ESTABLISHMENT OF NEURONAL CELL MODELS FOR THE STUDY OF LOW-INTENSITY PULSED ULTRASOUND THERAPY FOR NERVE REGENERATION

by

ARWA AHMED ABDULLAH AL-MASWARY

BDS, MDent

UNIVERSITY OF BIRMINGHAM

A thesis submitted to the University of Birmingham for the degree of

DOCTOR OF PHILOSOPHY

Institute of Clinical Sciences

School of Dentistry

College of Medical and Dental Sciences

University of Birmingham

March 2021

ABSTRACT

Although low-intensity pulsed ultrasound (LIPUS) is well highlighted as an adjunct therapeutic tool for bone regeneration, the potential therapeutic effect of LIPUS on nerve regeneration for regenerative endodontics and nerve injuries has been inadequately studied. This project aimed to investigate the effect of LIPUS as a potential non-invasive adjunct/therapeutic method for neuronal regeneration. Consequently, neuronal cell models were established by differentiation of two different cell types: human dental pulp stem cells (hDPSCs) and human neuroblastoma cell line (SH-SY5Y) for in vitro LIPUS experimentation. These neuronal cell models showed neuronal characteristics such as neuronal-like cell morphology, gene and immunocytochemical expression of neuronal markers, and neuro-electrophysiological recordings (sodium and potassium voltage-gated currents). These data indicated selective differentiation into a functional cholinergic sensory (nociceptive) neuronal lineage. The LIPUS study demonstrated that LIPUS induced cell proliferation of the neuronal cell models assessed by metabolic-based assays and cellular proliferation protein marker (Ki-67). The ERK/MAPK signalling pathway was activated in the neuronal differentiation of the neuronal cell models and LIPUS-induced proliferation processes assessed by phospho-ERK levels with either differentiation or proliferation assays. Therefore, this project mainly showed that hDPSCs can be differentiated into functional cholinergic sensory neuronal-like cells and LIPUS stimulates cell proliferation of the neuronal cell models which highlight the LIPUS as potential sole/adjunctive therapeutic approach for nerve/neuronal regeneration.

DEDICATION

This thesis is dedicated to three people for whom no words can describe my deep gratitude and thanks to them:

To Ar. Ahmed “my father”: the generous man who never let me need anything throughout my life. He named me after a Yemeni queen “Arwa Ahmed”. She was a sole ruler of Yemen for over 50 years in the 11th century CE. All Yemenis admire her and tell stories about her as a great female leader and her great achievements. Daddy, this PhD is for you to be proud of your queen!

To Mrs. Massara “my mother”: the earth angel who gives me unconditional love and keeps reminding me to be a good person regardless of the situation. And what others do or how others behave. This doctorate is for you, darling!

To Mr. Nashwan “my older brother” who stood by my side and risked travelling with me in dangerous circumstances at the time of the current Yemen war to protect and support his ambitious sister. Without you, my doctorate would not have been achieved. It was worthwhile, my rock!

ACKNOWLEDGEMENTS

I strongly believe “Successful people are always looking for opportunities to help others. Unsuccessful people are always asking, what is in it for me?”, Brian Tracy quote. So, I would like here to express my sincere thanks and appreciation to those successful people who I have met during my PhD journey. My sincere gratitude goes to my supervisors, Doctor Ben Scheven, Professor Paul Cooper, and Professor Damien Walmsley for their dedicated guidance, help, support, and patience. Without their guidance and support, this research project would not have been possible.

I would like to express my sincere thanks to Islamic Development Bank (IDB) for granting me this doctoral scholarship and School of Dentistry - University of Birmingham for covering the laboratory expenses. Without this generous fund, I would not have completed my postgraduate study. Special thanks to Dr Nazar El-Hilali, Mr Lakdhar Kadkadi, Mr Mahmud Aman, and Ms Bayan Filimban for their cooperation and help every time I contact IDB regarding the submissions and requests.

I would also like to thank all technical staff, in particular, Gay Smith, Michelle Holder, Jianguo Liu, Helen Wright and Khawla Doudin for their training and guidance in the lab. I am indebted to Justyna Folkert and Ania Mieszkowska who introduced me to the world of the real-time PCR. I would also like to thank Dr Huzaimi Haron (School of Pharmacy) for providing me the SH-SY5Y neuroblastoma cells. Furthermore, I am thankful to Dr Alessandro Di MaioI (School of Biosciences) and Dr Nina Vyas for training me to use the confocal microscopy and guidance in image analysis using ImageJ software. Great thanks also go to Professor Gabriel Landini for the guidance and advice regarding the ImageJ software. Many thanks go to collaborators from medical school, Dr Molly O'Reilly and Dr Andrew Holmes for measuring

the electrophysiological currents of my differentiated cells which made my research more valuable. I am so grateful to Dr Sayeed Haque for his training and advice regarding the statistical analysis of my data. My special thanks go to Professor Hatem Alhadainy, Professor Shokreia Ghoneim, Dr Niyaz Al-Sharabi, Dr Esam Halboub, Dr Firas Albaaj, and Dr Israa Alshalal for their advice and tips. I also have to thank Dr Abduraqeeb Alhaidari, our assistant deputy minister of health for his help every time I need to contact our embassy in London. Thanks also to all my fellow students for friendship, and company during my stay in Birmingham, in particular, Zinab, Haiyan, Candy, Ruba, Sonia, Soher, Nessma and Nina.

My deepest gratitude to my best friend Tahani Al-Jabi, my parents, sisters and brothers, in particular, Nashwan, Eman, Assma'a, Abdullah, Saher, Riyad, Shiama'a, and Sharif for their continuous caring, support, and encouragement. Also, my thanks go to my aunts, Fatehia and Aman for their continuous asking about me and checking if I need anything.

Finally, I would like to profoundly thank my students at Sana'a University for their kind and motivational words. These words really helped me immensely to continue and never let them down. I apologise for not mentioning their names, otherwise multiple pages would be needed. Thank you for believing in me.

TABLE OF CONTENTS

LIST OF FIGURES

CHAPTER 1: GENERAL INTRODUCTION

CHAPTER 2: MATERIALS AND METHODS

CHAPTER 3: OPTIMISING AND CHARACTERISING THE SH-SY5Y-DERIVED NEURONAL CELL MODELS

CHAPTER 4: DPSC DIFFERENTIATION INTO NEURONAL-LIKE CELLS AND CHARACTERISATION

CHAPTER 5: ROLE OF THE ERK1/2 MAPK SIGNALLING PATHWAY IN NEURONAL DIFFERENTIATION OF DPSCs AND SH-SY5Y CELLS

CHAPTER 6: PROLIFERATIVE EFFECTS OF LIPUS ON THE SH-SY5Y and DPSC-DERIVED NEURONAL CELL CULTURE MODELS

LIST OF TABLES

CHAPTER 1: GENERAL INTRODUCTION

CHAPTER 2: MATERIALS AND METHODS

CHAPTER 4: DPSC DIFFERENTIATION INTO NEURONAL-LIKE CELLS AND CHARACTERISATION

LIST OF ABBREVIATIONS

α-MEM	Alpha-modified minimum essential medium
AB	AlamarBlue
ACHE	Acetylcholinesterase
ATF-3	Activating transcription factor 3
ATRA	All trans-retinoic acid all-trans retinoic acid
AU	Airy unit
BDNF	Brain-derived neurotrophic factor
bFGF	Basic fibroblastic growth factor
BMP4/7	Bone morphogenic protein 4/7
B2M	Beta-2-microglobulin
BSA	Bovine serum albumin
cAMP	Cyclic adenosine monophosphate
CAMs	Cell adhesion molecule
CCK-8	Cell counting kit-8
CGRP	Calcitonin gene-related peptide
ChAT/CHAT	Choline O-acetyltransferase
CNPase	2',3'-Cyclic-nucleotide 3'-phosphodiesterase
Cp	Crossing point of gene amplification cycles
D609	Tricyclodecane-9-yl-xanthogenate
DAPI	4'-6-Diamidino-2-phenylindole
DAT	Dopamine acetyl transferase
dbcAMP	N^6, 2'-O-dibutyryladenosine 3', 5'-cyclic monophosphate (dibutyryl cAMP)
DBH	Dopamine beta-hydroxylase
DCX	Doublecortin
DMEM	Dulbecco's Modified Eagle's Medium
DMEM/F12	Dulbecco's modified Eagle's medium/Ham's nutrient mixture F12
DMEM/HG	High glucose Modified Eagle's Medium
DMSO	Dimethyl sulfoxide
DPSCs	Dental pulp stem cells
EDA	experimental design assistant
EGF/hEGF	Epidermal growth factor/Human epidermal growth factor
EN1	Engrailed homeobox 1
ENO2/NSE	Enolase 2/neuron-specific enolase
ERK	Extracellular signal-regulated kinase
FBS	Foetal bovine serum
EDTA	Ethylenediaminetetraacetic acid
FGF- FGF-8b	Fibroblast growth factor - fibroblast growth Factor 8b
GABA	Gamma-aminobutyric acid
GAD67	Glutamate decarboxylase 67
GAP43	Growth-associated protein 43
GAPDH	Glyceraldehyde-3-phosphate dehydrogenase
GATA3	GATA binding protein 3
GDF5	Growth differentiation factor 5
GDNF	Glial derived neurotrophic factor

GFAP	Glial fibrillary acidic protein
HB9	Homeobox 9
HDACi	Histone deacetylase inhibitor
hDPSCs	Human dental pulp stem cells
hESC	Human embryonic stem cells
HEPES	N-2-hydroxyethylpiperazine-N-ethanesulfonic acid
HPRT1	Hypoxanthine phosphoribosyltransferase
HRP	Horseradish peroxidase
Hz	Hertz
IBMX	Isobutyl methyl xanthine
IGF-1	Insulin-like growth factor 1
iPSCs	Induced pluripotent stem cells
ITS	insulin-transferrin-selenium
ITTS	Insulin-transferrin-sodium-selenite supplement
JNK	Jun N-terminal Kinase
KO DMEM/F12	Knockout DMEM/Nutrient Mixture
KO-ES	knockout-ES
LIF	Leukemia inhibitory factor
LIPUS	Low-intensity pulsed ultrasound
MAP2	Microtubule-associated protein 2,
MAPK	Mitogen-activated protein kinase
Mash1/ASCL1	Achaete-scute family bHLH transcription factor 1
MBP	Myelin basic protein
mESC	Mouse embryonic stem cells
MNX1	Motor neuron and pancreas homeobox 1
MSCs	Mesenchymal stem cells
MSI	RNA-binding protein Musashi
Nav1.6	Sodium Voltage-Gated Channel Alpha Subunit 8
NCAD	Neuronal cadherin
NCAM	Neural cell adhesion molecule
NEFM/NF-M	Neurofilament medium
NeuN	Neuronal nuclei protein
NEUROD1	Neuronal differentiation 1
NES	Nestin
NF1	Neurofibromin 1
NF-L	Neurofilament-light chain
NF-M	Neurofilament-medium chain
NF-H	Neurofilament-heavy chain
NG2	Neuron-glia antigen 2
NGN1	Neurogenin 1
NGN2	Neurogenin-2
NGF	Nerve growth factor
NSE	Neuron-specific enolase
NT2	Teratocarcinoma line Ntera2
NT-3	Neurotrophin-3
NTRK2	Neurotrophic receptor tyrosine kinase 2
NURR1/NR4A2	Nuclear receptor subfamily 4 group A member 2
Olig2	Oligodendrocyte transcription factor 2

p38 MAPK	38kDa mitogen associated protein kinase
PA	Pulse average
PAX6	Paired box 6
PBS	Phosphate-buffered saline solution
PDGF(aa)	Platelet-derived growth factor (AA)
PDGFR-α	Platelet-derived growth factor receptor alpha
p-ERK1/2	Phosphorylated ERK1/2 protein levels
PITX3	Paired like homeodomain 3
PLP1	Proteolipid protein 1
POU4F1	POU class 4 homeobox 1
PRPH	Peripherin
PSA-NCAM	Polysialic acid-neural cell adhesion molecule
PSD95	Postsynaptic density protein 95
PRF	Pulse repetition frequency
RET	Ret proto-oncogene
RPL13A	Ribosomal protein L13 (A)
S100β	Calcium-binding protein β
SA	Spatial average
SATA	Spatial-average temporal intensity
SCN1A	Sodium channel alpha subunit 1
SCN9A	Sodium channel alpha subunit 9
SHED	Stem cells from human exfoliated deciduous teeth
SHH	Sonic hedgehog
Shh-N	Sonic Hedgehog N Terminus
SLC6A3 (DAT)	Solute carrier family 6 member 3 (Dopamine acetyl transferase)
SNAP25	Synaptosome associated protein 25
SOX1	SRY-box transcription factor 1
SOX2	SRY-box transcription factor 2
SOX9	SRY-box transcription factor 9
SP	Spatial peak
SV2A	Synaptic vesicle protein
SYN1	Synapsin I
TA	Temporal average
TGF-β1/III	Transforming growth factor-beta1/III
TMB	3,3', 5,5"-tetramethylbenzidine
TNS	Trypsin neutralizing solution
TP	Temporal peak
TPA	12-O-Tetradecanoylphorbol-13-acetate (phorbol 12-myristate 13-acetate)
TRPM8	Transient receptor potential cation channel subfamily M number 8
TRPV1	Transient receptor potential cation channel subfamily V member 1
TUBB3/TUJ1/Tuj1	Tubulin beta 3 class III/βIII-tubulin
TH	Tyrosine hydroxylase
US	Ultrasound
VEGF	Vascular endothelial growth factor

CHAPTER 1: GENERAL INTRODUCTION

1.1. Introduction

Nerve loss occurs during pulp necrosis due to the consequences of dental infection. These pulpal nerves play a significant role in healthy pulp function, defence, and repair mechanisms (Lundy, El karim and Scheven, 2019; Byers, Suzuki and Maeda, 2003). There is a need for nerve regeneration in regenerative endodontics as a key component to achieving functional pulp regeneration (Nakashima and Iohara, 2011; Yang, Yuan and Chen, 2016). Furthermore, nerve loss due to injuries is a common problem worldwide and can affect anyone at any age; however, higher incidences occur in the younger population (Bekelis, Missios and Spinner, 2015; Missios, Bekelis and Spinner, 2014; Krivickas and Wilbourn, 2000; Bekelis, Missios and Spinner, 2014). The damaged nerves can result in patient suffering and diminished quality of life or even devastating effects in cases of severe nerve injuries (Huckhagel *et al.*, 2018; Rosberg *et al.*, 2005; de Albornoz *et al.*, 2011). Damage to dental divisions of the trigeminal nerves could lead to a range of outcomes of sensation loss (hypoesthesia to total anaesthesia) or chronic neurogenic pain which needs surgical intervention (Hillerup, 2007; Klazen *et al.*, 2018). The long-term outcomes of dental trigeminal nerve injuries might affect the quality of life, such as eating problems, speaking problems, depression, and persistent pain or neurosensory feeling disturbance (Pogrel *et al.*, 2011; Renton, 2011; Al-Sabbagh *et al.*, 2015).

Nerve regeneration is a clinical challenge to restore the neuronal loss in the peripheral nervous system, including dental branches of trigeminal nerves (Grinsell and Keating, 2014; Riccio *et al.*, 2019; Rosén, Tardast and Shi, 2016). Neurogenesis is the critical part of nerve regeneration, which involves differentiation into neuronal cells, proliferation, migration and then integration of these new functional neuronal cells within the surrounding tissue (Braun and Jessberger, 2014). In this context, it is understood that endogenous neurogenesis has the potential to repair the damaged or destroyed nerves (Duan *et al.*, 2016; Lim and Alvarez-Buylla,

2016). There remain controversial opinions regarding whether endogenous neurogenesis persists into adulthood (Sorrells *et al.*, 2018; Moreno-Jiménez *et al.*, 2019; Kempermann *et al.*, 2018). Furthermore, this endogenous regenerative capacity is limited to self-recovery of the damaged neurons which need therapeutic interventions to repair the defect (Riccio *et al.*, 2019). Current therapies show limitations, for example, incomplete functional recovery, and consequently, there is a need for creating new innovative therapies for nerve regeneration (Grinsell and Keating, 2014; Ventre and Koppes, 2016; Deumens *et al.*, 2010; Gordon, Sulaiman and Boyd, 2003; Gordon *et al.*, 2009).

Low-intensity pulsed ultrasound (LIPUS) is a clinical therapeutic approach for bone fracture healing, especially during delayed bone unions (Poolman *et al.*, 2017; Rutten *et al.*, 2016). Several studies have proposed LIPUS as a potential non-invasive therapeutic approach for nerve injury repair/regeneration. For example, it has been reported that LIPUS promoted inferior alveolar nerve healing after transection (Yang *et al.*, 2017a; Sato *et al.*, 2016), and enhanced neuronal differentiation and proliferation (Lv *et al.*, 2013; Zhao *et al.*, 2016). So far, however, few studies have investigated the effect of LIPUS on the regeneration of peripheral nerves, including dental-related trigeminal nerves. Furthermore, the majority of these LIPUS studies were conducted using rat cell or nerve models (see Table 1.2), which may not be entirely relevant to human responses (Bracken, 2009; Shanks, Greek and Greek, 2009). Thus, there is a clear need to investigate the effect LIPUS on neuro-regenerative ability using appropriate human models.

To investigate LIPUS therapeutic potential for nerve regeneration, neurons are needed for *in vitro* experimentation before transitioning the therapeutic method to the pre-clinical and clinical settings. The most appropriate option for such investigation is using human neurons; however, they are not accessible for research due to ethical issues. The most common option is

animal models which have provided us with good knowledge to understand neuronal-related responses such as neuronal circuitry in health and disease (Theyel, 2018; Nakajima and Schmitt, 2020). Notably, there are differences between animal and human neuronal responses which hinders translational research (Zhao and Bhattacharyya, 2018). For example, there is considerable variation in behavioural or biological aspects between animals and humans (Monteggia, Heimer and Nestler, 2018), which negatively affect the translation and interpretations of the results obtained. Hence, the development of *in vitro* human neuron cell models is necessary to investigate the neuron-related responses such as therapies, neurodevelopment, injury, and disease, which can be derived from human stem cells (Jones *et al.*, 2018). The development of neuronal cell models derived from stem cells are not only beneficial for *in vitro* studies, but also may provide neuronal cell replacements during neuro-regenerative transplantation therapies (Irion, Zabierowski and Tomishima, 2017; Grade and Götz, 2017). In this context, stem cells exhibit promising ability to differentiate into different cell types to replace the defective cells and tissues (Kalinina *et al.*, 2011). Dental pulp stem cells (DPSCs) are of neural crest origin and have potential neurogenic properties, making them a preferred stem cells for differentiation into neurons for regenerative endodontics and peripheral nerve injuries (Lundy, El karim and Scheven, 2019). Furthermore, DPSCs are an easily accessible source of stem cells derived from teeth extracted due to various dental reasons to be used in regenerative therapies (Kabir *et al.*, 2014). Hence, development of neuronal cell models using human DPSCs in comparison with a human neuronal cell line would be of interest and worthy of further investigation. The study of the effects of LIPUS on these neuronal cell models for dental pulp and nerve regenerative purposes could then be explored. In a broader context, further research in these areas might play a major role in addressing peripheral nerve injury treatments in regenerative medicine. Consequently, the regenerative endodontics and

nerve regeneration, peripheral nerve injuries (including dental-related injuries), LIPUS, and neuronal-cell models will be further discussed in this review.

1.2. Regenerative endodontics and nerve regeneration

Regenerative endodontics is defined as biological-based procedures designed to restore damaged dental structures, including cells of the pulp-dentine complex, dentine and root (Murray, Garcia-Godoy and Hargreaves, 2007). The ultimate goal of endodontic regeneration is to re-establish a genuine functional pulp tissue including innervation, immunity, vascularisation, and dentine formation ability (Law, 2013; Shi, Mao and Liu, 2020; Diogenes, 2020). Consequently, researchers have aimed to establish functional pulpal tissue, including pulpal innervation, via the main regenerative endodontic approaches: pulp revascularisation/revitalisation, cell transplantation, and cell homing.

1.2.1. Pulp revascularisation/revitalisation

The root canal or pulp revascularisation/revitalisation via blood clotting is the simplest and the traditional form of regenerative endodontics. This dental procedure is clinically indicated in necrotic pulp cases in immature and mature permanent, avulsed and traumatised teeth with and without external inflammatory root resorption (Saoud *et al.*, 2016). However, pulp revascularisation is recommended to be used in teeth with incomplete root formation to gain favourable outcomes (Kim *et al.*, 2018; Law, 2013). It is a bleeding-induced procedure from the periapical area to introduce the resident periapical stem cells into the root canal and blood clot acts as a cell scaffold (Chrepa *et al.*, 2015; Lovelace *et al.*, 2011). This approach can also be performed with platelet-rich fibrin or platelet-rich plasma placement without evoking bleeding from the apical area (Ulusoy *et al.*, 2019). The vast majority of the treated cases demonstrated an absence of pathological signs and symptoms, radiographic resolution of

periapical lesion, and signs of root completion (Geisler, 2012; Law, 2013; Hargreaves, Diogenes and Teixeira, 2013; Kandemir Demirci, Güneri and Çalışkan, 2020; Nageh, Ahmed and El-Baz, 2018; Neelamurthy *et al.*, 2018; Kahler *et al.*, 2014). However, a positive response to nerve vitality testing is generally not regained and estimated to occur in ~50% of the cases (Diogenes *et al.*, 2013; Diogenes, 2020). In addition, the thermal sensation in these regenerative endodontic cases is much weaker and still not conducted through the principal hydrodynamic mechanism like the normal healthy pulp (Diogenes, 2020).

Histologically, several animal models and human teeth studies have shown that the formed tissues after pulp revascularisation procedures were hard tissue-like structures such as cementum, and bone or periodontal ligament-like tissue but not pulp-like tissue (Wang *et al.*, 2010; da Silva *et al.*, 2010; Yamauchi *et al.*, 2011; Martin *et al.*, 2013; Shimizu *et al.*, 2013; Becerra *et al.*, 2014; Lei *et al.*, 2015). Also, root completion is attributed to cementum-like or bone-like tissue deposition (Saoud *et al.*, 2016). Subsequently, very few immunohistochemical studies have shown signs of pulpal innervation after root canal revascularisation. Lei *et al.* (2015) reported a presence of some nerve fibres, and Meschi *et al.* (2016) addressed few neurovascular bundles in the newly formed tissue within the canal system. Recently, Austah *et al.* (2018) demonstrated some nerve fibres like Schwann and sensory fibres expressing sensory markers (i.e. neuropeptide calcitonin gene-related peptide - CGRP). However, the authors reported that CGRP-expressing fibres were not co-localised with a pan-neuronal marker (Tubulin Beta 3/Class III - TUBB3) as in the control normal pulp tissue group, which might invalidate the presence of this sensory marker.

1.2.2. Cell transplantation

The early studies of cell transplantation were conducted on tooth slices/segments and subcutaneous implantation in immunocompromised mice. For example, using DPSCs, collagen

scaffolds, and dentine matrix protein 1 in dentine slices resulted in matrix formation of pulp-like tissue with rich angiogenesis (Prescott *et al.*, 2008). Other studies used a combination of deciduous DPSCs or stem cells from human exfoliated deciduous teeth (SHED) and a polylactic scaffold resulting in pulp-like tissue, odontoblast-like, and endothelial-like cells (Cordeiro *et al.*, 2008). Moreover, Huang *et al.* (2010) demonstrated that DPSCs, and a poly-D,L-lactide/glycolide scaffold resulted in formation of pulp-like tissue, dentine-like tissue and angiogenesis in the root segment. Other regenerative endodontic studies were performed in teeth of large animals, such as dogs and pigs/swine and resulted in a range of favourable outcomes from dentine formation to complete pulp regeneration, including neuronal tissue, in non-infected conditions of pulpotomy (Iohara *et al.*, 2004; Iohara *et al.*, 2009) or pulpectomy (Iohara *et al.*, 2011; Iohara *et al.*, 2013; Iohara *et al.*, 2018). Previous studies have contributed to a significant advancement in regenerative endodontics. However, these studies were conducted in healthy non-infected root canals which do not simulate the actual clinical scenario with infected or necrotic root canals and with no remaining healthy pulpal tissue. Verma *et al.* (2017) showed that residual bacteria negatively affect regeneration ability in both traditional revascularisation via blood clotting and transplanted DPSC-based pulp regeneration. In addition, Torabinejad *et al.* (2018) reported that the presence of the tiny amount of residual intact, healthy apical pulp tissue (1-4mm) could produce a complete normal pulp-dentine complex regeneration using the traditional revascularisation via blood clotting in animal models. This study suggested that the newly formed pulp tissue, including neuronal tissue, resulted from migrating and proliferation of remaining healthy pulp tissue. The concept of the residual healthy pulp tissue does not exist in the necrotic and irreversible pulpitis cases. Thus, regenerative endodontic studies are preferable for investigation into the pre-infected or necrotic

root canal to mimic the clinical scenario. Also, involving DPSCs in regenerative endodontic procedures might increase the chance of regaining a holistic pulp regeneration.

Interestingly, a randomised clinical trial achieved a total functional pulp-dentine complex regeneration with vascular and sensory nerve supply in necrotic immature teeth of paediatric patients using a combined approach of autologous deciduous DPSC implantation with traditional root canal revascularisation via blood clotting (Xuan *et al.*, 2018). Although the expression of the tested sensory nerve markers (i.e., TRPM8 and TRPV1) were shown in animal DPSCs before implantation and in hDPSCs implanted within rat ganglion, they were neither demonstrated in the newly regenerated pulp of animal nor human teeth. Notably, the neuronal nuclei (NeuN) marker was expressed in the regenerated pulp instead. The NeuN marker has also been expressed by undifferentiated mesenchymal stem cells (Foudah *et al.*, 2014). Hence, the importance of using multiple neuronal markers is proposed to make clear and definitive conclusions.

1.2.3. Cell homing

Cell homing is another emerging endodontic regenerative approach proposed by Kim *et al.* (2010). This approach relies on recruitment of the endogenous stem cells, followed by differentiation into pulp-dentine complex components under stimulation from exogenous bioactive molecules. The bioactive molecules include a collection of growth factors: VEGF, bFGF or PDGF with a basal set of BMP7 and NGF, encapsulated in a cell-free collagen gel scaffold. The outcome of this chemotaxis-based pulp regeneration step is pulp-like tissue with vascularisation (Kim *et al.*, 2010). Others have attempted to use only a single exogenous growth factor for pulp regeneration, including bFGF (Suzuki *et al.*, 2011; Takeuchi *et al.*, 2015), Granulocyte-colony stimulating factor (Takeuchi *et al.*, 2015), stem cell factor (Pan *et al.*, 2013; Ruangsawasdi *et al.*, 2017), and stromal cell-derived factor-1 (Zhang *et al.*, 2015; Yang *et al.*,

2015). Another approach for cell homing is to induce pulp-dentine complex regeneration through the release of endogenous growth factors from the dentine matrix (Smith *et al.*, 2016; Smith *et al.*, 2012; Sun *et al.*, 2011). Ethylenediaminetetraacetic acid (EDTA), the common chelating agent used to remove the smear layer in endodontic procedures, releases growth factors from dentine (Cassidy *et al.*, 1997; Zeng *et al.*, 2016; Tomson *et al.*, 2007). Recently, Austah *et al.* (2019) reported that the dentine matrix contains neurotrophic factors capable of increasing neurite outgrowth of trigeminal ganglion neurons. Moreover, Duncan *et al.* (2017) demonstrated that the histone deacetylase inhibitor (HDACi) is capable of releasing brain-derived neurotrophic factor (BDNF) more effectively from the dentine than EDTA solution whereas EDTA released more glial-derived neurotrophic factor (GDNF) than HDACi. Thus, the combination of EDTA and HDACi solutions or use in a sequential manner is most likely to increase neurogenesis in regenerative endodontic procedures.

Thus far, little attention has been paid to the role and importance of neurogenesis/innervation in regenerative endodontics. Inadequate innervation means losing the "alert" signal to detect the potential pathogenic stimuli, and the tooth becomes more vulnerable to future infections (Namour and Theys, 2014). This protective surveillance system in the normal pulp is conducted through nociceptors (Henry and Hargreaves, 2007; Dubin and Patapoutian, 2010). Thus, regenerative endodontic therapy could fail with a subsequent pathogenic invasion when the innate alerting system is absent. Pulpal innervations also regulate the pulpal blood flow (Olgart, 1996) and plays an essential role within the dental pulp defence and function (Olgart, 1985; Raab, 1992; Kerezoudis, Olgart and Edwall, 1994). Furthermore, neurogenic and angiogenic cytokines might be involved in the reparative process against low levels of inflammation (Cooper, Holder and Smith, 2014; Byers, Schatteman and Bothwell, 1990). It has been shown that pulpal nerves undergo sprouting into the infected areas and

stimulate the immunological and inflammatory responses via extravasation of immune cells to the injured site (Fristad, 1997; Kimberly and Byers, 1988; Byers *et al.*, 1990; Byers, Suzuki and Maeda, 2003). Sensory neuropeptides such as substance P and CGRP stimulated proliferation of pulp-derived fibroblast cells, and CGRP increased reparative dentine formation through inducing bone morphogenetic protein-2 release (Calland, Harris and Carnes, 1997; Trantor, Messer and Birner, 1995). This co-association of neuro-immunological activities and dentine formation was also demonstrated in human carious teeth (Couve, Osorio and Schmachtenberg, 2014).

Sensory denervation/deafferentation/dental nerve transection can negatively affect the health of the pulp and preapical tissues. It has been shown that sensory denervation accelerated loss of pulpal tissue, necrosis, and progression of pathogens and apical periodontitis formation after experimental pulp exposure (Byers and Taylor, 1993; Austah *et al.*, 2016). It was also shown that the dental nerve transection reduced the normal cell proliferation after experimental 1 mm depth cavity preparation within enamel and dentine (Chiego *et al.*, 1986). Thus, pulpal innervation is essential for maintaining pulpal tissue homeostasis, dental tissue repair and regeneration. Nerve regeneration and neuro-pulpal communication must be better appreciated and targeted in the research studies to re-establish a functional and holistic pulp-dentine complex (Nakashima and Akamine, 2005; Diogenes, 2020). Nerve regeneration is also critical to treat peripheral nerve injuries, including dental related nerve injuries.

1.3. Peripheral nerve injuries

Peripheral nerve injuries or damage are mostly the results of traumatic causes such as vehicle accident, and falls (Kouyoumdjian, 2006). Nerve injuries were first classified based on the anatomical extension of the nerve damage by Sir Herbert Seddon into neurapraxia,

axonotmesis, and neurotmesis (Seddon, 1942). Neurapraxia is myelin sheath damage without loss of the nerve continuity such as compression injuries and blunt trauma (mild damage). Axonotmesis is a loss of axonal continuity but with maintenance of the surrounding connective tissue sheath (moderate damage) whereas neurotmesis is the complete nerve transection, including its sheath (severe damage). Subsequently, Sunderland and Williams (1992) updated Seddon's classification by further dividing the axonotmesis into three subtypes according to the degree of nerve sheath involvement and adding an estimating prognosis for each one (See Table 1.1).

Table 1.1 Classifications of peripheral nerve injury (adapted from Lee and Wolfe (2000) and amalgamated with the recovery data from Sunderland and Williams (1992)).

Sunderland, and Williams, 1992	**Seddon, 1942**	**Pathophysiologic characteristics**	**Recovery**
Type 1	Neurapraxia	Localised damage of myelin causing impulse conduction block	Complete recovery takes (several days to weeks)
Type 2	Axonotmesis	Damage of axons	Full recovery (Months)
Type 3		Damage of the axons and endoneurium	Partial recovery
Type 4		Damage of the axons, endoneurium, and perineurium.	Minimal recovery
Type 5	Neurotmesis	Damage of the axons, endoneurium, perineurium, and epineurium (Complete nerve disruption).	Negligible recovery

The adverse effects of nerve injuries include loss of tactile perception (impaired stereognosis), disturbed thermal perception, and pain in some cases developing complex regional pain syndromes (CRPS 2) (Bruyns *et al.*, 2003; Rosén *et al.*, 2012). Other peripheral nerve injury patients experience a complete loss of sensation (anaesthesia), abnormal sensation (paraesthesia), and reduced sensation (hypesthesia), and increased sensitivity (hyperalgesia)

(Belzberg, 2006). In addition, the adverse psychological effects were reported after peripheral nerve injuries, including depression and stress (Wojtkiewicz *et al.*, 2015).

1.3.1. Dental related nerve injuries

The trigeminal nerve may be damaged or disturbed by many dental procedures such as implant insertion, dental-related surgeries, local anaesthetic injections, and root canal therapy (Pogrel, 2017; Agbaje *et al.*, 2016). However, the dental procedure most highly associated with the possibility of such injuries is the surgical removal of impacted mandibular third molar (Sarikov and Juodzbalys, 2014; Yadav, Verma and Sachdeva, 2014; Tojyo *et al.*, 2019). Furthermore, the inferior alveolar nerve block is another dental procedure which might cause nerve injury (Pogrel and Thamby, 2000; Kim, Hwang and Park, 2018; Renton *et al.*, 2010).

The inferior alveolar and lingual nerves are the main vulnerable nerves to be traumatised during dental practice (Veitz-Keenan and Keenan, 2015; Renton *et al.*, 2010). The most attributable risk factors of injuries to these nerves are their anatomical proximity to the operating area and the operator skills (Jerjes *et al.*, 2010; Sarikov and Juodzbalys, 2014). The incidence rate of these nerve injuries is generally low as most studies reported ≤ 1% (Renton *et al.*, 2013; Nguyen, Grubor and Chandu, 2014; Cheung *et al.*, 2010; Agbaje *et al.*, 2016), however Sarikov and Juodzbalys (2014) reported that this percentage could increase to 8.4% with inferior alveolar nerve injury.

Although most of these nerve injuries are temporary and self-recover within months, some of these nerve injuries are permanent (Sarikov and Juodzbalys, 2014; Nguyen, Grubor and Chandu, 2014; Cheung *et al.*, 2010). Valmaseda-Castellón *et al.* (2001) and Renton *et al.* (2013) reported that permanent damage is 25 - 29% of the total nerve injuries occurring during dental procedures, whereas Agbaje *et al.* (2016) reported a higher percentage rate of ~37.5%.

These nerve injuries may affect thermoception (hot and cold), nociception (pain), and mechanoreception (touch, pressure, and position) (Haas and Lennon, 1995; Day, 1994; Campbell, Shamaskin and Harkins, 1987). Thus, the patients may suffer from pain, oversensitivity, or abnormal sensation like hyperalgesia and allodynia, paraesthesia, or dysesthesia (Agbaje *et al.*, 2016; Renton *et al.*, 2010; Hartmann *et al.*, 2017). In addition, taste sensation may also be affected in some cases (Haas and Lennon, 1995; Renton *et al.*, 2010; Snyder and Bartoshuk, 2016). The change in sensation can be long-lasting or permanent (Smith and Lung, 2006; Tınastepe and Oral, 2013). Other functional implications might include speech, mastication difficulties, tongue and cheek biting (Zuniga and LaBanc, 1993; Sandstedt and Sörensen, 1995; Smith and Lung, 2006). There are also many psychological effects such as pain catastrophising and depression (Smith and Lung, 2006; Smith *et al.*, 2013).

1.4. Physiological nerve regeneration and limitations of current therapies

Physiologically, once peripheral nerve injury occurs, a sequence of processes is carried out to repair the resultant defect (Stoll and Müller, 1999; Rotshenker, 2011) as shown in Figure 1.1. Briefly, Wallerian degeneration is the first process to prepare the area for initiation of nerve repair/regeneration. In this process, macrophages and activated Schwann cells are chemoattracted to the injured site to eliminate the damaged axon and myelin sheath cells via phagocytosis. Subsequently, Schwann cells proliferate to form a path “the bands of Büngner” for guiding the sprouting axon from the intact remaining part of the nerve. Finally, the neuronal matrix is formed, and new axon fibres are sprouted from the intact end until regeneration of the lost area at an average of 2-3 mm/day in the nerve transection, and 3-4 mm/day in nerve crushes (Stoll and Müller, 1999).

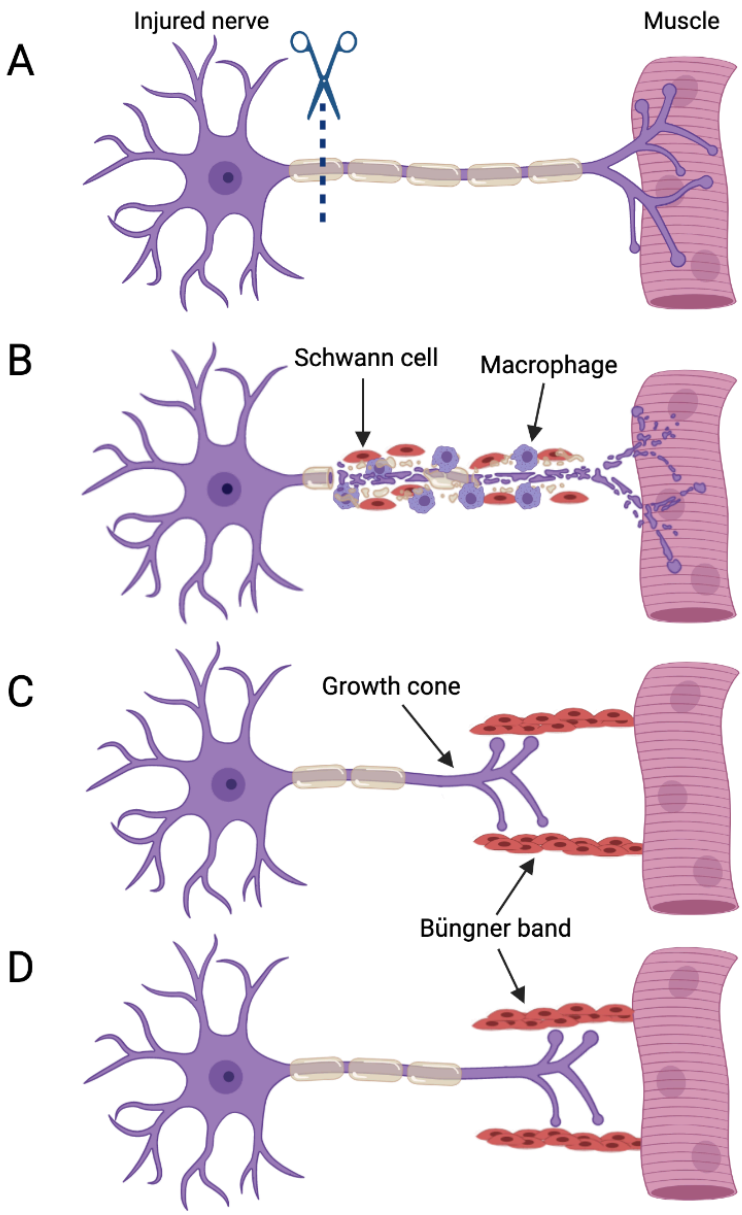

Figure 1.1 Physiological nerve regeneration after injury. A, complete nerve transection. B, Wallerian degeneration to remove the traumatised nerve. C, Growth-cone extension to regenerate the lost part. D, Büngner band guide the newly formed axon to the tissue target. The image was designed and created by the author using the Biorender designing website. (https://biorender.com).

From the molecular aspect, after nerve injury occurs, there is intracellular signalling for optimising the environment and conditions to achieve successful nerve regeneration. In this process, the status of affected neurons changes from "signal transmission mode" to

"regeneration and cell death mode" in which the cell death and regeneration coordinately stimulated to remove the damaged cell and replace them with new cells (Abe and Cavalli, 2008; Jessen and Mirsky, 2016). A cascade of intracellular molecules is activated to trigger nerve regeneration (Raivich and Makwana, 2007). The members of mitogen-activated protein kinase (MAPK): Jun N-terminal Kinase (JNK), 38kDa mitogen associated protein kinase (p38), and extracellular signal-regulated kinase (ERK) are involved in neurogenesis and the neuronal regenerative process after nerve injury (Raivich and Makwana, 2007). The JNK and p38-MAPKs are involved in cell apoptosis (Wada and Penninger, 2004; Kikuchi, Tenneti and Lipton, 2000; Cao *et al.*, 2004), whereas the ERK/MAPK is upregulated and involved in nerve regeneration and survival after nerve injury (Agthong *et al.*, 2006; Chierzi *et al.*, 2005; Raivich and Makwana, 2007; Wada and Penninger, 2004). The ERK1/2 proteins are rapidly activated and upregulated within 30 min after nerve injury, which is crucial for neuronal proliferation and regeneration (Mårtensson *et al.*, 2007; Agthong *et al.*, 2006). Subsequently, transcription factors, such as c-jun and activating transcription factor 3 (ATF-3), are activated triggering nerve regeneration and survival (Raivich *et al.*, 2004; Lindwall and Kanje, 2005; Patodia and Raivich, 2012).

Physiological regenerative processes are limited and cannot restore functional recovery, especially in severe injuries (Gonzalez-Perez, Udina and Navarro, 2013). For example, complete nerve transection often needs surgery or reconstruction to repair the nerve defect (Seddon, 1943; Gonzalez-Perez, Udina and Navarro, 2013). Although there is a common belief that the peripheral nerve injuries demonstrate better recovery outcomes after reparative surgical therapies, functional recovery is rare (Gordon, Sulaiman and Boyd, 2003). For instance, the conventional surgical reparative methods "bridging" such as tubularization (Hentz *et al.*, 1991; Ichihara, Inada and Nakamura, 2008), autografting, and allografting (Evans, 2001; Moore *et*

al., 2011) do not regain functional recovery in 50% or more of the cases (Grinsell and Keating, 2014; Lee and Wolfe, 2000). In addition, drawbacks of these conventional surgical methods include difficulty in scarifying or obtaining a nerve to be grafted into the defect area, accessibility to the donor's nerve, and surplus surgical methods (Griffin *et al.*, 2014; Yousefi *et al.*, 2019). Hence, further research is needed for creating alternative or adjunct therapies to boost nerve regeneration which might result in superior therapeutic outcomes and fewer drawbacks (Grinsell and Keating, 2014; Ventre and Koppes, 2016; Deumens *et al.*, 2010; Gordon, Sulaiman and Boyd, 2003; Gordon *et al.*, 2009). Ultrasound research is emerging and has been proposed to use as an adjunct stimulator for tissue regeneration (de Lucas *et al.*, 2020; Liu *et al.*, 2020), its application might also be beneficial for nerve regeneration.

1.5. Ultrasound (US)

Ultrasound (US) represents acoustic waves beyond the frequency range of the average human hearing (>20,000 hertz: Hz). Ultrasound has been widely used for diagnostic (Devey and Wells, 1978), therapeutic, and operative medical purposes (ter Haar, 2007; Crum *et al.*, 2010; Soler López, 2013). Moreover, ultrasonic equipment is also used in dentistry for clinical treatment applications such as periodontal scaling and root canal irrigation since the 1950s (Walmsley, Laird and Lumley, 1992).

1.5.1. US basic physical parameters

The main US parameters are frequency and intensity. US can be delivered in a continuous or pulsed mode. The pulsed US has additional main parameters which are the pulse repetition frequency (PRF) and duty cycle.

1.5.1.1. US frequency

US frequency is defined as the number of times the wave cycle is repeated in which the particle involved in compression and rarefication oscillations per second, expressed in Hz (Figure 1.2). Each wave cycle comprises one rarefaction and one compression. The wavelength is the distance occupied by one cycle (Schrope and Goel, 2014). The wavelength is either measured as the distance between two adjacent peaks of compressions or two adjacent troughs of rarefactions. It depends on numbers of frequency to be classified as low (20 to 200 kHz), medium (0.7-3.0 MHz), or high-frequency US (1-20 MHz). The low and medium frequency US are commonly specified for therapeutic purposes, whereas the high-frequency US is mostly used for diagnostic purposes (Ahmadi *et al.*, 2012; Xin *et al.*, 2016).

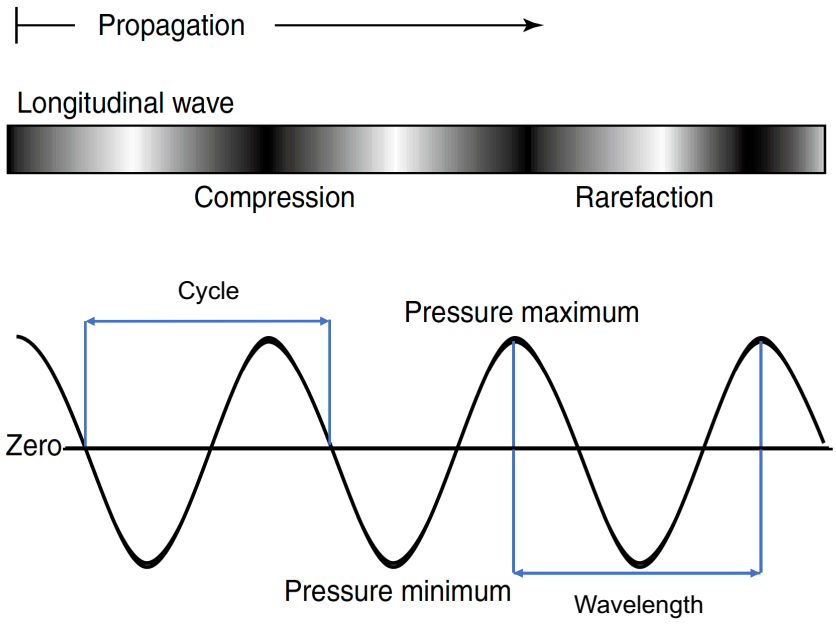

Figure 1.2 US wave frequency. Mechanical waves are propagated across the tissue as longitudinal waves and are parallel to the direction of the propagation. The wave cycle is one compression and one rarefaction. The image is adapted with permission from Schrope and Goel (2014) and the wavelength and cycle illustration arrows were added to the figure (blue lines).

1.5.1.2. Intensity

The US intensity is the acoustic energy placed per unit area and expressed in watts (W) or milliwatts (mW) per square centimetre (cm^2). US intensity can be described by the spatial, temporal, and spatial average-temporal average (SATA). The spatial average intensity is the average intensity measured over the cross-sectional area of US transmission, whereas temporal average intensity is measured over time. The US intensity ranges from 0.05 to 0.5 W/cm^2 in diagnostic imaging (Warden, 2003) and increases to 1000 W/cm^2 in the surgical therapies (ter Haar, 2007). However, most therapeutic US doses are 0.03-1.0 W/cm^2, for example physiotherapy and dental scaling (ter Haar, 1999; Karumuri *et al.*, 2016; Khanna *et al.*, 2009). The low-intensity US is less than 3 W/cm^2, whereas the high intensity is equal to or above the 3 W/cm^2 (Xin *et al.*, 2016). Low intensity is further subclassified according to the therapeutic dose into high (2–3 W/cm^2), medium (1–2 W/cm^2), and low (<1 W/cm^2) (Xin *et al.*, 2016).

1.5.1.3. Pulsed US and its physical parameters

Pulsed US is produced in a mode of pulse waves. These pulse waves are produced in an alternating manner between pulse wave output and rest "no pulses" (Figure 1.3A). The typical pulse ratios are 1:1 (equal time of pulse production and rest), and 1:4 (1-time interval pulse to 4-time intervals of rest), however, there are other available pulse ratios (Xin *et al.*, 2016). The ratio of pulse wave time to total time (pulse and rest time) is known as the duty cycle (Liu *et al.*, 2020). The duty cycle is given in percentage, such as 50% for 1:1, and 20% for 1:4 pulse ratios. The PRF are defined as the number of US pulses produced per second, expressed in Hz. The typical PRFs are either 100 or 1000 Hz (Xin *et al.*, 2016).

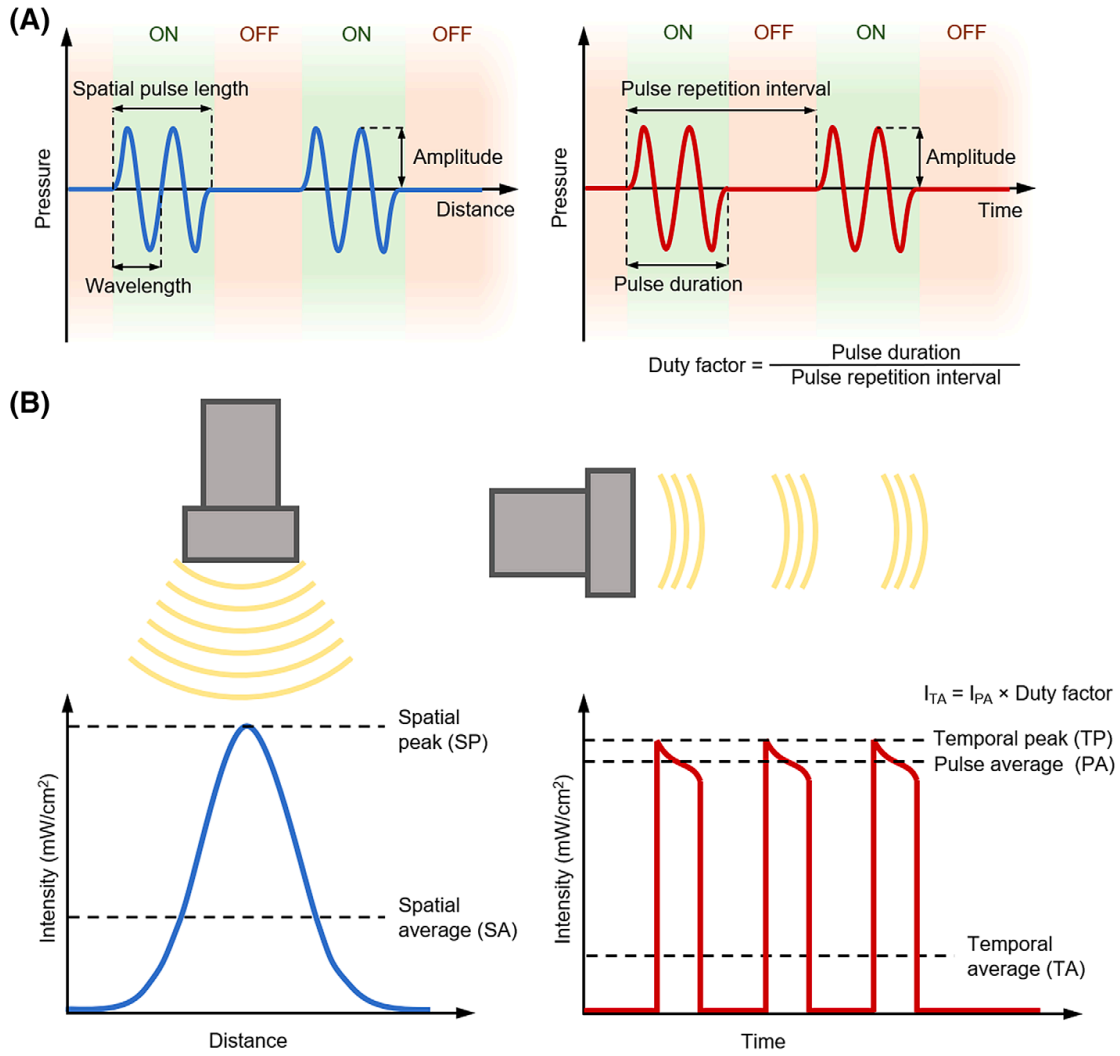

Figure 1.3 Pulsed-US parameters. A) Pulse wave parameters (spatial pulse length, pulse repetition interval, pulse duration, and amplitude) over space (left), and time (right). B) Spatial intensity parameters, including spatial average and peak (left), and temporal intensity parameters, including temporal average and peak, and pulse average (right). This image is adapted with permission from Liu *et al.* (2020).

Due to the pulse-mode US (on and off pulses), there is a difference between the spatial intensity (measures over the cross-sectional area) and temporal intensity (measures over on and off time) (Liu *et al.*, 2020). Thereby, the pulsed US intensity is described by various combinations of spatial and temporal intensities (Figure 1.3B). The spatial intensity measures are spatial average (SA) and spatial peak (SP). The SA and SP measured the intensity average and peak over the cross-sectional area of the US beam, respectively. In addition, temporal intensity measures are temporal average (TA), temporal peak (TP), and pulse average (PA).

The TA and TP measured the intensity average and peak over time, whereas PA measured the pulse average over the on-pulse interval. Hence, these measures are combined to make 6 combinations of the temporospatial intensities (SATA, SAPA, SATP, SPTA, SPPA, SPTP). The SATA is the most commonly used term to describe the intensity of the low-intensity pulsed US which the average of the spatial and temporal intensities (Ling *et al.*, 2017a; Zhao *et al.*, 2016; Zhang *et al.*, 2009; Daeschler *et al.*, 2018; Li, Zhang and Ren, 2012). However, many experimental studies do not specify the LIPUS intensity type, which make the reproducibility and comparison between studies difficult for determining standard therapeutic parameters (Liu *et al.*, 2020), for instance, only 3 out of 11 studies mentioned intensity type, see Table 1.2.

1.5.2. LIPUS and tissue regeneration

LIPUS is a therapeutic pulsed ultrasound characterised by low intensity (<1W/cm^2) and medium frequency (1-1.5 MHz) at pulse mode output (100 and 1000 Hz) (Karumuri *et al.*, 2016). An intensity range (I_{SATA}: 30-500 mW/cm^2) is considered to be useful for bone healing, but higher than 500 mW/cm^2 is harmful to the bone tissue (Tsai, Chang and Liu, 1992; Busse *et al.*, 2002; Reher *et al.*, 1997). One example showing the use of the LIPUS parameters is the Osteotron IV LIPUS device which delivers a range of low intensities (I_{SATA}: 30-60 mW/cm^2) at a frequency of 1.5 MHz or 750 kHz with pulse waves of 100 or 1000 Hz, and duty cycle 20%.

LIPUS is a relatively safe, non-invasive, inexpensive approach without the induction of thermal damage to the tissue (Pomini *et al.*, 2014; Tanaka *et al.*, 2015; Mukai *et al.*, 2005). It is approved by the United States Food and Drug Administration (FDA) for use as a therapeutic tool for delayed bone fracture healing (Rubin *et al.*, 2001). The overall concept is that low-intensity ultrasound has the therapeutic potential to promote effective tissue regeneration and repair (Scheven *et al.*, 2009; de Lucas *et al.*, 2020). Several studies investigated and reported

biological effects of LIPUS on different cell types. For example, it has been reported that LIPUS promoted cell proliferation of mesenchymal stem cells (MSCs) derived from different tissue types (Gao *et al.*, 2016b; Xie *et al.*, 2019; Ling *et al.*, 2017b; Yoon *et al.*, 2009; Huang *et al.*, 2020; Budhiraja, Sahu and Subramanian, 2018), osteoblasts (Alvarenga *et al.*, 2010), and chondrocytes (Takeuchi *et al.*, 2008; Nishikori *et al.*, 2002),. Other *in vitro* studies showed additional biological effects in different cell types such as inducing proliferation and migration of keratinocytes (Leng *et al.*, 2018), growth and stemness of periodontal ligament cells (El-Bialy, Alhadlaq and Lam, 2012), and cell viability and proliferation of osteoblasts (Miyasaka *et al.*, 2015). Moreover, some studies demonstrated the biological effects of LIPUS on bone-related tissues, such as osteogenic differentiation (Ren *et al.*, 2013; Sawai *et al.*, 2012; Suzuki *et al.*, 2009), and bone healing (Acar *et al.*, 2016; He *et al.*, 2015). In terms of stem cell-based tissue engineering, LIPUS may be used as a tool to induce and enhance regenerative therapy by enabling stem cell expansion, differentiation, and matrix production (Cui *et al.*, 2006; Ebisawa *et al.*, 2004; Lee *et al.*, 2006; Ling *et al.*, 2017b). However, Yang *et al.* (2014) reported that LIPUS did not promote repair of severe articular cartilage injury. Moreover, Xu *et al.* (2018) showed that LIPUS suppressed cellular proliferation and induced cell death in rat preadipocytes. Thus, there remain controversies as to whether LIPUS can induce tissue regeneration.

1.5.3. LIPUS and neuronal/nerve regeneration

Few studies have investigated the effect of LIPUS on neuronal regeneration by using *in vitro* neuronal cells, and experimental animal model studies for peripheral nerve injuries (Table 1.2: studies and LIPUS parameters). The *in vitro* studies reported that LIPUS induced proliferation and differentiation of neural stem cells, and iPSCs-NCSCs into neurons (Wu *et al.*, 2020b; Lv *et al.*, 2013), cell viability and proliferation of Schwann cells (Ren *et al.*, 2018). Moreover,

LIPUS induced the myelination ability of Schwann cells in co-culture of Schwann cell and adipose-derived stem cell culture model (Yue *et al.*, 2016). The *in vivo* animal models of peripheral nerve injuries demonstrated that LIPUS enhanced neuronal regeneration in the injured sciatic nerve (Crisci and Ferreira, 2002; Raso *et al.*, 2005). In addition, Sato *et al.* (2016) indicated that daily exposure of LIPUS on the transected inferior alveolar nerve promoted neuronal regeneration with functional recovery. Another study noted that LIPUS induced not only nerve regeneration and recovery of inferior alveolar nerve transection but also enhanced bone remodelling on the same jaw side (Yang *et al.*, 2017a). In addition, there are studies using LIPUS in combination with other therapeutic methods which demonstrated the improvement of clinical outcomes. For example, using LIPUS with nerve autograft improved nerve regeneration and functional recovery of the injured sciatic nerve compared with nerve autograft alone (Jiang *et al.*, 2016). Ning *et al.* (2019) and Lv *et al.* (2015) applied LIPUS with stem cell transplantation and demonstrated nerve regeneration with functional recovery in the contused spinal cord and transected sciatic nerve, respectively. Moreover, Kim *et al.* (2013) showed that combination of LIPUS, and nerve growth factor (NGF) with nerve guide conduit accelerated nerve regeneration and functional recovery compared with one therapeutic application of either LIPUS or NGF alone. Recently, another combination of LIPUS, iPSCs-NCSCs, and growth differentiation factor 5 (GDF5) was suggested to induce nerve regeneration with functional recovery of the injured sciatic nerve (Xia *et al.*, 2019). Thus, LIPUS has been proposed as a potential adjunct therapeutic tool for nerve regeneration of peripheral nerve injuries. However, Daeschler *et al.* (2018) reported that LIPUS did not induce axonal regeneration in median nerve transection with the intensity of 30 mW/cm^2. These initial studies suggest that LIPUS is a promising tool to induce neuroregeneration; however, more research to support these findings is needed.

Table 1.2 LIPUS studies for neuronal regeneration (therapeutic parameters, cell/tissue, and outcomes)

Study	Intensity-mW/cm^2 (type)	Frequency	Pulse repetition frequency	Duty cycle	Stimulation Time (days/weeks)	Cell/tissue source	Therapeutic outcomes
Wu *et al.* (2020b)	69.3 (-)	1 MHz	-	-	5 min (3 days)	Rat neural stem cells	-Proliferation -Differentiation
Xia *et al.* (2019)	500 mW/cm^2 300 mW/cm^2 (-)	1 MHz	100 Hz	20%	5-10 min (4 days)	Human iPSCs-NCSCs and transplanted in rat nerve	-Proliferation -Differentiation -Nerve regeneration with functional recovery
Ning *et al.* (2019)	50 mW/cm^2 (-)	1 MHz	-	-	3 min (3 days)	Rat bone marrow stem cells and transplanted in rat nerve	-Viability -Neurotrophic expression -Functional recovery
Daeschler *et al.* (2018)	30 mW/cm^2 (I_{SATA})	1.5 MHz	1000 Hz	20%	2 min (3 days/3 times a week)	Rat peripheral nerve injury (post-surgical reconstruction)	No difference in terms of axonal regeneration
Ren *et al.* (2018)	27.37 mW/cm^2 (-)	1 MHz	-	-	10 min (5 days)	Rat Schwann cells	-Viability -Proliferation
Sato *et al.* (2016)	30 mW/cm^2 (-)	1 MHz	-	-	20 min (28)	Rat inferior alveolar nerve (IAN) injury	-Nerve repair and regeneration
Jiang *et al.* (2016)	250 mW/cm^2 (I_{SATA})	1 MHz	1000 Hz	20%	5 min/another day for 2-12 weeks	Plus autograft transplantation in rat nerve injury	Improved autograft regeneration
Zhao *et al.* (2016)	30 mW/cm^2 50 mW/cm^2 (I_{SATA})	1 MHz	100 Hz	20%	10 min/day	Rat PC12 cells + NGF supplement	-Induced neurite outgrowth
Yue *et al.* (2016)	20 mW/cm² (-)	1 MHz	-	20%	10 min/day	Rat Schwann cells cocultured with rat adipose-derived stem cells	-Pro-myelination indicators' upregulation
Lv *et al.* (2015)	300 mW/cm^2 (-)	1 MHz;	100 Hz	20%	5 min/day for 2 weeks	Plus human iPSCs-NCSCs for rat transected sciatic nerve	Nerve repair and regeneration
Lv *et al.* (2013)	500 mW/cm^2 (-)	1 MHz	100 Hz	20%	10 min (2-4 days)	Human iPSCs-derived neural crest stem cells	-Cell viability -Proliferation -Neural differentiation

Note: The sign (-) indicates not mentioned.

1.5.4. LIPUS and neuronal/nerve regeneration for regenerative endodontics

To date, LIPUS has not been therapeutically applied for neuronal/nerve regeneration for pulp-dentine complex regeneration nor with the regenerative endodontic procedure to induce pulp regeneration. However, research on the effect of ultrasound or LIPUS on dental-related cells/tissue is emerging such as DPSCs (Gao *et al.*, 2016b), odontoblast-like cells (Scheven *et al.*, 2009; Man *et al.*, 2012; Ghorayeb *et al.*, 2013), and reparative dentine formation (Al-Daghreer *et al.*, 2013; Wang *et al.*, 2017a; Al-Daghreer *et al.*, 2012; Wang *et al.*, 2017b; Zuo *et al.*, 2018). Gao *et al.* (2016b) reported that LIPUS stimulated proliferation of DPSCs. Some studies showed that ultrasound significantly increased odontoblast-like cell numbers (Scheven *et al.*, 2009; Man *et al.*, 2012; Ghorayeb *et al.*, 2013). In addition, other two *in vitro* studies investigated the effect of LIPUS on tooth slices demonstrating upregulation of dentine repair-related genes after short-term incubation (24h), increase of the odontoblast number and pre-dentine thickness after 5-day incubation (Al-Daghreer *et al.*, 2013; Al-Daghreer *et al.*, 2012). Similar two *in vivo* studies on animal models demonstrated reparative dentine formation after LIPUS application on experimental cavity-prepared teeth (Wang *et al.*, 2017a; Zuo *et al.*, 2018). Zuo *et al.* (2018) reported the LIPUS-dentine formation is associated with Ca^{+2} transport-related protein expression. Whereas a further two studies reported the involvement of transforming growth factor beta 1 (TGF-β1), and its receptor regulators (Smad 2 and Smad 3) in LIPUS-induced dentine formation (Wang *et al.*, 2017a; Wang *et al.*, 2017b). These studies suggested that the reparative dentine formation induced by LIPUS is produced via the physiological inflammatory-reparative process (TGF-β1/Smad signal pathway). Furthermore, Gao *et al.* (2016b) and (2017) reported that ERK/MAPK signalling pathway is activated in LIPUS induced DPSC proliferation via mechanosensitive ion channels (Piezo1 and Piezo2) in the cell membrane. These studies suggested that LIPUS triggered different pathways depending

on the cell type. Overall, it appears that LIPUS might play a therapeutic role in enhancing neuronal/nerve regeneration which is critical for regenerative endodontics, dental nerve injuries and in a broader context for peripheral nerve injuries. To examine therapeutic device applications, and due to the inaccessibility to human neurons, human neuronal cell models are useful for *in vitro* testing before pre-clinical and clinical trials.

1.6. Neuronal cell models for *in vitro* experimentation

In vitro cell neuronal modelling is a widely recognised approach in neuroscience to study different research aspects related to neurons, such as neurogenesis (Azari and Reynolds, 2016), neuronal development, and injury (Jones *et al.*, 2018), screen drugs for nerve regeneration (Rayner *et al.*, 2018), brain simulation (D'Angelo *et al.*, 2013), studying neuroinflammation (Goshi *et al.*, 2020), and the modelling of central nervous system viral infection (D'Aiuto *et al.*, 2018). Different cell types have been used as *in vitro* neuronal cell models in the literature and the most frequently used cell types are reviewed below.

1.6.1. Cell line-derived neuronal cell models

One of the most common cell lines used in neuroscience studies is the SH-SY5Y human neuroblastoma cell line, which was derived via subcloning from metastatic bone tumour biopsy (Biedler, Helson and Spengler, 1973; Biedler *et al.*, 1978). SH-SY5Y cells have a mixed culture of neuroblast-like (N-type) and epithelial-like cells (S-type), expressing immature neuronal markers in the undifferentiated state (Påhlman *et al.*, 1984; Kovalevich and Langford, 2013). This neuronal cell line was subcloned three times; SH-SY, then SH-SY5, and to the ultimate form SH-SY5Y (Kovalevich and Langford, 2013) to yield a N-type neuroblastoma cell line which has a higher ability to differentiate into neuronal-like cells (Biedler, Spengler and Lyser, 1975). After neuronal differentiation, these cells became similar to primary neurons, for

instance, demonstrating mature neuronal markers, acquiring neuronal morphology and exiting the cell cycle and entering the nonproliferating phase (Påhlman *et al.*, 1984; Encinas *et al.*, 2000). The differentiated SH-SY5Y cell line has been used as a neuronal cell model for many neuronal-related responses, such as neurotoxicity, neurodegenerative diseases, and neuroprotective effects (Cheung *et al.*, 2009b; Nicolini *et al.*, 1998; de Medeiros *et al.*, 2019; Agholme *et al.*, 2010; Presgraves *et al.*, 2004; Xicoy, Wieringa and Martens, 2017).

Another less common human neuronal cell line used in neuroscience is the human teratocarcinoma line Ntera2 (NT2) which is derived from malignant carcinoma (Andrews, 1988; Podrygajlo *et al.*, 2009). The NT2-derived neurons (the differentiated form) have been used for *in vitro* modelling such as in neuron-astrocyte network signalling, neurodegenerative diseases, and neurotoxicity (Hill *et al.*, 2012; Esteves *et al.*, 2008; Taylor *et al.*, 2019; Stern *et al.*, 2014). Another commonly used cell line is the PC12 which is derived from a rat adrenal pheochromocytoma (Greene and Tischler, 1976) which has been used as *in vitro* modelling for neurotoxicity, neurotrophic activities, neurodegenerative diseases, and neural ischemia tolerance (Shafer and Atchison, 1991; Vaudry *et al.*, 2002; Rostamian Delavar *et al.*, 2018; Hillion *et al.*, 2005). Although these cancerous cell lines are rapidly grown in the laboratory to give many subsequent cell-culture passages with minimum variations between the cultures, their physiological properties are different from *in vivo* primary neurons (Gordon, Amini and White, 2013). Hence, the neuronal cell models derived from primary stem cell cultures are recommended as they are more able to simulate the physiological properties of neurons *in vivo* (Gordon, Amini and White, 2013; Randall, 2016; Sterneckert, Reinhardt and Schöler, 2014).

1.6.2. Stem cell-derived neuronal cell models

The *in vitro* modelling using neuronally differentiated stem cells is also widely recognised in the literature to assess neuronal-related responses (Wilson and Newell-Litwa, 2018;

Sterneckert, Reinhardt and Schöler, 2014; Scarnati, Halikere and Pang, 2019; Jones *et al.*, 2018). Regardless of the various types of stem cells, the most commonly used stem cells for *in vitro* modelling are induced pluripotent stem cells (iPSCs), followed by embryonic and neural stem cells. iPSCs were firstly reprogrammed from mouse embryonic and adult fibroblasts under embryonic stem cell culture conditions (Takahashi and Yamanaka, 2006). The neuronally differentiated iPSCs have been used as *in vitro* models to study many neuronal-related properties, for example, neurodegenerative diseases, neurodevelopment, pharmacological-related research, and synaptic development and degeneration (Israel *et al.*, 2012; Abud *et al.*, 2017; Hossini *et al.*, 2015; Wan *et al.*, 2015; Suga, Kondo and Inoue, 2019; Tamburini and Li, 2017; Chailangkarn, Acab and Muotri, 2012; Farkhondeh *et al.*, 2019; Akamatsu, 2017; Wilson and Newell-Litwa, 2018). There are some other studies that used neuronal cell models derived from embryonic stem cells to investigate neurodegenerative diseases, pharmacological-related research, synaptic integration, and neurodevelopment and injury (Amano *et al.*, 2009; Deshmukh, Kovács and Dinnyés, 2012; Koch *et al.*, 2009; Jones *et al.*, 2018). Lastly, the neuronal cell models derived from human neural stem cells have also been used to investigate Alzheimer's disease, and neuroinflammation (Choi *et al.*, 2014; Wang *et al.*, 2013) or neural stem cells without neuronal differentiation used as neuronal injury model (Vagaska, Gillham and Ferretti, 2020). The stem cell-derived neuronal cell models have also gained interest as neuronal cell replacements for nerve regeneration and are described below.

1.7. Stem cell-derived neuronal cell models for nerve regeneration

The use of stem cell-derived neuronal cell models has been proposed to identify better clinical outcomes for neuro-regenerative stem cell therapies instead of using undifferentiated stem cells in experimental animal research. For example, the transplantation of neuronal cell models differentiated from mesenchymal stem cells/stromal (MSCs) promoted nerve regeneration and

functional recovery in brain injury (Kim *et al.*, 2008; Dezawa *et al.*, 2004; Lu *et al.*, 2006; Yang *et al.*, 2013) and peripheral nerve injury (Dadon-Nachum *et al.*, 2011; Mimura *et al.*, 2004; Ishikawa *et al.*, 2009; Ladak *et al.*, 2011). Likewise, neuronal cell models derived from DPSCs also showed positive therapeutic outcomes through improvement of nerve regeneration and functional motor recovery in peripheral nerve injury (Zhang *et al.*, 2016a; Jang *et al.*, 2018), and neurological function in the brain injury (Király *et al.*, 2011). It has been reported that the transplantation of DPSC-derived neuronal cells is not only improved nerve regeneration of peripheral nerve injury but also enhanced angiogenesis (Sanen *et al.*, 2017). Another interesting concept suggested by Luo *et al.* (2018; 2021) is the transplantation of DPSCs and growth factors to enhance nerve regeneration and functional recovery. Thus, using neuronal cell models derived from DPSCs are considered efficient in inducing functional recovery and restore the lost neuronal cells in neuro-regenerative transplantation therapies (Shi, Mao and Liu, 2020; Jang *et al.*, 2018). Furthermore, the differentiated mesenchymal cells secreted greater amounts of neurotrophic factors which might boost the nerve regeneration (Dadon-Nachum *et al.*, 2011; Reid *et al.*, 2011). In this context, *in vitro* neuronal differentiation of hDPSCs might be useful for neuro-regenerative transplantation therapies, and *in vitro* modelling for neuronal-related experimentations.

1.7.1. DPSC neuronal differentiation

Several *in vitro* neuronal differentiation protocols have been proposed for use to differentiate human DPSCs into neuronal cells (see Table 1.3). These protocols are highly varied in their differentiating media, supplements, number of steps, and culturing duration. As seen in Table 1.3, the main differentiating supplements were growth factors in all studies except Jang *et al.* (2018) which used tricyclodecane-9-yl-xanthogenate (D609) to differentiate hDPSCs. However, D609 has been reported to cause T-lymphocytes death (Milhas *et al.*, 2012) which

might make the resultant neuronal cell model inappropriate for future clinical regenerative cell replacement therapies. The growth factors were either supplemented to special neuronal induction media such as neurobasal or neural proliferation medium or ordinary basal cell culture media such as DMEM/F12, and α-MEM as indicated in Table 1.3. Regardless of the media type used, the resultant differentiated hDPSCs in these studies expressed neural markers which indicate the neuronal differentiation is dependent on the growth factors rather than media type. Although all DPSC neuronal differentiation studies demonstrated expression of neuronal markers in the hDPSCs after neuronal differentiation, only a few of these studies examined the neuronal functionality, including electrophysiological profile (Li *et al.*, 2019; Ullah *et al.*, 2016; Gervois *et al.*, 2015; Arthur *et al.*, 2008; Király *et al.*, 2009) or intracellular Ca^{2+} analysis (Gonmanee *et al.*, 2020; Gonmanee *et al.*, 2018; Kanafi *et al.*, 2014; Osathanon *et al.*, 2014). The number of steps and culturing duration also showed much variation between DPSC differentiation studies. As shown in Table 1.3., the vast majority of studies utilised multiple differentiating steps whereas other studies performed one-step differentiation protocol (Luke *et al.*, 2020; Madanagopal, Franco-Obregón and Rosa, 2020; Zheng *et al.*, 2020; Wu *et al.*, 2020a; Jang *et al.*, 2018; Haratizadeh *et al.*, 2017; Zhang *et al.*, 2017; Zhang *et al.*, 2016a; Ullah *et al.*, 2016; Bonnamain *et al.*, 2013), ranging from 2-3 days (Geng *et al.*, 2017; Jang *et al.*, 2018) to 8 weeks (Goorha and Reiter, 2017).

Table 1.3 Neuronal differentiation studies of adult hDPSCs

Study	**Successful differentiation supplementation protocol** (all media containing 1% antibiotic supplement-Pen-Strep)	**Duration**	**Outcomes** (neuronal markers + characteristics)
Solis-Castro, Boissonade and Rivolta (2020)	Stage I: DMEM/F12 media supplemented with 2% B27, 1% N2, 50 ng/m IGF, 20 ng/ml bFGF, 20 ng/ml EGF and 10 ng/ml BMP4 for 4 weeks Stage II (neurosphere formation): adapted from Gervois et al., with modifications (DMEM:F12 with 2% B27, 1% N2, 20 ng/ml bFGF, and 20 ng/ml EGF and 10 ng/ml BMP4 in ultra-low attachment culture plates for 6-8 days). Stage III: The neurospheres are cultured in DMEM/F12 media with 2% B27, 1% N2, 1 mM dbcAMP, and 30 ng/ml NT3 in the Polyornithine (0.01%)/Laminin (2.5 μg/cm^2) coated-well plates for 2 weeks.	7 weeks	Neuronal-like cells expressing Peripherin, TUJ1, NFH, SYN1, TAU, and GAP43
Luke *et al*. (2020)	Serum-free human neural proliferation medium (StemCell Technologies, Canada) supplemented with 10 ng/ml bFGF and 20 ng/ml EGF.	21 days	Glial-like cells expressing TUBB3, GFAP, and oligodendrocyte marker.
Madanagopal, Franco-Obregón and Rosa (2020)	Neurobasal-A medium containing 1xB-27, 40 ng/ml bFGF, and 20 ng/ml EGF supplements.	21 days	Neuronal-like cells expressing NES, ENO-2, TUBB3, NF-M and NF-H
Zheng *et al.* (2020)	DPSCs were co-cultured with Chitosan scaffolds in serum-free low glucose DMEM/F12 medium supplemented with 2% B27, 2% N2, 25 ng/ml bFGF, and 25 ng/ml BDNF.	7 days	Neuronal-like cells expressing TUBB3, GFAP, and S100β.
Wu *et al.* (2020a)	Neurobasal A medium supplemented with 40 ng/ml bFGF, 20 ng/ml EGF, and 1× B27.	14 days	Neuronal-like cells expressing TUBB3, enolase, DCX, NCAD, NCAM and NEUROD1 and their transplantation improved neurological function in rat model of cerebral ischemia.

Table 1.3 Neuronal differentiation studies of adult hDPSCs (continued)

Study	**Successful differentiation supplementation protocol** (all media containing 1% antibiotic supplement-Pen-Strep)	**Duration**	**Outcomes** (neuronal markers +characteristics)
Kogo *et al.* (2020)	Stage I: 2.5% FBS-supplemented DMEM/F12, 10 ng/ml bFGF-2, and 10 μM azacytidine for 48h. Stage II: applied High K^+ BSS-Ca^{2+} buffer to the cells for 20 min. Stage III: DMEM/F12 with 250 μM3-isobutyl-1-Methylxanthine, 1% insulin-transferrin-selenium (ITS), 1 mM dibutyryl cyclic adenosine monophosphate, 200 nM tissue plasminogen activator, 50 μM forskolin, 10 ng/ml NGF, 10 ng/ml bFGF-22, and 30 ng/ml NT-3 for 72h.	5 days	Neuronal-like cells expressing PSD95, TUBB3, and NES.
Laudani *et al.* (2020)	Stage I: Cell culture in the basic medium for 6 days. Stage II: DMEM supplemented with 0.5 mM Isobutyl Methyl Xanthine (IBMX), 1 mM dbcAMP, 40 ng/ml bFGF, 20 ng/ml EGF, 10 ng/ml NGF, and 10 ng/ml BDNF for 10 days. Stage III: DMEM supplemented with 10% FBS and 10 mM retinoic acid for 15 days. Stage IV: the differentiated cells seeded in bone marrow stem cell-derived decellularized extracellular matrix for 7 days	38 days	Neuronal-like cells expressing PAX6, NF-L, NF-M, NF-H, and MAP2.
Gonmanee *et al.* (2020)	Stage I: Adapted neurosphere induction stage from Gonmanee *et al.* (2018) method (DMEM/F12 with 20 ng/ml bFGF, 20 ng/ml EGF, 2% B-27 in low attachment wells) for 5 days. Stage II: cell transplantation in rat auditory brainstem slices for 2-4 weeks.	3-5 weeks	Functional neuronal-like cells expressing Tuj1, SV2A, and Gata3 with intracellular calcium oscillations.

Table 1.3 Neuronal differentiation studies of adult hDPSCs (continued)

Study	**Successful differentiation supplementation protocol** (all media containing 1% antibiotic supplement-Pen-Strep)	**Duration**	**Outcomes** (neuronal markers + characteristics)
Rafiee *et al.* (2020)	Stage I (neurosphere induction): KO DMEM/F12 with 20 ng/ml bFGF, 20 ng/ml EGF, and 10 µg/ml heparin in low attachment wells for 3 day. Stage II: incubation in serum-free media for 3 days. Stage III: 10% FBS-supplemented DMEM/HG for 10 days.	16 days	Neuronal-like cells expressing NES, MAP2, and NGN1.
Goudarzi *et al.* (2020)	Stage I (neurospheres induction): the hDPSCs were cultured in serum-free DMEM/F12 containing 5% rat embryonic cerebrospinal fluid for 2 days. Stage II: the neurospheres were cultured in DMEM/F12 containing 10^{-6} µm retinoic acid, 2% B27, 5% FBS, 100 ng/ml GDNF and 200 ng/ml BDNF for 6 days.	8 days	Neuronal-like cells expressing NES and MAP2 with presence of Nissl bodies in cytoplasm.
Li *et al.* (2019)	Stage 1 (Neurosphere formation): Serum-free DMEM/F12 with 2% B27 supplement, 20 ng/ml bFGF, and 20 ng/ml EGF for 6–8 days. Stage 2: Poly-D-lysine coating, serum-free neurobasal medium with 2 mM L-glutamine, 1% N2, 2% B27, 30 ng/ml NT-3, and 1 mM N^6,2'-O-dibutyryladenosine 3', 5'-cyclic monophosphate (dbcAMP) for 4 weeks	5–6 weeks	Functional neuronal like cells expressing TUBB3, synapsin, GFAP, CNPase, MAP2, NFM, GAD67, Nav1.6, NF1, NSE, and PSD95 with neuro-electrophysiological profile.
Gonmanee *et al.* (2018)	Stage 1 (neurosphere induction): DMEM/F12 with 20 ng/ml bFGF, 20 ng/ml EGF, 2% B-27 in low attachment wells. Stage 2: poly-L-ornithine and laminin coating, DMEM/F12 with 20 ng/ml NT-3, 20 ng/ml BDNF, 20 ng/ml GDNF, 2% N-2, and 2% B-27 supplement.	19-23 days	Function spiral ganglion neuronal-like cells expressing Tuj1/TUBB3, GFAP and spiral ganglion neuronal markers (GATA3, and NTRK2) with intracellular calcium activity.

Table 1.3 Neuronal differentiation studies of adult hDPSCs (continued)

Study	**Successful differentiation supplementation protocol** (all media containing 1% antibiotic supplement-Pen-Strep)	**Duration**	**Outcomes** (neuronal markers + characteristics)
Jang *et al.* (2018)	Geltrex LDEV coating 10% FBS advanced Dulbecco's modified Eagle's medium (ADMEM) containing 4 μg/ml tricyclodecane-9-yl-xanthogenate (D609).	3 days	Neuroanl-like cells expressing cholinergic neurotransmitter (ChAT), and motor neuronal markers; homeobox (HB9).
Bonaventura *et al.* (2018)	Stage 1: DMEM with 40 ng/ml bFGF, 20 ng/ml hEGF, 1 mM dbcAMP, 0.5 mM IBMX, 10 ng/ml BDNF, and 10 ng/ml NGF for 6 days. Stage 2: maintaining media10% FBS DMEM with 10 mM retinoic acid for 20 days.	26 days	Neuronal-like cells expressing NF-M, NF-H, NSE and MAP2.
Geng *et al.* (2017)	Stage 1: DMEM media with 15 mM resveratrol for 12h. Stage 2: DMEM/F12 with 500 mM β-mercaptoethanol, 10 ng/ml bFGF, and 10% FBS for 24h. Stage 3: Serum-free DMEM/F12 with 2% dimethyl sulfoxide, 100 Mm butylated hydroxyanisole for 6h.	2 days	Neuronal-like cells express NF-M, NES, and Musashi.
Haratizadeh *et al.* (2017)	DMEM/F12 with 10^{-7} μm Retinoic acid and 10% Sprague-Dawley rat cerebrospinal fluid.	8 days	Neuronal glial-like cells express MAP2, and GFAP markers.
Moayeri *et al.* (2017)	Stage 1: 5% FBS DMEM-F12 with 1M retinoic acid for 4 days. Stage 2: DMEM/F12 medium with 10 ng/ml bFGF, and 5 ng/ml PDGF for 8 days.	12 days	Oligoprogenitor cells expressing NES, glial markers (NG2, Olig2, and protein O4), and oligoprogentor markers (PDGFR-α and Olig2 genes)

Table 1.3 Neuronal differentiation studies of adult hDPSCs (continued)

Study	**Successful differentiation supplementation protocol** (all media containing 1% antibiotic supplement-Pen-Strep)	**Duration**	**Outcomes** (neuronal markers + characteristics)
Goorha and Reiter (2017)	Stage 1 (Epigenetic reprogramming): 2.5% FBS DMEM:F12 with 10 µM 5-Azacytidine, and 10 ng/ml bFGF in Poly-D-Lysine coating wells. Stage 2 (neural differentiation): 250 µm IBMX, 50 µM Forskolin, 200 nM TPA (Phorbol 12-myristate 13-acetate), 1 mM dbcAMP, 10 ng/ml NGF, 10 ng/ml bFGF, 30 ng/ml NT-3, 1% insulin-transferrin-sodium selenite premix (ITS). Stage 3 (neuronal maturation): Neurobasal-A Medium, 1mM dbcAMP, 1% N2 supplement, 1% B27, 30 ng/ml NT-3, and 1× Glutamax.	6-8 weeks	Mixed neuronal-like cell (astrocyte and pyramidal neuronal-like cell) expressing TUJ1, NeuN, GFAP, synaptic and ion channel markers.
Zhang *et al.* (2017)	Serum-free low glucose DMEM/F12 medium supplemented with 2% N2, 2% B27, 25 ng/ml BDNF, 25 ng/ml bFGF, and 100 ng/ml NGF.	7 days	Neuronal-like cells expressing NES, MAP-2, βIII-tubulin, and GFAP
Gnanasegaran *et al.* (2016)	Stage 1: Neurobasal media with B27 supplement, 20 ng/ml bFGF and 20 ng/ml EGF for 9 days. Stage 2: Neurobasal media with 200 ng/ml SHH, 100 ng/ml fibroblast growth factor 8 (FGF8), 10 ng/ml BDNF and 10 µmol/L forskolin for 7 days.	16 days	Dopaminergic neuronal-like cells expressing dopamine acetyl transferase (DAT), TH, NES, TUBB3, PAX6, GFAP, MSI, NCAM, and NURR1.
Jung *et al.* (2016)	Stage 1: DMEM/F12 medium supplemented with 1% B27, 1% N2, 100 ng/ml SHH, 100 nM retinoic acid, 10 ng/ml GDNF, 10 ng/ml BDNF, and 10 ng/ml insulin-like growth factor-1 on type I and IV collagen, laminin and fibronectin (10μg/ml) coated-well plate for 2 weeks. Stage 2: adding 1mM dbcAMP and 10 μM forskolin for 1 week.	3 weeks	Neuronal-like cells expressing the following markers (TUBB3, Olig2, Pax6, Mash1, DCX, Map2, nestin, NeuroD1, NCAD, NCAM, Sox1, and Sox2).

Table 1.3 Neuronal differentiation studies of adult hDPSCs (continued)

Study	**Successful differentiation supplementation protocol** (all media containing 1% antibiotic supplement-Pen-Strep)	**Duration**	**Outcomes** (neuronal markers + characteristics)
Chun *et al.* (2016)	Stage 1: gelatin-coating with recombinant mouse leukemia inhibitory factor (LIF)-containing knockout-ES (KO-ES/LIF) medium, which is composed of DMEM, MEM non-essential AA, FBS and β-mercaptoethanol for 3-4 days. Stage 2: KO-ES medium without LIF for 4 days Stage 3: DMEM/F-12 with human ITS or fibronectin medium with L-glutamine, glucose, NaHCO3, and bovine fibronectin for 6-8 days. Stage 4: poly-L-ornithine or fibronectin-coating with N-2-supplemented medium with bFGF, FGF-8b, Shh-N, and ascorbic acid for 4-6 days. Stage 5: N-2 or ascorbic acid medium for 10-15 days	27-37 days	Dopaminergic neuronal-like cells expressing TH, NES, TUBB3, GFAP, MBP, and *PAX6.*
Ullah *et al.* (2016)	Adapted Media A of Arthur *et al.* (2008) with minor changes; Geltrex LDEV coating, and using neural basal A media with B27 supplement, 30 ng/ml bFGF, and 20 ng/ml EGF.	3 weeks	Functional neuronal like expressing TUBB3, MAP2, NF-M, NF-H, NGF, TAU, synapsin and synaptophysin with neuro-electrophysiological profile.
Zhang *et al.* (2016a)	2% N2, 2% B27, 40 ng/ml NGF, 25 ng/ml BDNF, and 25 ng/ml bFGF in the chitosan scaffolds	14 days	Neuronal-like cells expressing nestin, GFAP, MAP-2, and CNPase improved functional recovery upon implantation in spinal cord injury
Gervois *et al.* (2015)	Stage I (neurosphere induction): DMEM/F12 containing 2% B27, 20 ng/ml bFGF, and 20 ng/ml EGF in low attachment dishes for 6–8 days. Stage II: Neurobasal medium supplemented with 2% B27, 1% N2, 2 mM L-glutamine, 1 mM dbcAMP, 30 ng/ml NT-3 on poly-L-ornithine and Laminin coated-well plate/dishes for 4 weeks.	5 weeks	Functional neuronal-like cells expressing NeuN, MAP2, GAP43, neural CAMs, synapsin I, and synaptophysin. In addition, secretion of NGF, VEGF, and BDNF with neuro-electrophysiological profile.

Table 1.3 Neuronal differentiation studies of adult hDPSCs (continued)

Study	**Successful differentiation supplementation protocol** (all media containing 1% antibiotic supplement-Pen-Strep)	**Duration**	**Outcomes** (neuronal markers + characteristics)
Chang *et al.* (2014)	Basic neural induction media: DMEM/F12 serum-free media containing N2, heparin, nonessential amino acids -Motor neural induction: Stage 1: basic neural induction with 0.1 µm ATRA. Stage 2: basic neural induction with 100 ng/ml sonic hedgehog (SHH) and 0.1 µm ATRA. Stage 3: basic neural induction with 0.1 µm retinoic acid, 100 ng/ml SHH, 1 µm Cyclic adenosine monophosphate (cAMP), and 200 ng/ml ascorbic acid. Stage 4: basic neural induction with 10 ng/ml BDNF, 10 ng/ml GDNF, 10 ng/ml IGF-1, 1 µm cAMP, and 200 ng/ml ascorbic acid. -Dopaminergic neural induction: Stage 1: N2 media and DMEM/F12 with N2-A, and 300 ng/ml noggin supplements. Stage 2: BASF media containing N2 medium, 50 mg/ml BDNF, 50 mg/ml SHH 200 mM ascorbic acid, and 50 mg/ml FGF-8b. Stage 3: BASF medium without bFGF. Stage 4: BCT-GA medium containing N2 medium, BDNF 50 mg/ml, ascorbic acid 200 mM, GDNF 10 ng/ml, TGF-bIII 2 mg/ml, and cAMP 200 mM.	15 days	Dopaminergic and cholinergic neuronal like cells expressing TUBB3 and NES, and GFAP. Moreover, TH in dopaminergic neuronal-like cells, and CHAT in cholinergic neuronal-like cells.

Table 1.3 Neuronal differentiation studies of adult hDPSCs (continued)

Study	**Successful differentiation supplementation protocol** (all media containing 1% antibiotic supplement-Pen-Strep)	**Duration**	**Outcomes** (neuronal markers + characteristics)
Osathanon *et al.* (2014)	Stage I: Neurobasal medium containing 2 mM L-glutamine, 2% B27, 5 µg/ml amphotericin B, 20 ng/ml bFGF, and 20 ng/ml EGF in low attachment dishes for 7 days. Stage II: Neurobasal medium supplemented with 10^{-7} nM retinoic acid, 2 mM L-glutamine, 2% B27, 5 µg/ml amphotericin B, 20 ng/ml bFGF, and 20 ng/ml EGF for 7 days on Collagen IV coated dishes.	14 days	Functional neuronal-like cells expressing SOX2, SOX9, TUBB3, and GABA neurotransmitter receptors with intracellular Ca^{+2} activity.
Kanafi *et al.* (2014)	Stage 1: Neurobasal medium containing 0.5% B27, 100 ng/ml FGF8, 50 ng/ml bFGF, and 200 ng/ml SHH for 3 days. Stage 2: Neurobasal media containing 0.5% B27 and BDNF for 6 days.	9 days	Functional dopaminergic neuronal-like cells expressing dopaminergic neuronal makers (TH, Nurr1, En1, and Pitx3) with intracellular Ca^{+2} activity
Martens *et al.* (2014)	Stage 1: Free FBS α-MEM medium containing 2 mM l-glutamine and 1 mM β-mercaptoethanol for 24h. Stage 2: 10% FBS α-MEM medium with 35 ng/ml ATRA for 72h. Stage 3: 10% FBS α-MEM medium with 5 µM forskolin, 5 ng/ml platelet-derived growth factor AA (PDGFaa), 10 ng/ml b-FGF, and 200 ng/ml heregulin-β-1 for 2 weeks.	18 days	Schwann-like cells expressing NES, GFAP, and neurotrophic factors (b-NGF, BDNF, GDNF, and NT-3).
Bonnamain *et al.* (2013)	Basal medium (serum-free) supplemented with 2 ml N2, 10 ng/ml EGF, 25 ng/ml bFGF, and 0.2% heparin solution.	4 weeks	Neural-like cells expressing NES, TUBB3, NF-M, and Oligodendrocyte marker (PLP1).

Table 1.3 Neuronal differentiation studies of adult hDPSCs (continued)

Study	**Successful differentiation supplementation protocol** (all media containing 1% antibiotic supplement-Pen-Strep)	**Duration**	**Outcomes** (neuronal markers + characteristics)
Király *et al.* (2009)	Stage I: DMEM/F12 supplemented with 10 µM 5-azacytidine, 10 ng/ml bFGF, 2.5% FCS on poly-L-lysine coated-well plate for 48h. Stage II: DMEM/F12 containing 50 µM forskolin, 250 µM IBMX, 200 nM TPA, 1 mM dbcAMP, 10 ng/ml NGF, 10 ng/ml bFGF, 30 ng/ml NT-3, and 1% ITS for 3 days. Stage III: Neurobasal A media containing 1% N2, 1% B27, 1 mM dbcAMP, and 30 ng/ml NT-3 for 3–7 days.	8-12 days	Neuronal-like cells expressing N-tubulin, NSE, NF-M, NGN2, NeuN and GFAP with functional activity of voltage-activated sodium and potassium channels.
Arthur *et al.* (2008)	Media A: Neurobasal with B27 supplement, 20 ng/ml EGF, and 40 ng/ml bFGF for 3 weeks on Laminin-coated wells. Media B: Stage 1: using Media A for 7 days. Stage 2: DMEM/F12 media and ITTS + 40 ng/ml FGF for 7 days. Stage 3: DMEM/F12 media, ITTS, 40 ng/ml FGF, and 0.5 µM retinoic acid for 7 days.	3 weeks.	Functional neuronal like cells expressing TUBB3 and NES, PSA-NCAM, NF-M and NF-H with neuro-electrophysiological profile

Notably, serum supplementation also demonstrated much variation in the DPSC differentiation protocols as is presented in Table 1.3, for example, several studies used a standard serum level of 10% at least in one of the differentiation steps (Laudani *et al.*, 2020; Rafiee *et al.*, 2020; Jang *et al.*, 2018; Bonaventura *et al.*, 2018; Geng *et al.*, 2017; Chun *et al.*, 2016; Martens *et al.*, 2014), and other studies used reduced serum levels (2.5 to 5%) to differentiate hDPSCs (Kogo *et al.*, 2020; Goudarzi *et al.*, 2020; Moayeri *et al.*, 2017; Goorha and Reiter, 2017; Király *et al.*, 2009). Relatively few studies have used completely serum-free media without using serum alternative supplements (Luke *et al.*, 2020; Chang *et al.*, 2014; Bonnamain *et al.*, 2013). However, the majority of the presented DPSC differentiation studies used serum-free media but supplemented with serum alternative supplement (B27) (Chen *et al.*, 2008; Brewer *et al.*, 1993; Brewer, 1995). In this context, it is understood that reduction or removal of serum levels increased the neuronal differentiation in neuronal cell lines and DPSCs (Kumar and Katyal, 2018; Darmon, Bottenstein and Sato, 1981; Chang *et al.*, 2014). In contrast, Croft and Przyborski (2006) reported that serum removal from culture is an environmental culture stressor which resulted in pseudo-neuronal morphology and expressions. The concept of serum removal from cell culture media has other reasons such as risk of pathogen transmission, and serum variability which would affect the properties of cells and reproducibility of results (Karnieli *et al.*, 2017; McGillicuddy *et al.*, 2018). However, indeed, it would be of interest to investigate whether the reduction of the serum level in neurogenic media would increase neuronal differentiation. Overall, it is presently clear that it is debatable whether DPSCs can in fact be differentiated into bona fide neuronal cells and no consensus exists regarding the optimal method to differentiate the hDPSCs into neuronal cell models. It would be of interest to investigate whether the successful differentiation protocol of neuroblastoma cell line (SH-SY5Y) (Encinas *et al.*, 2000) could differentiate hDPSCs into

neuronal cell models which may offer a useful human neuronal model for *in vitro* testing and neuronal cell replacement therapies. Furthermore, LIPUS has the potential to induce neuronal cell proliferation which is critical to the success of nerve regeneration for regenerative endodontics and nerve injuries, including dental divisions of trigeminal nerve. Consequently, the current studies were designed to examine whether serum levels would potentiate the neuronal differentiation in neuroblastoma cell line (SH-SY5Y) and develop the neuronal cell models derived from hDPSCs and SH-SY5Y. Subsequently, these neuronal cell culture models were used to investigate potential effects of LIPUS, and study whether the reported neuro-reparative signalling (ERK signalling pathway) is involved in the neuronal cell differentiation and proliferation.

1.8. Hypotheses

It is hypothesised that human DPSCs may be differentiated into functional neuronal cells *in vitro.* This differentiation cell model may facilitate the study of LIPUS use for nerve regeneration. Therefore, it would be possible to promote neuronal progenitor proliferation, thereby positively affecting the therapeutic outcome in neuronal regeneration.

1.9. Aims and objectives

1.9.1. Aims

The overall aim of this PhD research was to investigate LIPUS as a therapeutic modality for nerve regeneration and therefore might provide a new avenue of potential treatment regimes in regenerative endodontics and nerve injury treatment.

1.9.2. Objectives

- Establish and characterise neuronal differentiation models using the SH-SY5Y human neuroblastoma cell line.
- Develop and characterise a hDPSC-derived neuronal cell culture model.
- Investigate the effect of LIPUS on the hDPSC and SH-SY5Y-derived neuronal-like cells.
- Evaluate the role of the ERK/MAPK signalling pathway in the hDPSC and SH-SY5Y-derived neuronal cell model differentiation and LIPUS effect.

CHAPTER 2: MATERIALS AND METHODS

2.1. Cell culture

2.1.1. SH-SY5Y Cell culture

The SH-SY5Y neuroblastoma cell line (ATCC® CRL-2266™, USA) was cultured in a T75 flask with 10 ml of complete growth media containing Dulbecco's modified Eagle's medium/Ham's nutrient mixture F12 (DMEM/F12) (Sigma Aldrich, UK) with 1% antibiotics (penicillin/streptomycin (100 IU.ml− 1) (Sigma-Aldrich, UK), and 10% foetal bovine serum (FBS) (Biosera, UK). Cells were incubated in a humidified incubator (Heracell 150i, Thermo Scientific, UK) at 37 °C with 5% CO_2. Medium change was every 3-4 days.

The cells were subcultured twice per week when the cells reached 80-90% confluence. These cultures displayed a mixture of detached (N-type) and adherent cells (S-type). The supernatant containing the detached cells was transferred to 50 ml falcon tube, and the adherent cells were detached using 0.25% trypsin-ethylenediaminetetraacetic acid (Trypsin-EDTA) (Sigma, UK), and reincubated for 1-2 min at 37 °C with 5% CO_2. Trypsinisation was stopped by adding a double volume of complete growth media with gentle agitation of the flask to remove the cells, and then transferring this to combine with the detached cells in the previously described 50 ml falcon tube. The collected cell suspension was then centrifuged at 220 x g for 3 min, and the resulting pellet was re-suspended in 1 ml complete growth media; the cells were then counted as mentioned in section 2.3 to have $1x10^4$ cells/cm^2 for subculturing seeding or $1x10^6$ cells/ml per vial for cryopreservation.

Cryopreservation was performed by resuspension of the cells with cryopreserved media (20% FBS, 10% dimethyl sulfoxide (DMSO) (Sigma, UK), and 70% DMEM/F12 media), and aliquoted into 1 ml of cell suspension/vial. Vials were then labelled and kept in Mr. Frosty freezing container (Thermo Scientific, UK) at -80 °C freezer overnight before final transfer to

the vapour phase of liquid nitrogen for long term storage. Passages 18 to 22 were used for the studies described in this thesis. All other materials were obtained from Sigma-Aldrich (Dorset, UK) and all plasticware from Thermo Scientific, UK unless otherwise stated.

2.1.2. DPSC culture

Human DPSCs were purchased from two different suppliers (see the details in Table 2.1). hDPSCs were initially cultured and subcultured using the suppliers' commercial media and other supplements until a sufficient stock of frozen cells with low passages (1-3) were generated. Cultures were incubated at 37 °C in a humidified atmosphere containing 5% CO_2 until 80-90% confluence. The cells were either subcultured or cryopreserved using the method described in section 2.1.1, but the trypsinisation time was 3 min. Cells were subcultured at 5-6 x 10^3 cells/cm^2 density and cryopreserved at 5 x 10^5 to 1 x 10^6/ml in 7.5% DMSO, and 92.5% complete media according to the suppliers' recommendations. Cryopreserved cells were revived using the standard alpha-modified minimum essential medium (α-MEM) (Biosera, UK) with 2 mM L-glutamine supplemented and 1% antibiotics (penicillin/streptomycin - 100 IU.ml− 1), and 10% FBS. Passage 2-4 were used for conducting the studies.

Table 2.1 Data for hDPSCs used in this project

Reported Information	**DPSCs (Lonza, Slough, UK)**	**DPSCs (Axol, Cambridge, UK)**
Product code	PT-5025	ax3901
Donor gender	Male	Female
Donor age	16 yrs.	14 yrs.
Tooth	Third molar	Third molar
Stem cell markers	≥ 90% positive for CD105, CD166, CD29, CD90 and CD73 markers. ≤ 10% positive for CD34, CD45, and CD133 markers.	> 90% positive for CD29, CD44, CD90, and CD105 markers. < 10% positive for CD34 and CD45 markers.
Multilineage differentiation ability	Osteogenic, adipogenic, and chondrogenic, and neurogenic differentiation.	Osteogenic, adipogenic, and chondrogenic differentiation.
Virus and Microbiological testing	Negative	Negative
The culturing and subculturing materials to prepare a good cryovial stock.	- DPSC BulletKit™ Medium (PT-3005, Lonza) supplied as 1 ml/5 cm^2 includes: DPSC basal Medium (PT-3927, Lonza) DPSC Growth Medium (PT-4516); contains 50 ml DPSC growth supplement, 10 ml L-glutamine, 5.0 ml Ascorbic Acid; 0.5 ml Gentamicin/Amphotericin-B to -Reagent Pack™ Subculture Reagents (CC-5034, UK); HEPES Buffered Saline Solution, 0.25% Trypsin/EDTA, and Trypsin Neutralizing Solution (TNS).	- Alpha-modified minimum essential medium (α-MEM) (Biosera, UK) with 2 mM L-glutamine, 1% antibiotics (penicillin/streptomycin (100 IU.ml−1), and 10% FBS. - Standard subculturing materials; (0.25% Trypsin/EDTA, and 10% FBS complete media).

2.2. Neuronal differentiation method

The cells were seeded with the standard 10% FBS media at an initial density of 5000/cm^2 (SH-SY5Y), and 625/cm^2 (DPSCs) which had been previously determined during preliminary experiment growth curves. Depending on the assay and the experiment and the cells were either cultured in 35-mm Petri dish, in 6-well plate with collagen-I coating, or in T25 flasks (Thermo Fisher Scientific, UK) and left overnight. For immunocytochemistry, the cells were cultured onto laminin/collagen-coated coverslips (Electron Microscopy Sciences, UK). The neuronal differentiation was induced by the following 2 supplementation protocols in DMEM/F12 media with 1% antibiotics (Sigma-Aldrich, UK): (1) 10 µM all-trans retinoic acid (ATRA) with 5% or 10% FBS for 12 days and (2) 10 µM ATRA with 5% or 10% FBS for 5 days followed by 50 ng/ml brain-derived neurotrophic factor (BDNF) exposure in serum-free media for 7 days as illustrated in Figure 2.1. These test groups were performed in parallel with controls: (3) 5% or 10% FBS-media for 12 days and (4) 10 µM ATRA with 5% or 10% FBS-media for 5 days followed by serum-free media for 7 days. The ATRA-supplemented groups were incubated with foil coverage to avoid ATRA degradation due to light exposure (Sharow, Temkin and Asson-Batres, 2012). All cultures were washed twice with non-supplemented media before the final 7-day differentiation stage. The cells were incubated at a temperature of 37 °C, and 5% CO_2 concentration, and media changed after 2-3 days for the initial 5 days and after 3-4 days for the final 7 days.

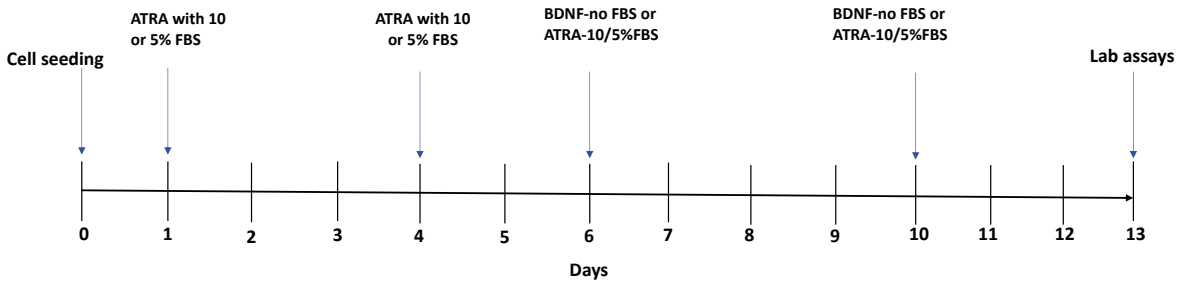

Figure 2.1 Summary of timeline and interventions for neuronal differentiation methods.

2.3. Trypan Blue exclusion assay

Cell suspensions prepared following Trypsin/EDTA treatment were mixed with an equal volume (20 µl) of 0.4% (w/v) Trypan blue cell dye (Life Technologies, Thermo Fisher Scientific, UK). This mixture was transferred to the haemocytometer's chamber (an improved Neubauer haemocytometer; Hawksley, UK); the number of stained, and unstained cells (viable cells) were manually counted under a phase-contrast microscope (Zeiss, Carl Zeiss Limited, UK). All samples were counted twice. The average number of cells per chamber was taken and multiplied by 10^4 and the dilution factor to obtain the number of viable cells per ml.

2.4. AlamarBlue assay

The AlamarBlue (AB) assay is a fluorometric/colorimetric assay based on metabolic activity and was used to assess cell viability, proliferation, and cytotoxicity (Fields and Lancaster, 1993; O'Brien *et al.*, 2000; Monteiro *et al.*, 2012). The assay utilises an oxidation-reduction indicator that changes the blue colour of the AB (resazurin: the oxidised form) to a pink colour (resorufin: the reduced form); the more oxygen uptake from the resazurin structure by respiring cells, the greater the intensity of the pink colour due to the increased resorufin produced. AlamarBlue powder (Sigma Aldrich, UK) was dissolved in phosphate-buffered saline (PBS) at a ratio of 0.15mg/ml (stock solution). This stock solution was diluted in the blank culture media to give a final concentration of 10%. The AlamarBlue prepared media was added to the cells in each well and then incubated up to 3.5h at 37 °C with 5% CO_2 with tin foil coverage to protect photosensitive AB from light exposure (Rampersad, 2012). Moreover, negative control wells (prepared AlamarBlue media added to wells without cells) were used for the method validity and calculation purposes (i.e., were used as "blank"). After incubation, 100 µl of the solution was transferred to a well of the 96-well plate (Nunc™, Thermo Fisher Scientific, UK) having at least 10 replicates wells of each group (control, and test, and blank wells). Absorbance was

read at 570 nm and 600 nm using a Spark microplate reader (Tecan Trading AG, Switzerland/ELX 800; Biotek Instruments Inc, UK). The reduction percentage of AlamarBlue was calculated using the following equation:

$$Percentage\ reduction\ of\ AlamarBlue = \frac{(O2 \times A1) - (O1 \times A2)}{(R1 \times N2) - (R2 \times N1)} \times 100$$

Where:
O1 = molar extinction coefficient (E) of oxidized AlamarBlue (Blue) at 570 nm
O2 = E of oxidized AlamarBlue at 600 nm
R1 = E of reduced AlamarBlue (Red) at 570 nm
R2 = E of reduced AlamarBlue at 600 nm
A1 = absorbance of test wells at 570 nm
A2 = absorbance of test wells at 600 nm
N1 = absorbance of negative control well (media plus AlamarBlue but no cells) at 570 nm
N2 = absorbance of negative control well (media plus AlamarBlue but no cells) at 600 nm

2.5. Morphological analyses

Morphological changes such as neurite outgrowth are characteristic of neuronal cells and determinants of neuronal cell health, connectivity, and subsequently function through signal transmission (Reese and Drapeau, 1998; Polleux and Snider, 2010). They are also considered as a vital indicator of neuronal development and regeneration (Polleux and Snider, 2010; Alberts *et al.*, 2002). Two different approaches were selected to assess the neuronal differentiation depending on the neurite formation, namely: image analysis and neurite outgrowth assay (automated cell membrane quantification).

2.5.1. Image preparation and analysis

All images were captured under X10 and X40 magnification using phase-contrast inverted microscopes (Axiovert 25, Zeiss, UK/Nikon Eclipse TE300 microscope, Japan). All phase contrast images were background corrected using the flat-field correction technique

(https://imagej.net/Image_Intensity_Processing): the experimental image intensity was divided by the intensity of the flat-field image (image without cells) and multiplied by mean of all images (experimental images and flat-field image). Subsequently, all experimental images were converted to black and white 8-bit images. This background correction was processed in Fiji (ImageJ, U. S. National Institutes of Health, Bethesda, Maryland, USA) (Schindelin *et al.*, 2012) using image calculator plus plugin (https://imagej.nih.gov/ij/plugins/calculator-plus.html). Flat-field and experimental images were captured under the same parameters such as magnification, contrast-phase ring, and light.

The neurite-like extensions were analysed using semi-automatic tracing plugin - NeuronJ (Meijering *et al.*, 2004; Meijering, 2010) in Fiji ImageJ software. The most apparent (longest) extended neurites (n = 10) were measured in ten random images taken from 9 equal sectors of each experimental group's well (100 neurite measurements per group). NeuronJ was calibrated for micrometre scale and phase contrast images. All measurements were exported to a Microsoft Excel file (XLS extension), and tracings were stored for future reference.

The differentiation percentage was calculated using a Cell Counter plugin (https://imagej.nih.gov/ij/plugins/cell-counter.html) in Fiji ImageJ software. The cells were considered as differentiated when the cell had one or more apparent neurites of length ≥50µm (Påhlman *et al.*, 1981; Påhlman *et al.*, 1984; Nicolini *et al.*, 1998; Brown *et al.*, 2005). Both total and differentiated cells were counted, and the labelling index was blue for total cell count and had a red index for cells with neurite-like extension ≥ 50 µm. The total number of differentiated cells was divided by the total cell number and then multiplied by 100 to convert to a percentage. The average was taken from 10 random images per each group.

2.5.2. Neurite outgrowth assay

Since the neurite outgrowth emanating from the cell bodies change the total amount of cell membrane surface area, the neurite outgrowth assay using cell membrane stain was used to quantify neurite projections alongside calcein AM stain (a cell-permeable esterase substrate) as a reporter of the cell viability (Hancock *et al.*, 2015). Hence, the neurite outgrowth staining assay kit (Thermo Fisher Scientific, USA) was used according to the manufacturer's instructions. The working solution was prepared of cell membrane stain (a measure for neurite outgrowth) and cell viability indicator in blank PBS or PBS containing 4% paraformaldehyde (Alfa Aesar, UK). This solution was applied to cells with an incubation time of 15 min at standard culture conditions and then was replaced by a background suppression solution. Free-cell wells were also included for background subtraction. The relative fluorescence quantification was immediately read using the bottom mode of the Spark microplate reader (Tecan Trading AG, Switzerland) with the reading parameters described in Table 2.2. For confocal microscopy scanning, the coverslips were mounted on microscope slides and scanned using the parameter settings mentioned in Table 2.3.

Table 2.2 The fluorescent intensity reading parameters

Dye (colour)	Excitation (nm)	Emission (nm)	Bandwidth (nm)
Cell membrane stain (orange-red)	554	567	5
Cell viability indicator (green)	483	525	12

2.6. Immunocytochemistry

Cells were fixed using 4% paraformaldehyde in PBS (Alfa Aesar, UK) for 10 min, and then gently washed twice with PBS. The permeabilization step with 0.5% Triton X-100 in PBS for

10 min was only performed for the intracellular antibody (Anti-Ki67), and then gently washed with PBS (3x10 min). Subsequently, the cells were blocked for 1h with block solution (3% bovine serum albumin BSA, 0.1% Triton X-100, and 10% goat serum (#G-9023, Sigma, UK) in PBS). The cells were then incubated with the desired diluted primary antibody (diluent buffer: 3% BSA and 0.05% tween-20 in PBS; see the antibodies and dilutions in Table 2.4) and kept overnight at -4 °C. The negative controls were incubated with antibody diluent buffer alone (without the primary antibody). The cells were gently washed with PBS (3x10 min) and then incubated for 1h with the diluted secondary antibody (see the antibodies and dilutions in the Table 2.4) in a dark box or covered with foil to protect the conjugated secondary antibody from the light exposure. Finally, the cells were gently washed with PBS (3x10 min) and mounted on microscopy slides with mounting containing DAPI (Abcam, UK) or incubated with DAPI for 5 min, and then mounted with aqueous mounting media (Abcam, UK). The slides were stored in the dark at 4 °C until microscopy scanning was performed.

All slide groups were multi-track scanned under 40x-oil lens magnification using the Zen 2011 software (Zeiss LSM software, Germany) of the confocal microscopy (Zeiss LSM 700 confocal microscope, Germany) with the acquisition parameters described in the Table 2.3.

Table 2.3 Imaging settings for confocal microscopy

Dyes	**Wavelength (colour)**	**Laser**	**Gain (master)**	**Digital gain (offset)**	**Pinhole size**	**Speed**	**Scan mode**	**Averaging**
Alexa 488	488 (green)	15	500-600	1 (0)	1 *AU (32.8)	7	Frame	4
Alexa 555	555 (red)	15	450-500	1 (0)	1 *AU (33.6)	7	Frame	4
DAPI	405 (blue)	15-20	600-700	1 (0)	1 *AU (28.8)	7	Frame	4

*AU = airy unit (recommended unit for detection efficiency and depth discrimination).

Table 2.4 Immunofluorescence antibodies and dilutions used

Antibody	Type	Host species	Description	Dilution	Reactivity	Product number	Supplier
Anti-βIII-tubulin (2G10)	Primary	Mouse	Monoclonal	1:400	Human, rat, mouse	T8578	Sigma-Aldrich, UK
Anti-βIII-tubulin (2G10)	Primary	Mouse	Monoclonal	1:500	Human, mouse, rat, rabbit, chicken, cow, cat, quail	ab78078	Abcam, UK
Anti-160kD Neurofilament Medium	Primary	Rabbit	Polyclonal	1:1000	Human, rat, cow	ab9034	Abcam, UK
Anti-GFAP	Primary	Rabbit	Monoclonal	1:500	Human, rat	ab33922	Abcam, UK
Anti-Ki67	Primary	Rabbit	Polyclonal	1:200	Human, mouse, rat	ab66155	Abcam, UK
Alexa Fluor 488	Secondary	Goat	Monoclonal	1:400	Anti-mouse	A20181	Invitrogen, Thermo Fisher Scientific, UK
Alexa Fluor 555	Secondary	Goat	Polyclonal	1:500	Anti-Rabbit	ab150078	Abcam, UK

2.7. Electrophysiological recordings

The cell patch-clamp method was used to investigate the functionality of the established neuronal-like models in comparison with controls. After the 12-day differentiation protocol (section 2.2), the cells were detached with trypsin as described in section 2.1 and suspended in 10% FBS DMEM/F12. The cell suspensions were transferred with numeral coding to ensure blinded recordings regardless of the group status. The sodium (Na^+) and potassium (K^+) channel ions voltage recordings were conducted as follows:

2.7.1. Na^+ channel ions voltage recordings

Cells were placed in a microscope chamber which was perfused at 3 ml/min with an extracellular solution containing (in mM): 145 NaCl, 4.5 KCl, 2 $NiCl_2$, 1.8 $CaCl_2$, 1.2 $MgCl_2$, 10 HEPES and 10 glucose, adjusted to pH 7.4 with CsOH. Voltage-clamp recordings were performed at room temperature using an Axopatch 200B amplifier (Molecular Devices, CA, USA), a CED micro1401 driven by Signal v6 (CED, UK), and borosilicate glass pipettes (tip resistance 1.5–3 MΩ). This borosilicate glass pipette had an internal solution containing (in mM): 115 CsCl, 5 NaCl, 0.5 $MgCl_2$, 10 EGTA, 5 Mg-ATP, 10 HEPES and 20 TEA, adjusted to pH 7.2 with CsOH. The sodium currents were set at 50 kHz with 20 kHz low-pass filtration, and the series resistance was in the range of 6-8 MΩ (the compensation between 80% and 100%). To test the current-voltage relationships, the 100 ms step depolarisations was used over membrane potentials in the range of -40 mV to +60 mV at a holding potential of -100 mV with 5 mV increments. The currents were normalised to the cell membrane capacitance to remove any differentiation change effect on the cell size and then expressed in pA/pF as current density. Due to clear I_{Na} voltage magnitudes (below2nA), using low sodium external solution was not needed, and a sufficient control was established as demonstrated in the bell-shaped I/V plot

results. The current-voltage (I-V) relationship curve data were fitted using the following modified Boltzmann equation (Spencer *et al.*, 2001):

$$INa = \frac{Gmax(Vm - Vrev)}{1 + \exp\left[\frac{V0.5 - Vm}{k}\right]}$$

Where:

INa = sodium peak current density at an equivalent test potential (Vm)

Gmax = maximal conductance (nS)

Vrev = reversal potential,

V0.5 = membrane potential at half-maximal current activation

k = slope constant factor

2.7.2. K^+ channel ions voltage recordings

The K^+ currents were recorded with the same external solution, but the internal pipette solution contained the following (in mM): 135 KCl, 5 NaCl, 10 EGTA, 3 Mg-ATP, 0.5 Na3GTP, 10 HEPES and 5 glucose; pH adjusted to 7.2 using KOH. The Ca^{2+} independent K^+ currents were evoked at a holding potential of -70 mV using 5 mV interval step depolarisations (500 ms duration) and obtained over the range of membrane potentials of -60 mV to +40 mV, and the voltage dependent was at 1 Hz. In some minimally inactivated currents cells, the duration was adjusted to 300 ms after the initial pulse. The K^+ currents were also corrected against the cell membrane capacitance to remove any effect on the cell size due to differentiation and then expressed in pA/pF as current density. Non-measurable currents were also used in the analysis.

2.8. Gene expression

Quantitative real-time polymerase chain reaction (qPCR) was used to analyse and compare the gene expression levels between control and treated groups.

2.8.1. RNA Isolation

RNA was extracted from all DPSC and SH-SY5Y cell culture groups using a Qiagen RNeasy Mini kit according to the manufacturer's instructions. The cell cultures were washed twice with PBS to remove any remaining media followed by lysis in 350-700 µl of Buffer RLT depending on the cell number (350 µl per ≈ $5x10^6$ cells) and transferred to an Eppendorf tube (Nunc, UK). The lysed cells were stored at -80 °C until isolation of RNA.

The cell lysate was used to isolate pure RNA for reverse transcription cDNA synthesis. An equal volume of 70% ethanol was added to the cell lysate with gentle mixing, and the whole amount was transferred to a spin column assembly. The column assembly was centrifuged at 10000 rpm for 30s, and the flow-through was discarded. Then 350 µl of Buffer RW1 was added to the column and centrifuged at 10000 rpm for 30s. Total RNA was digested by adding Deoxyribonuclease I (DNase I) (Qiagen, UK) to the spin column assembly. DNase I was prepared in a buffer (10:70 µl ratio) depending on the number of samples used. Then 80 µl of DNase I incubation mix was added to the spin column assembly and incubated for 15 min. Subsequently, the RNA was purified by several washes and centrifugation using wash buffers (Buffer RW1 and Buffer RPE). Then 20-30 µl of DEPC-treated water was added to the column assembly to elute RNA and centrifuged at 10000 rpm for 1 min. The eluted RNA was stored at -80 °C until used.

2.8.2. RNA Quantification and visualisation

The RNA concentration and purity were measured at 260/280 nm (optical density) using a Spectrophotometer (BioPhotometer Plus, Eppendorf, Germany). The device was blanked with 70 µl of water in a clean cuvette (Eppendorf, Germany). Then, 2 µl of RNA sample was added to 68 µl of RNase free water in another cuvette, which measured with adjusting the device according to the used dilution (2:68 µl). The RNA with a concentration value greater than 50

µg/ml and with a high purity ration (ranging from 1.8-2.0) was used for complementary DNA conversion.

RNA integrity was visualised using a 1% agarose gel. The gel was synthesised by combining 0.6 g of Agarose (Bioline, UK) in 60 ml of 1x TAE buffer (Fermentas, Lithuania) with 5 µl of SYBR Gold (Invitrogen, USA). The RNA loading was prepared using 1 µl of the isolated RNA, and 5 µl 1X loading buffer (Promega, USA). Then loading of 5 µl of the mixture into wells in the agarose gel, and electrophoresis was performed at 120 V for 20 min. Images of the SYBR gold nucleic acid stained gel were captured using a gel doc system (G:Box, Syngene, UK) to determine isolated RNA integrity and absence of contaminants such as genomic DNA or proteins.

2.8.3. Complementary DNA (cDNA) conversion

RNA was used to produce cDNA using the Tetro cDNA Synthesis Kit (Bioline, UK). Following the manufacturer's instructions, 2 µg out of the total RNA concentration was determined. The priming premix included: 1 µl of Oligo $(dT)_{18}$ primer, 1 µl of 10 mM dNTP mix, 4 µl of 5x RT Buffer, 1 µl of RiboSafe RNase Inhibitor, and 1 µl of Tetro Reverse Transcriptase (200 u/µl). Subsequently, 8 µl of priming premix was added to 12 µl of the diluted RNA to make a total of 20 µl solution. The RNA samples were heated to 45 ºC for 45-60 min and subsequently incubated at 85 °C for 5 min to allow the synthesis reaction of cDNA using a thermal cycler (Applied Biosystems™ Veriti™ 96-Well Thermal Cycler, UK). The samples were stored at -20 ºC before use for real-time PCR.

2.8.4. Quantitative real-time PCR

The reference and target genes were selected from the literature, and several primers were purchased as ready-designed pair primers (Invitrogen/Sigma, UK) (see the primers details in

Table 2.5). The PCR was performed using LightCycler® 480 SYBR Green I Master (Roche, UK) by combining 10 µl LightCycler® 480 SYBR Green I Master, 0.5 µM of forward and reverse primers, 1 µl of cDNA and RNase-free water to have a total volume of 20 µl per well. All gene primer assays were run with 1 µl of cDNA except for CHAT and MNX1 as they appeared to be relatively lowly expressed genes (used 2 µl of cDNA), and TUBB3 showed relatively high expression as detected at early cycle numbers in DPSCs (used 0.5 µl of cDNA) which were optimised in the primer's efficiency validation. Subsequently, 20 µl mix was placed on a white 96-well plate (LightCycler® 480 multi-well plate, Roche, UK); the plate was then sealed with sealing foil (LightCycler® 480 sealing foil, Roche, UK), and centrifuged for 3 min at 1500 rcf (Universal 320R centrifuge, Hettich, UK). After that, the plate was cycled using the protocol described in Table 2.6 in the LightCycler® 480 software (Roche diagnostics version 1.5.0.39), and the Roche LightCycler® 480 II machine PCR system. All samples had duplicate or triplicate wells and two negative controls of "no cDNA or no template-RNase free water" per each primer pair in every run to identify the presence of genomic contamination. Finally, gene expression data were computed as crossing point (Cp) values using the fit-points methods on the LightCycler 480 software following the manufacturer's instructions. The melting curve of each sample was checked to ensure that the PCR product contained no primer dimers, i.e., a single uniform melting curve for each primer. Selected qPCR products were analysed by the gel electrophoresis to determine if the product exhibited the correct molecular weight size.

2.8.5. PCR primer validation

All gene of interest and housekeeping primers were analysed for Real-time PCR efficiency as previously recommended by Pfaffl (2001) to reveal the number of amplification folds. Pooled cDNA of all groups was diluted (1, 1:1, 1:100, 1:1000), and each dilution was run in duplicate samples (see Figure 2.2A). The melting curve was checked to ensure that all groups of each

primer exhibited a single peak amplicon (no primer dimer), and no-template (negative) controls exhibited no melting curve (see Figure 2.2B). The efficiency value was logarithmically calculated using LightCycler® 480 software by creating a standard curve of the serial dilutions per each primer (slope of the regression between Ct values and the log values) (see Figure 2.2C). Double fold increases in every cycle gives a value of 2, which is considered 100% efficient. All primer efficiency values are shown in Table 2.5.

2.8.6. Housekeeping gene selection

Four housekeeping genes (GAPDH, HPRT1, B2M and RPLA13) were compared to identify the most stable housekeeping reference among the groups to enable normalisation of quantitative PCR data that are widely recommended and used (Pfaffl *et al.*, 2004; Li *et al.*, 2016). The most two suitable reference genes were selected according to the statistical algorithm analysis program "Normfinder" (Andersen, Jensen and Orntoft, 2004). The Normfinder calculated the variation between groups based on the geometric mean of the Cp values and standard deviation (SD) along with the coefficient of variance. The SD value should be less than one to be considered as a stable reference gene, and the lowest SD value is the most stable (Piehler *et al.*, 2010). Both HPRT1 and RPL13A references genes were the most stable and consistent for both used cell types analysed and were therefore selected for qPCR data quantification (see stability data in Appendix I).

2.8.7. Gene expression data analysis

The gene expression was calculated as a ratio of fold change compared with the housekeeping genes using the Pfaffl method (Pfaffl, 2001), which includes the efficiency values of the gene of interest and housekeeping in the gene fold-change calculation. If the PCR product exhibited a double or irregular melting curve, it was excluded in the calculation, and the data was discarded.

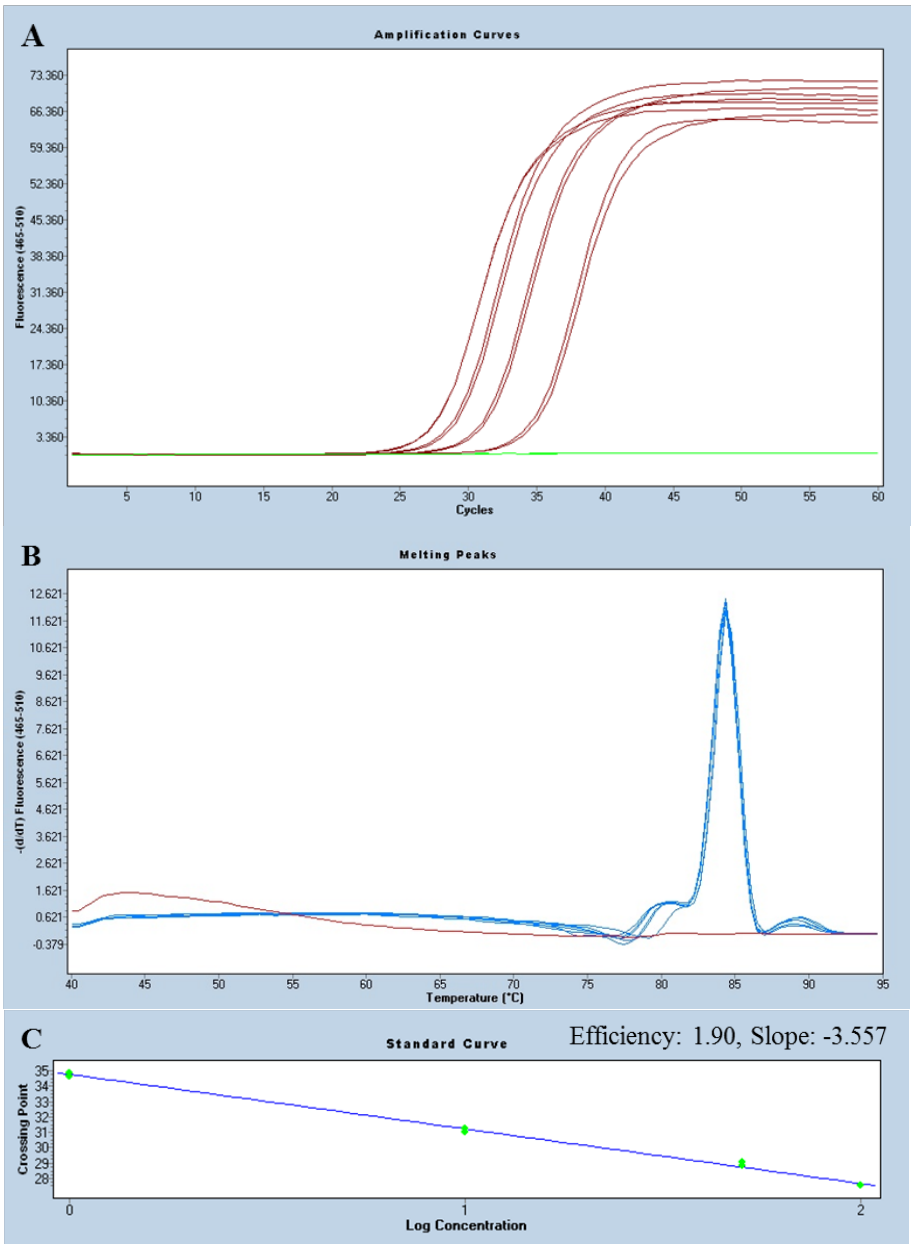

Figure 2.2 Representative images of SNAP25 primer efficiency validation with DPSCs. (A) Amplification curves for the cDNA serial dilutions (brown curves) including 2 no-template controls (green lines). These sequential brown curves represent the serial dilutions (1, 1:1, 1:100, 1:1000) used by the LightCycler® 480 software to generate the standard efficiency curve. (B) Melting curve of all concentration samples (blue lines) including negative controls (red lines). (C) The standard efficiency curve indicates a good primer with the efficiency value of 1.9 and the slope value of -3.56.

Table 2.5 The primer details used for real-time PCR

Gene	Primer sequence (5→3)	Amplicon size (bp)	Accession number (NCBI)	Efficiency value	
				SH-SY5Y	DPSCs
Housekeeping genes					
GAPDH	(F) CTCCTGTTCGACAGTCAG (R) GCCCAATACGACCAAATC	111	NM_002046.7	1.70	1.80
RPL13A	(F) CCTGGAGGAGAAGAGGAAAGAGA (R) TTGAGGACCTCTGTGTATTTGTCAA	126	NM_012423.4	1.90	1.70
B2M	(F) ACCCCCACTGAAAAAGATGA (R) ATCTTCAAACCTCCATGATG	114	NM_004048.3	1.60	1.90
HPRT1	(F) GACCAGTCAACAGGGGACAT (R) AACACTTCGTGGGGTCCTTTTC	195	NM_000194.3	1.90	1.70
Target genes					
ENO2 (NSE)	(F) CTGAAGCCATCCAAGCGTGC (R) CCCACCACCAGGTCAGCAAT	109	NM_001975.2	1.85	1.92
NES	(F) GAGAACTCCCGGCTGCAAAC (R) CCAGCTTGGGGTCCTGAAAG	70	NM_006617.1	1.83	1.93
RET	(F) ACAGGGGATGCAGTATCTGG (R) CTGGCTCCTCTTCACGTAGG	154	NM_020975.6	1.86	2.00
TUBB3	(F) CATCCAGAGCAAGAACAGCA (R) CTCGGTGAACTCCATCTCGT	235	NM_006086.4	1.94	1.76
SYN1	(F) AATACTGGCTCTGCGATGCT (R) TGACCACGAGCTCTACGATG	223	NM_006950.3	1.94	1.78

Table 2.5 The primer details used for real-time PCR (continued)

Gene	Primer sequence (5→3)	Amplicon size (bp)	Accession number (NCBI)	Efficiency value	
				SH-SY5Y	DPSCs
Target genes					
SNAP25	(F) CTGCTCGTGTAGTGGACGAA (R) CGATCTGGCGATTCTGTGTA	186	NM_003081.4	1.86	1.90
GFAP	(F) CCATTCCCGTGCAGACCTTC (R) TCTGAGAGGCAGGCAGCTAAC	180	NM_001131019.2	2.07	1.60
PRPH	(F) AGATCGCCACCTACCGCAAG (R) CCCATTCCGGGTCTCAATGGT	170	NM_006262.3	2.08	1.85
MAP2	(F) TGGCATTGACCTCCCTAAAGAG (R) TTGCTTCCGTTGGCATTTCG	77	NM_001363910.1	1.91	2.04
SCN1A	(F) CATTTTGTCACGCATCAATC (R) GAAACATACCTACAATGGAGAG	149	NM_001165963	2.04	2.10
SCN9A	(F) GGCAACTTCTGATGACAGCG (R) GTGCAAATCTGTACCACCAAGG	200	NM_001365536.1	2.01	2.05
DBH	(F) CAGATATCTCCGCCTGGAAG (R) TGCAGTAGCCAGTGAGGATG	197	NM_000787.3	1.76	_
POU4F1	(F) TTGCCATGCATCCCACCCTC (R) TGAAAGGATGGCTCTTGCCCT	198	NM_006237.3	2.03	1.60
CHAT	(F) TCCAACGAGGACGAGCGTTT (R) ATCATGTCCAGCGAGTCCCG	122	NM_001142934.1	2.10	1.93

Table 2.5 The primer details used for real-time PCR (continued)

Gene	Primer sequence (5→3)	Amplicon size (bp)	Accession number (NCBI)	Efficiency value	
				SH-SY5Y	DPSCs
Target genes					
ACHE	(F) CCTCCTTGGACGTGTACGAT (R) AAACAGCGTCACTGATGTCG	218	NM_001302622.2	1.64	1.72
NEFM (NF-M)	(F) GCTGCGTACAGAAAACTC (R) CCTTGGGTTTCTGAATCTTAC	127	NM_005382	2.10	2.02
GAP43	(F) CAGAATTAAAAGGGAACCTGG (R) TGTGACTCATTTTCCTTGTG	93	NM_001130064	2.04	2.10
MNX1	(F) GTTCAAGCTCAACAAGTACC (R) GGTTCTGGAACCAAATCTTC	98	NM_001165255	1.65	1.88
SLC6A3 (DAT)	(F) TGCCGAGTACTTTGAACGTG (R) ACCACCTTCCCTGAGGTCTT	159	NM_001044.5	_	_

Abbreviations: GAPDH (glyceraldehyde-3-phosphate dehydrogenase); RPL13A (ribosomal protein L13-A); B2M (beta-2-microglobulin); HPRT1 (hypoxanthine phosphoribosyl transferase 1); ENO2/NSE (enolase 2/neuron-specific enolase); NES (nestin); RET (ret proto-oncogene); TUBB3 (tubulin beta 3 class III); SYN1 (synapsin I); SNAP25 (synaptosome associated protein 25); GFAP (glial fibrillary acidic protein); PRPH (peripherin); MAP2 (microtubule associated protein 2); SCN1A (voltage-gated sodium channel alpha subunit 1); SCN9A (voltage-gated sodium channel alpha subunit 9); DBH (dopamine beta-hydroxylase); POU4F1 (POU class 4 homeobox 1); CHAT (choline O-acetyltransferase); ACHE (acetylcholinesterase); NEFM (neurofilament medium); GAP43 (growth associated protein 43); MNX1 (motor neuron and pancreas homeobox 1); SLC6A3 (solute carrier family 6 member 3).

Table 2.6 The qPCR cycling conditions [adapted from (Forster *et al.*, 2016)]

PCR Step	Temperature (˚C)	Time (s)	Cycles
Denaturation	95	300	1
Amplification	95 60 72	30 30 30	45-60
Melting curve	95 40 90-95	15 90 0.11˚C/s	1
Cooling	40	1800	1

2.9. LIPUS set up, dosage and experimental conditions

The LIPUS exposure device (Osteotron IV LIPUS, ITO, Tokyo, Japan) has two transducers with each head diameter of 32 mm; both transducers were adhered to two adjacent well floors of 6-well plate using an adherent material as shown in Figure 2.3A. These transducers were coated with a thin layer of transmission gel (Aquasonic 100 ultrasound transmission gel, Parker Laboratories, USA) and two separate 35 mm Petri dishes were placed on the two mounted transducers as shown in Figure 2.3B. In certain experiments, a 6-well plate was used in which only the peripheral wells were treated without using the middle wells (the middle wells were filled with PBS). The cells in the LIPUS exposure groups were treated, while those in the control group received a sham treatment (the LIPUS device was switched off). To choose the optimal spatial-average temporal intensity (I_{SATA}), the cells were treated with the available different intensities (including 30 mW/cm^2, 45 mW/cm^2, 60 mW/cm^2), and then assessed by AlamarBlue assay (the results are presented in the chapter 6, section 6.2.1). The resultant highest absorbance intensity (60 mW/cm^2) with other LIPUS parameters (frequency of 1.5 MHz, pulse of 100 Hz ratio of 1:5 (duty cycle 20%), and time of 20 min) were applied for subsequent experiments.

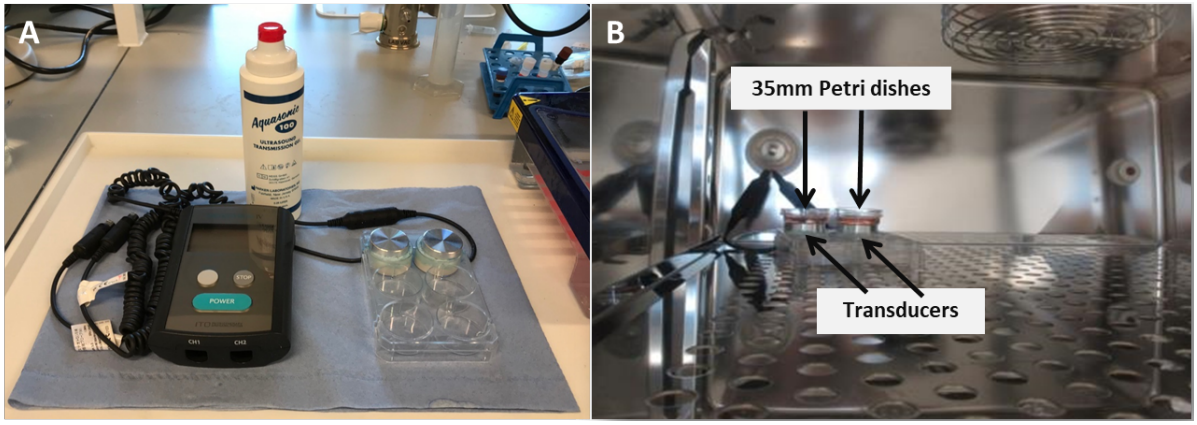

Figure 2.3 The set-up used to deliver the LIPUS to *in vitro* cultured cells. (A) The two transducers of the Osteotron LIPUS device were attached to the adjacent wells of 6-well plate using Aquasonic 100 gel to coat the transducer surfaces before dishes were located for LIPUS exposure. (B) The LIPUS treatment was conducted in 35-mm Petri dishes inside the incubator to keep the tissue culture conditions as demonstrated.

In the LIPUS experiments, the cell seeding was at an initial density of 1250/cm^2 for DPSCs, and 10000/cm^2 for SH-SY5Y and these samples were differentiated using the resultant optimised method described in chapter 3 and 4. After 12 days of differentiation, the BDNF-supplemented serum-free media was replenished, and the cells were either exposed to a single- or three-fold treatment (once daily for three consecutive days). Subsequently, the laboratory tests were conducted after 15 days, as demonstrated in Figure 2.4.

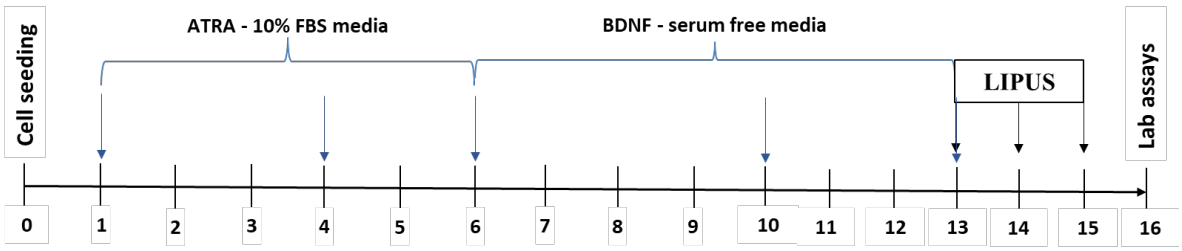

Figure 2.4 The schematic diagram illustrating the cell culture differentiation protocol (blue arrows) and LIPUS exposure regimen (black arrows) throughout the time (days).

2.10. Proliferation assays

In this study, 2 different approaches were used to assess the cell proliferation, namely measurement of cellular metabolism: Cell counting kit-8 assay (CCK-8) and AlamarBlue assays (described in section 2.4) reflecting the number of viable cells, and the expression of proliferation protein markers (Ki-67).

2.10.1. Cellular metabolism/viability: Cell counting kit-8 assay (CCK-8)

The CCK-8 assay utilises the reduction of water-soluble tetrazolium salt WST-8 [2-(2-methoxy-4-nitrophenyl)-3-(4-nitrophenyl)-5-(2,4-disulfophenyl)-2Htetrazolium, monosodium salt] to a yellow-orange coloured formazan by dehydrogenases activity. The higher dehydrogenases activity in the cells is directly proportional to the number of viable cells which produce more coloured formazan compound. This metabolic colorimetric assay has been used for proliferation (Lin *et al.*, 2020; Ling *et al.*, 2017b) and cytotoxicity studies (Yoshimura *et al.*, 2002; Han *et al.*, 2011).

To check the method validity, the calibration curve was generated using known cell densities (12500, 25000, 50000, and 100000) seeded in a 96-well plate (the results are presented in the chapter 6, section 6.2.3). The cells were preincubated at 37 °C with 5% CO_2 for 6h to allow the cells to adhere to the cell culture surface and then 10 µl of CCK-8 solution (Sigma-Aldrich, UK) was added to 90 µl blank medium to enable a final concentration of 10% in each well. Then, the cells were incubated for 3h in standard culture conditions. Negative control wells (no cells) also contained the same 10% CCK-8 concentration in the medium for method validity and background correction. The absorbance was read at a wavelength of 450 nm with a reference filter at 460 nm using the Spark microplate reader (Tecan Trading AG, Switzerland). The actual absorbance values were used for comparison analysis.

2.10.2. Ki67 proliferation assay

The K-i67 labelling method was used to determine the percentage of the newly formed cells. The staining and scanning were conducted as previously detailed in section 2.6. The fluorescent K-i67 immunopositive cells were counted using a Cell Counter plugin (https://imagej.nih.gov/ij/plugins/cell-counter.html) in Fiji ImageJ software. The percentage of Ki67 immunopositive cells was calculated among the total DAPI-stained cells number in each microscopic field. The average was taken from 24-33 images per group.

2.11. ERK1/2 (p44/42MAPK) signalling

The p44/42MAPK (ERK1/2) assay (PathScan® Phospho-p44/42MAPK (Thr202/Tyr204) Sandwich ELISA Kit) and ERK1/2 inhibitor (MEK1/2 inhibitor: U0126) were purchased from Cell Signalling Technology, USA to quantify the phosphorylation of p44/42MAPK (ERK1/2) of the neuronal differentiation and LIPUS groups. Furthermore, immunocytochemistry, neurite outgrowth, and CCK-8 assays were assessed in the presence and absence of the ERK1/2 inhibitor.

2.11.1. ERK1/2 signalling and neuronal differentiation

The SH-SY5Y and DPSCs were treated with 10 µM ATRA in 10% FBS-DMEM/F12 medium for 5 days as a preparatory phase. The cells were then washed twice with blank media, and serum starved by incubating them in blank media for 5h. Subsequently, the cells were preincubated either with or without 10 µM U0126 inhibitor in serum-free medium for 1h, and then supplemented with 50 ng/ml BDNF. The groups were either 5-min incubated and lysed for ELISA assay or 48h incubated in presence and absence of the U0126 inhibitor for neurite outgrowth assay and immunocytochemistry.

2.11.2. ERK1/2 signalling and LIPUS stimulation

The neuronal-like models were pretreated with or without 10 µM U0126 inhibitor for 1h in the presence of BDNF-supplemented DMEM/F12 media as standard media and subsequently exposed to LIPUS (I_{SATA} = 60 mW/cm^2; time = 20 min) or sham treatment. Then, the cells either were immediately lysed for ELISA or further incubated for 48h for Ki67 immunostaining.

2.11.3. Phospho-p44/42 MAPK (ERK 1/2) - Sandwich ELISA

Cell lysis and the ERK1/2 ELISA were carried out according to the manufacturer's instructions. In brief, the cultures were rapidly rinsed twice with cold-PBS to remove the residual media and then lysed with provided lysis buffer[1] (Cell Signalling Technology, USA) in a ratio of 400 µl/10 cm^2 cell culture area for 5-min incubation on ice. The cells were then removed from the culture surface with a cell scraper (CytoOne Cell Scraper, Starlab, UK), and briefly sonicated (~30s) on ice. The samples were centrifuged for 10 min at 14,000 rpm in 4 °C cold microcentrifuge (Centrifuge 5415 R, Eppendorf, Germany), and cell lysate supernatants were stored in aliquots at -80 °C until ELISA procedure.

All the groups' cell lysates and desired number of the phospho-p44/42MAPK-coated microwell strips were brought to room temperature, and 100 µl of undiluted lysate of each group was added to duplicate wells of the 96-well plate, which was then sealed and incubated overnight at 4 °C. Subsequently, the wells were washed 4 times in an automated plate washer (Bio-Tek Instruments, USA) using the prepared wash buffer. Reconstituted detection antibody (100 µl) was added to each well, sealed and incubated for 1h at 37 °C (Heracell 150i incubator, Thermo Scientific, UK). The washing step was repeated, and then 100 µl of reconstituted HRP (Horseradish peroxidase)-linked secondary antibody was added to each well and incubated for

[1] Supplemented with 1 mM Phenylmethylsulphonyl fluoride (PMSF) (Sigma-Aldrich, UK) as a protease inhibitor.

30 min at 37 °C. After incubation, the washing step was again repeated; 100 µl of TMB (3,3', 5,5"-tetramethylbenzidine) substrate was then added to each well, sealed, and incubated for 10 min at 37 °C. To terminate the assay reaction, 100 µl of stop solution was added, gently shaken, and the absorbance was then read at 450 nm using the Spark microplate reader.

2.12. Statistical analysis

All individual experiments were repeated 3-4 times with at least 2-4 technical replicates per group. The data were statistically analysed by IBM SPSS Statistics version 26 and 27, USA. The Kolmogorov-Smirnov tests were used to check the normality of the data, whether data follow the normal distribution or not. Subsequently, the statistical test was chosen for either parametric analysis if the data followed the normal distribution or for non-parametric test if the data did not follow the normal distribution with an appropriate post-hoc test for multiple pairwise comparisons. Hence, the groups with parametric data were compared using means of One-way ANOVA either followed by Tukey or Games-Howell post hoc test for pairwise comparisons based on the results of the homogeneity test of variances (Levene's test). Whereas the groups with non-parametric data were compared using Kruskal-Wallis test followed by Bonferroni post-hoc test or Dunn's test for pairwise comparisons. These statistical tests were the main tests used to analyse the data unless otherwise stated. All statistical analysis tests were performed at a significance level of $p < 0.05$. Data in graphs were generated using GraphPad Prism 8 software package (GraphPad, San Diego, CA, USA), and presented as mean ± standard error of the mean (SEM) unless otherwise stated. Statistical significance level in graphs was indicated as *$p < 0.05$, ** $p < 0.01$, and *** $p < 0.001$.

CHAPTER 3: OPTIMISING AND CHARACTERISING THE SH-SY5Y-DERIVED NEURONAL CELL MODELS

3.1. Introduction

Testing new therapies for nerve regeneration requires in-vitro studies as the first steps in understanding the response of neuronal tissue prior to the *in-vivo* setting. The animal neuronal tissue taken from rodent does not accurately represent the human tissue due to differences in gene expression and transcription factor signalling (Lin *et al.*, 2014; Cheng *et al.*, 2014; Hodge *et al.*, 2019). This is in addition to other ethical issues in using animals in research (Festing and Wilkinson, 2007). Obtaining human embryonic neurons for studies involve even higher ethical difficulties. Furthermore, the primary cells undergo a postmitotic fate once they have differentiated, which results in a finite number being available for ongoing experimental screening. The SH-SY5Y neuronal neuroblastoma cell line is considered a good neural tissue model as it is derived from a human tissue (Biedler, Helson and Spengler, 1973). It exhibits a high throughput cell population which is needed for experimental research (Forster *et al.*, 2016). The primary form is the SK-N-SH cell line which contains S-type and N-type cells (Biedler, Helson and Spengler, 1973; Ross, Spengler and Biedler, 1983). This neuronal cell line has been subcloned three times to give the SH-SY5Y form (Kovalevich and Langford, 2013) which is a high N-type cell line with a higher ability to differentiate into neuronal-like cells (Biedler, Spengler and Lyser, 1975; Ross, Spengler and Biedler, 1983). Furthermore, this cell line is used in neuroscience as a representative neurological tissue for different studies such as for neurodegenerative diseases including Parkinson and Alzheimer's diseases (Gatta *et al.*, 2011; Zhang *et al.*, 2016b), neurotoxicity (Ng and Say, 2018; Wang *et al.*, 2019), energetic neuronal vulnerability (Forster *et al.*, 2016), pathogenesis of viral infection (Sun *et al.*, 2010; Christensen *et al.*, 2011; Gimenez-Cassina, Lim and Diaz-Nido, 2006), and MSC secretome effects on neuritogenesis and differentiation (Pires *et al.*, 2014; Gervois *et al.*, 2017).

It has been demonstrated that the neuronal differentiation of neuroblastoma cells is induced by the reduction of serum, and this is shown by an increase in neuronal characteristics such as neurite outgrowth (Seeds *et al.*, 1970; Kumar and Katyal, 2018). It was also reported that the neuronal differentiation of SH-SY5Y neuroblastoma cells is highly dependent on the differentiating supplement and the culture substrates used but not on FBS content (Buttiglione *et al.*, 2007). Hence, there are still conflicting theories as to whether the serum concentration should be reduced in the differentiating media when aiming to enhance the neuronal SH-SY5Y differentiation and maturation. Some SH-SY5Y differentiation studies have used the standard serum level from 10% to 15% (Constantinescu *et al.*, 2007; Agholme *et al.*, 2010; Bell *et al.*, 2013; Encinas *et al.*, 2000) whereas others have applied reduced serum concentration from 1%, to 5% (Cheung *et al.*, 2009a; Forster *et al.*, 2016; Shipley, Mangold and Szpara, 2016; Lopes *et al.*, 2010; de Medeiros *et al.*, 2019).

Several supplements have been used to induce SH-SY5Y differentiation (Påhlman *et al.*, 1995; Cheung *et al.*, 2009a; Constantinescu *et al.*, 2007; Forster *et al.*, 2016; Buttiglione *et al.*, 2007; Brown *et al.*, 2005; Chen *et al.*, 1990; Kume *et al.*, 2008). Notably, all-trans retinoic acid (ATRA) is the most documented compound used to differentiate the SH-SY5Y cells into neuronal-like cells (Brown *et al.*, 2005; Cheung *et al.*, 2009a; Constantinescu *et al.*, 2007; Kovalevich and Langford, 2013; Påhlman *et al.*, 1984). This approach was optimised by adding 2nd stage supplementation with brain-derived growth factor (BNDF) to produce a functional homogenous cell neuronal model (Encinas *et al.*, 2000). This study aimed to investigate the effects of lowering FBS concentration on the differentiation and compare different neurogenic differentiation protocols using the SH-SY5Y neuroblastoma cell line. It also aimed to characterise these SH-SY5Y neuronal models morphologically, biochemically, and electro-physiologically. The grouping and assays conducted are illustrated in Figure 3.1.

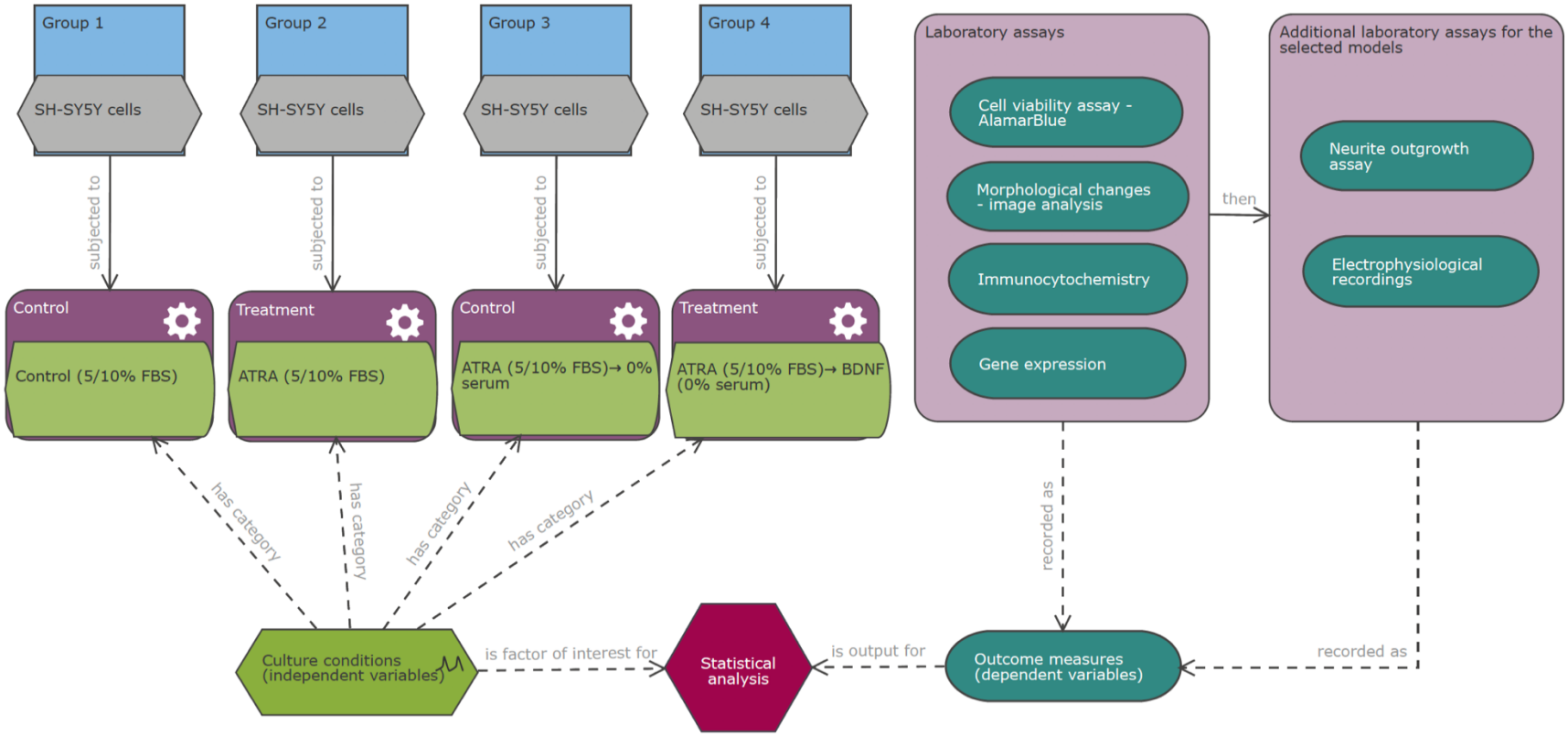

Figure 3.1 Schematic diagram showing the groups and assays used to investigate whether the serum reduction increase the neuronal differentiation of SH-SY5Y neuroblastoma cell line and characterise the established neuronal-like model. The diagram was designed by the author using the experimental design assistant (EDA) tool in the link (https://eda.nc3rs.org.uk).

3.2. Results

3.2.1. Selection of the cell seeding density and FBS level

The growth curve of different cell seeding numbers ($1.25x10^3/cm^2$, $2.5x10^3/cm^2$, $5x10^3/cm^2$, and $10^4/cm^2$) was established using Trypan Blue Exclusion Assay (viable cell count) throughout the 7 days to select the optimal cell seeding for the subsequent experiments (Figure 3.2). Although only the highest cell seeding densities ($5x10^3/cm^2$, and $10^4/cm^2$) showed obvious exponential growth increase over time, all cell densities presented significant increases over the time (non-linear regression - exponential model, regression coefficient = 0.53 ± 0.06, adjusted $R^2 = 0.75 \pm 0.03$, *p*-value = 0.00). These data indicated that the average of the viable cell number increased by approximately half (0.53) for each day and this exponential model could explain about 75% of the variability in viable cell number counts (showing a good fit of the model). The groups were also compared within each day which showed that the highest cell seeding densities ($5x10^3/cm^2$ and $10^4/cm^2$) were significantly higher than the lowest cell seeding ($1.25x10^3/cm^2$) throughout the 7 days ($p = 0.013 \pm 0.02$ and 0.000 for $5x10^3/cm^2$ and $10^4/cm^2$, respectively) but only the $10^4/cm^2$ cell seeding group exhibited a significantly higher cell number than the $2.5x10^3/cm^2$ group ($p = 0.008 \pm 0.01$). Furthermore, there was no significant difference in viable cell number between $5x10^3/cm^2$, and $10^4/cm^2$ cell seeding groups ($p = 0.086 \pm 0.055$), so both cell seedings were considered for future studies. The planned differentiation duration was 12 days, and the $10^4/cm^2$ cell seeding showed high cell confluence growth on the 7th day of culture whereas the $5x10^3/cm^2$ group showed a reasonable growth that allows adequate intercellular space for neurite outgrowth projections in differentiation stage. Thus, the $5x10^3/cm^2$ cell seeding was therefore chosen for the differentiation experiments.

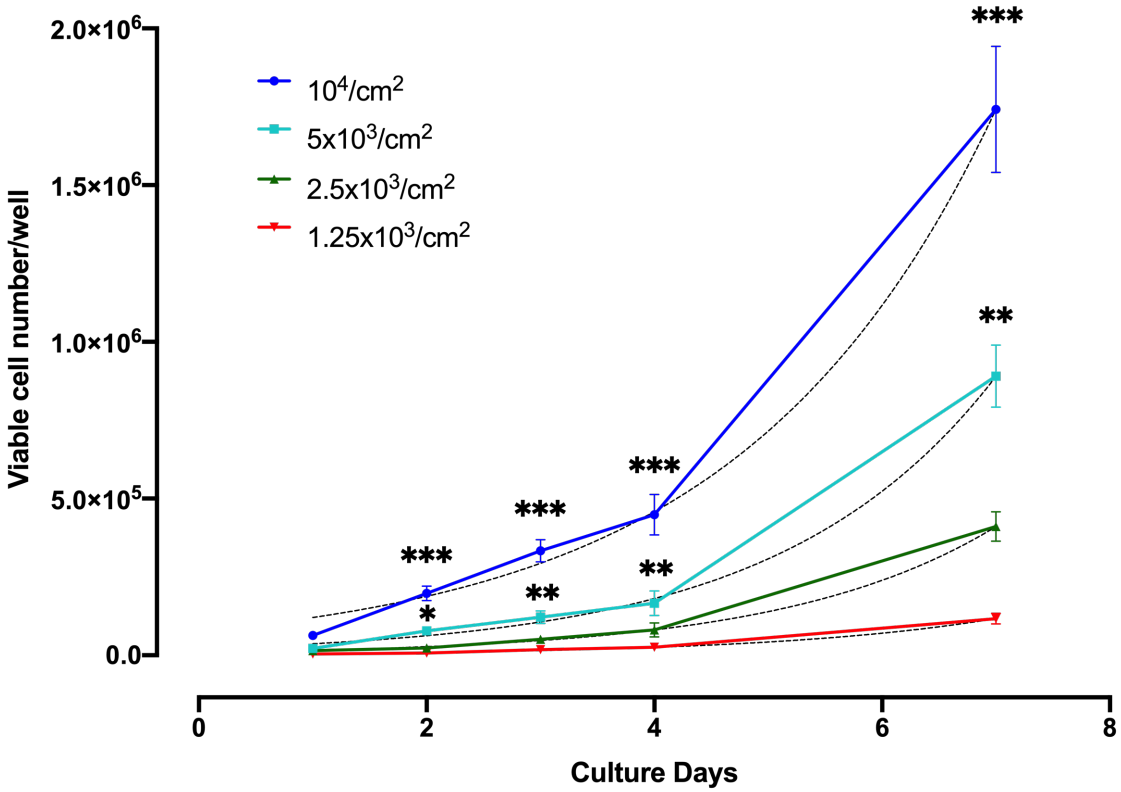

Figure 3.2 Growth curve of the SH-SY5Y cell line over time (7 days). The highest cell seeding groups ($5x10^3/cm^2$ and $10^4/cm^2$) demonstrated significant cell number growth (compared by Kruskal-Wallis test with pairwise comparison; the significance values were adjusted by Bonferroni correction for multiple tests. The data are mean ± SEM (n = 9; *$p < 0.05$, ** $p < 0.01$, and *** $p < 0.001$). The dotted lines are the best curve estimation fitting of the non-linear regression (exponential model).

To select reduced FBS levels, lower FBS concentrations (5%, 2.5%, and 1.25%) were tested in parallel with the standard FBS level (10%) (Figure 3.3). The cells were seeded at the chosen density of $5x10^3$ cells/cm^2 in 6-well plate and were counted after 48h. There was a significant increase in 5% and 10% FBS supplementation groups ($p = 0.002$ for 5% and 0.000 for 10%) while 2.5% and 1.25% FBS groups showed a significant reduction after 48h in comparison with the initial cell seeding number ($p = 0.000$). These results showed that 2.5% and 1.25% FBS negatively affected cell viability and growth, but not 5%. Hence, the 5 and 10% FBS conditions were chosen for the subsequent experiments as they induced cell viability and cell growth.

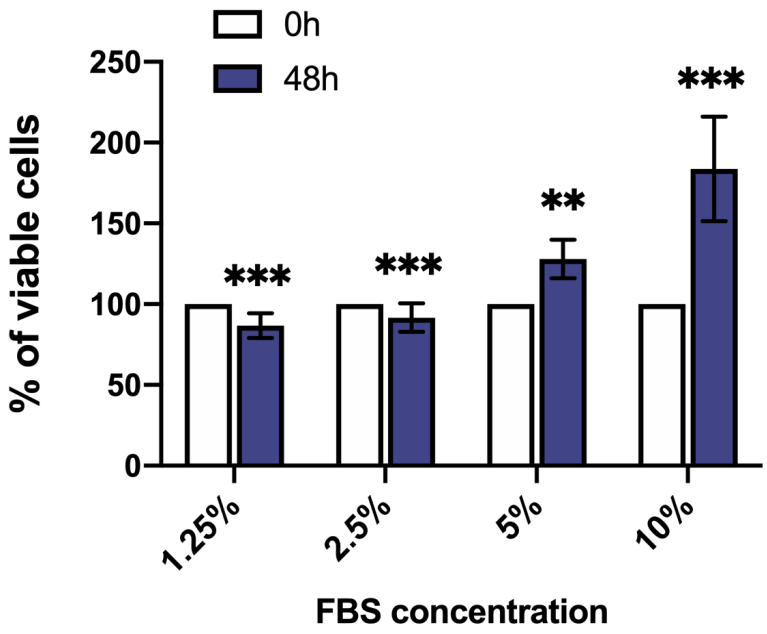

Figure 3.3 Effects of FBS concentrations on cell numbers. The viable cell numbers were significantly greater in 10% and 5% FBS groups and lower in 2.5% and 1.25% after 48h. Data (n = 9) are analysed by Mann-Whitney test and presented as mean ± SD and the statistical significance: *$p < 0.05$, **$p < 0.01$, and ***$p < 0.001$.

3.2.2. Cell viability of differentiated groups

To assess the effect of the differentiation methods on cell viability with the two selected FBS conditions (5% and 10%), AlamarBlue assay was used to represent the percentage of viable cell numbers. The calibration/standard curve (Figure 3.4) was performed using known cell number densities (0, 12500, 25000, 50000, and 100000 cells) of SH-SY5Y neuroblastoma cell line. The cells were seeded in a 96-well plate and preincubated at 37 °C with 5% CO_2 for 6h to allow the cells to adhere to the cell culture surface. Subsequently, the assay and calculations were conducted as previously mentioned in the section 2.4, chapter 2. The average of % AB absorbance per each group was used to generate the calibration/standard curve and statistically analyse to assess the linear relationship between the % AB absorbance and cell numbers using linear regression analysis.

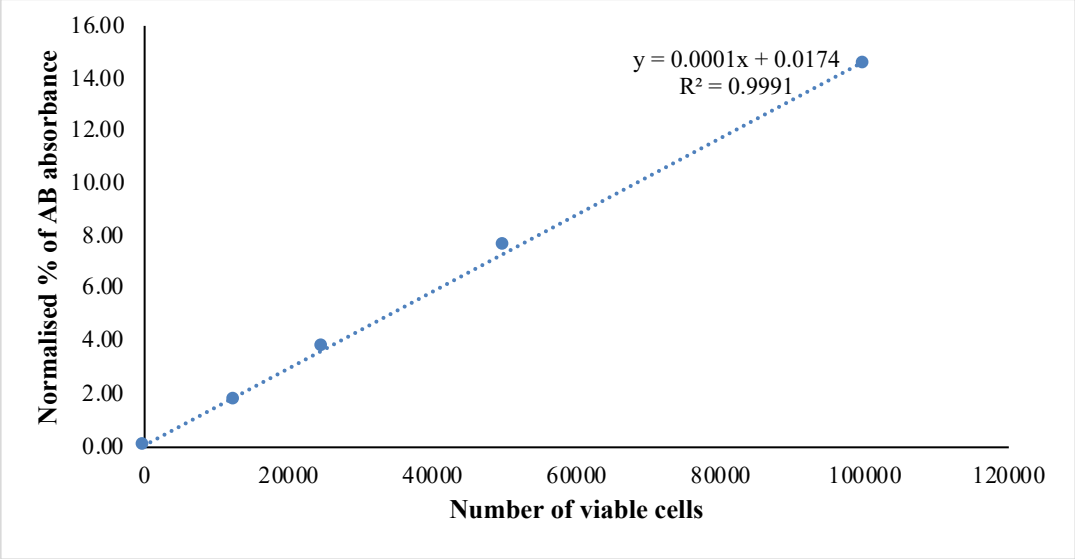

Figure 3.4 Representative calibration curve of AlamarBlue (AB) assay for SH-SY5Y neuroblastoma cell line to examine the calculated percentage of AB absorbance reflecting the change in the number of viable cells. The linear regression equation and R^2 coefficient (>0.9) are shown next to the line of the best fit of all different cell densities' means.

The 10% FBS supplemented or pre-supplemented (in ATRA stage) groups had significantly higher percentage of viable cells than their counterpart groups in 5% FBS condition ($p = 0.000$) (Figure 3.5). The sequential exposure (ATRA→BDNF) groups in both FBS conditions demonstrated significantly higher percentage of viable cells than their controls (ATRA→0% serum) ($p = 0.042$ for 5% and 0.000 for 10% FBS), however they showed significantly lower viable cells than the standard cell culture controls ($p = 0.000$). Although the percentage of viable cells in ATRA→BDNF group in the 10% FBS group was significantly less than that of the standard 10% FBS culture, percentage of viable cells were significantly more than that of the standard 5% FBS cell culture ($p = 0.001$). These data indicated that the 10% FBS pre-/supplemented groups maintained more viable cells than 5% FBS groups, and the 10% FBS sequential treatment (ATRA→BDNF) preserved a considerable cell viability for the differentiated cells.

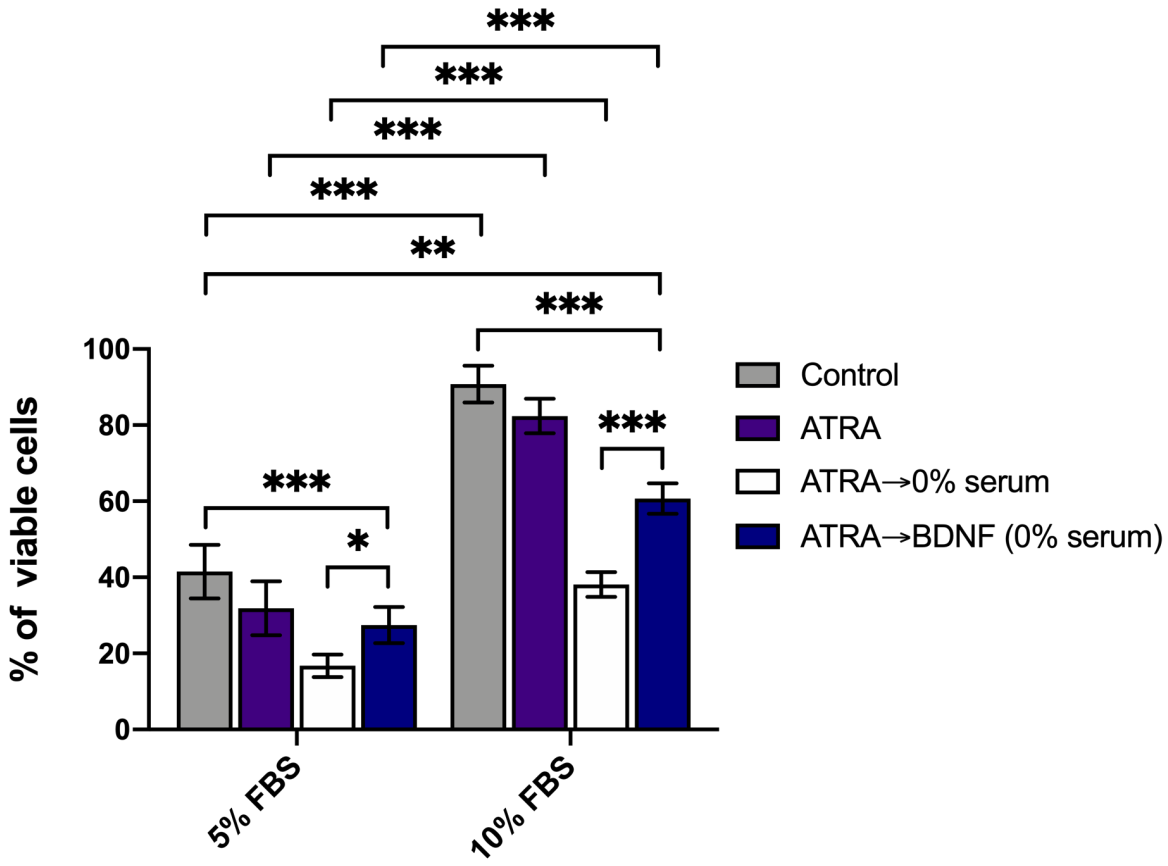

Figure 3.5 Viable cell percentage in the SH-SY5Y differentiation groups. The 10% FBS pre-/supplemented groups were highly significant than their similar 5% FBS groups (Kruskal-Wallis test with pairwise comparison; the significance values were adjusted by Bonferroni correction for multiple tests. The data are plate-reader absorbance values, and these values were then calculated to have a percentage of the mean ± SEM (n = 30; *$p < 0.05$, ** $p < 0.01$, and *** $p < 0.001$).

3.2.3. Neuronal morphological changes

To assess the neuronal morphological characteristics after neuronal differentiation, phase contrast images were captured, and images were analysed using FIJI ImageJ software to measure the neurite extension length and determine the percentage of the differentiated cells (defined as cells with one or more neurite of length ≥ 50μm).

Regarding FBS concentration effect, no noticeable difference in the morphological appearance between the similar groups in both conditions (5 and 10% FBS) was noted. The

10% FBS pre-/supplemented groups (ATRA alone or ATRA→BDNF) demonstrated more cells with neurite extensions in comparison with the similar groups in 5% FBS condition (Figure 3.6A-H). However, image analysis revealed that there was also no statistically significant difference between the similar groups in both FBS conditions in neurite length (p = 0.66 between ATRA groups and p = 1 between ATRA→BDNF groups) or percentage of the cell with neurite(s) (p = 0.64 between ATRA groups and p = 0.37 between ATRA→BDNF groups) (Figure 3.7A-B). These results indicated that the higher number of differentiated neuronal-like cells in 10% FBS groups did not mean higher neuronal characteristics (neurite length and percentage of differentiated cells). Consequently, there was no difference in the neuronal differentiation between 5% and 10% FBS groups.

The 5% FBS control cell culture (without differentiating supplement) showed an increase in neurite length. This increase was not significantly higher than the 10% FBS control (p = 0.06) nor ATRA→0% serum group in both FBS concentrations (p = 0.68 in 5% FBS and p = 0.88 in 10% FBS group) (Figure 3.7A). This result indicated that the FBS reduction alone in the SH-SY5Y cell culture can induce neurite outgrowth, albeit is not statistically higher compared with the 10% FBS control groups.

The two differentiation protocols (ATRA alone or ATRA→BDNF) clearly resulted in the cells acquiring extended neuritic projections (Figure 3.6C, D, G, and H) compared with the untreated cell cultures (Figure 3.6A-B). Nevertheless, the two-stage protocol (ATRA followed by BDNF) groups showed the highest level of differentiation. This neuronal differentiation was demonstrated by the emergence of a homogenous cell population with typical neuronal morphological features which included a phase-bright cell body with extended neurite and neurite arborization forming intercellular network (Figure 3.6G-H). The ATRA groups

displayed heterogeneous cell population of less differentiated cells (more likely N-type) as demonstrated by having less phase-bright cell bodies with extended neurites with no apparent intercellular network. There were also other undifferentiated cells (more likely S-type) which resembled glial cells rather than neuronal cells (Figure 3.6C-D). The control group (ATRA followed by serum-free media) displayed a considerable loss of the differentiated cells with their extensions as seen with ATRA step (Figure 3.6E-F). These morphological observations were confirmed by image analysis (Figure 3.7A-B). Regardless of the FBS conditions, the ATRA group demonstrated significantly higher neurite length (p = 0.014 in 5% FBS and p = 0.005 in 10% FBS group) and percentage of the cell with neurite(s) than control groups (p = 0.049 in 5% FBS and p = 0.018 in 10% FBS group). However, the two-stage protocol (ATRA followed by BDNF) revealed the highest significant difference among groups (p = 0.000 for Neurite length, and percentage of cell with neurite).

These data indicated that the differentiated SH-SY5Y cells acquired comparable neuronal morphological hallmarks in both FBS conditions, and the sequential treatment approach (ATRA→BDNF) induced the highest neuronal morphological features.

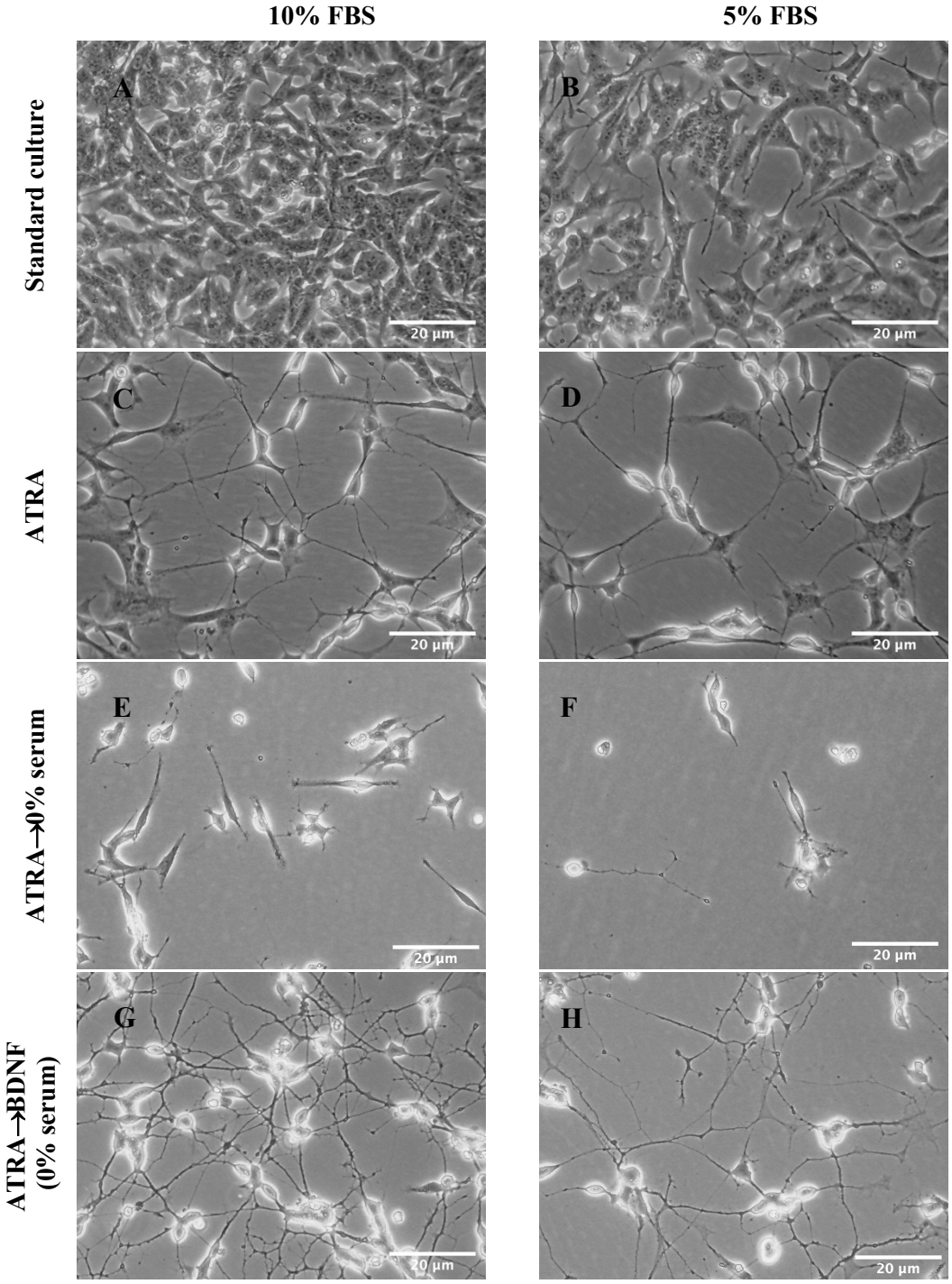

Figure 3.6 Representative morphological appearance of the differentiation groups as evaluated by phase-contrast microscopy. (A-B) non-treated cell culture. (C-D) ATRA groups showed differentiated N-type cells and undifferentiated S-type cells. (E-F) ATRA→0% serum demonstrated a loss of cells and neurites in the absence of FBS or BDNF. (G-H) ATRA→BDNF groups revealed the most extensive and elongated neurites with homogenous neuronal-like cell population. It was also evident that 10% FBS produced a greater number of differentiated cells (G) than 5% FBS (H). Scale bars are shown.

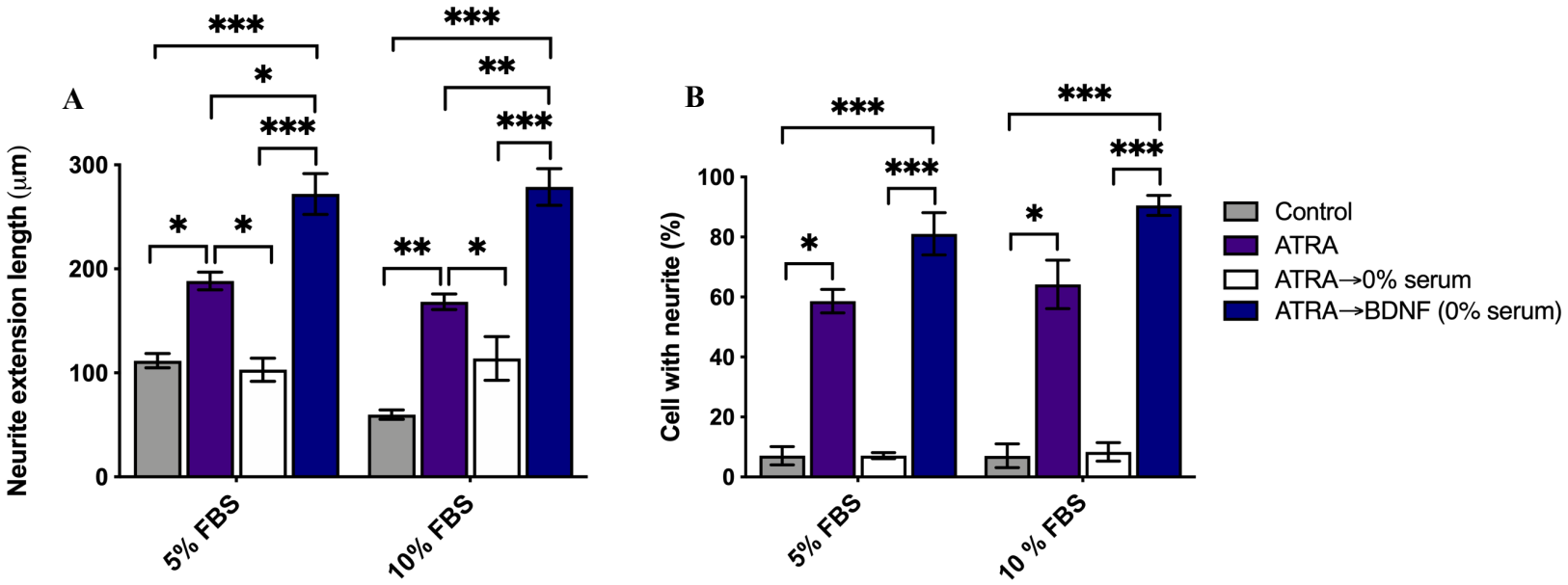

Figure 3.7 Quantitative image analysis of neurite length and percentage of the cell with neurite(s). The image analysis was performed on captured phase contrast images at 10x magnification to measure the neurite extension length (A) and percentage of cell with neurite (B). The ATRA→BDNF groups showed the most significant increase in the average of the neurite length (One-way ANOVA: the F ratio is 51.09 with 7 and 78 degrees of freedom (df)). (A), and the percentage of differentiated cells "neurite-bearing cells" (Kruskal-Wallis test with pairwise comparison; the significance values were adjusted by Bonferroni correction for multiple tests (B). The data are mean ± SEM (n = 11; *$p <$ 0.05, **$p < 0.01$, and ***$p < 0.001$).

3.2.4. Immunocytochemistry

To investigate the expression of neuronal protein markers[2], immunofluorescence staining was performed using general neuronal cytoskeleton marker (βIII-tubulin/TUBB3), mature marker (NF-M) and glial astrocyte cell marker (GFAP).

Immunocytofluorescence staining showed that the immunopositivity of neuronal markers (TUBB3, NF-M, and GFAP) were comparable between the similar groups in both FBS conditions (10% and 5% FBS) **(**Figure 3.8 - Figure 3.11). Regarding the expression of the differentiated groups, the ATRA treatment increased expression of neuronal protein markers (TUBB3 and NF-M) in comparison with the control. TUBB3 and NF-M was highly expressed in the differentiated N-type cells with their evident neurites but not in the undifferentiated S-type cells of the same cell culture. Whereas the sequential differentiation approach (ATRA→BDNF) produced the highest extensive uniform expression of both neuronal markers (TUBB3 and NF-M) in the differentiated N-type cells with fewer numbers of undifferentiated S-type cells (Figure 3.8 and Figure 3.9).

In contrast, the GFAP expression (glial astrocyte cell marker) was only weakly detected in the controls and was reduced in both differentiated groups (ATRA alone and ATRA→BDNF) for both FBS concentrations (Figure 3.10 and Figure 3.11). The accompanying βIII-tubulin (TUBB3) expression confirmed the observations reported above. These data suggested that the ATRA followed by BDNF protocol induced the highest neuronal differentiation toward mature neuronal cells rather than glial cells. Next, the expression of these neuronal markers were also investigated by quantitative gene expression along with other neuronal-related markers to profile and confirm the neuronal nature of these models.

[2] The references of the specificity of the neuronal markers are mentioned in Appendix II.

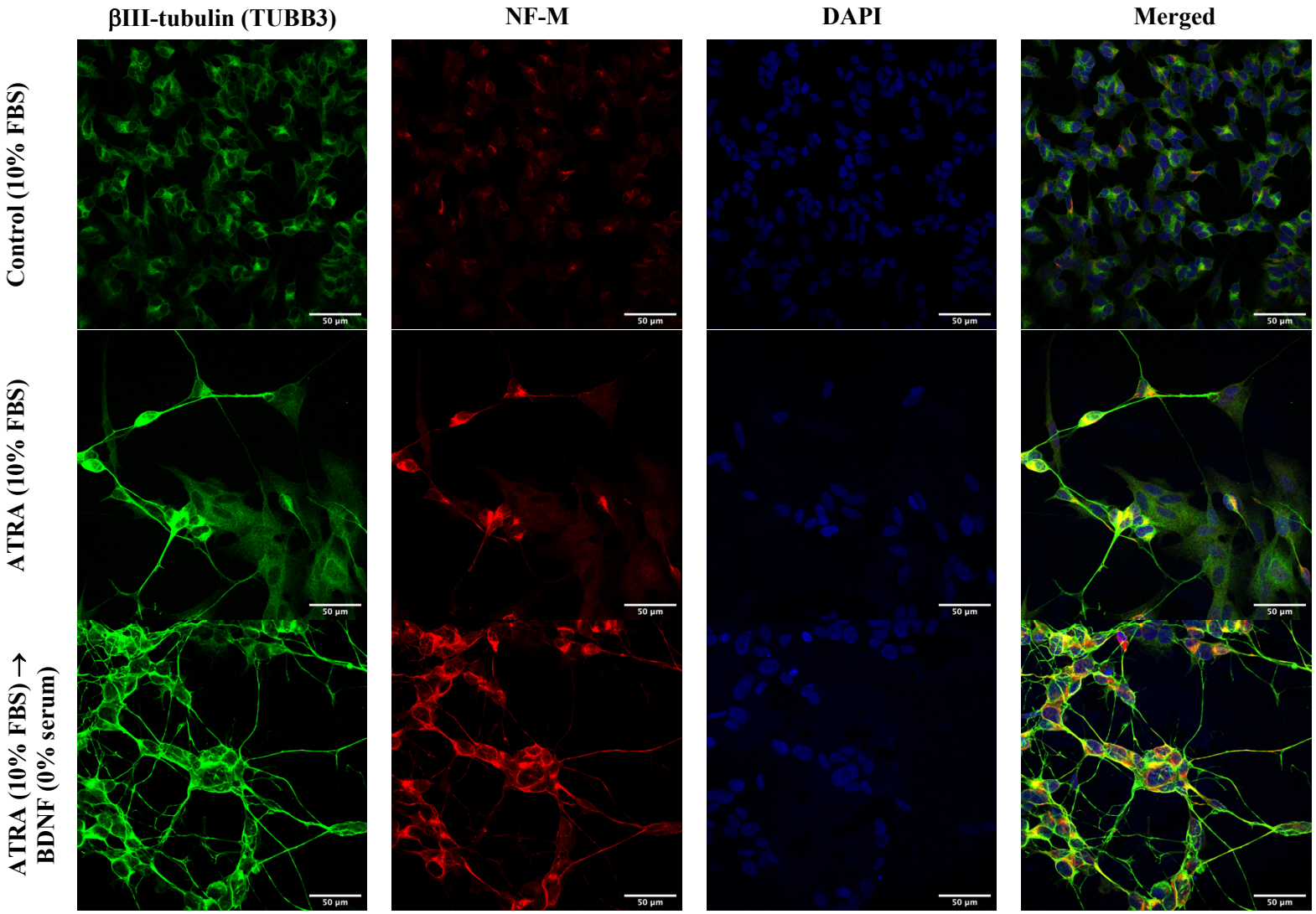

Figure 3.8 Immunocytofluorescence expression analysis of TUBB3 and NF-M neuronal markers in 10% FBS pre-/supplemented groups. The ATRA→BDNF treatment approach induced the highest immunopositive staining amongst the groups; TUBB3 and NF-M were highly expressed in the differentiated N-type cells, but not in the undifferentiated S-type cells in the ATRA group. Scale bars are shown.

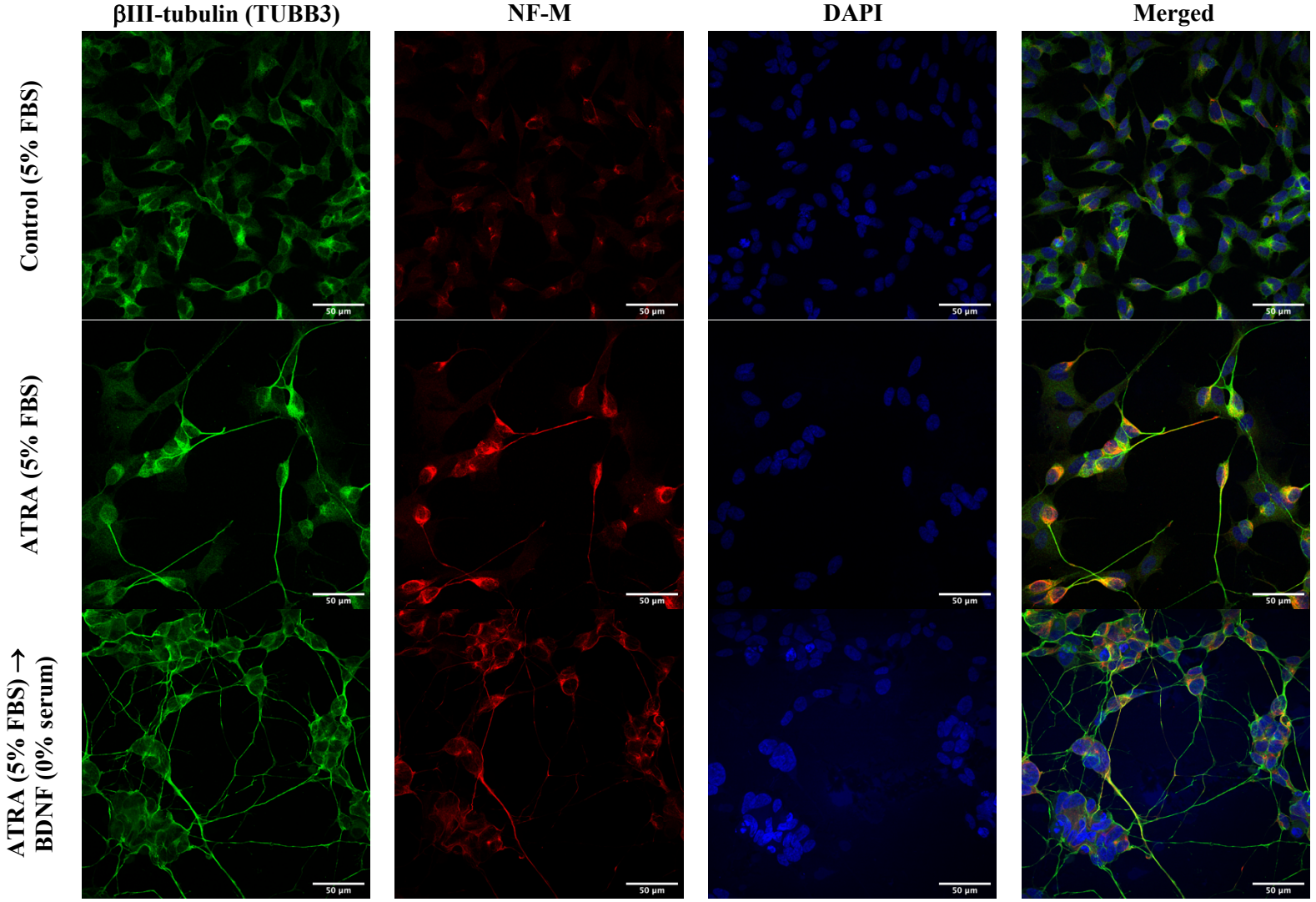

Figure 3.9 Immunocytofluorescence expression analysis of TUBB3 and NF-M neuronal markers in 5% FBS pre-/supplemented groups. The ATRA→BDNF approach produced the highest immunostaining and TUBB3 and NF-M were highly expressed in the differentiated N-type cells, but not in the undifferentiated S-type cells in the ATRA group. Scale bars are shown.

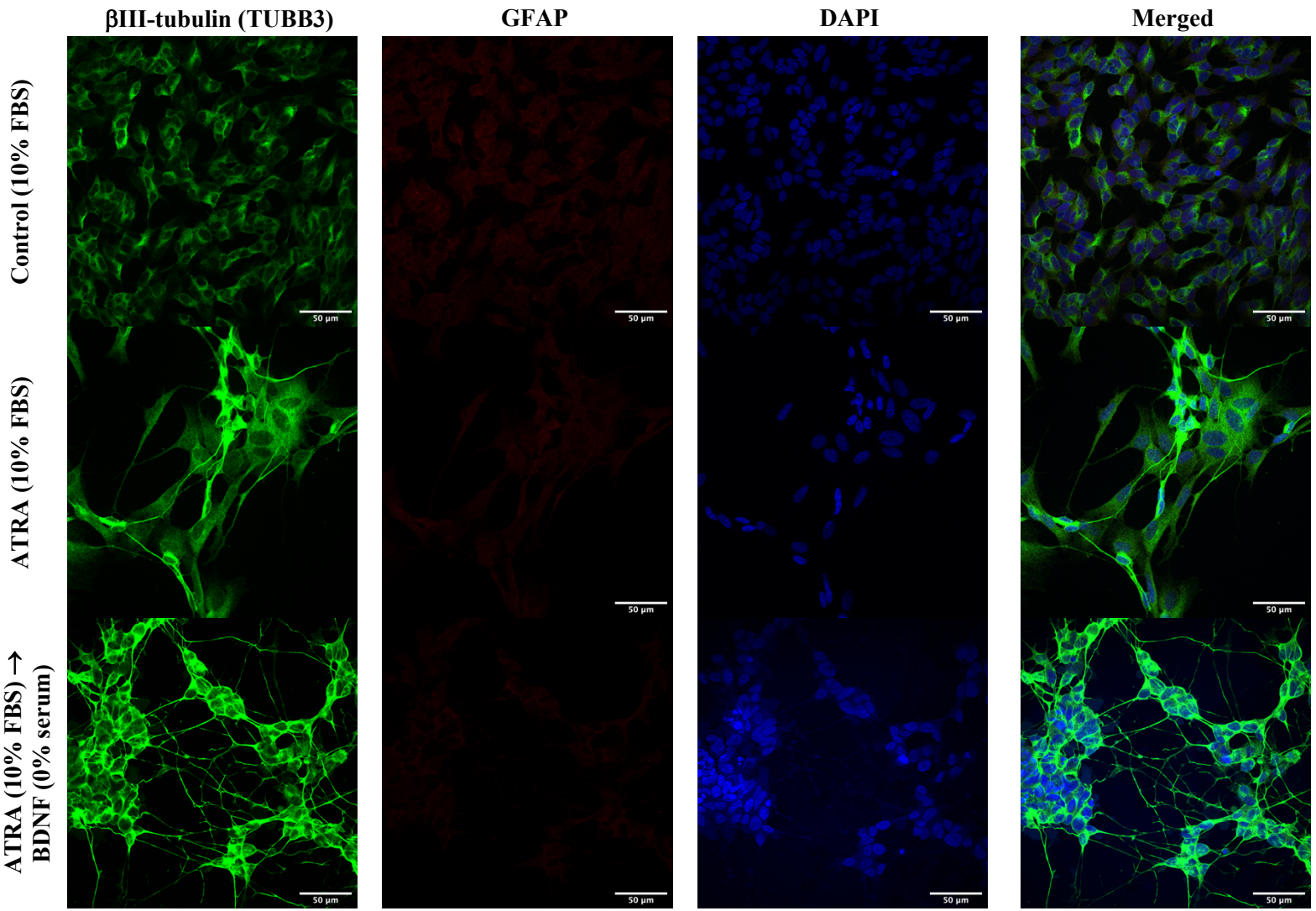

Figure 3.10 Immunocytofluorescence expression analysis of GFAP astrocyte marker in 10% FBS pre-/supplemented groups along with TUBB3 to express the cytoskeleton. Differentiated SH-SY5Y cells demonstrated reduction of the glial astrocyte marker (GFAP) in comparison with the weak expression in control. The ATRA→BDNF group displayed the lowest GFAP staining. Scale bars are shown.

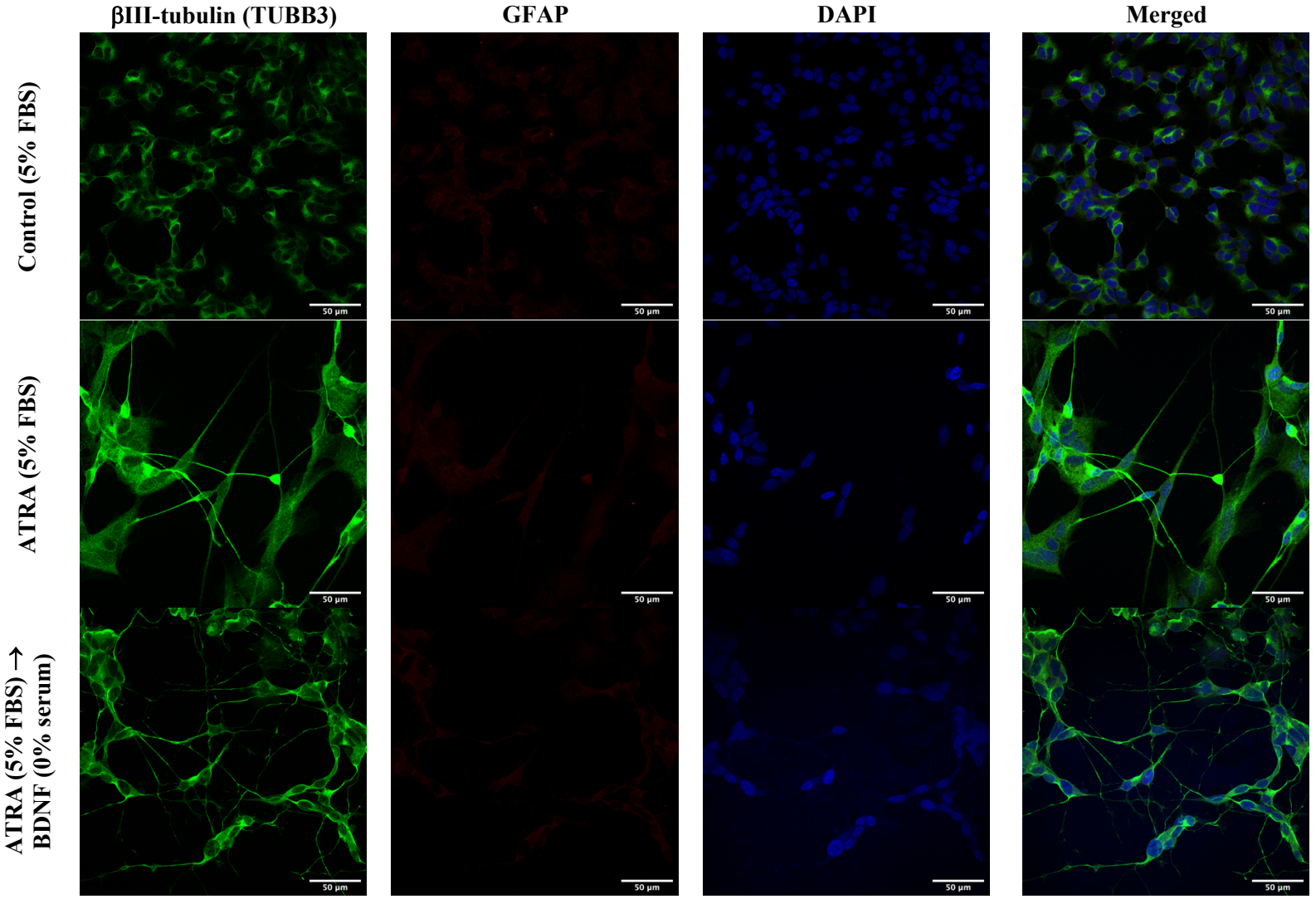

Figure 3.11 Immunocytofluorescence staining of the GFAP astrocyte marker in 5% FBS pre-/supplemented groups. Control cells showed minimal staining of GFAP while differentiated SH-SY5Y cells revealed reduction of GFAP in the ATRA group, and more in ATRA→BDNF group. Scale bars are shown.

3.2.5. Neuronal gene expression

Quantitative PCR analysis (Figure 3.12 - Figure 3.16) was conducted to determine whether there was a difference in gene expression levels for specific neuronal markers[3] between both FBS conditions (10% and 5%) and the differentiation models (ATRA alone and ATRA→BDNF).

Regarding the FBS effect, the differentiated groups of 10% FBS groups displayed significant higher gene expression upregulation for mature neuron specific marker (ENO2) compared with those of the 5% FBS treatment groups (p = 0.019 between ATRA groups and 0.004 between ATRA→BDNF groups) (Figure 3.13). The general cytoskeleton (TUBB3) and peripheral nervous system (PRPH) markers were also expressed at significantly higher levels in 10% FBS ATRA than in 5% FBS ATRA group (p = 0.000 for TUBB3 and 0.002 for PRPH) (Figure 3.12 and Figure 3.16). The sensory voltage-gated sodium channel sodium (SCN9A) was significantly upregulated in 10% FBS ATRA→BDNF group (p = 0.010) but not in 5% FBS ATRA→BDNF group (p = 0.263). In contrast, the synaptic marker (SYN1) was significantly increased in 5% FBS ATRA compared with the 10% FBS ATRA group (p = 0.036) (Figure 3.15). However, the vast majority of the other neuronal markers revealed no difference in the gene expression between the similar groups in both FBS conditions. These results indicated that there was no clear difference between the FBS level conditions and FBS level concentration did not affect gene expression of the neuronal markers.

In the differentiation models, the ATRA alone and ATRA→BDNF methods induced statistically significant upregulation in gene expression of the following neuronal markers: neuroepithelial (NES), development (RET), mature (NF-M and ENO2), cholinergic (ACHE

[3] The references of the specificity of the neuronal markers are mentioned in Appendix II.

and CHAT), synaptic (SYN1 and SNAP-25), nociceptive voltage-gated sodium ion channel (SCN9A), general cytoskeleton (TUBB3) and peripheral nervous system (PRPH)[4] markers (Figure 3.12 - Figure 3.16). However, the growth (GAP-43) marker was only significantly increased in the ATRA→BDNF treatment group (GAP-43: $p = 0.012$ in 5% and 0.008 in 10% FBS) (Figure 3.12). This GAP-43 gene upregulation in ATRA→BDNF group was also significantly higher than ATRA group ($p = 0.019$ in 5% and 0.001 in 10% FBS). In contrast, GFAP was significantly reduced for both differentiation methods ($p = 0.011$ for ATRA and 0.004 for ATRA→BDNF group in 5% FBS whereas $p = 0.000$ for ATRA and ATRA→BDNF in 10% FBS) (Figure 3.13). The other neuronal markers (dendritic: MAP2, adrenergic/norepinephrine: DBH, dopaminergic: DAT, general neuronal voltage-gated sodium channel: SCN1A, sensory marker: POU4F1, and motor: MNX1) showed no to minimal change (Figure 3.13 - Figure 3.16). These gene expression data suggested that the sequential supplementation method (ATRA→BDNF) induced more neuronal gene upregulations than ATRA alone method.

[4] *NES*: $p = 0.000$ was for ATRA and ATRA→BDNF groups in 5% FBS and $p = 0.000$ was for ATRA and 0.001 was for ATRA→BDNF group in 10% FBS, *RET*: $p = 0.000$ was for ATRA groups in both FBS and $p = 0.047$ was for 5% FBS ATRA→BDNF group whereas $p = 0.017$ was for 10% FBS ATRA→BDNF group, *NF-M*: $p = 0.005$ was for ATRA and 0.004 was for ATRA→BDNF group in 5% FBS whereas $p = 0.000$ was for ATRA and $p = 0.047$ was for ATRA→BDNF groups in 10% FBS, *ENO2*: $p = 0.000$ was for ATRA and 0.002 was for ATRA→BDNF in 10% FBS, *ACHE*: $p = 0.000$ was for ATRA and 0.021 was for ATRA→BDNF in 5% FBS whereas $p = 0.000$ was for ATRA and 0.003 was for ATRA→BDNF in 10% FBS, *CHAT*: $p = 0.043$ was for ATRA and 0.005 was for ATRA→BDNF in 5% FBS whereas $p = 0.000$ was for ATRA and 0.047 was for ATRA→BDNF in 10% FBS, *SYN1*: $p = 0.000$ was for ATRA and 0.003 was for ATRA→BDNF in 5% FBS whereas $p = 0.000$ was for ATRA and 0.043 for ATRA→BDNF in 10% FBS, *SNAP-25*: $p = 0.000$ was for ATRA and 0.006 was for ATRA→BDNF in 5% FBS whereas $p = 0.000$ was for ATRA and 0.001 was for ATRA→BDNF in 10% FBS, *SCN9A*: $p = 0.001$ was for 5% FBS ATRA whereas $p = 0.000$ was for ATRA and 0.039 was for ATRA→BDNF in 10% FBS, TUBB3: $p = 0.007$ in 5% ATRA→BDNF, 0.004 in 10% FBS ATRA, and 0.000 in ATRA→BDNF, *PRPH*: $p = 0.015$ was for 5% FBS ATRA→BDNF whereas $p = 0.000$ was for ATRA and 0.033 was for ATRA→BDNF in 10% FBS.

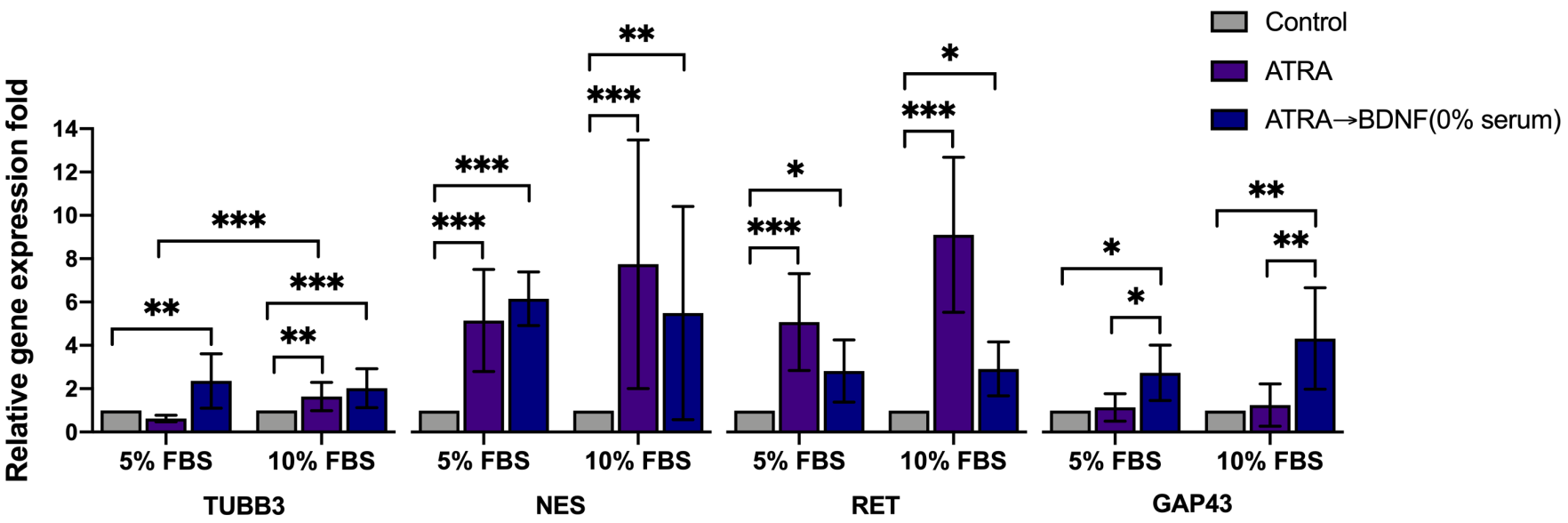

Figure 3.12 Neuronal gene expression following neurogenic induction analysed by real-time qPCR. The differentiated SH-SY5Y cells demonstrated significant upregulation in the neuroepithelial (NES), and neuronal development (RET) gene markers whereas the general cytoskeleton (TUBB3) and growth (GAP43) gene markers were only significantly increased in ATRA→BDNF group. Moreover, there was no significant difference between 5% and 10% FBS except TUBB3 was significantly higher in 10% ATRA than 5% FBS ATRA. The gene expression fold calculations were normalised against two housekeeping genes (HPRT1and RPLA13). The data are mean ± SD analysed by Kruskal-Wallis test with pairwise comparison; the significance values were adjusted by Bonferroni correction for multiple tests (n = 9; *$p < 0.05$, **$p < 0.01$, and ***$p < 0.001$).

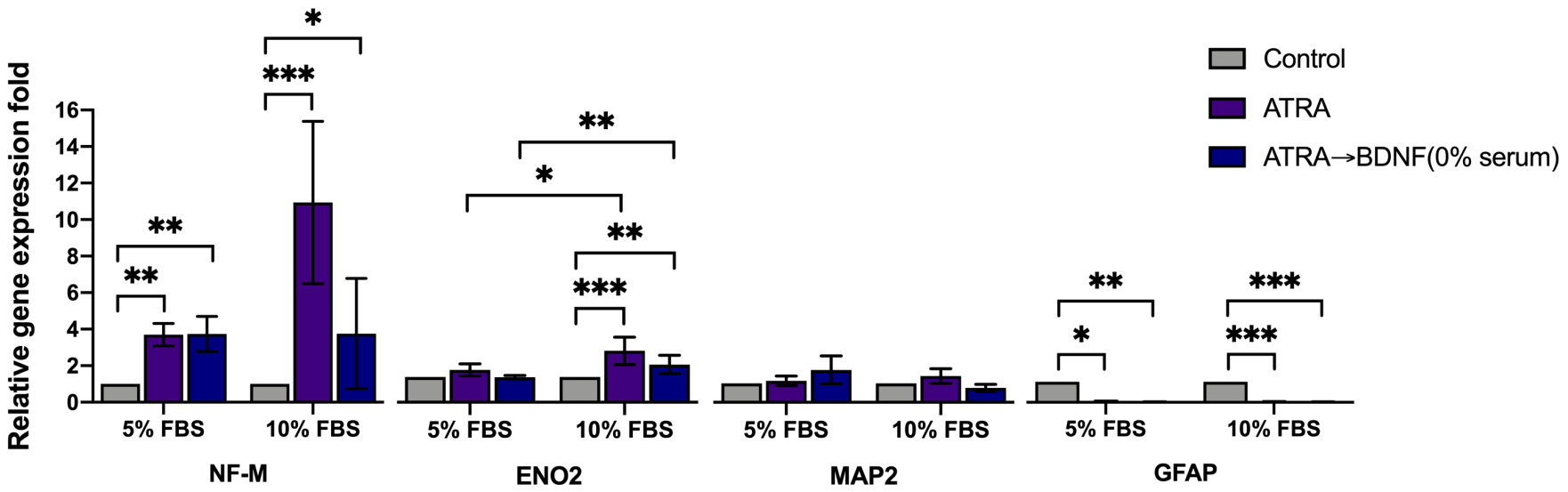

Figure 3.13 Mature neuronal and astrocyte gene expression following neurogenic induction analysed by real-time qPCR. There was no significant difference in gene expression between 5% and 10% FBS groups except ENO2 neuronal marker was significantly higher in 10% than 5%. All maturation gene makers of the main neuronal cells (NF-M and ENO2) except dendritic marker (MAP2) were significantly upregulated in ATRA and ATRA→BDNF differentiated groups whereas the glial astrocyte gene (GFAP) was reduced in both differentiation methods. This significant increase in mature gene expression and decrease in glial neuronal gene markers in both differentiated groups indicated that the differentiation was induced toward mature neuronal main cells rather than glial cells. The gene expression fold calculations were normalised against two housekeeping genes (HPRT1 and RPLA13). The data are mean ± SD analysed by Kruskal-Wallis test with pairwise comparison; the significance values were adjusted by Bonferroni correction for multiple tests (n = 9, except for NF-M, n= 6; *$p < 0.05$, **$p < 0.01$, and ***$p < 0.001$).

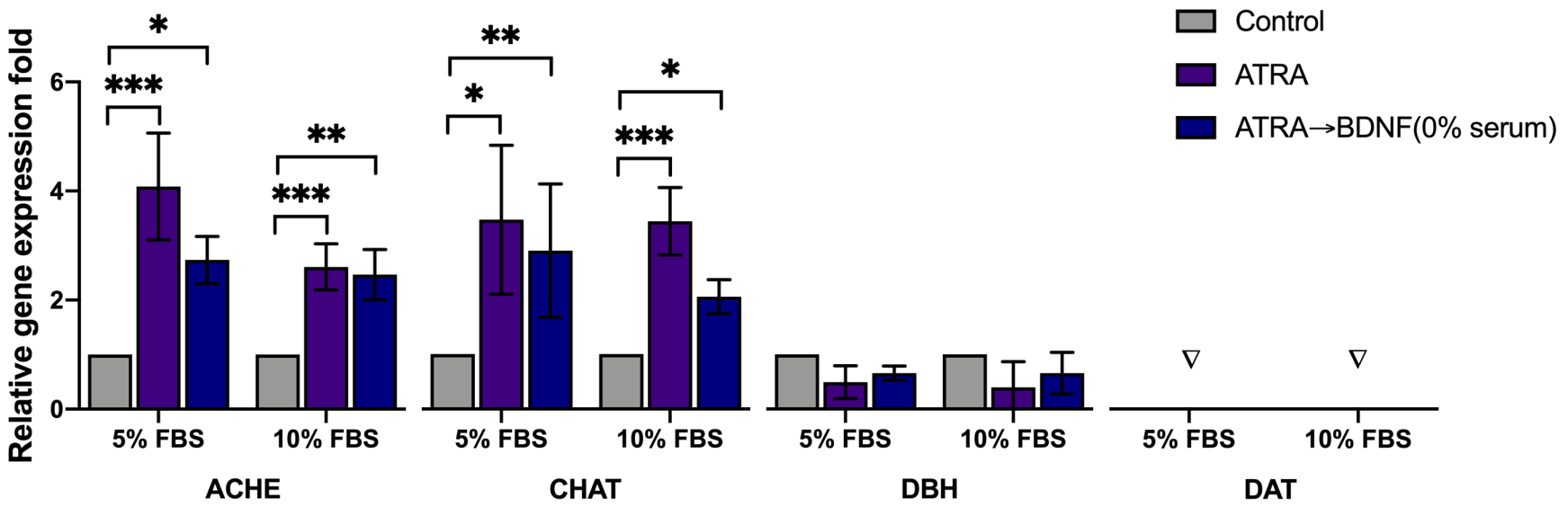

Figure 3.14 Neurotransmitter gene expression following neurogenic induction analysed by real-time qPCR. There was no difference between 5% and 10% FBS groups in the gene expression of the neurotransmitter gene markers. The differentiated groups revealed upregulation in the cholinergic markers (ACHE and CHAT) and reduction in adrenergic (DHB) marker whereas the dopaminergic (DAT) marker was not detected. This indicate that the differentiated cells were specifically cholinergic neuronal-like cells. The gene expression fold calculations were normalised against two housekeeping genes (HPRT1 and RPLA13). The data are mean ± SD analysed by Kruskal-Wallis test with pairwise comparison; the significance values were adjusted by Bonferroni correction for multiple tests (ACHE: n = 6, CHAT: n = 3, and DBH: n= 9; *$p < 0.05$, **$p < 0.01$, and ***$p < 0.001$). Note: ∇ indicates not detected.

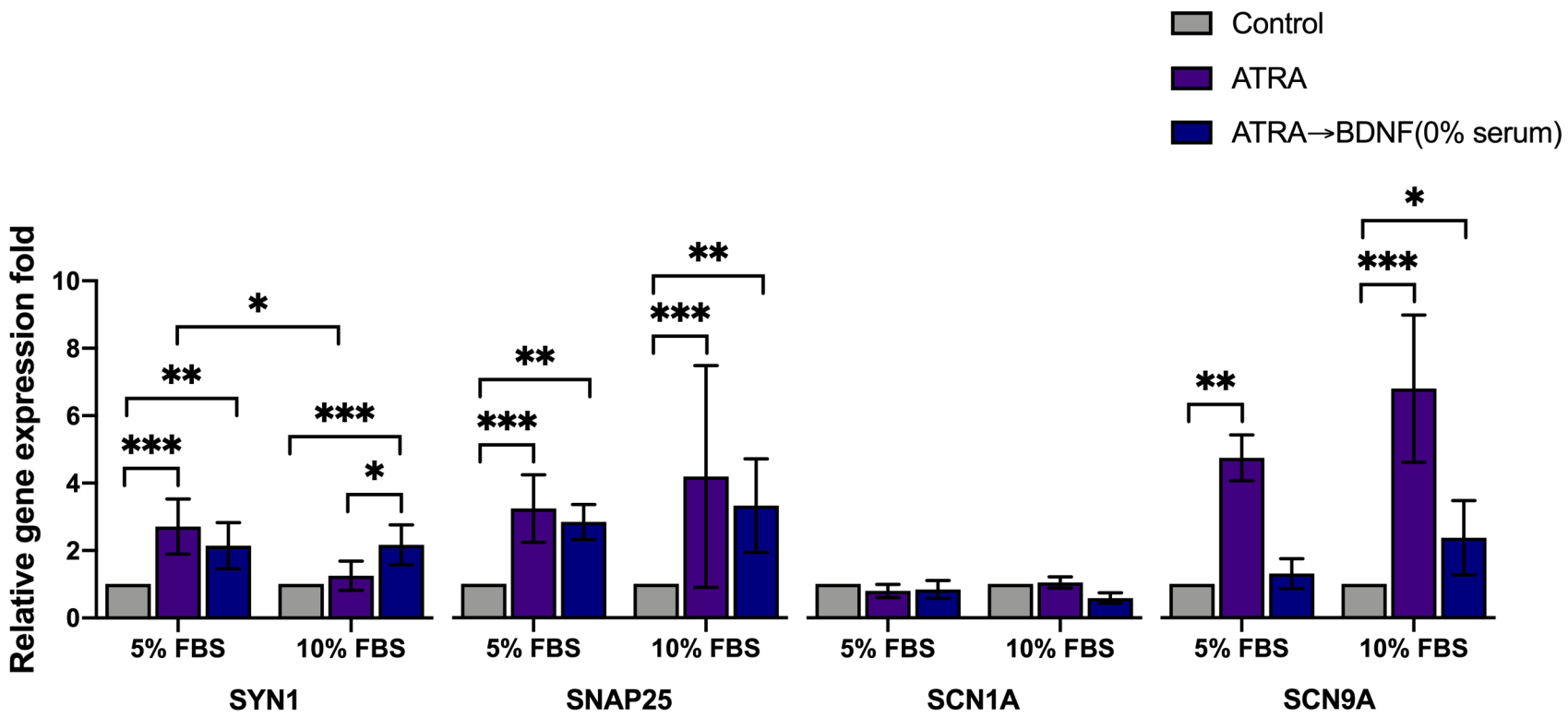

Figure 3.15 Synaptic and voltage-gated Na^{+2} channels gene expression following neurogenic induction analysed by real-time qPCR. There was no significant difference in gene expression between 5 and 10% FBS groups except synaptic marker (SYN1) which was higher in 5% FBS ATRA than 10% FBS ATRA. The differentiated SH-SY5Y cells demonstrated significant upregulation in synaptic (SYN1 and SNAP25) and sensory voltage-gated sodium channel (SCN9A) markers, but not general neuronal voltage-gated sodium channel (SCN1A). This indicated that the differentiated cells were sensory neuronal-like cells. The gene expression fold calculations were normalised against two housekeeping genes (HPRT1 and RPLA13). The data are mean ± SD analysed by Kruskal-Wallis test with pairwise comparison; the significance values were adjusted by Bonferroni correction for multiple tests (n = 9, except for SCN1A, n = 3; *$p < 0.05$, **$p < 0.01$, and ***$p < 0.001$).

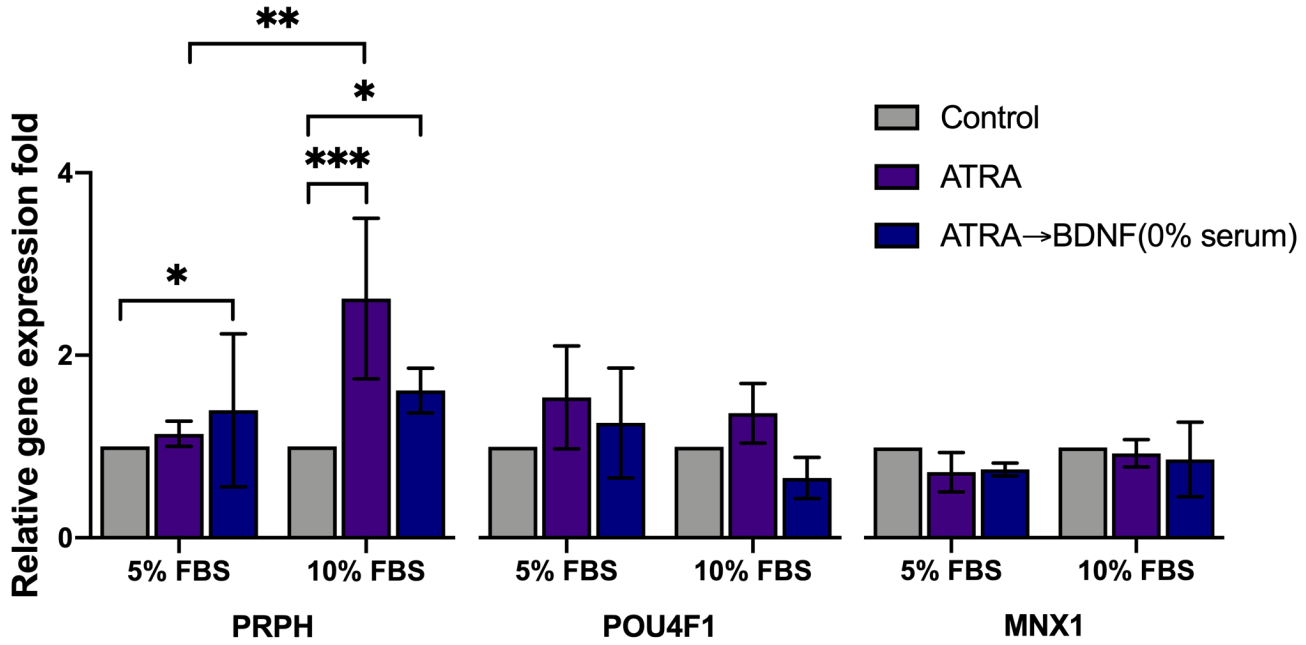

Figure 3.16 Sensory and motor gene expression following neurogenic induction analysed by real-time qPCR. There was no difference in sensory and motor gene expression between 5 and 10% FBS groups except PRPH which was only significantly higher in 10% FBS ATRA than 5% FBS ATRA. The differentiated SH-SY5Y cells showed significantly increase in expression of the peripheral nervous system maker (PRPH) and decrease in motor marker (MNX1) expression. This indicate the resultant neuronal-like cells are not motor neuronal-like cells. The gene expression fold calculations were normalised against two housekeeping genes (HPRT1 and RPLA13). The data are mean ± SD analysed by Kruskal-Wallis test with pairwise comparison; the significance values were adjusted by Bonferroni correction for multiple tests (PRPH: n = 9, POU4F1 and MNX1: n = 3; *$p < 0.05$, **$p < 0.01$, and ***$p < 0.001$).

3.2.6. Quantitative neurite outgrowth staining assay

The neurite outgrowth assay was performed for the 10% FBS treatment groups to support the image analysis of neuronal morphological changes. The assay results indicated that the ATRA→BDNF treatment resulted in the highest outgrowth among all groups and showed significant differences compared with both controls (10% FBS standard culture: $p = 0.001$ and ATRA→0% serum: $p = 0.011$), however it was not significantly higher than ATRA alone approach ($p = 0.073$) (Figure 3.17). This assay also demonstrated that there was a significant reduction in the cell viability of the ATRA→0% serum control ($p = 0.000$) and ATRA→BDNF ($p = 0.02$) groups in comparison with the standard 10% FBS culture (Figure 3.17). This data suggested that the sequential treatment (ATRA→BDNF) induced a significant neurite outgrowth which confirmed the quantitative image analysis findings. Also, the cell viability of this assay showed the same trend results previously obtained by the AlamarBlue assay which demonstrated reduction in cell viability with differentiation (section 3.2.2).

3.2.7. Neuronal electrophysiological recording

To evaluate the neuronal functionality of the differentiated cells in comparison with undifferentiated controls (standard cell culture), the I-V relationships of voltage-dependent sodium and potassium currents were recorded using the whole-cell patch-clamp (Figure 3.18A-B).

The inward voltage-dependent sodium currents were detected in all groups and activated at a threshold between -40 and -20 mV (Figure 3.18C). However, a statistically significant increase was only observed at membrane potentials of −10 to +20 mV in control and ATRA groups, and of −10 to +40 mV in sequential protocol of ATRA and then BDNF group (Friedman repeated measure ANOVA, $X^2 = 135.28$ for control, 156.96 for ATRA, 143.25 for BDNF, df

(10), $p = 0.000$). A peak value (negative value) was measured as follows: control (-7.83 ± 1.79 pA/pF), ATRA (-10.05 ± 2.02 pA/pF), and ATRA→BDNF (-19.93 ± 3.80 pA/pF). These sodium-current recordings were also compared between groups. The ATRA→BDNF group was significantly higher than control ($p = 0.019 \pm 0.005$) and ATRA treatment groups ($p = 0.025 \pm 0.013$), and no significant difference between control and ATRA groups ($p = 1$) (Figure 3.18C).

Similarly, the outward voltage-dependent potassium currents were detected in all groups, which were triggered at a membrane potential of -20 mV (Figure 3.18D). The significant increase was reached at 0 mV for control ($p = 0.005$) and at -10 mV for ATRA ($p = 0.016$) and ATRA→BDNF groups ($p = 0.003$), and then more significant positive currents (Friedman repeated measure ANOVA, $X^2 = 164.459$ for control, 164.863 for ATRA, 228.075 for ATRA→BDNF, df (11), $p = 0.000$). The peak value of 16.72 ± 3.3.99 pA/pF, 19.59 ± 5.25 pA/pF, 46.31 ± 6.79 pA/pF was measured for control, ATRA, and ATRA→BDNF groups, respectively. The outward potassium recordings in the ATRA→BDNF group were significantly higher than in control ($p = 0.001$) and ATRA groups ($p = 0.024 \pm 0.015$) (Figure 3.18D). Although the ATRA group induced marginally higher outward sodium currents than the control, this difference was not significant at all measuring voltages ($p = 0.928 \pm 0.073$).

Moreover, the sequential approach (ATRA→BDNF) promoted a significantly higher cell membrane capacitance (the cell membrane ability to respond to current impulses) than control and ATRA groups ($p = 0.000$), whereas there was no difference between control and ATRA groups ($p = 0.475$) (Figure 3.18E). These data suggested that the sequential method (ATRA→BDNF) induced the highest electrophysiological neuronal profile in SH-SY5Y cells.

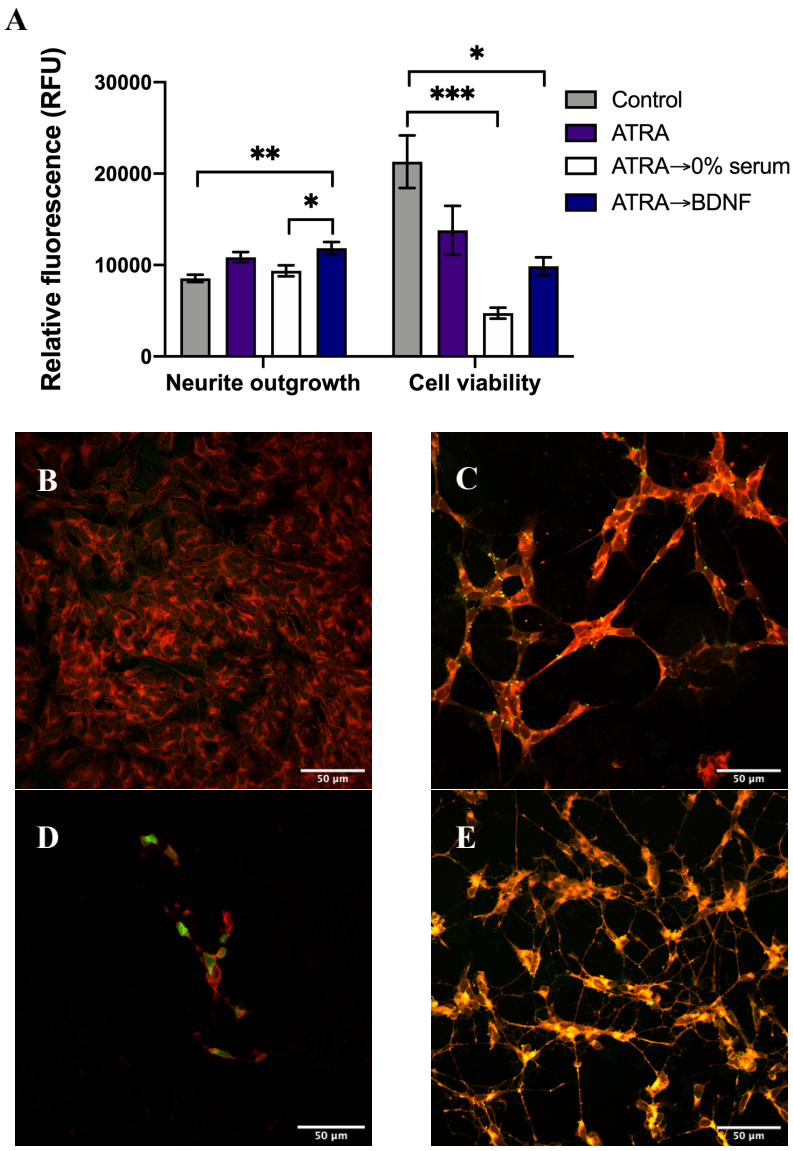

Figure 3.17 Neurite outgrowth assay (a plate reader quantification of neurite growth). (A) Relative quantification of neurite outgrowth and cell viability fluorescence intensity (orange-red fluorescent cell membrane stain indicator for neurite outgrowth, along with green stain indicator for cell viability; RFU = relative fluorescence unit). (B-E) Merged images are presented for a visual reference of the groups: (B) untreated control, (C) ATRA, (D) ATRA→0% serum, and (E) ATRA→BDNF. Data plotted are mean ± SEM analysed by Kruskal-Wallis test with pairwise comparison; the significance values were adjusted by Bonferroni correction for multiple tests (Neurite outgrowth: n = 9; cell viability: n = 8, except for ATRA→0% serum (n = 5); *$p < 0.05$, **$p < 0.01$, and ***$p < 0.001$). Scale bars are shown.

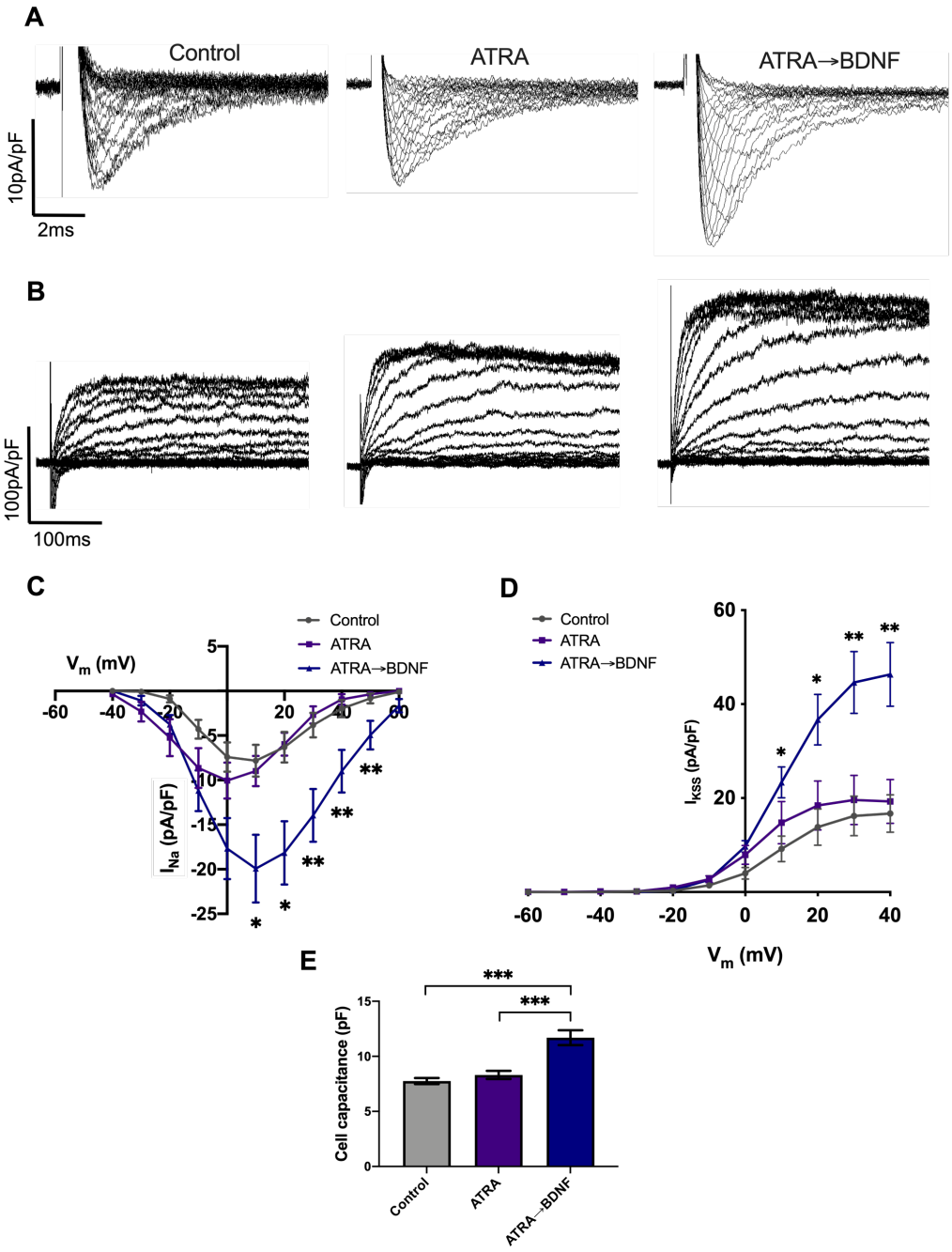

Figure 3.18 Electrophysiological membrane currents induced by neuronal differentiation. (A, B) Representative voltage-dependent sodium (A) and potassium currents (B) evoked in the experimental groups (control, ATRA, ATRA→BDNF) for visual reference. (C) The I-V relationship of inward sodium currents recorded in the experimental groups: control standard culture condition (n = 23), ATRA (n = 25), and ATRA→BDNF (n = 21). (D) The I-V relationship of outward potassium currents recorded in the groups: control (n = 22), ATRA (n = 18), and ATRA→BDNF (n = 23). (E) Cell membrane capacitance measured in the experimental groups: control (n = 45), ATRA (n = 43), ATRA→BDNF (n = 43). The comparison between groups in C, D and E graphs were analysed by Kruskal-Wallis test with pairwise comparison; the significance values were adjusted by Bonferroni correction for multiple tests. Data are mean ± SEM (*$p < 0.05$, **$p < 0.01$, and ***$p < 0.001$).

3.2.8. Selection of the maintenance media for the neuronal-like model

To determine the suitable maintenance media condition for subsequent experiments such as for the LIPUS study (see chapter 6), the selected SH-SY5Y neuronal model: ATRA (10% FBS)→BDNF (0% serum) was incubated in three different media conditions (BDNF with serum-free media, 10% FBS media, and 10% FBS ATRA-supplemented media). Subsequently, phase contrast images were captured after 24 and 72h incubation (Figure 3.19).

The images showed that to maintain the pre-produced neuronal morphological characteristics it was necessary to continuously culture the cells in BDNF with serum-free media (Figure 3.19A-B). In contrast, incubating in 10% FBS plain media or 10% FBS ATRA-supplemented media resulted in a loss of the established neuronal morphology. Culture in 10% FBS plain media resulted in loss of the rounded and phase-bright cell bodies with reduced intercellular networks and also reoccurrence of S-type cells (Figure 3.19C-D). Unexpectedly, 10% FBS ATRA-supplemented media led to a considerable loss of the established neuronal morphological characteristics (rounded and phase-bright cell bodies, neurite extensions, and intercellular network) and the shape of the cells exhibited a glial-like cell morphology (Figure 3.19E-F).

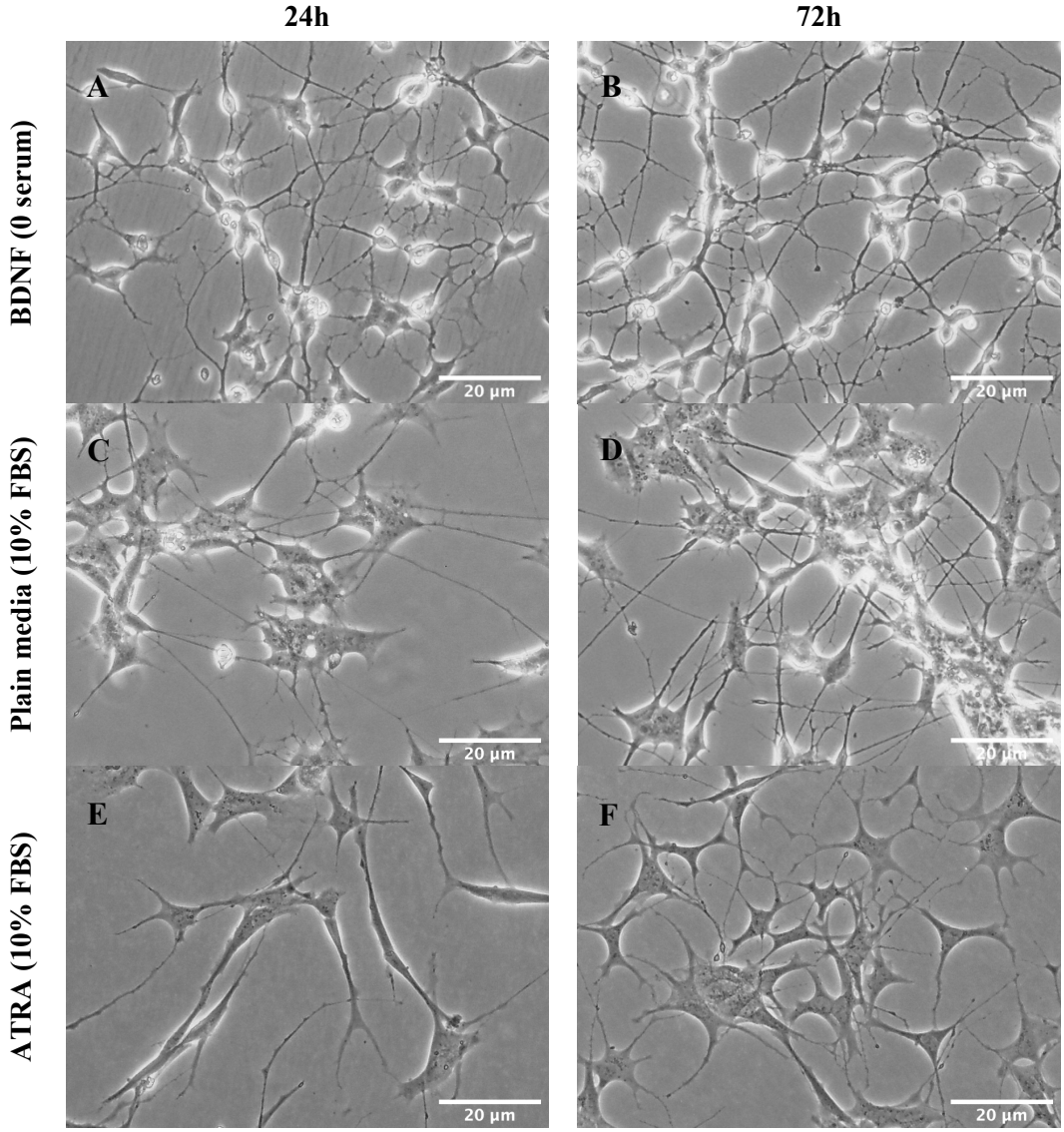

Figure 3.19 SH-SY5Y neuronal-like cells appearance after continued culture in different media following the initial differentiation protocol. (A-B) BDNF supplementation maintained the established neuronal morphological landmarks after 24 and 72h incubation. (C-D) Partial loss of the established neuronal landmarks (flattened cell bodies and S-type reoccurrence) after 24 and 72h incubation in standard 10% FBS media. (E-F) Distinct loss of the established neuronal characteristics and exhibition of a glial-like cell phenotype after 24 and 72h incubation in ATRA-supplemented media. Scale bars are shown.

3.3. Discussion

The findings presented in this chapter demonstrate that the reduction of the FBS concentration from the standard 10% FBS concentration in combination with differentiating media (ATRA or ATRA→BDNF) did not increase neuronal differentiation morphologically, immunocytochemically, or even transcriptionally. Furthermore, this study confirmed the neuronal lineage identity of the SH-SY5Y differentiated model.

In this study, the greatest number of differentiated cells as observed in ATRA→BDNF groups in both FBS conditions demonstrated a significant reduction in percentage of viable cells compared with their controls under standard cell cultures. This is a common phenomenon which is considered as normal biological switch of the cells from proliferative to differentiative phase for the development of neuronal cells (Hardwick and Philpott, 2014). This reduction in number of cells with differentiation was previously reported in many neuronal differentiation studies (Cheung *et al.*, 2009a; Påhlman *et al.*, 1995; Bell *et al.*, 2013; Encinas *et al.*, 2000). Inhibition of cell proliferation is considered necessary at the initiation of the differentiation process in order to upregulate specific differentiation-associated transcripts (Ruijtenberg and van den Heuvel, 2016). Although the 10% FBS (ATRA→BDNF) showed a reduction in the number of viable cells, these cultures had significant higher percentage of viable cells than the control 5% FBS culture. This finding suggested that 10% FBS supplementation in the ATRA stage is a more optimal condition for cell survival and expansion prior to differentiation.

The data of the present study are consistent with the results of Buttiglione *et al.* (2007) who studied the effect of the FBS reduction alone (without any differentiating supplement) on differentiation of the SH-SY5Y cells. They reported no significant increase in neurite length in the reduced FBS (2%) compared with the standard FBS concentration (10%). The present study

also showed FBS reduction alone (5%) induced insignificant greater neurite length than 10% FBS standard cell culture. Furthermore, there was no difference in neurite length between the same differentiated groups under both FBS concentrations. This indicated that FBS reduction alone could induce simple neurite extension in SH-SY5Y cells, but it does not produce greater neurite length in combination with differentiating media. In the comparison between the differentiated method groups, ATRA produced heterogeneous cell population of differentiated N-type cells and undifferentiated S-type. These data are in agreement with other studies (Arcangeli *et al.*, 1999; Kovalevich and Langford, 2013; Encinas *et al.*, 2000). In contrast, the sequential approach (ATRA→BDNF) yielded homogenous differentiated cell population with few numbers of undifferentiated S-type cells which is agreed with findings of Encinas *et al.* (2000).

The immunocytochemistry analyses demonstrated no differences in the immunoreactivity of the neuronal markers (β-III tubulin, NF-M, and GFAP) between the similar groups in both FBS concentrations. These data were consistent with another neuronal maker (NF-H) expression showed by Buttiglione *et al.* (2007) who reported that the immunoreactivity was only strictly induced by differentiation supplements and surface substrates but not by FBS concentrations. Regarding the differentiation groups, the ATRA alone treatment approach induced an increase in expression of the general cytoskeleton β-III tubulin and the mature marker NF-M compared with control group. Notably, NF-M was highly expressed in the differentiated neuronal-like cells. This specific expression could be explicable by the heterogeneity of the SH-SY5Y cell population which is a mixture of N-type and S-type cells in which N-type cells do mainly express specific neuronal markers (Sadée *et al.*, 1987; Ciccarone *et al.*, 1989). The increased NF-M immunoreactivity finding is similar to that reported by Cheung *et al.* (2009a). The increase in β-III tubulin is also comparable with

methodologically slight different study (Constantinescu *et al.*, 2007). The sequential protocol (ATRA→BDNF) produced the highest and homogenous expression of β-III tubulin and NF-M in the whole cell culture. The β-III tubulin expression in this group was comparable to a study which used the BDNF alone or with other combinations (Agholme *et al.*, 2010) while the increase in NF-M immunopositivity was consistent with another neurofilament marker (NF-H) expression analysed in similar studies (Encinas *et al.*, 2000; Arcangeli *et al.*, 1999). In contrast, there was a reduction in glial astrocyte cell marker GFAP in both ATRA and ATRA→BDNF groups compared with the control. These results suggest differentiation and maturation towards neuronal-like cells rather than glial cells particularly with the ATRA→BDNF treatment groups.

Although the ATRA alone and sequential method (ATRA→BDNF) induced the same gene expression trends, the only ATRA→BDNF method resulted in significant gene upregulation of the growth neuronal marker (GAP-43). These findings suggested that BDNF step enhanced neuronal maturation and growth rather than more differentiation. The upregulation of these neuronal markers (NES, RET, ACHE, SYN1, SNAP-25, and TUBB3) in ATRA→BDNF method is similar to gene expression findings reported by Forster *et al.* (2016) who used a slightly different methodology. The significant expression of cholinergic markers (ACHE, and CHAT) associated with no expression in adrenergic (DBH) and dopaminergic (DAT) markers indicated the cholinergic lineage of the established neuronal models resulting from ATRA alone or the ATRA→BDNF protocol. The findings of cholinergic marker expression are in agreement with a study by de Medeiros *et al.* (2019) who used a slightly different methodology. Furthermore, the nociceptive voltage-gated sodium channel marker (SCN9A/Na_v 1.7) and lack of expression of motor marker (MNX1) indicated the sensory identity of these neuronal models. This finding is in agreement with a transcriptomic study of undifferentiated SH-SY5Y reported by Yin *et al.* (2016), who observed the presence of SCN9A

and suitability of SH-SY5Y cells to represent sensory neurons. In addition, SCN9A/Na_v 1.7 expression was reported in another study by Vetter *et al.* (2012) which highlighted its significant role in changing membrane potential and producing action potential in SH-SY5Y cells. The significant expression of mature markers (NF-M and ENO2) and reduction of glial astrocyte cell marker (GFAP) indicate that these differentiation protocols induce mature neuronal-like cells rather than glial astrocyte cells. The GFAP expression has been reported in neuronal precursors and stem cells (Casper and McCarthy, 2006; Liu *et al.*, 2010; Zhang and Jiao, 2015) so this could explain the expression of GFAP in the control cell cultures.

The electrophysiological recordings were conducted to verify the functionality of the differentiated models (10% FBS groups) in comparison with the control. As SH-SY5Y cells are neuroblastoma cell line, all groups presented inward sodium and outward potassium currents. However, the only ATRA→BDNF approach induced the significant currents. These electrophysiological findings were in agreement with other studies by Arcangeli *et al.* (1999), and Gervois *et al.* (2017) who used BDNF in the differentiation of SH-SY5Y cells. Moreover, it has been reported that BDNF enhances the neurotransmitter release and synaptic activity (Shinoda *et al.*, 2014; Tyler and Pozzo-Miller, 2001). Hence, the BDNF supplement could have played a key role in substantially inducing neuronal electrophysiological activities.

In this study, using the 10% FBS standard media as maintenance media resulted in S-type cells reoccurrence. The occurrence of S-type cells of the SH-SY5Y cell line was observed in serum-supplemented media but not in serum-free media incubation (Leventhal *et al.*, 1995; Encinas *et al.*, 2000) so this may therefore justify their reoccurrence. In contrast, the ATRA-supplemented 10% FBS media as maintenance media caused a loss of neuronal morphological characteristics (neuronal-like extensions, and cell-body features) and the cells resembled a glial cell morphology after 72h incubation. A possible explanation for this phenomenon could be the

ability of the SH-SY5Y cell subtypes to transdifferentiate between N-type and S-type (Ross, Spengler and Biedler, 1983) where N-type can differentiate into neuronal-like cells but not S-type (Encinas *et al.*, 2000). S-type cells were reported to differentiate into glial cells such as Schwann cells (Tsokos *et al.*, 1987) or melanocytes (Slack *et al.*, 1992). Moreover, retinoic acid was observed to induce a dual differentiation effect on neural crest cells into neurons and melanocytes (Dupin and Le Douarin, 1995). The observations reported here may suggest that ATRA incubation transdifferentiated the SH-SY5Y neuronal-like model into glial cells/melanocytes. Finally, the BDNF-supplemented media was the optimal maintenance media in keeping the neuronal characteristics of the established neuronal cell model which was selected for the subsequent studies.

3.4. Conclusion

Lowering FBS to 5% in combination with differentiating media diminishes the cell viability and growth without additional differentiation potential of SH-SY5Y cells. In addition, this study confirms that there is a reduction in cell numbers of SH-SY5Y cells due to the differentiation process (biological switch from proliferative phase to differentiative phase). Consequently, there is no need for additional inhibition of cell growth by serum deprivation which does not enhance the neuronal differentiation of the SH-SY5Y cells. The sequential protocol of ATRA and BDNF supplementation substantially induces greater morphological, biochemical, and electro-physiological differentiation of the SH-SY5Y cells compared with the ATRA alone supplementation. The results indicate that ATRA and BDNF supplementations guide the differentiation towards a functional mature cholinergic sensory “nociceptive” neuronal model. This neuronal cell model may be useful as *in vitro* cell model for testing any

therapeutic approach or studying disease related to cholinergic nociceptive sensory nerves. Furthermore, this model can be beneficial for studying pain signalling mechanism, and neuroinflammation.

CHAPTER 4: DPSC DIFFERENTIATION INTO NEURONAL-LIKE CELLS AND CHARACTERISATION

4.1. Introduction

Nerve regeneration using stem cells has received particular attention over the last decades to enable treatment of nerve injuries and as part of regenerative therapies, including regenerative endodontics. Using undifferentiated stem cells in transplantation studies however has limitations such as only a small proportion of the transplanted stem cells differentiate towards a neuronal lineage and also there is a risk of unwanted differentiation or/and unfavourable outcomes, such as fibrotic scar tissue formation which inhibits the subsequent regenerative therapy (Heng *et al.*, 2016; Jones *et al.*, 2019). It has therefore been suggested that using *in vitro* differentiated stem cell-derived neuronal cells offers particular promise for *in vivo* nerve repair or regeneration (Pavlova *et al.*, 2012; Abeysinghe *et al.*, 2015; Hu *et al.*, 2017; Yamamoto *et al.*, 2020; Lee *et al.*, 2007). Furthermore, the establishment of neuronal cell models from stem cells may be beneficial in non-therapeutic applications, such as *in vitro* testing of neurotoxicity and neuropharmacological screening of new drugs (Yap *et al.*, 2015). Stem cell-derived neuronal models can also be used for experimental studies such as neurodevelopment, neuron injury, and neurodegenerative diseases (Srikanth and Young-Pearse, 2014; Jones *et al.*, 2018).

Dental stem cells, particularly DPSCs, have gained considerable interest due to their neurogenic potential (Isobe *et al.*, 2016; Pagella *et al.*, 2020) and immunomodulation properties which prevent the dilemma of immune rejection as is observed in other cell stem therapies (Pierdomenico *et al.*, 2005; Gao *et al.*, 2016a). In addition, DPSCs are readily obtained from extracted third molar teeth or teeth extracted for orthodontic purposes. DPSC transplantation have been recommended to be used and showed positive regenerative ability for dental pulp and neuronal regeneration (Lambrichts *et al.*, 2017; Nakashima and Iohara, 2011; Nakashima *et al.*, 2017; Ibarretxe *et al.*, 2012), spinal cord and peripheral nerve injuries (Luo *et al.*, 2021;

Yang *et al.*, 2017b; Sakai *et al.*, 2012) and treating neurological diseases (Zhang *et al.*, 2018; Shamir, Venugopal and Dhanushkodi, 2015).

There are different protocols described which involve complex combinations of supplements to differentiate DPSCs into neuronal-like cells (see Table 1.3, chapter 1 literature review); however, there is no clear consensus regarding the best method for use. Notably, the relatively simple 2-component differentiation method (ATRA followed by BDNF) was reportedly an effective method to differentiate human neuroblastoma cell line (SH-SY5Y) into mature neuronal models (Encinas *et al.*, 2000; Goldie, Barnett and Cairns, 2014; de Medeiros *et al.*, 2019; Jämsä *et al.*, 2004). To the best of my knowledge, this supplementation method has not been adequately highlighted for differentiation of DPSCs. Hence, the aim of this chapter was to investigate whether this method can differentiate DPSCs into mature functional neuronal cells and compare it with those of the ATRA method alone. This study also aimed to characterise the neuronal cell models established. The methodological approach and assays conducted in this study are illustrated in Figure 4.1.

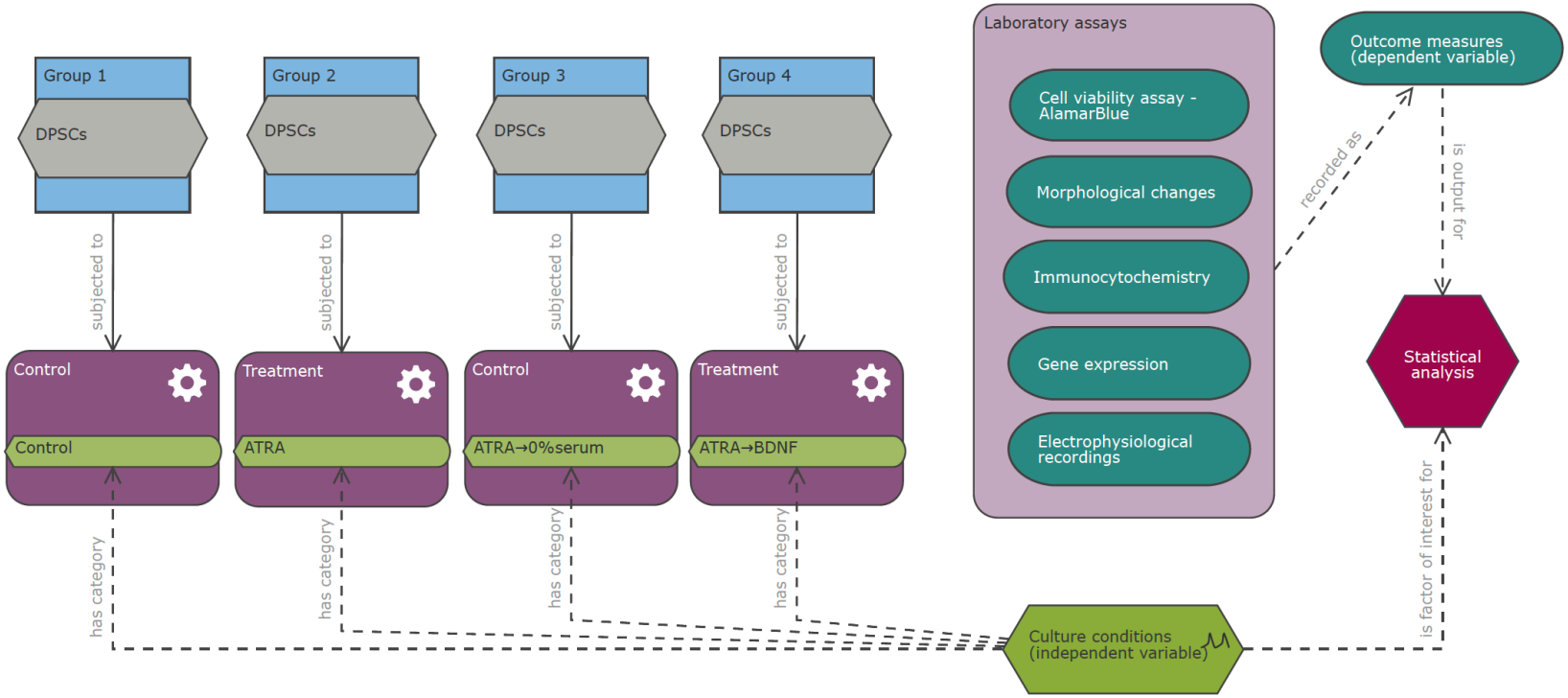

Figure 4.1 Schematic diagram showing the groups and assays used to investigate the neuronal differentiation of DPSCs using ATRA alone or the sequential supplementation method (ATRA→BDNF). The diagram was designed by the author using the EDA https://eda.nc3rs.org.uk.

4.2. Results

4.2.1. Calibration/standard curve of AlamarBlue (AB) assay

The AlamarBlue (AB) assay was used to represent the percentage of viable cell numbers. The calibration/standard curve (Figure 4.2) was performed using known cell number densities of DPSCs (0, 12500, 25000, 50000, and 100000 cells). The cells were seeded in a 96-well plate and preincubated at 37 °C with 5% CO_2 for 6h to allow the cells to adhere to the cell culture surface. Subsequently, the assay and calculations were conducted as previously mentioned in the section 2.4, chapter 2. The average of % AB absorbance per each group was used to generate the standard curve and statistically analyse to assess the linear relationship between the % AB absorbance and cell numbers using linear regression analysis.

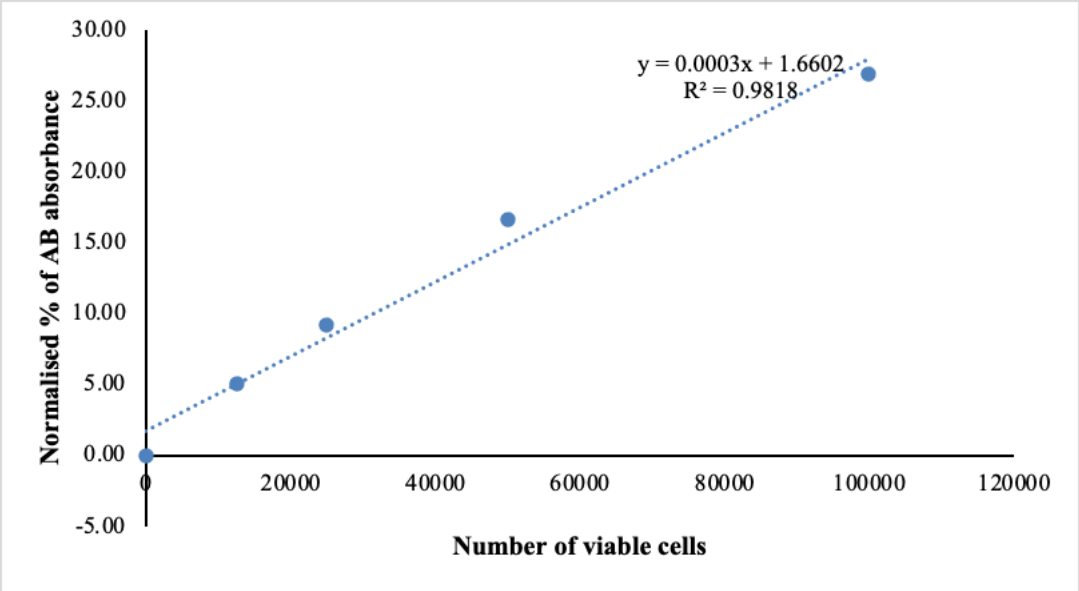

Figure 4.2 Representative calibration curve of AlamarBlue (AB) assay for DPSCs to examine the change in the calculated percentage of AB absorbance reflecting the change in the number of viable cells. The linear regression equation and R^2 coefficient (>0.9) are shown next to the line of the best fit of all different cell densities' means.

4.2.2. Selection of the cell seeding density

To select the optimal cell seeding for the subsequent experiments, the AlamarBlue (AB) assay was performed for a range of cell seeding numbers ($6.25x10^2/cm^2$, $1.25x10^3/cm^2$, $2.5x10^3/cm^2$, and $5x10^3/cm^2$) (Figure 4.3A). The cells were cultured for 12 days as it is the duration of the subsequent differentiation experiments based on previous SH-SY5Y studies. Results revealed that the lower cell seeding densities ($6.25x10^2/cm^2$ and $1.25x10^3/cm^2$) produced a significantly higher percentage of viable cell readings than the higher cell seeding densities ($2.5x10^3/cm^2$ and $5x10^3/cm^2$; $p = 0.000$) which showed increased confluency in terms of cell growth. Moreover, there was no significant difference in % of viable cell readings between the lower cell seeding densities ($6.25x10^2/cm^2$ and $1.25x10^3/cm^2$; $p = 0.806$) nor between the higher cell seeding densities ($2.5x10^3/cm^2$ and $5x10^3/cm^2$; $p = 1$). The phase contrast images of these groups demonstrated the increased confluency of the higher cell seeding densities ($2.5x10^3/cm^2$ and $5x10^3/cm^2$) compared with the lower cell seeding densities ($6.25x10^2$ and $1.25x10^3/cm^2$) (Figure 4.3B-E). Hence, the lower cell seedings were used for future studies (Figure 4.3B-C). The lowest cell seeding density ($6.25X10^2/cm^2$) was selected for differentiation experiments due to its high number of viable cells without reaching cell confluency “cell-cell contact inhibition”. Also, these cell culture exhibited considerable intercellular spaces which would enable neurite outgrowth projections during the differentiation stage (Figure 4.3B).

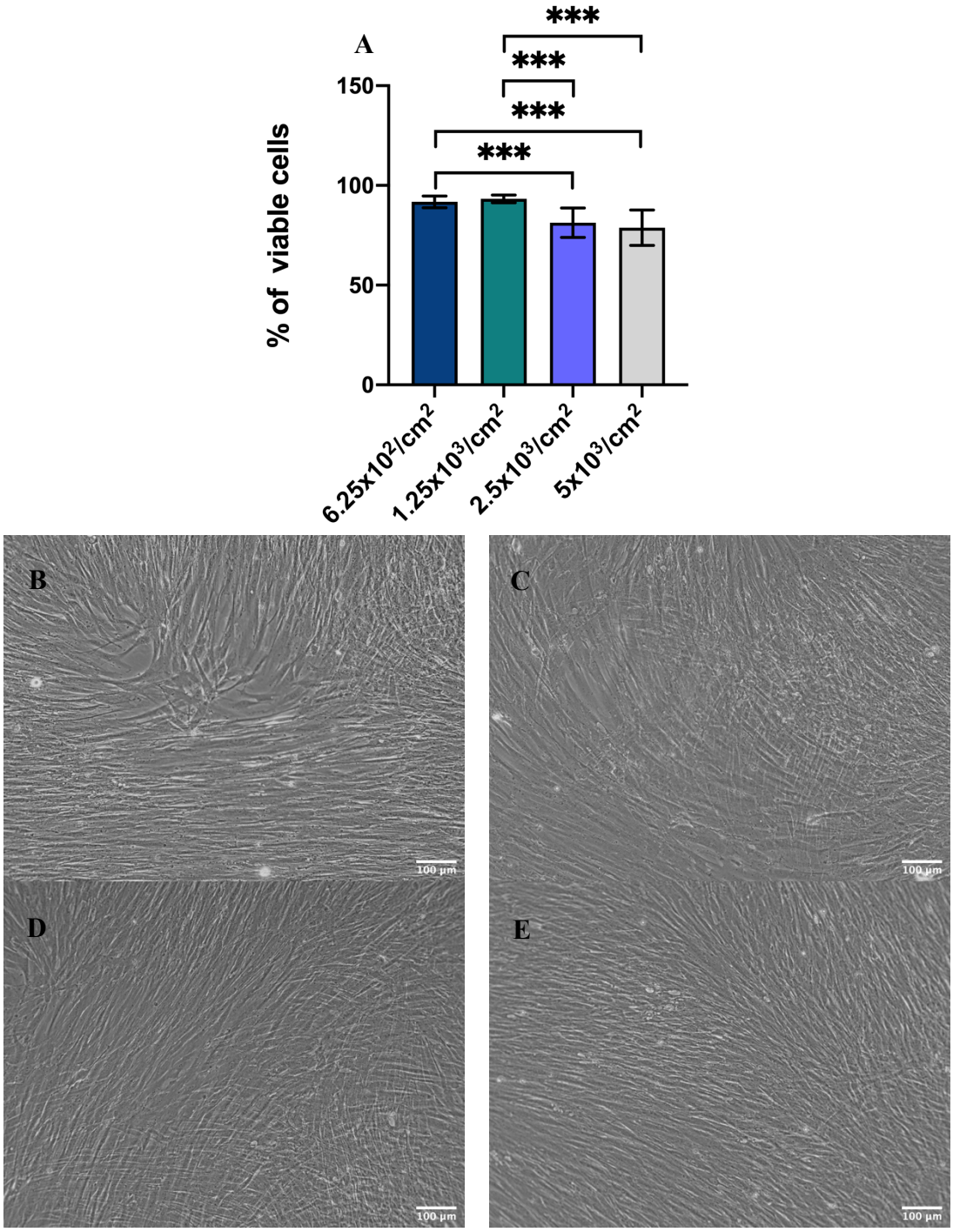

Figure 4.3 Relative AlamarBlue readings reflecting viable cell numbers for the different cell seeding densities after 12 days of culture. (A) Percentage of AlamarBlue readings data. These plate-reader data were calculated and presented as mean ± SD of % viable cells. (B-E) Phase contrast images of cell seeding densities groups for visual reference (B: $6.25x10^2/cm^2$, C: $1.25x10^3/cm^2$, D: $2.5x10^3/cm^2$, E: $5x10^3/cm^2$). The data were analysed by Kruskal-Wallis test with pairwise comparison; the significance values were adjusted by Bonferroni correction for multiple tests (n = 36; ***$p < 0.001$). Scale bars are shown.

4.2.3. Assessment of viable cell numbers after differentiation

Next, the effect of the differentiation methods on viable DPSC numbers was assessed using AlamarBlue assay (Figure 4.4). Although the differentiation groups (ATRA and ATRA→BDNF) showed significantly lower % of viable cell numbers than the standard cell culture control (p = 0.000), they demonstrated significantly higher % of viable cell numbers than the other control (ATRA→0% serum) (p = 0.001 with ATRA and 0.040 with ATRA→BDNF). There was also no significant difference in data between ATRA and ATRA→BDNF groups (p = 0.225). These data indicated that the differentiation methods (ATRA and ATRA→BDNF) still preserved adequate viable cell numbers after differentiation.

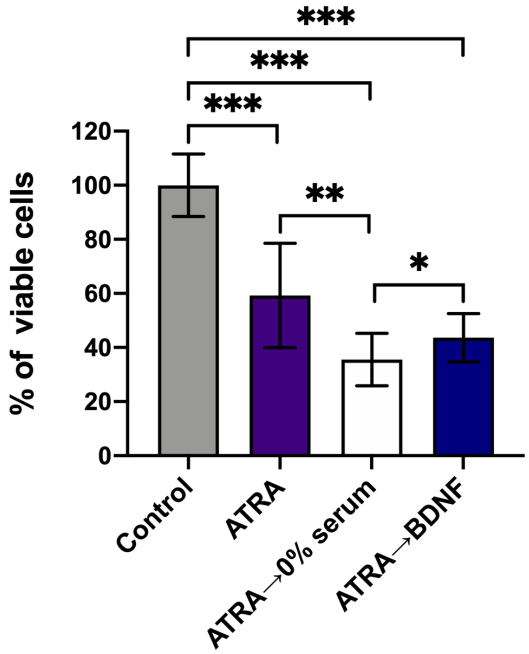

Figure 4.4 Relative cell numbers in DPSCs after differentiation. The data are plate-reader AB absorbance values which were calculated to have a percentage. The plotted data are mean ± SD of % viable cell numbers which were analysed by Kruskal-Wallis test with pairwise comparison; the significance values were adjusted by Bonferroni correction for multiple tests (n = 28; *p < 0.05, **p < 0.01, and ***p < 0.001).

4.2.4. Morphological changes

4.2.4.1. Neuronal morphological observations

DPSCs underwent morphological changes throughout the differentiation process generating neuronal-like cell features (Figure 4.5). In standard cell culture conditions, the cells displayed heterogeneity in shape and size exhibiting a spindle-shaped and fibroblast-like appearance (Figure 4.5A-B). These cells differentiated into bipolar elongated cells with ATRA treatment (Figure 4.5C-D), and they became more defined as bipolar elongated cells following BDNF supplementation in the two-stage protocol (ATRA→BDNF) (Figure 4.5G). Some cells following ATRA→BDNF application acquired typical neuronal-like characteristics exhibiting a phase-bright cell body with well-defined neurite/axon-like extensions and with relatively minor lateral branching (Figure 4.5H). Contrastingly, the comparable culture in the absence of BDNF supplementation (ATRA→0% serum) displayed a loss of elongated cells as seen with the ATRA step in which the cells appeared flattened (Figure 4.5E-F).

The neuronal-like cells in ATRA→BDNF group showed variations in shape and size (Figure 4.6). Cultures included cells presenting with bipolar and multipolar structures as neuronal-like cells, although the bipolar-phenotype cells were predominant (Figure 4.6A-B). There were also different sizes of bipolar (Figure 4.6C-D) and multipolar neuronal-like cells (Figure 4.6E-F). These morphological observations were supported by further quantitative neurite outgrowth assay.

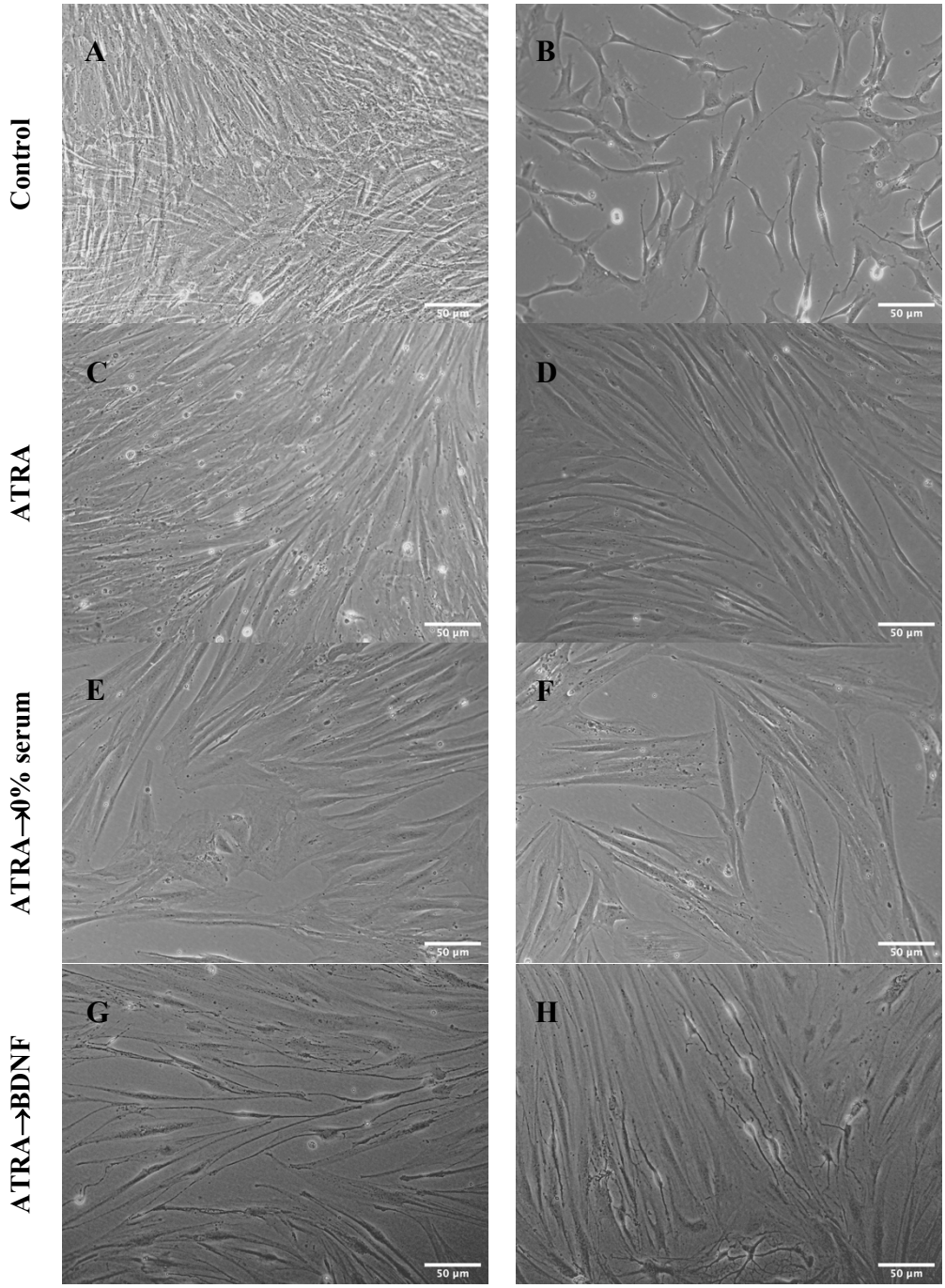

Figure 4.5 Representative morphological appearance of the differentiation groups as evaluated by phase-contrast microscopy. (A-B) Non-treated cell culture (A: Cells are confluent at the end of the experiment, B: Standard DPSC culture displayed spindle-shape and fibroblast-like phenotypes). (C-D) Cells exhibited bipolar elongation after ATRA treatment. (C: in majority of the culture, D: in less dense area). (E-F) ATRA→0% serum demonstrated less and flattened cells in the absence of FBS or BDNF. (G-H) ATRA→BDNF groups revealed the most neuronal differentiation exhibiting well-defined oval cell-bodies with bipolar elongated processes (G) and some cells demonstrated typical bipolar neuronal-like cellular phenotype (H). The images were taken at 20X magnification. Scale bars are shown.

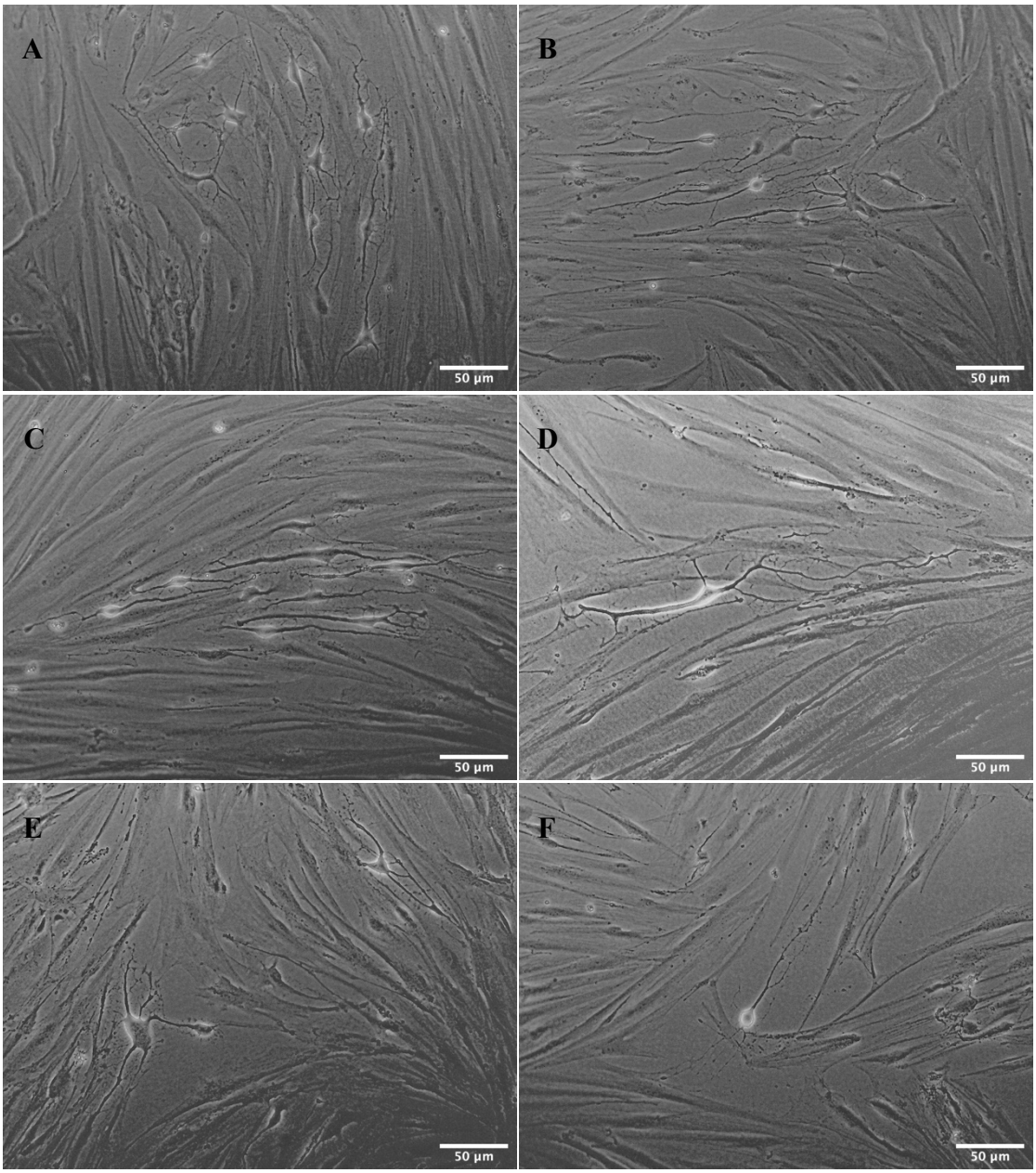

Figure 4.6 Representative morphological variations of the typical neuronal-like DPSCs were cultured in ATRA→BDNF conditions and imaged under phase-contrast microscopy. (A-B) Mixed differentiated DPSC cultures of bipolar and multipolar neuronal morphologies. (C-D) Cultures exhibited different sizes of bipolar neuronal-like cells with lateral ramifications. (E-F) Cells also displayed different sizes of multipolar neuronal-like cells. Images were taken at 20X magnification. Scale bars are shown.

4.2.4.2. Quantitative neurite outgrowth staining assay

Data demonstrated that the ATRA→BDNF group exhibited the highest neurite outgrowth compared with other experimental groups (Figure 4.7). This experimental group exhibited

significantly higher neurite outgrowth compared with both controls (p = 0.045 with standard cell culture and p = 0.001 with ATRA→0% serum group); however, this was not significantly higher than the ATRA group alone (p = 1). The ATRA group showed no significant difference in neurite outgrowth quantification compared with the standard cell culture control (p = 0.784); however, this value was significantly higher than the other experimental control (ATRA→0% serum: p = 0.006) (Figure 4.7A). Confocal microscopy images indicated that the ATRA→BDNF group displayed higher staining and neuronal morphological characteristics than the ATRA group (Figure 4.7B-E).

The results also showed that there were differences in the cell viability between groups (Figure 4.7A) which were in agreement with data obtained from AlamarBlue assay (Figure 4.4). Although there was a reduction in the fluorescent cell viability readings in ATRA and ATRA→BDNF groups, this reduction was not significantly lower than that derived for cells cultured under standard conditions (p = 1 with ATRA and 0.136 with ATRA→BDNF). Fluorescent cell viability readings in the differentiation groups were also insignificantly higher than other experimental control (ATRA→0% serum: p = 0.381 with ATRA and p = 1 with ATRA→BDNF group). There was also no significant difference in cell viability between both differentiation methods used (ATRA and ATRA→BDNF groups: p = 1). The only significant difference was between controls in which the ATRA→0% serum control was lower than the standard cell culture control (p = 0.01). The neuronal morphological observations and neurite outgrowth data indicated the superiority of the relatively simple sequential protocol (ATRA→BDNF) to induce morphologically neuronal-like features while simultaneously preserving adequate cell viability in the differentiated cell cultures.

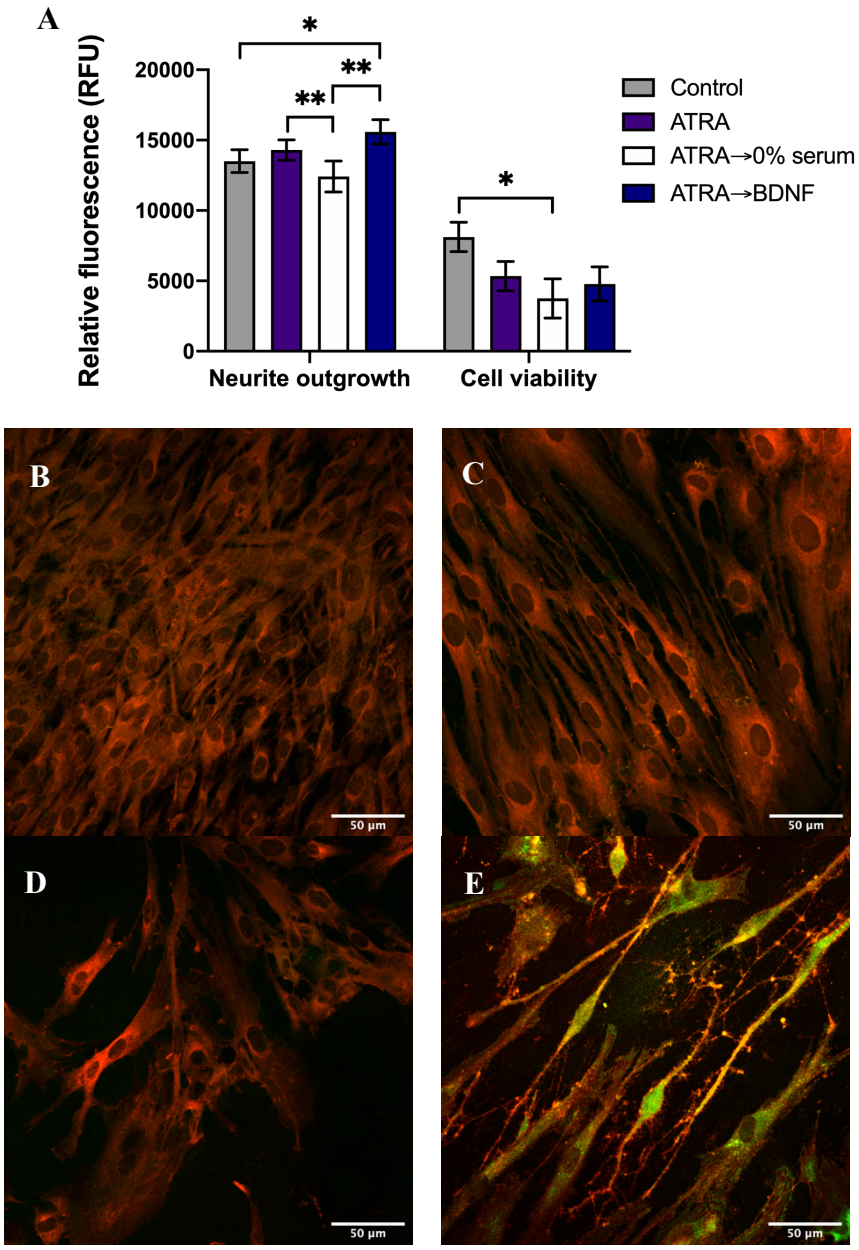

Figure 4.7 Neurite outgrowth assay. (A) Relative quantification of neurite outgrowth and cell viability as determined by fluorescence intensity (orange-red fluorescent cell membrane stain indicator for neurite outgrowth, along with green stain indicator for cell viability). These fluorescence intensity values were quantified by spectrophotometer plate reader; RFU = relative fluorescence unit). (B-E) Merged images are presented for a visual reference of the groups: (B) Untreated control, (C) ATRA, (D) ATRA→0% serum, and (E) ATRA→BDNF. Data plotted are mean ± SEM which were analysed by Kruskal-Wallis test with pairwise comparison; the significance values were adjusted by Bonferroni correction for multiple tests (neurite outgrowth: n = 9, except for ATRA→0% serum, n = 5; cell viability: n = 8, except for ATRA and ATRA→0% serum, n = 5; *$p < 0.05$, and **$p < 0.01$). Scale bars are shown.

4.2.5. Immunocytochemistry

To investigate the immunoreactivity of neuronal protein markers[5] on the differentiated DPSCs, immunofluorescence staining was performed using the general neuronal cytoskeleton marker (βIII-tubulin/TUBB3), mature marker (NF-M) and astrocyte glial cell marker (GFAP) (Figure 4.8 - Figure 4.10).

Immunocytofluorescence staining demonstrated that the neuronal cytoskeleton marker (βIII-tubulin/TUBB3) was increased in the ATRA experimental group and levels were higher in the ATRA→BDNF experimental group compared with the control group. The mature marker (NF-M) was only immunopositively detected in the differentiated experimental groups; the highest levels were detected in the ATRA→BDNF experimental group (Figure 4.8). In contrast, GFAP expression was not detected in all groups, and the accompanying βIII-tubulin (TUBB3) expression was in agreement with the observations reported with NF-M expression (Figure 4.9). The glial-like differentiated cells in the ATRA→BDNF group were also stained with TUBB3, NF-M, and GFAP to check their neuronal immunopositivity. TUBB3 was the only marker detected, and no expression of the NF-M or GFAP marker was detected (Figure 4.10). For methodological validity, no immunofluorescent staining was observed in the negative controls. These immunocytochemical observations indicated that the ATRA followed by BDNF supplementation protocol induced the highest neuronal differentiation towards a mixed population of mature neuronal cells and neuroglia-like cells (not astrocyte cells due to lack expression of GFAP). Subsequently, the expression of these neuronal markers were also investigated by quantitative gene expression along with other neuronal-related markers to profile and identify the neuronal nature in these differentiated models.

[5] The references of the specificity of the neuronal markers are mentioned in Appendix II.

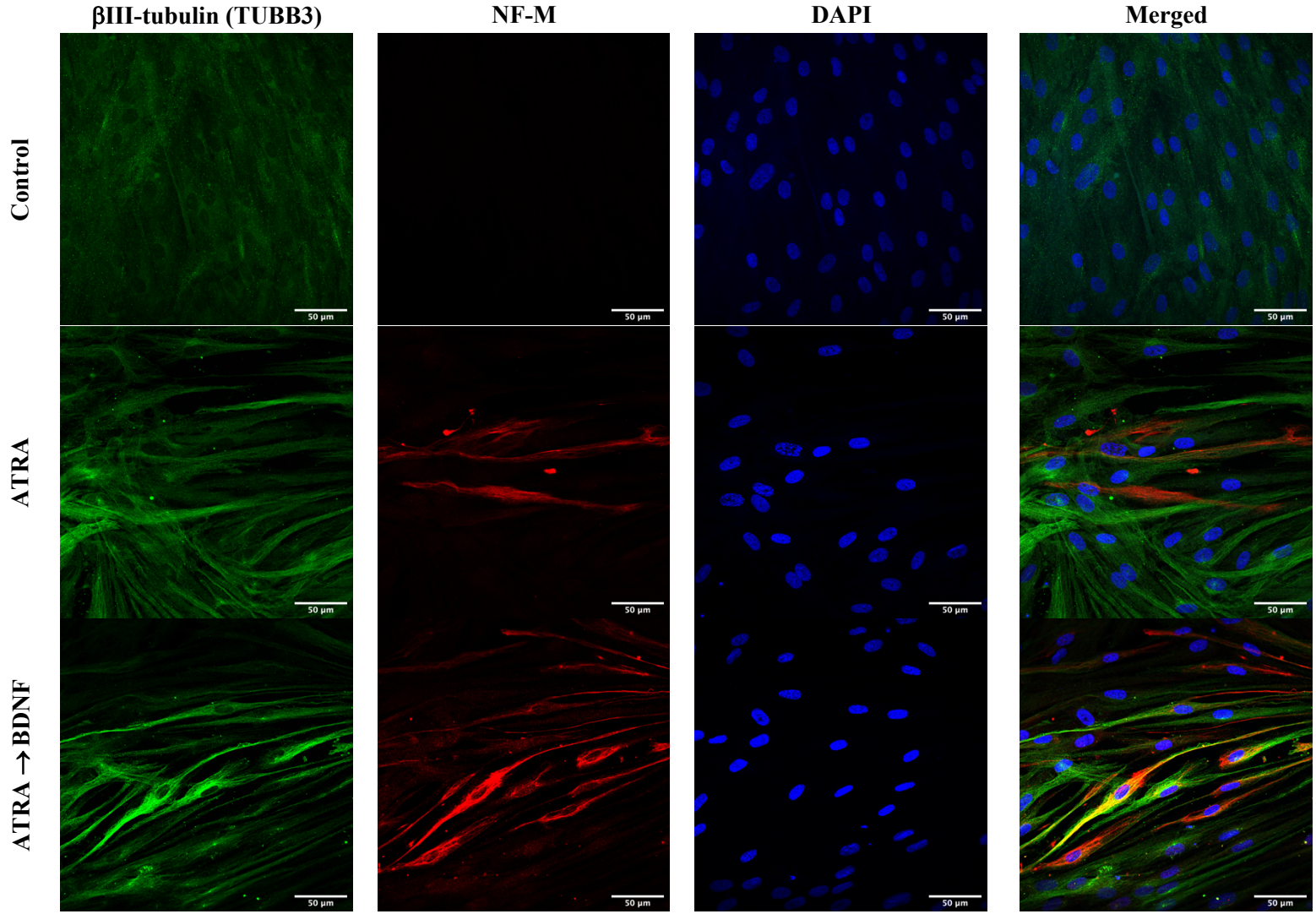

Figure 4.8 Immunocytofluorescence analysis of the NF-M and TUBB3 markers in the differentiated DPSC experimental groups. The ATRA→BDNF supplementation protocol induced the highest expression of these markers. Scale bars are shown.

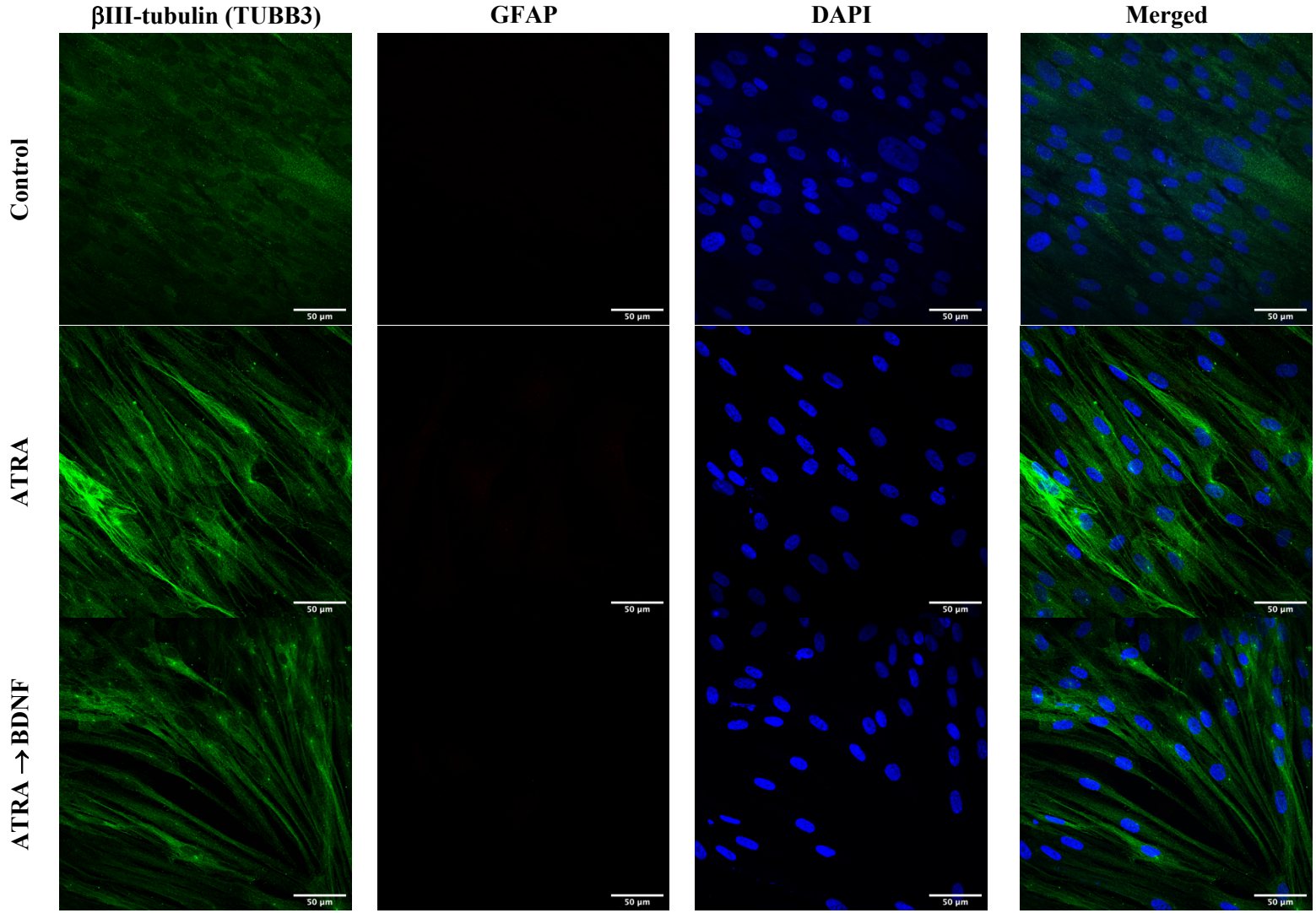

Figure 4.9 Immunocytofluorescence analysis of the GFAP and TUBB3 markers in the differentiated DPSC experimental groups. GFAP expression was not detected in all experimental groups. Scale bars are shown.

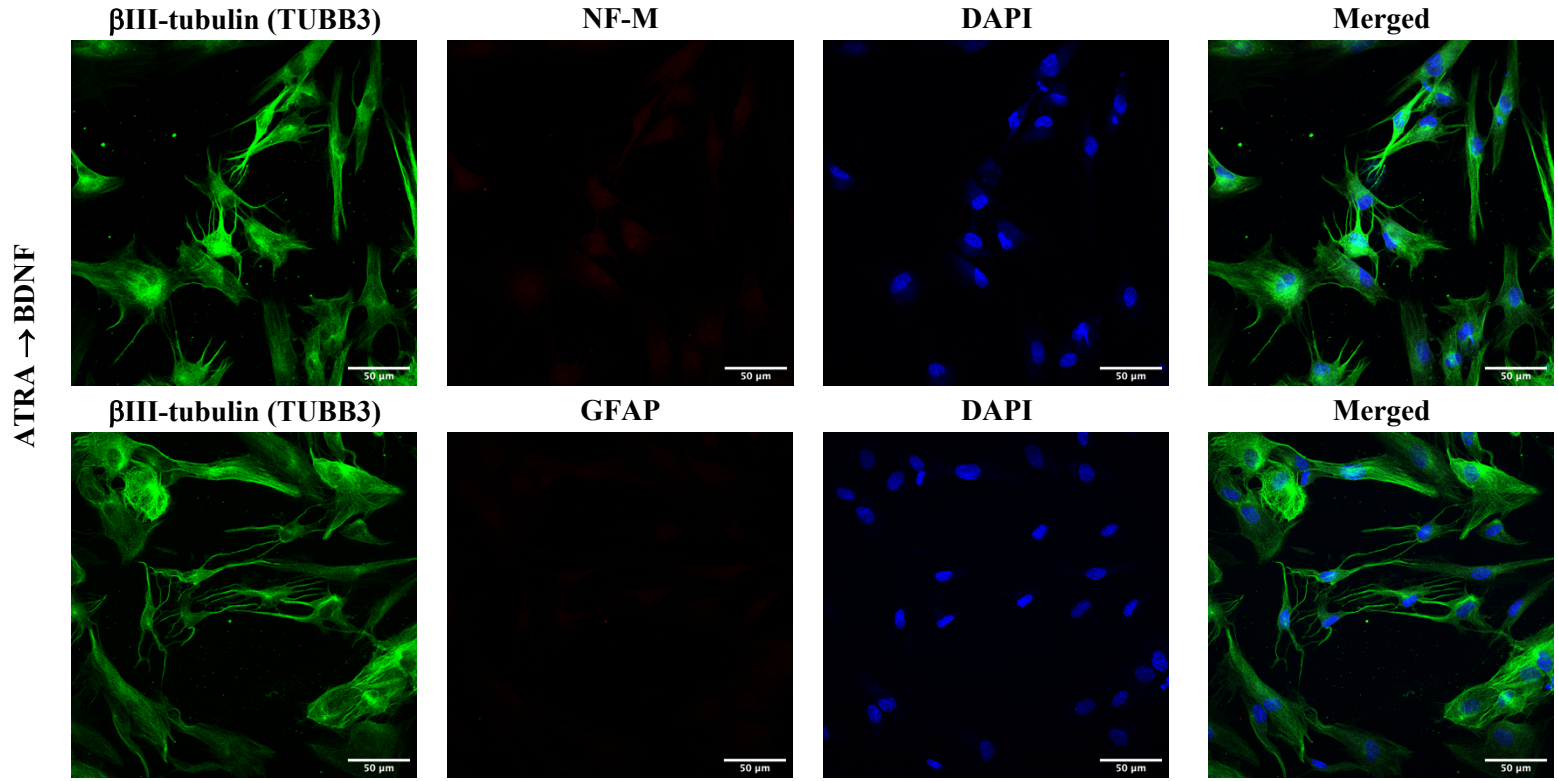

Figure 4.10 Immunocytofluorescence analysis of the NF-M, and GFAP markers in the glial-like differentiated DPSCs. Both mature neuronal (NF-M) and glial astrocyte (GFAP) markers were not expressed. Scale bars are shown.

4.2.6. Neuronal gene expression

To compare gene expression levels for neuronal markers, quantitative PCR analysis was performed. A panel of gene markers was selected to assess the neuronal differentiation and to determine the cellular outcome (neuronal lineage). Neuronal markers[6] were studied including general, mature and astrocyte glial, neurotransmitters, synaptic and voltage-gated sodium channels, sensory and motor neuronal markers (Table 4.1 and Figure 4.11 - Figure 4.15).

The sequential supplementation method (ATRA→BDNF) induced significant gene upregulation of more neuronal markers than ATRA alone supplementation method compared with controls (Table 4.1). Some of these neuronal markers in ATRA→BDNF group were also expressed at significantly higher levels than in the ATRA alone supplementation group, including TUBB3 ($p = 0.005$), GAP43 ($p = 0.001$), ACHE ($p = 0.010$), and PRPH ($p = 0.001$) (Figure 4.11 and Figure 4.15). In contrast, there was a reduction in gene expression of some neuronal markers in both differentiation methods compared with control such as GFAP, SCN1A, and MNX1 (Table 4.1). Furthermore, there were also no to minimal gene expression of some neuronal markers such as DBH, DAT, and MAP2 (Table 4.1). The reduction and no changes in gene expression of these neuronal markers indicated selective neuronal differentiation towards specific neuronal lineage.

Gene expression data indicated that the ATRA→BDNF differentiation method induced increased neuronal gene upregulation compared with the ATRA method, and also the differentiation appeared more specialised towards a cholinergic sensory mature neuronal-like cell identity.

[6] The references of the specificity of the neuronal markers are mentioned in Appendix II.

Table 4.1 Significant change in gene expression of neuronal markers compared with control

Specificity of neuronal markers	Gene of interest	ATRA	ATRA→BDNF
General cytoskeleton marker	TUBB3	—	↑ (p = 0.001)
Neuroepithelial marker	NES	—	↑ (p = 0.011)
Mature marker	NF-M	↑ (p = 0.002)	↑ (p = 0.016)
	ENO2	↑ (p = 0.001)	↑ (p = 0.004)
Cholinergic marker	CHAT	↑ (p = 0.007)	↑ (p = 0.000)
	ACHE	—	↑ (p = 0.002)
Synaptic marker	SYN1	↑ (p = 0.040)	↑ (p = 0.002)
	SNAP-25	—	↑ (p = 0.019)
Neuronal development and growth	GAP43	—	↑ (p = 0.031)
	RET	—	↑ (p = 0.019)
Peripheral nervous system	PRPH	—	↑ (p = 0.042)
Sensory marker (nociceptive voltage-gated sodium channel)	SCN9A	↑ (p = 0.000)	↑ (p = 0.000)
Sensory marker	POU4F1	—	↑ (p = 0.000)
Motor marker	MNX1	—	↓ (p = 0.005)
Astrocyte glial marker	GFAP	↓ (p = 0.032)	↓ (p = 0.001)
General voltage-gated sodium channel	SCN1A	↓ (p = 0.011)	↓ (0.007)
Adrenergic/norepinephrine marker	DBH	—	—
Dopaminergic marker	DAT	—	—
Dendritic maker	MAP2	—	—

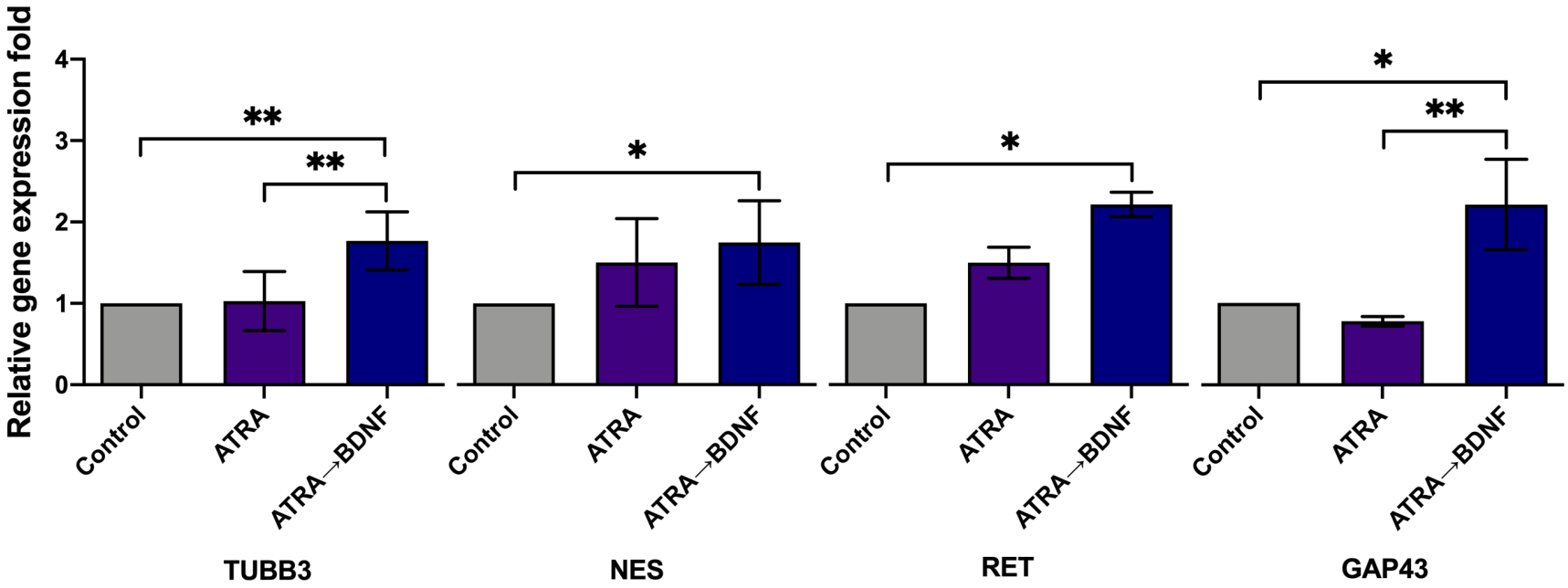

Figure 4.11 Neuronal gene expression in DPSC cultures following neurogenic induction were analysed by real-time qPCR. Only differentiated DPSCs in the ATRA→BDNF group showed significant upregulation of the cytoskeleton (TUBB3), the neuroepithelial (NES), and neuronal development and growth (RET and GAP43) gene markers. Gene expression fold calculations were normalised against two housekeeping genes (HPRT1and RPLA13). The data presented are mean ± SD analysed by Kruskal-Wallis test with pairwise comparison; the significance values were adjusted by Bonferroni correction for multiple tests (TUBB3: n = 9, NES: n = 6, RET: n = 3, and GAP-43: n = 6; *$p < 0.05$, and **$p < 0.01$).

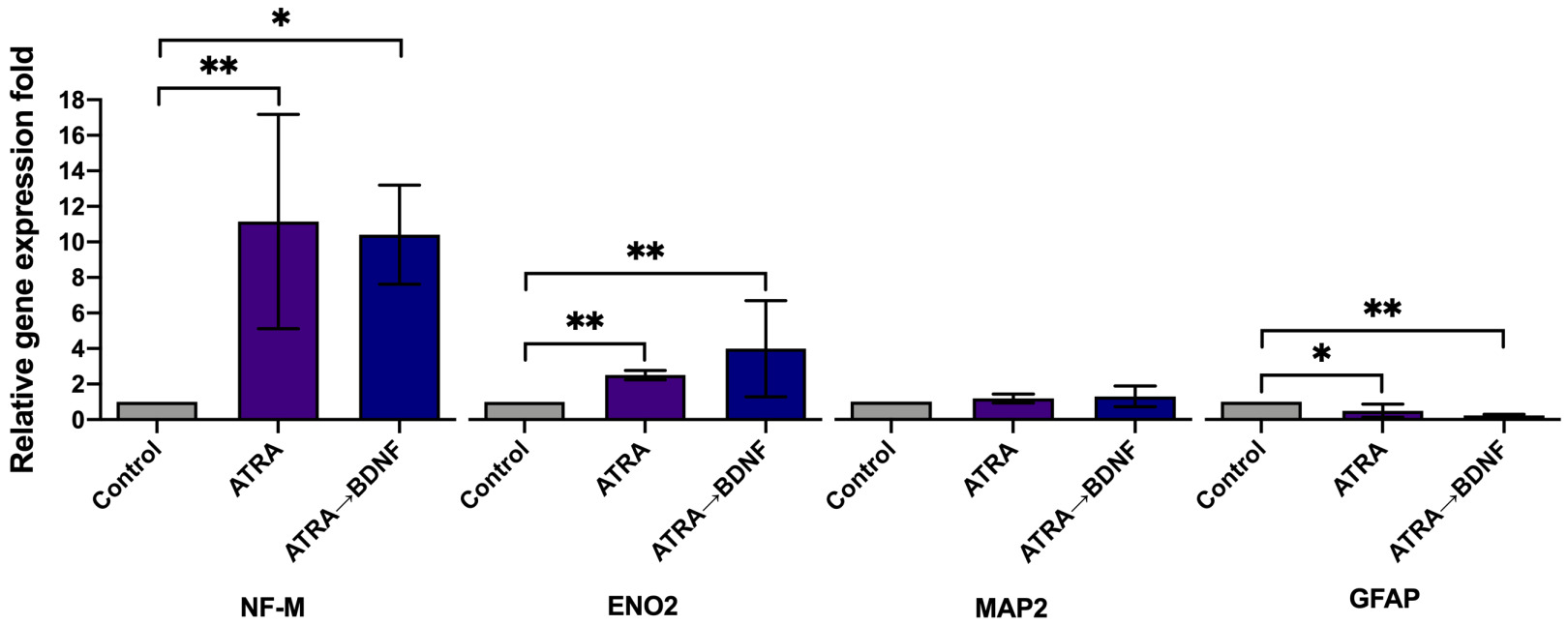

Figure 4.12 Mature neuronal and astrocyte glial gene expression following neurogenic induction were analysed by real-time qPCR. All mature gene makers for the main neuronal cells (NF-M and ENO2) except dendritic marker (MAP2) were upregulated in differentiated DPSC groups, whereas astrocyte marker (GFAP) levels were reduced in both groups. This significant increase in mature markers and decrease in astrocyte gene marker indicated that the differentiation was induced towards mature neuronal cells. Gene expression fold calculations were normalised against two housekeeping genes (HPRT1 and RPLA13). Data are mean ± SD analysed by Kruskal-Wallis test with pairwise comparison; the significance values were adjusted by Bonferroni correction for multiple tests (NF-M: n = 6, ENO2: n = 9, MAP2: n = 6, and GFAP: n = 7; *$p < 0.05$, **$p < 0.01$).

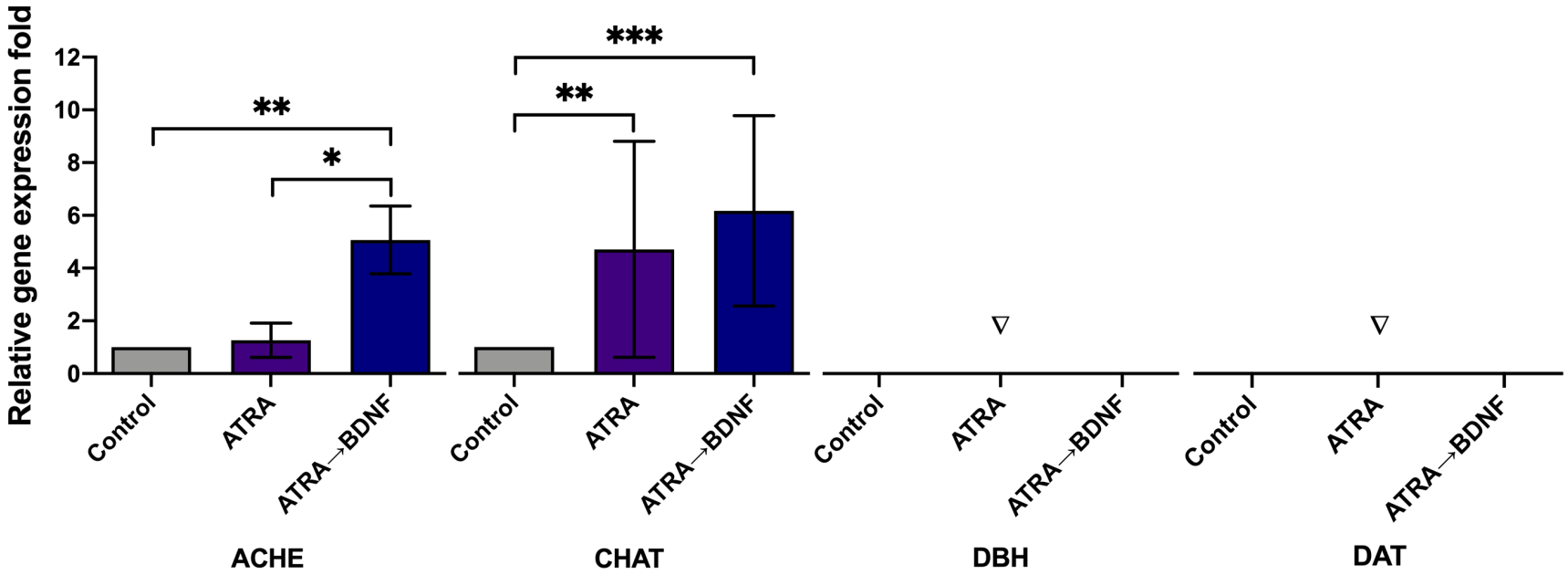

Figure 4.13 Neurotransmitter gene expression following neurogenic induction were analysed by real-time qPCR. The cholinergic markers (ACHE and CHAT) were both upregulated in ATRA→BDNF group whereas only CHAT was upregulated in the ATRA group. The adrenergic (DHB) and dopaminergic (DAT) markers were not observed. The DBH gene marker was detected and reduced with differentiation in the positive control cells (SH-SY5Y) as mentioned in chapter 3 (Figure 3.14). This upregulation in the cholinergic markers and no detection in other neurotransmitters suggested that the differentiated DPSCs were cholinergic neuronal-like cells. Gene expression fold calculations were normalised against two housekeeping genes (HPRT1 and RPLA13). The data are mean ± SD analysed by Kruskal-Wallis test with pairwise comparison; the significance values were adjusted by Bonferroni correction for multiple tests (ACHE: n = 6, and CHAT: n = 9; *$p < 0.05$, **$p < 0.01$, and ***$p < 0.001$). Note: ∇ indicates not detected.

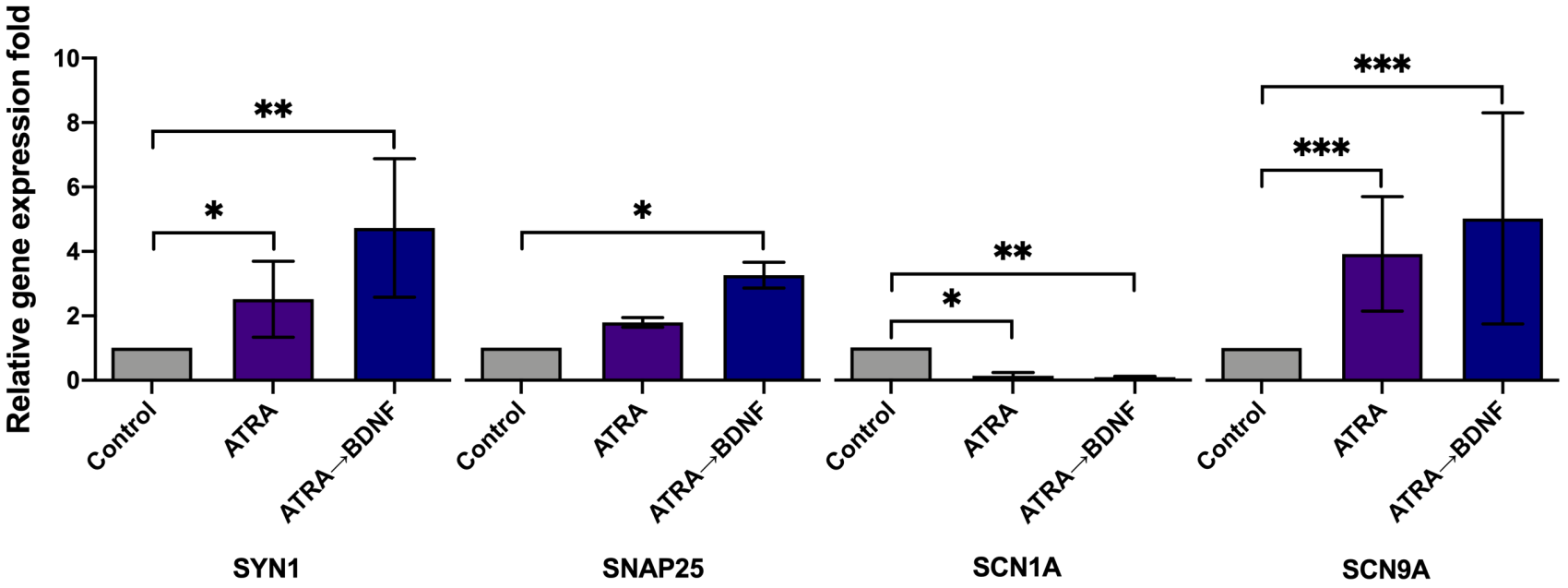

Figure 4.14 Synaptic and voltage-gated sodium channels gene expression following neurogenic induction were analysed by real-time qPCR. More synaptic (SYN1, SNAP25) and sensory/nociceptive voltage-gated sodium (SCN9A) markers were upregulated in the ATRA→BDNF group compared with the ATRA group (SYN1 and SCN9A). The general neuronal voltage-gated sodium channel (SCN1A) marker was reduced in expression following application of both supplementation protocols. These upregulations in synaptic and sensory voltage-gated sodium channel (SCN9A) markers and simultaneously reduction in general neuronal voltage-gated sodium channel (SCN1A) marker indicated that the differentiated DPSCs were sensory neuronal-like cells with synaptic activity. Gene expression fold calculations were normalised against two housekeeping genes (HPRT1 and RPLA13). Data are mean ± SD analysed by Kruskal-Wallis test with pairwise comparison; the significance values were adjusted by Bonferroni correction for multiple tests (SYN1: n = 6, SNAP25: n = 3, SCN1A: n = 6, and SCN9A: n = 9; *$p < 0.05$, **$p < 0.01$, and ***$p < 0.001$).

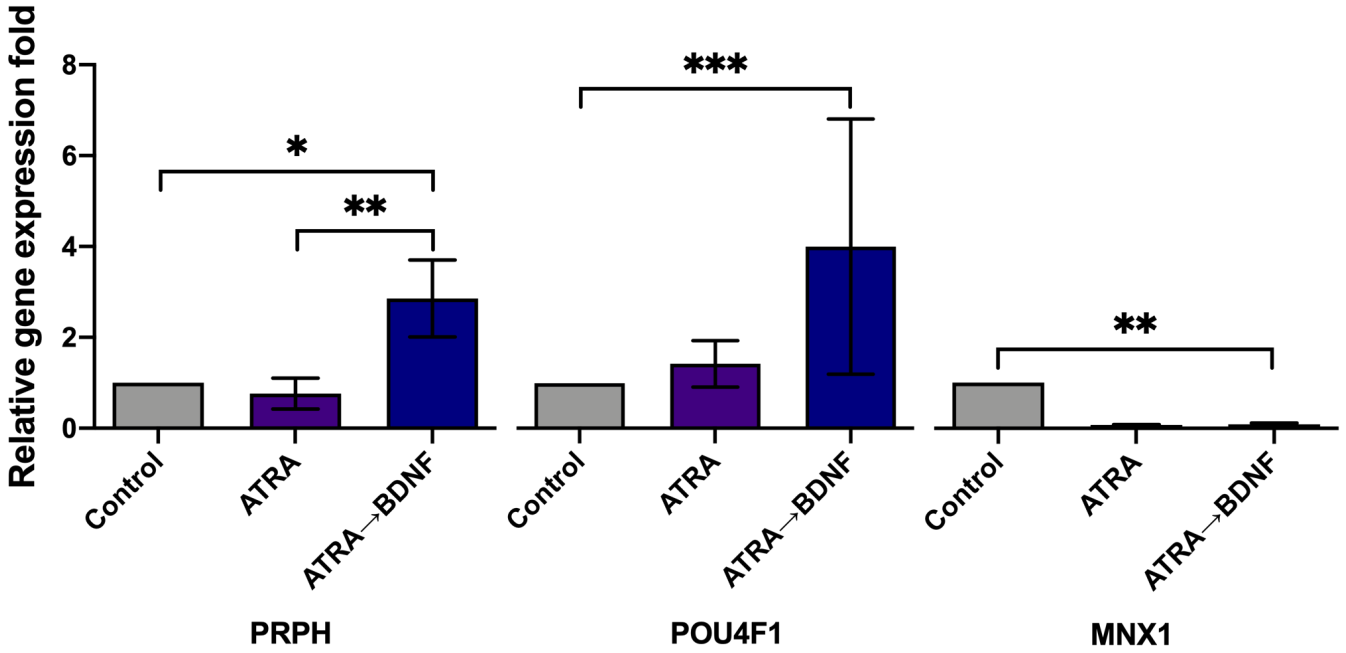

Figure 4.15 Sensory and motor gene expression following neurogenic induction were analysed by real-time qPCR. The peripheral nervous system maker (PRPH) and sensory marker (POU4F1) were only significantly increased in the ATRA→BDNF group, whereas motor marker (MNX1) was significantly decreased in both differentiation groups. This increase in sensory marker (plus SCN9A marker in Figure 4.13) and decrease in motor marker suggested that differentiation was induced towards sensory rather than motor neuronal-like cells. Gene expression fold calculations were normalised against two housekeeping genes (HPRT1 and RPLA13). The data are mean ± SD analysed by Kruskal-Wallis test with pairwise comparison; the significance values were adjusted by Bonferroni correction for multiple tests (PRPH: n = 6, POU4F1: n = 9, and MNX1: n = 6; *$p < 0.05$, **$p < 0.01$, and ***$p < 0.001$).

4.2.7. Neuronal electrophysiological recordings

Whole-cell patch-clamp was performed to investigate the neuronal functionality of the differentiated DPSCs in comparison with undifferentiated cells (standard cell culture). This approach was used to record the voltage-dependent sodium and potassium currents (Figure 4.16A-B).

The differentiated DPSC groups presented inward voltage-dependent sodium currents; however, untreated DPSCs did not. These currents were triggered at a threshold of between -40 and -20 mV (Figure 4.16C). A statistically significant increase was only detected at membrane potentials of −10 to +30 mV in ATRA group, and of −10 to +40 mV in the ATRA→BDNF group (Friedman repeated measure ANOVA with df (10); control: $X^2 = 13.40$ ($p = 0.202$), ATRA: $X^2 = 51.30$ ($p = 0.000$), and BDNF: $X^2 = 101.77$ ($p = 0.000$)). A peak value (negative value) was measured as follows: control (-0.08 ± 0.06 pA/pF), ATRA (-3.61 ± 2.09 pA/pF), and ATRA→BDNF (-8.79 ± 2.19 pA/pF). These sodium-current recordings were also compared between groups. The ATRA→BDNF group exhibited significantly higher values than the control ($p = 0.007 \pm 0.003$) whereas no significant difference between the control and ATRA groups ($p = 0.525 \pm 0.098$) nor the ATRA and ATRA→BDNF groups ($p = 0.129 \pm 0.041$) was observed (Figure 4.16C).

Likewise, the outward voltage-dependent potassium currents were detected in the differentiated experimental groups but not in untreated DPSCs. These currents were evoked at a membrane potential of -30 mV (Figure 4.16D). Although the K^+ currents in the ATRA group were recorded, these currents were not statistically significantly increased at different measured membrane potentials ($p = 0.749 \pm 0.098$). The significant increase in the ATRA→BDNF-treated group of DPSCs exhibited onset at -10 mV ($p = 0.043$), and subsequently at more

significantly positive currents (Friedman repeated measure ANOVA with df (10); control: X^2 = 0.00 (p = 1), ATRA: X^2 = 33.27 (p = 0.749), and ATRA→BDNF: X^2 = 97.80 (p = 0.000)). The peak value of 0 ± 00 pA/pF, 0.53 ± 0.22 pA/pF, 3.341 ± 0.42 pA/pF was measured for control, ATRA, and ATRA→BDNF treated groups, respectively. The potassium recordings in the ATRA→BDNF were significantly higher than the control (p = 0.000) and ATRA groups (p = 0.020 ± 0.004). Although the ATRA treated group induced marginally higher outward potassium currents than the control, this difference was not significant at all measured voltages (p = 0.872 ± 0.076) (Figure 4.16D).

The cell membrane capacitance (i.e., it determines how rapidly the cell membrane responds to current impulse conduction) was also calculated (Figure 4.16E). The ATRA treated group demonstrated relatively high cell membrane capacitance values; however, they were not significantly higher than the control (p = 0.211). Whereas the sequential treatment approach (ATRA→BDNF) demonstrated a significantly higher cell membrane capacitance values compared with the control group (p = 0.011). However, there was no statistical difference between the ATRA and ATRA→BDNF groups (p = 1).

These data indicated that only the sequential differentiation method (ATRA→BDNF) induced functional electrophysiological neuronal profile in differentiated DPSCs.

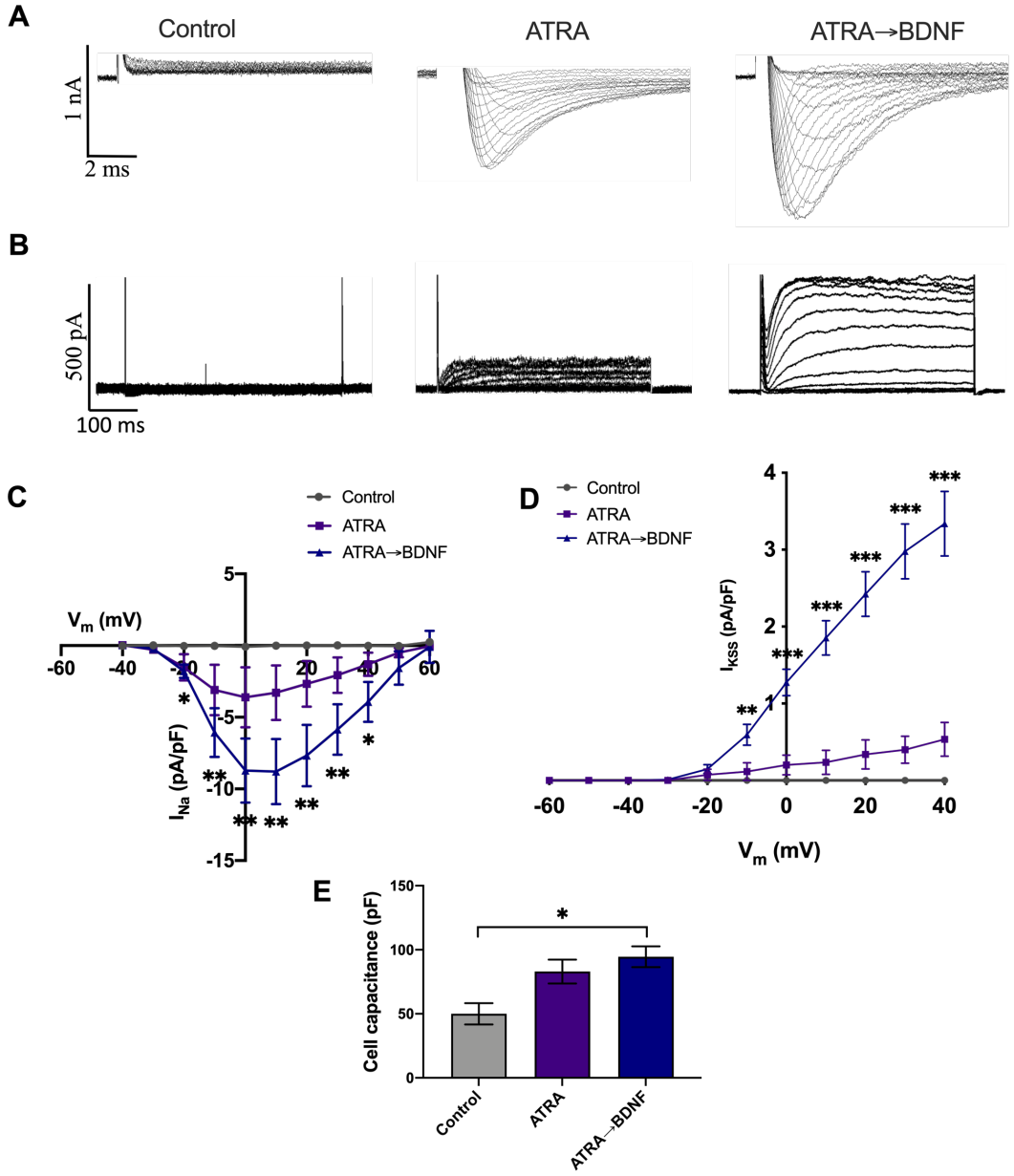

Figure 4.16 Electrophysiological membrane currents were induced by neuronal differentiation. (A, B) Representative voltage-sodium (A) and potassium currents (B) evoked in the experimental groups (control, ATRA, and ATRA→BDNF) for visual reference. (C) The I-V relationship of inward sodium currents were recorded in the experimental groups: control standard culture condition (n = 6), ATRA (n = 10), and ATRA→BDNF (n = 14). (D) The I-V relationship of outward potassium currents were recorded in the groups: control (n = 7), ATRA (n = 6), and ATRA→BDNF (n = 10). (E) Cell membrane capacitance was measured in the experimental groups: control (n = 8), ATRA (n = 6), and ATRA→BDNF (n = 23). The comparison between groups in C, D and E graphs were analysed by Kruskal-Wallis test with pairwise comparison; the significance values were adjusted by Bonferroni correction for multiple tests. Data are mean ± SEM (*$p < 0.05$, **$p < 0.01$, and ***$p < 0.001$).

4.3. Discussion

The present chapter reports on how DPSCs were successfully differentiated into neuronal-like cells as determined by cytomorphology, immunoreactivity, gene expression, and electrophysiological profile. The DPSCs were differentiated into neuronal-like cells using the established and relatively straightforward sequential differentiation protocol (ATRA followed by BDNF) as has been reported for SHS-Y5Y cells (Encinas *et al.*, 2000). In addition, the neuronal lineage identity of the differentiated DPSCs was identified.

Although the ATRA treatment alone stimulated morphologically bipolar elongation in the DPSCs, only the sequential approach (ATRA→BDNF) induced the greatest neuronal morphological features via neurite outgrowth quantification. These results were consistent with those previously reported in SH-SY5Y studies by Encinas *et al.* (2000) and Goldie *et al.* (2014) in which they reported that the ATRA→BDNF differentiation method gave superior neuronal morphological features than the ATRA alone method. In addition, only the differentiated DPSCs in the ATRA→BDNF group in the current study displayed a combination of typically bipolar, and fewer multipolar neuronal phenotype cells. This finding is consistent with a study by Luzuriaga *et al.* (2019) who used BDNF with other supplements in specialised neuronal differentiating media and reported that BDNF reprogrammed DPSCs into neuronal- and glial-like cells lineages.

The current chapter presents data on neuronal-like cell appearance established by DPSC differentiation. However, these neuronal-like cells were a relatively small population among the more dominant elongated cells and other cells which appeared relatively unchanged. The possible explanation for this was that while the DPSCs were characterised as stem cells, they were not sorted for stem cells markers and consequently resulted in low percentage of stem

cells. The presence of bipolar and multipolar differentiated neuronal-like cells in the same culture could also support the heterogeneity of the tested DPSCs. This combination of the two different neuronal phenotypes could be produced due to the presence of specific markers in the undifferentiated DPSCs of the same culture which result in neuronal and glial lineages (Young *et al.*, 2016; Harrington, Sloan and Waddington, 2014). However, further investigations are required to determine other possible reason(s) why the same population of DPSCs behave differently in response to the same differentiating supplementation.

Even though there was increased immunoreactivity of the neuronal cytoskeleton (β-tubulin III) and mature marker (NF-M) with both differentiation methods, the ATRA→BDNF method resulted in the greatest expression levels. The β-tubulin III expression finding is in agreement with previous studies which used ATRA and BDNF supplements along with other stimulants to differentiate human embryonic stem cells (hESC) (Li *et al.*, 2005; Lee *et al.*, 2007) and DPSCs into neuronal-like cells (Chang *et al.*, 2014; Jung *et al.*, 2016). However, the β-tubulin III expression was also observed in the uninduced control DPSC groups. This expression indicates that the detection of this marker is not necessarily an indicator of neuronal differentiation, but the increase in the expression most likely does. This observation is consistent with previous studies which found β-tubulin III expression in undifferentiated mesenchymal stem cell cultures, including DPSCs (Foudah *et al.*, 2014; Martens *et al.*, 2012; Tamaki *et al.*, 2013). The immunoexpression of the mature maker (NF-M) in bipolar but not in multipolar differentiated cells indicated that the bipolar differentiated cells were mature neuronal-like cells, whereas the multipolar cells were supportive glial-like cells. The immunoexpression of the mature maker (NF-M) was also supported by transcript upregulation for mature markers (NF-M and ENO2). The immunoexpression of the mature neurofilaments was comparable to those expression levels reported by Wichterle *et al.* (2002) who used the

ATRA and BDNF supplements along with other differentiating stimulants to differentiate mouse embryonic stem cells (mESC) into neuronal-like cells.

Surprisingly, GFAP immunoexpression was not detected in any experimental groups, and this observation was supported by the reduction in GFAP gene expression. Thereby, these results indicated that neither method (ATRA or ATRA→BDNF) produced astrocyte glial cells and the multipolar glial-like cells presented in ATRA→BDNF group were potentially glial cells but not an astrocyte subtype. Because of their multipolar appearance, they may be either oligodendrocytes or microglia; hence, further investigation is needed to reveal the identity of these multipolar glial-like cells. Notably, these GFAP expression results are not in agreement with that of the study performed by Chang *et al.* (2014) who reported GFAP expression after neuronal differentiation. This outcome may have been due to one of their other multiple differentiating supplements such as the presence of glial cell line-derived neurotrophic factor (GDNF), which is not present in the current study. GDNF is known for activating glial cells and producing astrogliosis (new astrocytes) used for neuronal repair and regeneration (Deng *et al.*, 2011; Walker and Xu, 2018).

The sequential method (ATRA→BDNF) resulted in enhanced gene upregulation of neuronal markers compared with the ATRA alone method which simulated relative few gene changes. The upregulation of the general neuronal markers (NES and β-tubulin) due to ATRA→BDNF supplementation agrees with results reported by Chang *et al.* (2014) and Jung *et al.* (2016). Both studies used ATRA and BDNF in combination with other supplements to differentiate DPSCs into neuronal-like cells. The increase in the gene expression of cholinergic and synaptic markers (ACHE, CHAT, and SNAP25) in this study is similar to findings reported by Lee *et al.* (2007). They also used ATRA and BDNF with other supplement combinations to

differentiate hESC into neuronal-like cells. Furthermore, the increased gene expression in cholinergic markers corresponded with the immunostaining of cholinergic markers showed by Li *et al.* (2005) and Wichterle *et al.* (2002) who used ATRA and BDNF in their complex differentiating media to differentiate hESC and mESC, respectively. Also, in SH-SY5Y differentiation studies where ATRA and BDNF were used, a cholinergic identity of the differentiated cells was reported (de Medeiros *et al.*, 2019; Goldie, Barnett and Cairns, 2014). This agreement in data suggests that ATRA and BDNF supplements are inducers of the cholinergic synaptic activity of the resultant differentiated cells.

The distinct expression of sensory marker (POU4F1), nociceptive voltage-gated sodium channel marker (SCN9A/Na_v 1.7) and lack of expression of motor marker (MNX1) indicated the sensory identity of these DPSC-derived neuronal-like cells. This finding was not in agreement with the upregulation of motor neuronal marker (HLXB9/HB9/MNX1) reported by others (Lee *et al.*, 2007; Li *et al.*, 2005; Wichterle *et al.*, 2002). These studies concluded a motor phenotypic identity of their stem cell-derived neuronal-like cells. The possible explanation for this difference is the presence of sonic hedgehog (SHH) supplement in their differentiating media which is reported to guide the differentiation towards a motor neuronal phenotype (Li *et al.*, 2008; Wichterle and Peljto, 2008). In addition, very low concentrations of ATRA (1 nM to 2 µM) and BDNF (10-20 ng/ml) supplements were used which may not be sufficient to induce the sensory neuronal-like cells in comparison with the current study (ATRA: 10 µM and BDNF: 50 ng/ml).

It has previously been reported by Lu et al (2004) that the morphological changes of stem cells into neuronal-like cells and certain neuronal markers' upregulation could be induced by chemical stress or cellular toxicity from components in the differentiating media rather than due to guided neuronal differentiation. Therefore, electrophysiological recordings were

established for all groups to investigate the functionality and support the molecular and cellular data of the differentiated DPSCs. Only the differentiated DPSCs generated by the sequential method (ATRA→BDNF) displayed a marked neuronal electrophysiological profile. This finding is consistent with distinct electrophysiological results reported by Lee *et al.* (2007) and Li *et al.* (2005) who used ATRA and BDNF in their differentiating media to differentiate hESC into neuronal-like cells. The consistency with those studies could suggest that the BDNF supplement stimulated the neuronal electrophysiological characteristics towards functional neuronal-like cells, whereas ATRA alone is not sufficient. This interpretation is in agreement with Goldie *et al.* (2014), who concluded that the ATRA supplementation alone method produced intermediate differentiation and only with the additional supplementation of BDNF could maturity and synaptic functionality of differentiated SHS-Y5Y cells be induced.

4.4. Conclusion

This study demonstrates that only the sequential protocol of ATRA followed by BDNF supplementation effectively induces morphological, biochemical, and electro-physiological differentiation of DPSCs into neuronal-like cells compared with ATRA alone protocol. The sequential supplementation (ATRA→BDNF) enables DPSCs to differentiate towards a functional mature cholinergic sensory (nociceptive) neuronal-like phenotype. These DPSC-derived neuronal-like cells could be used as a neuronal component of a constructive/engineered tissue structure or transplanted with other targeted cells to replace any desired tissue loss in the dental and medical fields. As this neuronal-like model is derived from DPSCs, the best fit may be as neuronal component of the dental pulp regenerative therapy. They could also be adopted for the *in vivo* regenerative neuronal transplantation therapies to restore the defective neuronal

tissue due to nerve injuries, instead of undifferentiated stem cells. However, further investigation is required to study the suitability of this neuronal-like model for clinical use. Furthermore, it could be used as a preclinical *in vitro* neuronal-like model for investigating therapies, and neuronal-related problems.

CHAPTER 5: ROLE OF ERK/MAPK SIGNALLING IN NEURONAL DIFFERENTIATION OF DPSC AND SH-SY5Y CELL CULTURES

5.1. Introduction

The neuronal differentiation of stem cells involves various and complex underlying signalling pathways (Gage, 2000). Elucidating these pathways that govern neural stem cell-fate determination (neuronal or glial cells) is crucial for creating new specialised therapies that could provide points of intervention to limit neuronal loss or stimulate neuronal repair and regeneration (Navarro Quiroz *et al.*, 2018; Chuang, Tung and Lin, 2015; Tzeng *et al.*, 2015).

There are a variety of signalling pathways involved in specific neuronal cell fate differentiation. For example, mature neuronal differentiation is induced via cyclic adenosine monophosphate (cAMP) signalling (Kim *et al.*, 2005), and the extracellular-regulated kinases/mitogen-activated protein kinase (ERK/MAPK) signalling pathway (Tzeng *et al.*, 2015). Astrocytic differentiation is achieved via Janus kinases/signal transducer and activator of transcription proteins (JAK/STAT) and ERK/MAPK signalling pathways (Nakanishi *et al.*, 2007). Oligodendrocyte differentiation is activated via p38 MAPK signalling pathway (Haines *et al.*, 2015; Chew *et al.*, 2010). Schwann cell differentiation is trigged via cAMP signalling (Arthur-Farraj *et al.*, 2011; Monk *et al.*, 2009) and the phosphatidylinositol 3-kinase/Akt protein kinase B (PI3K/Akt) pathway (Heller *et al.*, 2014).

Although the MAPK signalling pathways are commonly involved in cell growth and proliferation (Chang and Karin, 2001; Zhang and Liu, 2002), there are several studies reporting its involvement in the differentiation of several cell types (Lovicu and McAvoy, 2001; Traverse *et al.*, 1992; Jaiswal *et al.*, 2000). The MAPK and PI3K/Akt pathways are considered the main signalling pathways in the nervous system stimulated by neurotrophins, including BDNF (Kaplan and Miller, 2000; Frebel and Wiese, 2006). It has been previously reported in neuronal cell line (SH-SY5Y) and stem cell studies that the ERK/MAPK was responsible for neuronal

differentiation and maturation whereas the PI3K/Akt pathway was involved for sustaining cell survival during differentiation (Encinas *et al.*, 1999; Tzeng *et al.*, 2015). Thus, the ERK/MAPK pathway was selected to investigate whether the established mature cholinergic sensory DPSC-derived neuronal-like cells (the neuronal model described in chapter 4) is also achieved via this signalling pathway. This investigation was conducted in parallel with SH-SY5Y-derived neuronal-like cells as positive control cells (the neuronal model described in chapter 3).

The mitogen-activated protein kinase 1/2 (MEK1/2) is the primary form of the active phosphorylated form (p-MEK1/2/MAPKKs) in ERK/MAPK signalling. These p-MEK1/2 proteins are responsible for the phosphorylation of the ERK1/2 into the active phosphorylated form (p-ERK1/2/MAPK) which stimulates biological responses, such as cell proliferation and differentiation (Rubinfeld and Seger, 2005; Murphy and Blenis, 2006). The MEK inhibitors (U0126 and PD98059) have been widely used in research to investigate the role of ERK/MAPK signalling pathway in neuronal differentiation (Encinas *et al.*, 1999; Phonchai *et al.*, 2019; Lee *et al.*, 2016; Yin *et al.*, 2014; Chan *et al.*, 2013). Notably, U0126 inhibits the MEK1 and MEK2 (Favata *et al.*, 1998) whereas PD98059 inhibits only the MEK1 (Alessi *et al.*, 1995). Consequently, the MEK1/2 (U0126) inhibitor was selected in the present study as it subsequently inhibits the phosphorylation of both ERK1 and ERK2 rather than the partial inhibition of this signalling pathway (see the proposed pathway of study is illustrated in Figure 5.1). Also, the methodological approach and assays conducted in this study are illustrated in Figure 5.2.

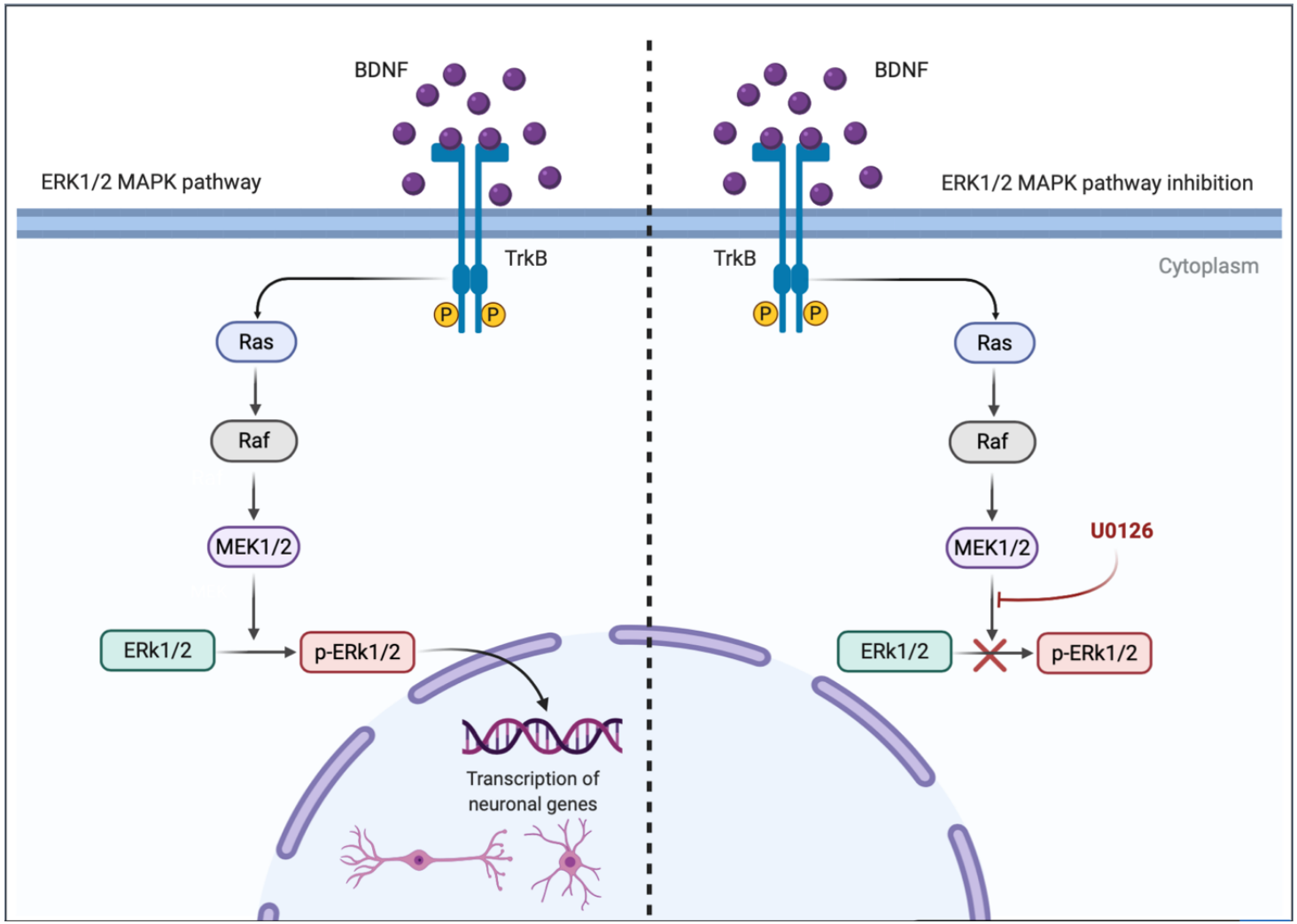

Figure 5.1 A proposed schematic diagram demonstrating how BDNF could trigger the ERK/MAPK signalling pathway to induce the neuronal differentiation and maturation of DPSCs (the diagram was designed by the author using the Biorender designing website https://biorender.com).

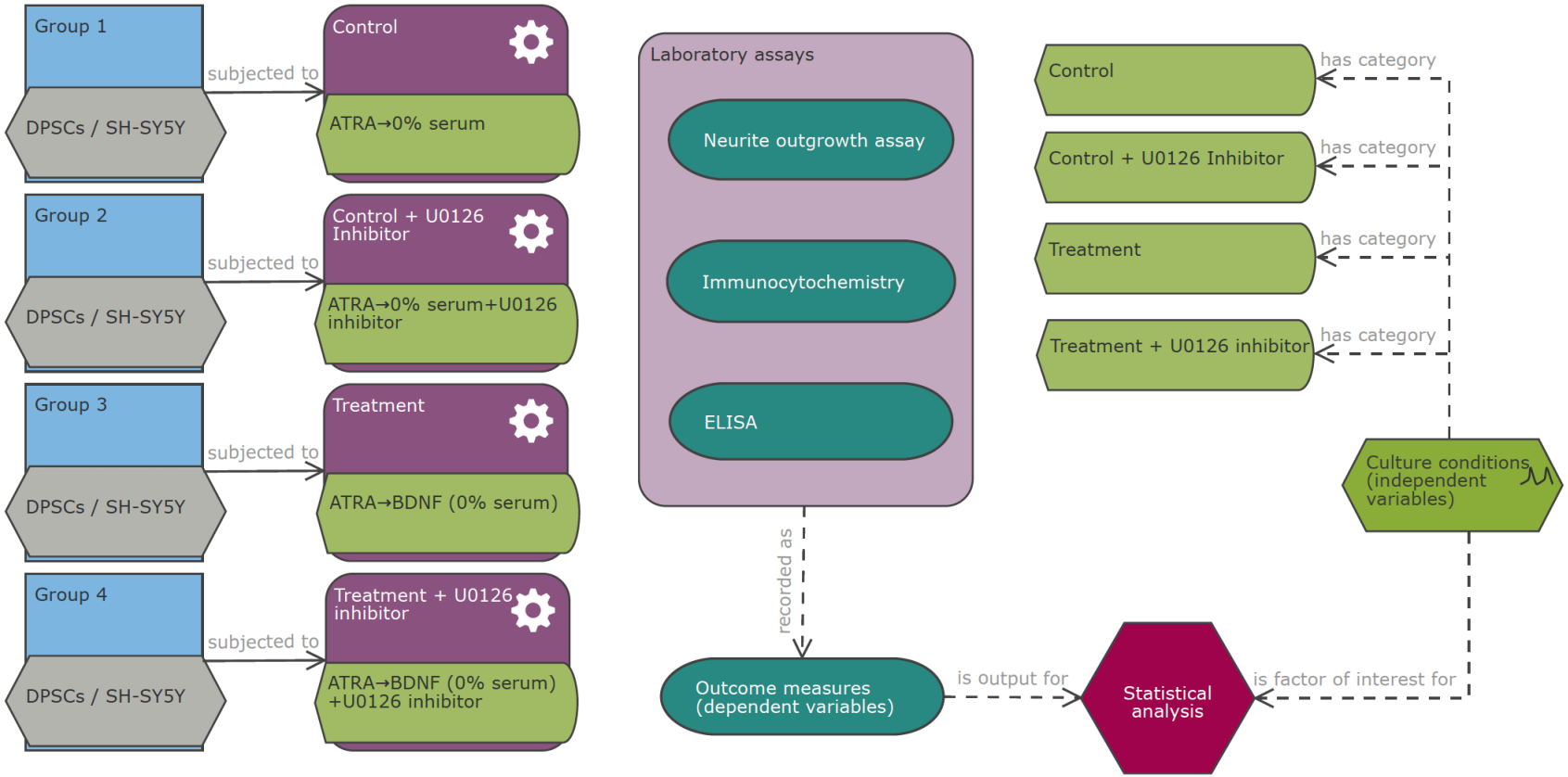

Figure 5.2 Schematic diagram showing the groups and assays used to investigate the involvement of ERK signalling in the neuronal differentiation of DPSCs in comparison with SH-SY5Y cells. The diagram was designed by the author using the EDA https://eda.nc3rs.org.uk.

5.2. Results

To determine whether the differentiation effect following application of the sequential protocol (ATRA→BDNF) on DPSCs (with SH-SY5Y cells used as positive controls) was dependent upon the ERK/MAPK signalling pathway, the ATRA-differentiated cells were pretreated with and without the ERK1/2 inhibitor (MEK1/2 inhibitor: U0126) (Wu and Park, 2015; Favata *et al.*, 1998) for 1h. Subsequently, the cultures were incubated in BDNF-supplemented or serum-free media (control) for 48h with and without the application of the U0126 inhibitor. The neurite outgrowth assay (described in section 2.5.2), and βIII-tubulin/TUBB3 and NF-M immunofluorescent staining (described in section 2.6) were conducted to assess the differentiation effect in the presence and absence of the U0126 inhibitor. ELISA was also performed to quantify the phosphorylated ERK1/2 (phsopho-p44/42 MAPK/p-ERK1/2) levels (described in section 2.11.3).

5.2.1. Quantitative neurite outgrowth staining assay

The experimental cell types (SH-SY5Y and DPSCs) demonstrated comparable results (Figure 5.3). The BDNF-supplemented group resulted in the highest neurite outgrowth staining amongst all the experimental groups tested after 48h incubation; however, this was not statistically significantly higher compared with the control group (SH-SY5Y: $p = 0.578$ and DPSCs: $p = 0.634$). In contrast, the U0126-treated (MEK/ERK-inhibited) groups (BDNF+U0126 and control+U0126) demonstrated a highly significant reduction in neurite outgrowth readings compared with the BDNF-supplemented group ($p = 0.000$ in both cell types: SH-SY5Y and DPSCs). In addition, there was no difference in neurite outgrowth readings between the U0126-treated groups in the presence and absence of BDNF supplementation (SH-SY5Y and DPSCs: $p = 1$; p-values were adjusted by Bonferroni

correction for multiple tests). These U0126-treated groups were also significantly lower in neurite outgrowth readings compared with the control group (SH-SY5Yand DPSCs: $p = 0.002$ was for control vs BDNF+U0126 whereas SH-SY5Y: $p = 0.000$ and DPSCs: $p = 0.002$ were for control vs control+U0126).

The associated cell viability staining of the neurite outgrowth assay revealed comparable results in both cell types (SH-SY5Y and DPSCs) with the BDNF-supplemented group producing the highest cell viability readings amongst the experimental groups tested (Figure 5.3). The BDNF-supplemented group showed significantly higher readings compared with those of the control (SH-SY5Y: $p = 0.025$ and DPSCs: $p = 0.000$) and the control plus U0126 inhibitor (SH-SY5Y and DPSCs: $p = 0.000$). Moreover, there was no significant difference in cell viability readings between the BDNF-supplemented groups in presence and absence of U0126 inhibitor (SH-SY5Y: $p = 0.845$ and DPSCs: $p = 0.245$). The BDNF plus U0126 inhibitor group demonstrated higher cell viability readings compared with those of the control with and without application of the U0126 inhibitor in DPSCs and SH-SY5Y cells. Nonetheless, the BDNF plus U0126 inhibitor groups demonstrated only statistically significantly higher cell viability readings compared with those of the control plus the U0126 inhibitor group in DPSC cell type (BDNF+U0126 vs control+U0126 in DPSCs: $p = 0.005$ and SH-SY5Y: $p = 0.123$; BDNF+U0126 vs control in DPSCs: $p = 0.241$ and SH-SY5Y: $p = 0.752$).

Data captured using confocal microscopy images for the experimental groups supported the quantitative data obtained by plate reader in which the BDNF-supplemented groups exhibited the highest immunofluorescent staining and most neuronal morphological features amongst all the experimental groups (Figure 5.4). The neurite outgrowth/cell membrane and cell viability staining data from the BDNF-supplemented group displayed markedly higher staining and neuronal-like branching in SH-SY5Y cells compared with those of the BDNF plus

U0126 inhibitor and controls with and without inhibitor. Similarly, the BDNF-supplemented group of DPSC cultures exhibited higher staining and neuronal-like cell elongation with some branching compared with cultures supplemented with BDNF plus the U0126 inhibitor and controls with and without inhibitor. In contrast, the control and the U0126-supplemented groups (BDNF+U0126 and control+U0126) demonstrated decreased cell membrane staining and no apparent morphologically neuronal-like change. Furthermore, the BDNF-supplemented groups in the presence or absence of MEK/ERK inhibitor showed higher cell viability staining (green stain) compared with the control groups with or without MEK/ERK inhibitor supplementation.

These neurite outgrowth assay results demonstrated that BDNF supplementation enhanced the neuritogenesis and viable cell survival/growth in the DPSC and SH-SY5Y cell cultures. Furthermore, the presence of the MEK/ERK inhibitor (U0126) markedly blocked neuritogenesis and to some degree the cell viability in the BDNF-supplemented groups. These results indicate that the ERK/MAPK pathway was involved in neuritogenesis but may not be involved in cell viability/survival during differentiation.

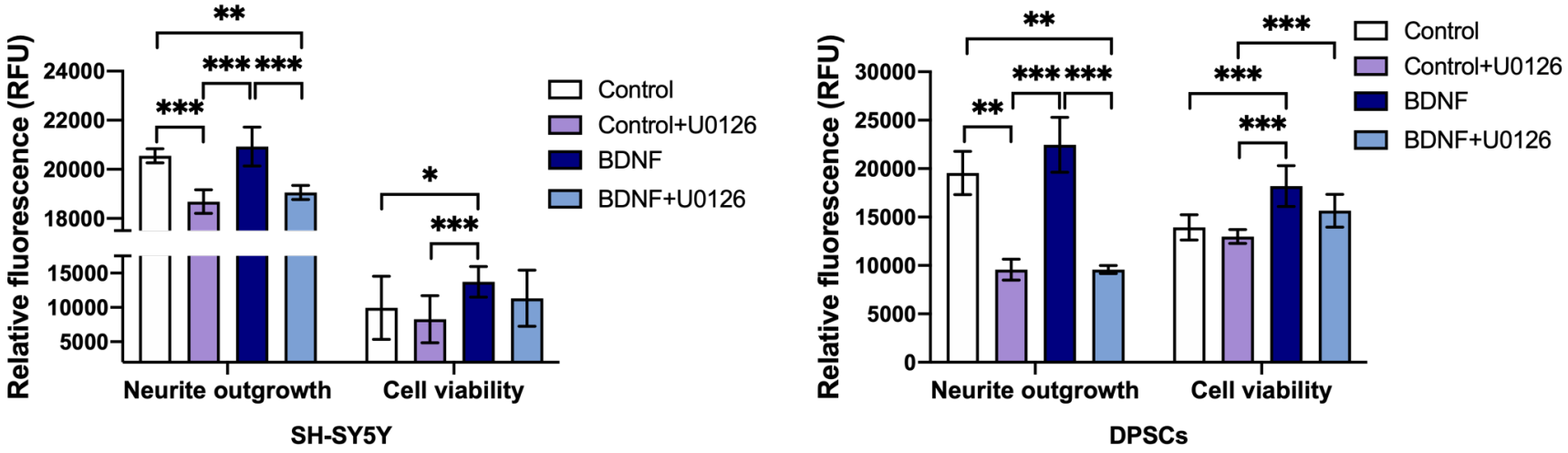

Figure 5.3 Relative neurite outgrowth quantification as measured by neurite outgrowth staining kit. The relative quantification of neurite outgrowth and viable cell staining intensities readings were performed after 48h incubation in the presence or absence of the MEK/ERK inhibitor (U0126) in both cell types tested (SH-SY5Y and DPSCs). Data plotted are mean ± SD and was analysed using the Kruskal-Wallis test with pairwise comparison; the significance values were adjusted by Bonferroni correction for multiple tests (n = 12; *$p < 0.05$, **$p < 0.01$, and ***$p < 0.001$). Note: RFU = relative fluorescence unit.

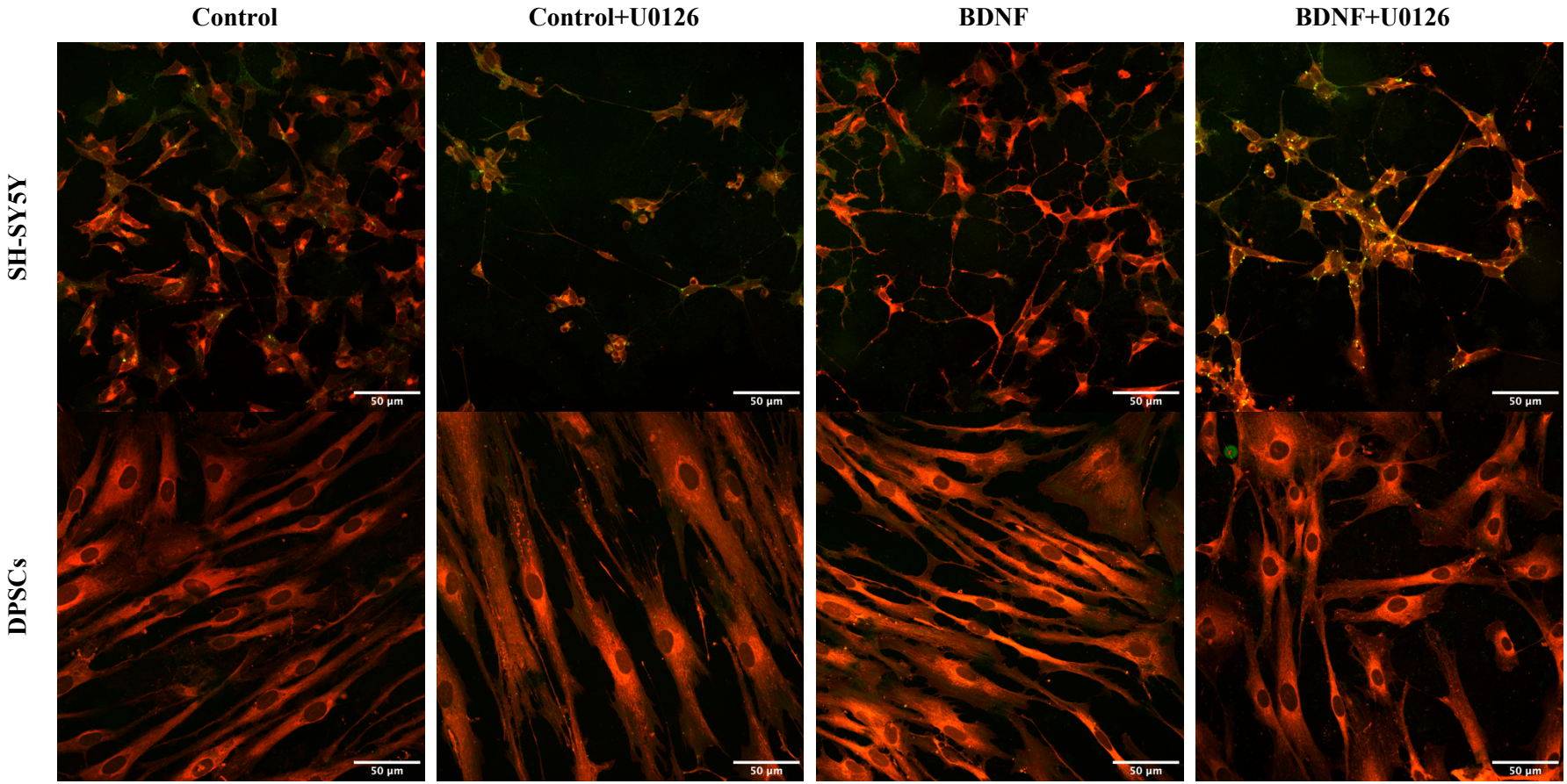

Figure 5.4 Representative images of relative neurite outgrowth quantification. Images were captured immediately after plate reading of fluorescent intensities using confocal microscopy at a 40X magnification. The images are 2-stain merged channels of the orange-red fluorescent cell membrane stain as an indicator for neurite outgrowth and green stain as an indicator for viable cells (n = 12). Scale bars are shown.

5.2.2. Immunocytochemistry

The immunocytofluorescence staining demonstrated that the tested cell types (SH-SY5Y and DPSCs) showed comparable results (Figure 5.5 and Figure 5.6). The highest expression of the mature neuronal marker (NF-M) was detected in the BDNF-supplemented group compared with all other experimental groups. In contrast, the presence of the MEK/ERK inhibitor with BDNF-supplementation (BDNF+U0126 group) resulted in markedly lower expression of this neuronal marker. The expression of the NF-M in the BDNF+U0126 group was similar to that of control groups in the absence or presence of MEK/ERK inhibitor. Whereas the cytoskeleton marker (βIII-tubulin/TUBB3) was comparable between the experimental groups.

In both cell types (SH-SY5Y and DPSCs), Immunocytofluorescence staining revealed the highest neuronal morphological features in the BDNF-supplemented group compared with all other experimental groups (Figure 5.5 and Figure 5.6). Immunostaining in the BDNF-supplemented group revealed higher neuronal-like branching in SH-SY5Y cells compared with that of the BDNF plus U0126 inhibitor and the control groups in the absence or presence of the U0126 inhibitor. Similarly, the immunostaining in the BDNF-supplemented group in DPSC cultures displayed more bipolar neuronal-like cell elongation compared with that of the BDNF plus U0126 inhibitor and the control groups in the absence or presence of the U0126 inhibitor. Furthermore, there was no morphological difference between BDNF plus U0126 inhibitor and the control groups with or without U0126 inhibitor supplementation. These neuronal-like morphological observations in the absence and presence of the U0126 inhibitor supported the observations of the neuronal-like morphological features which were previously reported in the neurite outgrowth results (section 5.2.1).

These immunocytochemical observations indicated that the BDNF supplementation induced neuronal-like differentiation at 48h incubation. Moreover, the inhibition of ERK

signalling abrogated the BDNF-induced upregulation of mature neuronal marker (NF-M) and neuronal-like morphologically changes, albeit no change in expression of general cytoskeleton marker (βIII-tubulin) was observed. These results suggest that ERK signalling is required for BDNF-induced neuronal differentiation.

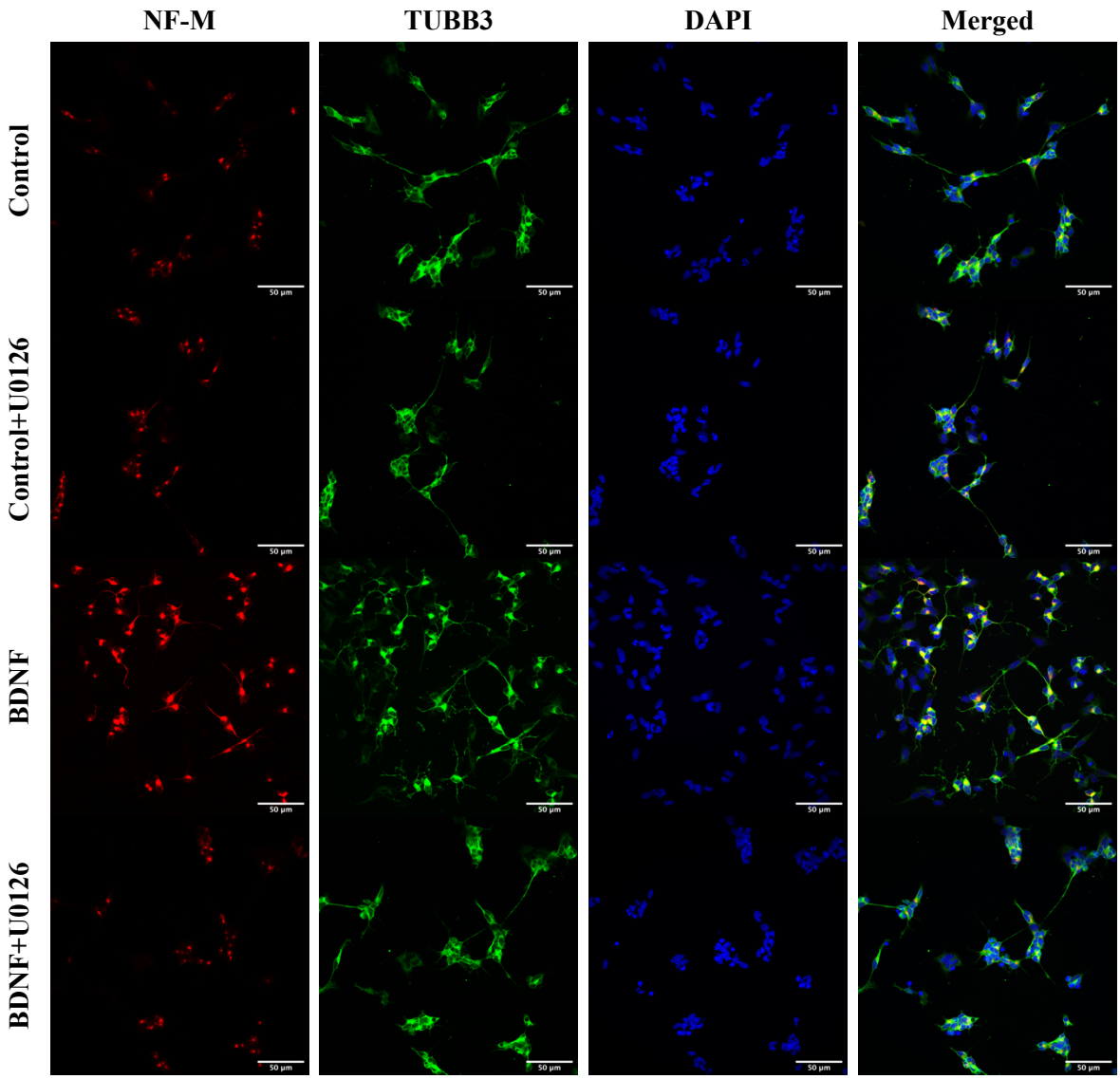

Figure 5.5 Representative immunocytochemical staining of the NF-M and TUBB3/βIII-tubulin in the control and BDNF-supplemented groups with or without U0126 inhibitor supplementation in SH-SY5Y cells. All groups were preincubated with ATRA for 5 days as a preparatory step before ERK inhibition studies (n = 12). Scale bars are shown.

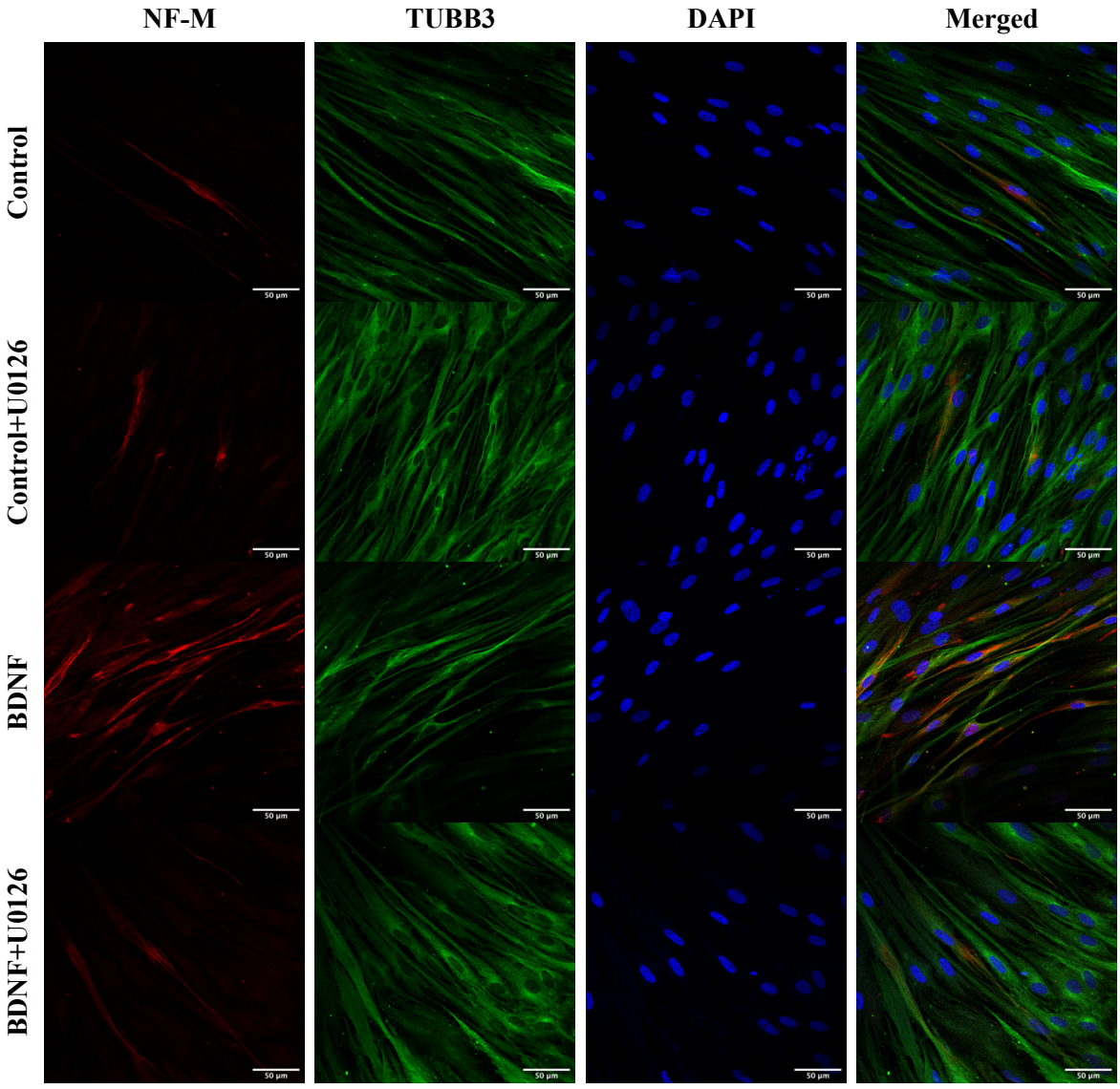

Figure 5.6 Representative immunocytochemical staining of NF-M and TUBB3/βIII-tubulin in the control and BDNF-supplemented groups in the presence or absence of the MEK/ERK (U0126) inhibitor supplementation in DPSCs. All groups were preincubated with ATRA for 5 days as a preparatory step before ERK inhibition studies (n = 12). Scale bars are shown.

5.2.3. ELISA

The BDNF-supplemented group in both tested cell types showed the highest phosphorylation of ERK1/2/MAPK (phospho-p44/42MAPK/phospho-ERK1/2) compared with all the other experimental groups (Figure 5.7A). The BDNF-supplemented group demonstrated higher percentage of phospho-ERK1/2 protein levels than control in the absence of the MEK/ERK

(U0126) inhibitor (SH-SY5Y: 54.20 ± 10.33% and DPSCs: 18.97 ± 10.03%), albeit there was no statistically significant difference compared with control group (see Figure 5.7B). Furthermore, these BDNF-supplemented groups resulted in highly significant higher phospho-ERK1/2 levels than those of the BDNF plus U0126 inhibitor group (SH-SY5Y and DPSCs: $p = 0.000$), and the control plus U0126 inhibitor group (SH-SY5Y: $p = 0.000$ and DPSCs: $p = 0.043$). There was also no significant difference detected between both U0126-inhibited groups in the absence or presence of BDNF supplementation (control+U0126 and BDNF+ U0126; SH-SY5Y: $p = 1$ and DPSCs: $p = 0.853$).

The pre-treatment with the MEK/ERK (U0126) inhibitor in both cell types (SH-SY5Y and DPSCs) did not only significantly reduce the phospho-ERK1/2 levels in the BDNF-supplemented group but also decreased levels of phospho-ERK1/2 in the control (serum-free media) (Figure 5.7). Nonetheless, it was only statistically significantly lower in SH-SY5Y ($p = 0.001$), but not statistically significantly lower in DPSC cultures ($p = 0.166$) compared with the control without the inhibitor applied. Levels of phospho-ERK1/2 in the BDNF plus inhibitor group were also significantly lower than in the control without inhibitor applied (SH-SY5Y: $p = 0.008$ and DPSCs: $p = 0.000$).

These phospho-p44/42MAPK (p-ERK1/2) quantification results indicated that the BDNF supplementation induced upregulation of phospho-ERK1/2 protein, which was effectively blocked by the U0126 inhibitor pre-treatment. Hence, this indicates that the phosphorylation and activation of ERK1/2 were involved in neuronal differentiation of the SH-SY5Y cells and DPSCs.

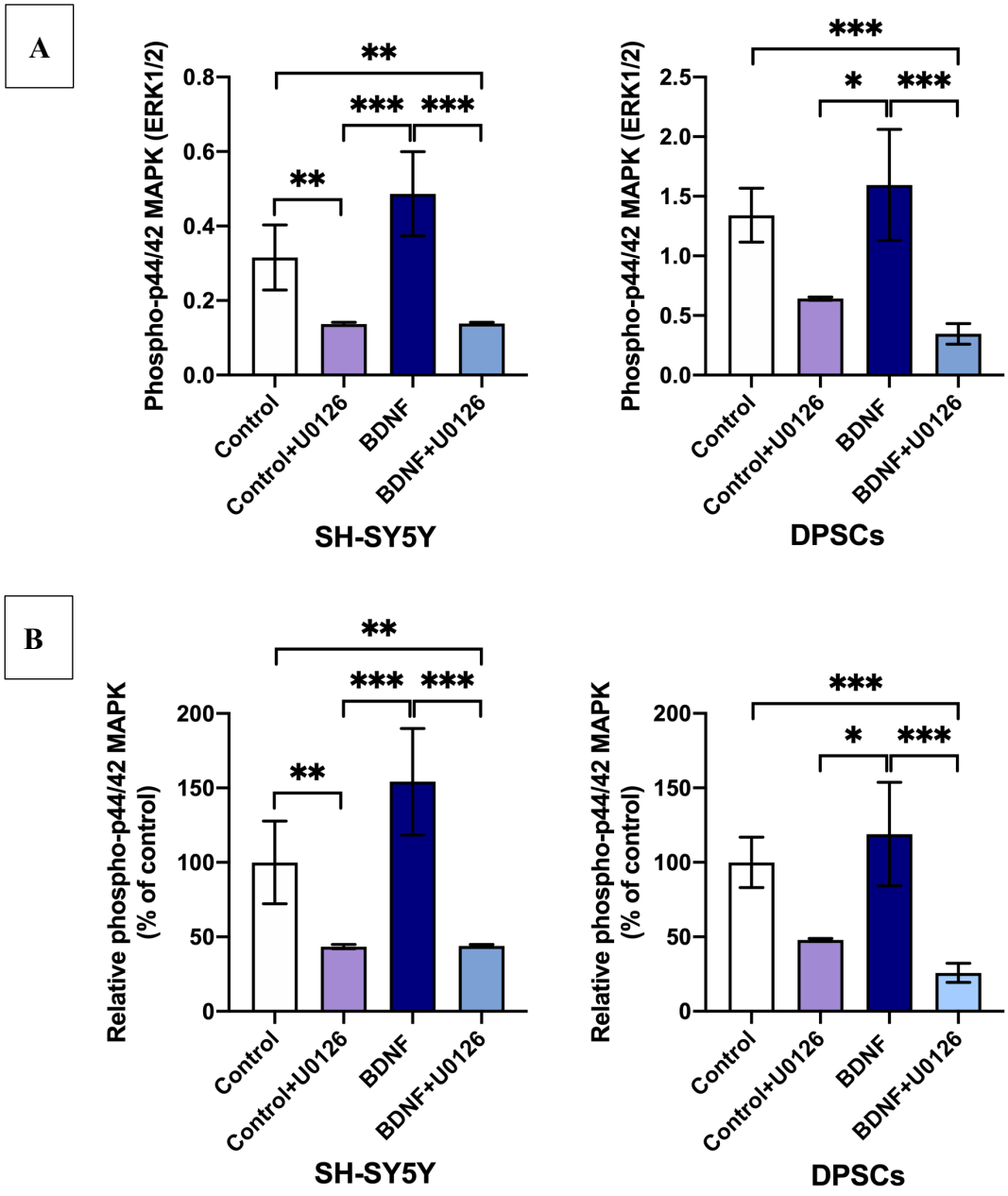

Figure 5.7 Phosphorylation of p44/42 MAPK (phosho-ERK1/2) in control and BDNF-supplemented groups in the presence and absence of MEK/ERK inhibitor (U0126). A, Phosho-ERK1/2 protein quantification levels. B, Relative percentage of phosho-ERK1/2 protein quantification levels in the experimental groups to those of the control group. These phosphorylation data were detected by quantitative sandwich ELISA, and absorbance readings were recorded at 450 nm. Data plotted are mean ± SD analysed by Kruskal-Wallis test with pairwise comparison; the significance values were adjusted by Bonferroni correction for multiple tests (n = 12, except for DPSC control+U0126 group, n = 6; *p < 0.05, **p < 0.01, and ***p < 0.001).

5.3. Discussion

In the present chapter, the crucial role of the ERK1/2 signalling pathway in the neuronal differentiation of BDNF-induced DPSCs was explored in comparison with that of the positive control cells (SH-SY5Y cells). This activated pathway was assayed by neurite outgrowth quantification, neuronal protein expression, and phosphorylated ERK1/2 MAPK protein quantification in the absence and presence of the ERK1/2 inhibitors (MEK1/2 inhibitor).

Experimental groups were incubated with ATRA for 5 days before the ERK/MAPK investigation as a preparatory phase. This incubation approach was necessary as the higher neuronal differentiation and maturation was detected after the 2nd stage (BDNF supplementation) of the sequential protocol (ATRA→BDNF) not in ATRA supplementation stage as reported in previous studies (see chapter 3 and chapter 4) in agreement with work done by others using SH-SY5Y cells (Encinas *et al.*, 2000; Goldie, Barnett and Cairns, 2014). Furthermore, it is known that ATRA activates the TrkB cell membrane receptor, which increases the binding of and responsiveness to BDNF supplementation (Kaplan *et al.*, 1993). This TrkB receptor activation reached a peak after 5 days of ATRA supplementation (Encinas *et al.*, 2000). Thus, the cells were pretreated with ARTA for 5 days before the further investigation of the control and BDNF-supplemented groups in the presence or absence of the inhibitor.

The analysis of relative neurite outgrowth and associated confocal microscopic images showed that the MEK/ERK inhibitor blocked neuritogenesis induced by BDNF supplementation. Also, there was no difference detected between the control and BDNF-supplemented group in the presence of the inhibitor. These results are consistent with results described by Encinas *et al.* (1999), who used a similar methodology to differentiate the neuroblastoma cell line (SH-SY5Y) into neuronal-like cells. These results were also in

agreement with those of Gakhar-Koppole *et al.* (2008) and Tzeng *et al.* (2015) who used a different methodology to differentiate human neural and bone marrow stem cells into neuronal-like cells, respectively. Indeed, these studies reported the lack of morphological neuronal-like features in the presence of the MEK/ERK inhibitor. This consistency in the neurite outgrowth results for these different differentiation studies supports a key role for ERK/MAPK signalling in neuritogenesis regulating neuronal differentiation regardless of the cell type and method used.

Neuritogenesis was noticeably increased in the BDNF-supplemented group in both cell types. However, the quantitative neurite outgrowth data in this group were not significantly higher than that of the control in the absence of the MEK/ERK inhibitor. The possible explanation for this is that for morphological neuronal differentiation induction, more than one-time application of BDNF-supplementation is required to produce a significant increase in neurite length. Furthermore, the time of incubation analysed in this study was 48 hours which was sufficient to investigate the inhibition effect of MEK/ERK inhibitor on neurite outgrowth but may not be sufficient to detect differences in increases in neurite length significantly. For example, the neurite outgrowth reported in this chapter was not as significant as the increases reported in previous chapters (Figure 3.17 and Figure 4.7) in which the same cells were incubated for a longer incubation period with frequent changes of the differentiating media. Furthermore, the previously highlighted comparable signalling pathway studies did not show neurite length quantification data to enable morphological assessment of neuronal-like changes. Indeed, Encinas *et al.* (1999) reported the counting of neurites per cell body rather than actual neurite length, and Tzeng *et al.* (2015) presented phase contrast images to exhibit the cell morphology change without any quantification. Also, the Gakhar-Koppole *et al.* (2008)

reported that the significant increase in the neurite outgrowth was observed in already differentiated neurons and not in neural progenitor cells after only hours of incubation.

The accompanying cell viability and staining data demonstrated that BDNF supplementation significantly increased the cell viability reading, which was not significantly affected by MEK/ERK inhibition. Comparable results have been previously reported by a study using a similar methodology (Encinas *et al.*, 1999) as well as a further study using a different methodology (Tzeng *et al.*, 2015). These studies concluded that the cell viability and survival of the SH-SY5Y and the bone marrow stem cells during neuronal differentiation, respectively, were not induced via the ERK/MAPK signalling pathway, but via PI3K/Akt signalling. Hence, the ERK/MAPK signalling pathway was not central to sustaining the cell viability and survival/growth during neuronal differentiation following BDNF supplementation.

The immunostaining data also demonstrated that the ERK1/2 inhibitor markedly inhibited morphological neuronal differentiation and expression of the neuronal mature protein markers (NF-M) induced by BDNF supplementation. Other neuronal differentiation studies have also observed a reduction in neuronal protein markers following MEK/ERK inhibitor supplementation (Zheng *et al.*, 2020; Lang *et al.*, 2019; Phonchai *et al.*, 2019; Lim *et al.*, 2011). Data indicated that the ERK/MAPK signalling pathway was involved in neuronal differentiation of DPSCs and other mesenchymal stem cells, respectively. Thus, the ERK/MAPK signalling pathway could also mechanistically regulate neuronal protein expression.

Levels of the phosphorylated p44/42 MAPK (p-ERK1/2) protein increased after BDNF supplementation, and these levels were subsequently lower when cultures were pretreated with MEK/ERK inhibitor before BDNF supplementation. These results were in agreement with

similar studies analysing the neuronal-like differentiation of stem and SH-SY5Y cells using a range of methodologies (Tzeng *et al.*, 2015; Lang *et al.*, 2019; Phonchai *et al.*, 2019; Lim *et al.*, 2011; Lim *et al.*, 2008; Encinas *et al.*, 1999). These studies reported an upregulation of the p-ERK protein following application of the differentiation inducing supplement, which significantly reduced following MEK/ERK inhibitor pre-treatment. Consequently, it is highly possible that the sequential protocol (ATRA→BDNF) also induced the DPSC neuronal differentiation through the phosphorylation and activation of ERK1/2.

5.4. Conclusion

The established mature cholinergic sensory DPSC-derived neuronal-like cells (described in chapter 4) and SH-SY5Y-derived neuronal-like cells (described in chapter 3) are induced via ERK/MAPK signalling pathway as determined both morphologically and biochemically. The MEK/ERK (U0126) inhibitor substantially inhibited the neuronal differentiation and ERK phosphorylation of both cell types (DPSCs and SH-SY5Y) induced by BDNF supplementation. These findings indicate the involvement of the proposed ERK/MAPK pathway in the neuronal differentiation as illustrated in Figure 5.1. Hence, targeting the ERK/MAPK pathway by specific inducers could be useful to stimulate neuronal repair and regeneration. In contrast, this study also indicates that ERK1/2 MAPK signalling is not the main pathway involved in cell viability/survival during neuronal differentiation of DPSCs and SH-SY5Y cells. However, the underlying signalling pathway that sustains cell viability/survival during neuronal differentiation of these cells requires further investigation.

CHAPTER 6: PROLIFERATIVE EFFECTS OF LIPUS ON THE SH-SY5Y and DPSC-DERIVED NEURONAL CELL CULTURE MODELS

6.1. Introduction

LIPUS induces cell proliferation in different cell types, including mesenchymal stem cells (Gao *et al.*, 2016b; Ling *et al.*, 2017b; Xie *et al.*, 2019), neural stem cells (Lv *et al.*, 2013; Wu *et al.*, 2020b), chondrocytes (Takeuchi *et al.*, 2008; Nishikori *et al.*, 2002), and keratinocytes (Leng *et al.*, 2018). However, to the best of my knowledge, LIPUS effects have not been investigated in *in vitro* differentiated neuronal-like cells derived from DPSCs and the SH-SY5Y neuroblastoma cell line. As it is known that once neuronal differentiation is established, the cells exit the cell cycle and subsequently lose their proliferative capacity (Hardwick *et al.*, 2015; Buttitta and Edgar, 2007; Järvinen *et al.*, 2010). Therefore, it is of interest to investigate whether LIPUS can induce cell proliferation in the differentiated neuronal-like models derived from SH-SY5Y and DPSCs. These neuronal cell models are kept in differentiating culture environment during LIPUS experimentation. This study attempted to determine the potential of using LIPUS as a pre-stimulator or a combined application with differentiated neuronal-like cells for future use in transplantation therapies or other regenerative tissue engineering approaches, including regenerative endodontics. Furthermore, using human-derived neuronal-like cell culture models to assess the proliferative effect of LIPUS may be more predictable of human nerve responses compared with animal models (Shanks, Greek and Greek, 2009; Bracken, 2009; Jansen *et al.*, 2020). The proliferative effect of LIPUS may also be useful for *in vitro* cell expansion of human-derived neuronal-like models when use in different laboratory testing purposes for neuronal-related problems and therapeutics.

The ERK/MAPK signalling pathway is the principal underlying mechanism for many biological cellular processes in several cell types, including neurons, such as cellular proliferation, differentiation, and homeostasis (Chambard *et al.*, 2007; Cruz and Cruz, 2007). This pathway plays a crucial regulating role in neuroinflammation and neuronal cell survival,

particularly in sensory neurons (O'Brien *et al.*, 2015). At least 160 ERK-activated substrates have been identified in the nucleus or the cytoplasm regulating a range of cellular functions (Yoon and Seger, 2006). It has also been proposed that the ERK signalling pathway underpins cell proliferation following LIPUS exposure in several cell types (Ling *et al.*, 2017b; Gao *et al.*, 2016b; Xia *et al.*, 2019; Zhou *et al.*, 2004). However, it has not been investigated if ERK signalling mediates LIPUS-induced cell proliferation in differentiated cells, including neuronal-like cells.

Therefore, this study aimed to investigate the proliferative effect of LIPUS exposure in established neuronal-like cells derived from DPSCs and the SH-SY5Y neuroblastoma cell line (chapter 3 and 4). A secondary aim was to evaluate whether the number of LIPUS exposures influenced the cell proliferative response. A tertiary aim was to investigate whether the ERK signalling pathway is involved in the proliferative effect of LIPUS on the neuronal-like cell cultures derived from DPSCs and SH-SY5Y neuroblastoma cell line. The grouping and assays conducted in this study are illustrated in Figure 6.1 and Figure 6.2.

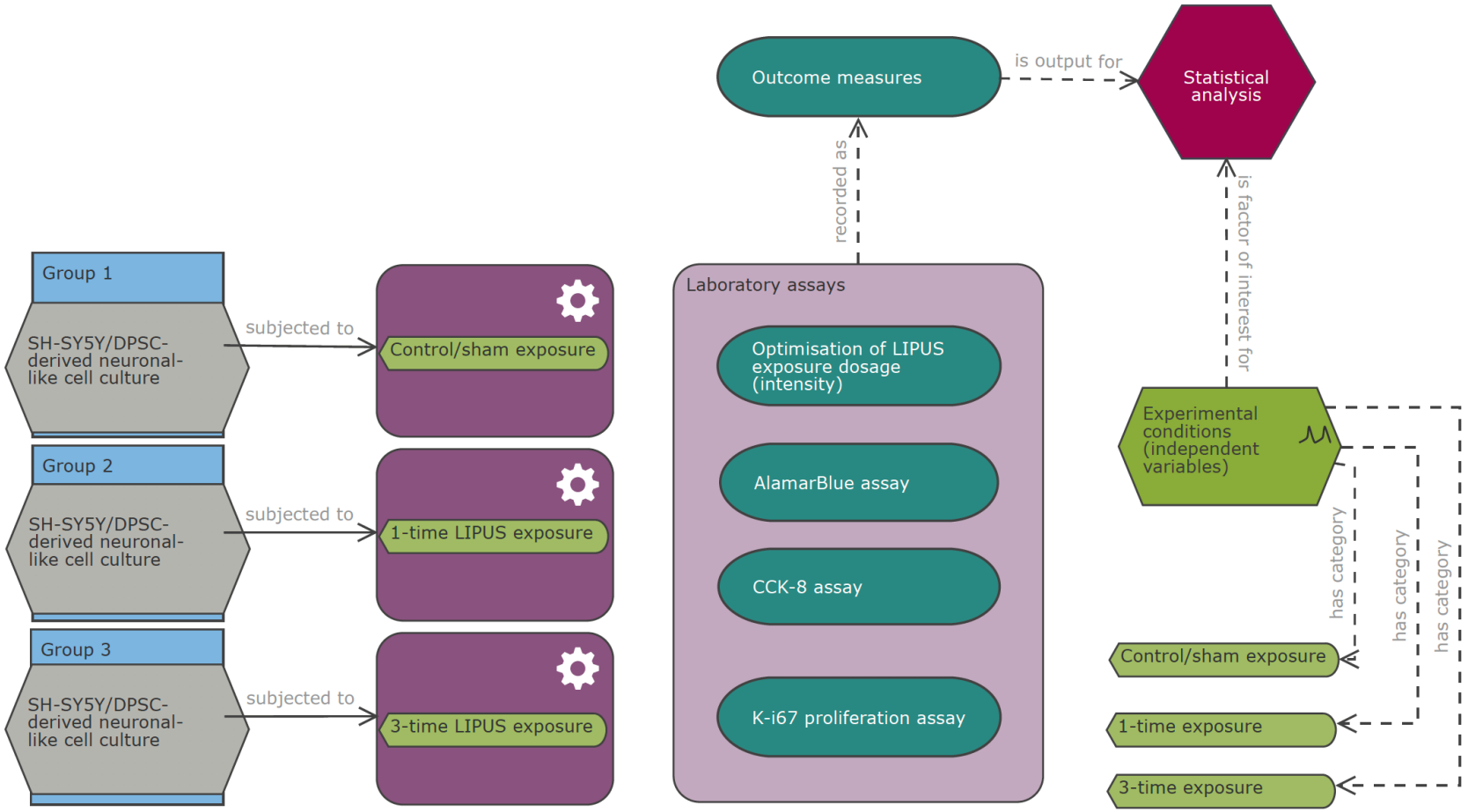

Figure 6.1 Schematic diagram showing the groups and assays used to study the proliferative effect of LIPUS on SH-SY5Y and DPSC-derived neuronal-like cell cultures. The diagram was designed by the author using the EDA https://eda.nc3rs.org.uk.

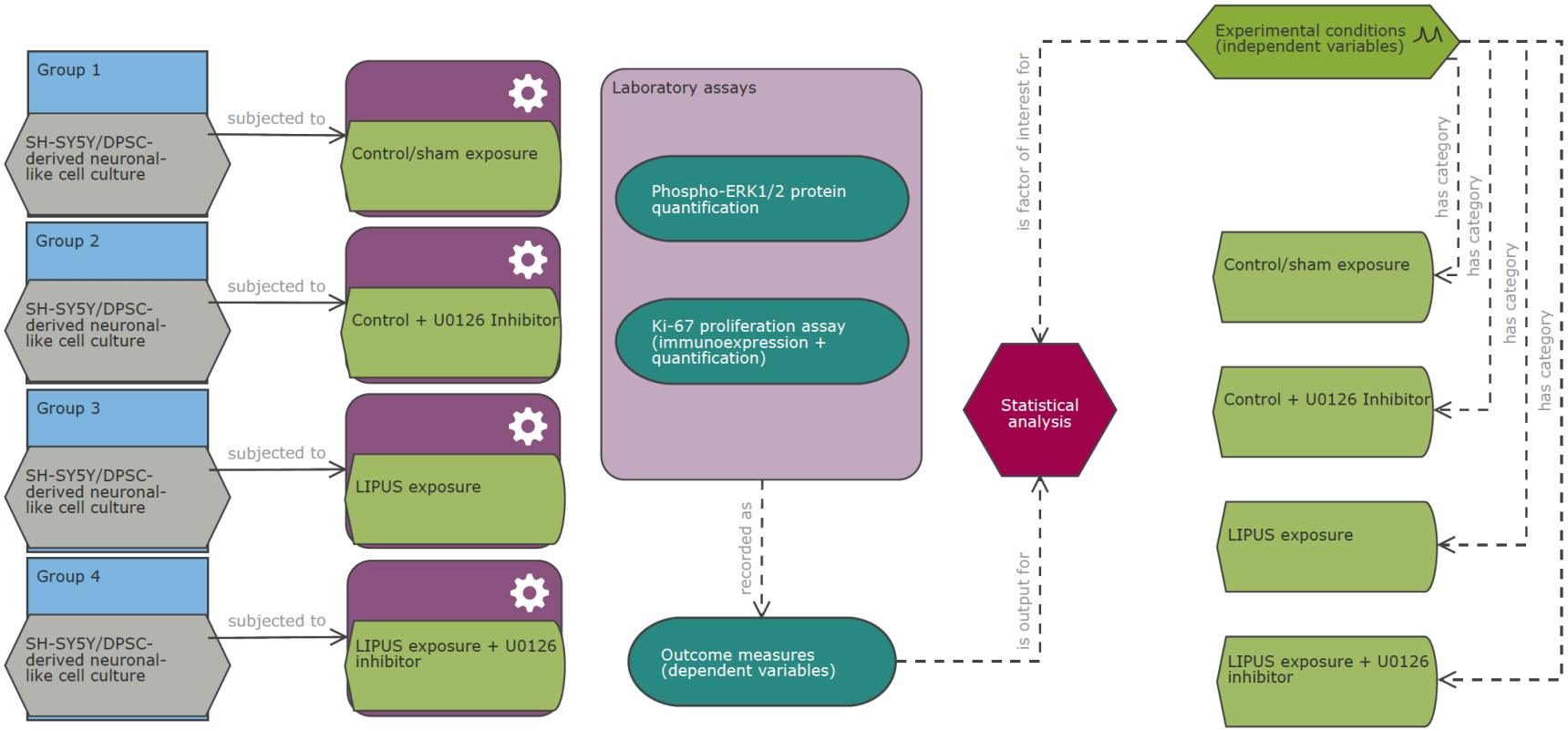

Figure 6.2 Schematic diagram showing the groups and assays used to study the involvement of the ERK/MAPK signalling in the proliferative effect of LIPUS on SH-SY5Y and DPSC-derived neuronal-like cell cultures. The cell cultures were either immediately lysed for ELISA to quantify the levels of phosphorylated ERK1/2 (phsopho-p44/42/MAPK/p-ERK1/2) or 48h-incubated for Ki67 immunostaining assay. The diagram was designed by the author using the EDA https://eda.nc3rs.org.uk.

6.2. Results

The proliferative effect of LIPUS on differentiated SH-SY5Y and DPSCs (d-SH-SY5Y and d-DPSCs) was assessed using cellular metabolic-based assays, including the AlamarBlue (AB) assay and the Cell Counting Kit-8 (CCK-8) assay. These cellular metabolic-based assays can be used to assess the number of cells present in each experimental group. The experimental groups were also studied to determine levels of the proliferation protein marker (Ki-67), and data was used to calculate the proliferation ratio.

6.2.1. Determination of optimal LIPUS stimulation dose

To identify the optimal spatial-average temporal intensity (I_{SATA}), the 10% FBS SH-SY5Y cell cultures were treated with ATRA supplementation for 5 days and then exposed to a range of intensities (30 mW/cm^2, 45 mW/cm^2, 60 mW/cm^2) using the Osteotron LIPUS device, and incubated for 24h. Subsequently, the experimental groups were assessed by AB assay.

The AB absorbance results reflected cell numbers per experimental group as shown in the calibration curves of both cell types (see SH-SY5Y: Figure 3.4 in chapter 3 and DPSCs: Figure 4.2 in chapter 4). The LIPUS-treated groups with I_{SATA} of 45 mW/cm^2 and 60 mW/cm^2 were statistically significantly higher than the sham/control (0 mW/cm^2) or 30 mW/cm^2 groups (Figure 6.3; Kruskal-Wallis test - test statistics (df) = 200.523 (3), p = 0.000). While there was neither significant difference between the sham/control (0 mW/cm^2) and 30 mW/cm^2 groups (p = 0.156) nor between the 45 mW/cm^2, and 60 mW/cm^2 groups (p = 0.969). Thus, the resultant exposure group exhibiting the highest absorbance intensity/cell numbers (60 mW/cm^2) was selected for subsequent studies using additional LIPUS parameters (frequency of 1.5 MHz, pulse of 100 Hz ratio of 1:5 (duty cycle 20%), and time of 20 min based on previous studies as discussed in section 6.3.

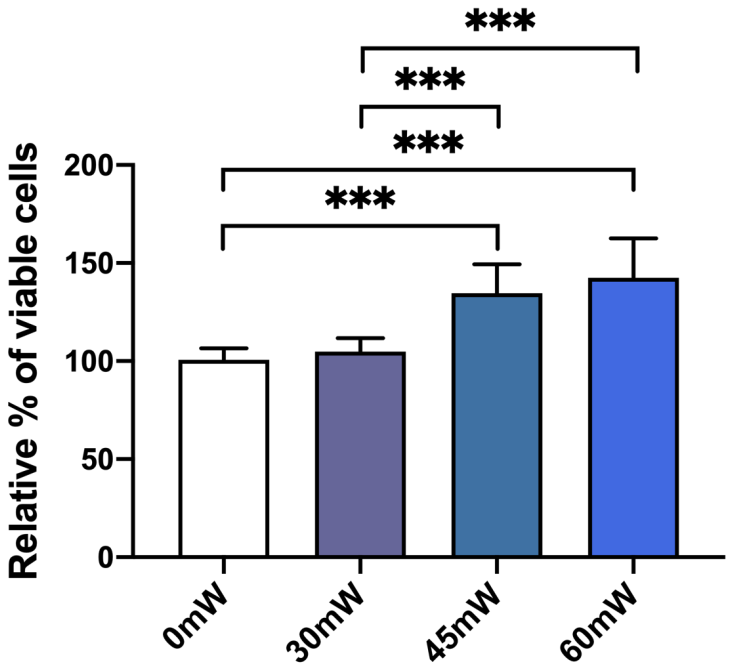

Figure 6.3 Determination of the optimal I_{SATA} exposure dose analysed by AB assay. The AB reduction and oxidative absorbance data were obtained at the wavelengths of 570 nm and 600 nm, respectively (24h after LIPUS exposure). Both data were calculated to provide the relative percentage of AlamarBlue solution reduction levels (% viable cell numbers). The plotted data are mean ± SD analysed by Kruskal-Wallis test with pairwise comparison; the significance values were adjusted by Bonferroni correction for multiple tests (n = 12; ***$p < 0.001$).

6.2.2. Cell numbers after LIPUS exposure assessed by AlamarBlue assay

The AB results demonstrated that the LIPUS-treated groups showed higher statistically significant relative cell numbers compared with controls for both cell types (Figure 6.4; Kruskal-Wallis test - test statistics (df): the d-SH-SY5Y = 29.333 (2) and the d-DPSCs = 33.422 (2), $p = 0.000$). The 1-time LIPUS exposure group (20-min exposure) showed a statistically significantly higher percentage of viable cell numbers than the control/sham (d-SH-SY5Y: $p = 0.011$ and d-DPSCs: $p = 0.041$). The 3-time LIPUS exposure group (daily 20-min exposure for

3 consecutive days) demonstrated the highest statistically significant percentage of viable cell numbers compared with the control group (d-SH-SY5Y and d-DPSCs: $p = 0.000$), and also this was significantly higher than 1-time LIPUS exposure group (d-SH-SY5Y: $p = 0.035$ and d-DPSCs: $p = 0.003$). The AB results indicated that both LIPUS exposures induced increase in the percentage of cell numbers compared with the control/sham group. Also, the greater number of the LIPUS exposure performed, the greater the percentage of the cell numbers produced.

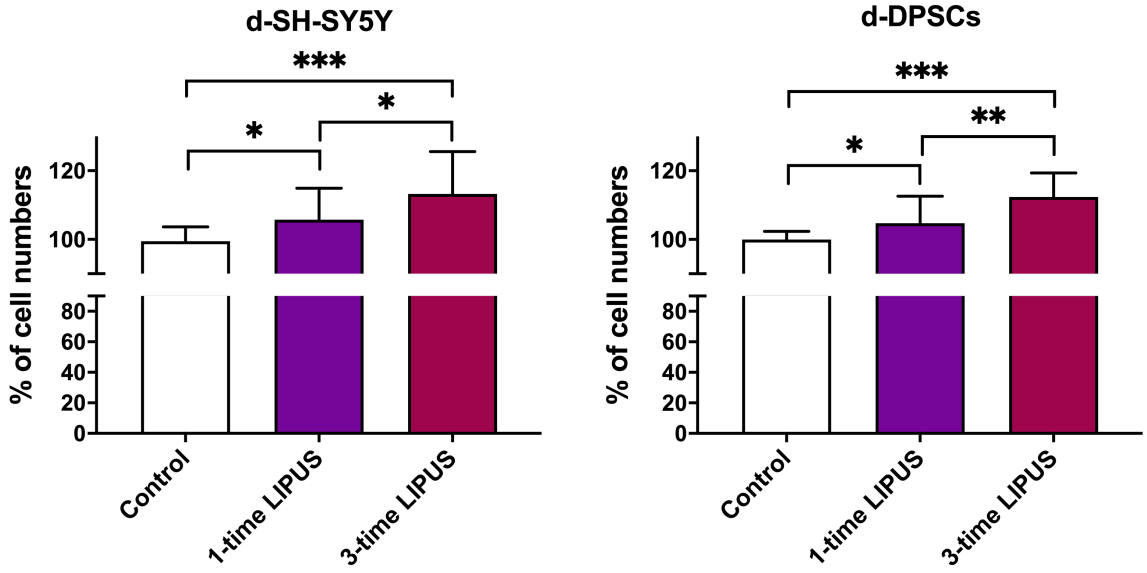

Figure 6.4 Relative cell numbers as determined by AB assay. The data are optical density (OD) values at 570 nm and 600 nm (24h after 3-time LIPUS stimulation) and the relative percentage of AlamarBlue solution reduction levels (% cell numbers) was calculated. The plotted data are mean ± SD analysed by Kruskal-Wallis test with pairwise comparison; the significance values were adjusted by Bonferroni correction for multiple tests (d-SH-SY5Y: n = 32, d-DPSCs: n = 27; *$p < 0.05$, **$p < 0.01$, and ***$p < 0.001$).

6.2.3. Cell counts after LIPUS exposure assessed by Cell Counting Kit-8 assay

To assess cell proliferation by Cell Counting Kit-8 assay (CCK-8 assay), calibration curve was generated using known cell densities (12500, 25000, 50000, and 100000) which were incubated for 6h. Then, the experimental groups were assessed by CCK-8 assay. The calibration curve

demonstrated that the absorbance results reflected cell numbers per experimental group (Figure 6.5).

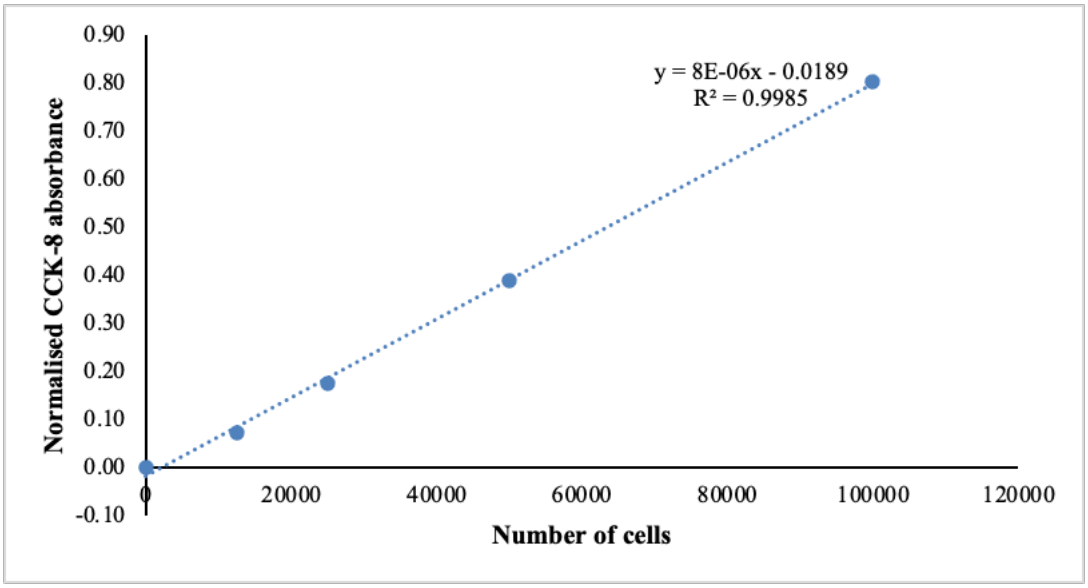

Figure 6.5 Representative calibration curve of CCK-8 assay using SH-SY5Y neuroblastoma cell line. The linear regression equation and R^2 coefficient (>0.9) are shown next to the line of the best fit of all different densities' means.

Consequently, the LIPUS-treated groups showed higher statistically significant absorbance levels relating to cell counts compared with the control groups for both neuronal-like cell culture models (Figure 6.6; Kruskal-Wallis test - test statistics (df): the d-SH-SY5Y = 13.197 (2), p = 0.001 and d-DPSCs = 8.772 (2), p = 0.012). Levels for the 1-time LIPUS exposure group demonstrated statistically significantly higher cell count absorbance values compared with the control/sham group in d-SH-SY5Y cell culture (p = 0.035), but not in d-DPSC cell culture (p = 0.988). While the 3-time LIPUS exposure group resulted in statistically significant cell count absorbance values compared with the control group in both cell cultures (d-SH-SY5Y: p = 0.001 and d-DPSCs: p = 0.032); these data were only statistically significantly higher than values derived from the 1-time LIPUS exposure group in d-DPSC cell

culture (d-DPSCs: $p = 0.030$ and d-SH-SY5Y: $p = 0.941$). The CCK-8 results indicated that LIPUS exposure resulted in increased cell numbers compared with the control/sham group. Also, there was a trend that indicated that for an increasing number of LIPUS exposure performed, there was an increasing number of cells, albeit there was no statistically significant difference between the 1-time and 3-time LIPUS-treated groups in d-SH-SY5Y cell culture.

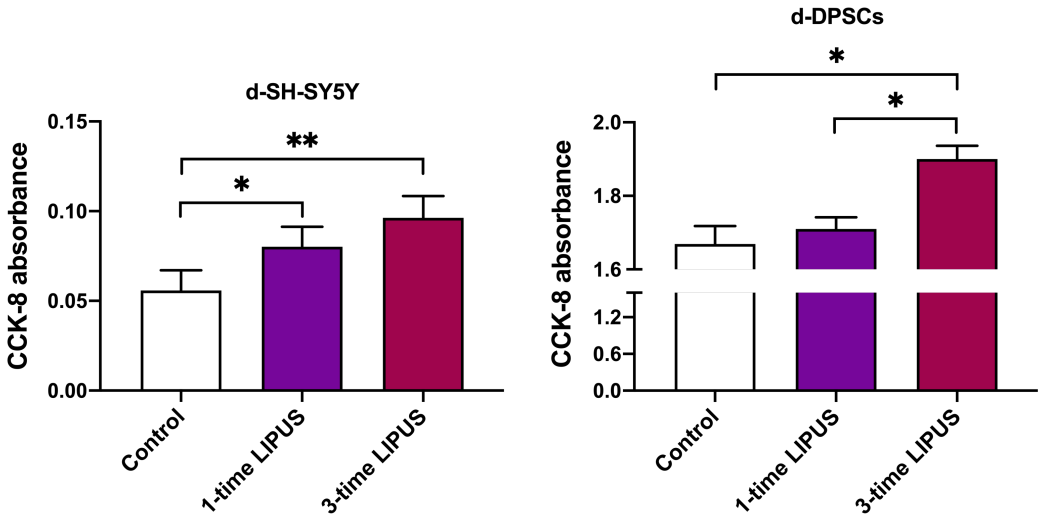

Figure 6.6 Assessment of the cell numbers as determined by CCK-8 assay. The data shown are plate-reader absorbance values at 450 nm (24h after 3-time LIPUS stimulation). The data are normalised for background levels and presented as mean ± SEM. The statistical comparison was performed through Kruskal-Wallis test with pairwise comparison; the significance values were adjusted by Bonferroni correction for multiple tests (d-SH-SY5Y: n = 12, d-DPSCs: n = 14; *$p < 0.05$, **$p < 0.01$, and ***$p < 0.001$).

6.2.4. Proliferation ratio after LIPUS exposure assessed by Ki67 indicator

Cellular proliferation was assayed using the Ki67 staining marker in both neuronal-like cell culture models. Immunocytochemical data showed that LIPUS treatment distinctively increased the number of nuclear immunopositive labelling with the Ki67 marker compared with the control/sham group (Figure 6.7 and Figure 6.8). In addition, the 3-time LIPUS group showed higher immunopositive Ki67 nuclei than the 1-time LIPUS group.

Consequently, the Ki67 staining index was calculated (percentage of the Ki67 stained nuclei to the nuclei number of the whole cell population) in both neuronal-like cell culture models; the number of the cell population was revealed by DAPI stain. The results revealed that the LIPUS-treated groups demonstrated a higher proliferation ratio of Ki67 positive cells compared with the control group (Figure 6.9). Statistical analysis revealed that there was a significant difference in mean proliferation ratio of Ki67 positive cells between the experimental groups (One-way ANOVA test - F statistics (df): the d-SH-SY5Y: F (2,97) = 32.597, p = 0.000 and d-DPSCs: F (2,96) = 8.291, p = 0.000). The 1-time LIPUS group had a statistically significantly higher percentage of Ki67 immunopositive cells compared with the control/sham group (d-SH-SY5Y: p = 0.000 and d-DPSCs: p = 0.003). Likewise, the 3-time LIPUS group was statistically significantly higher in the percentage of Ki67 immunopositive cells than that of the control (d-SH-SY5Y: p = 0.000 and d-DPSCs: p = 0.001). Although, the 3-time LIPUS showed higher percentage of Ki67 immunopositive cells compared with the 1-time LIPUS, there was no significant difference between the 1-time LIPUS and the 3-time LIPUS groups (d-SH-SY5Y: p = 0.527 and d-DPSCs: p = 0.839).

These results further supported LIPUS inducing significant cell proliferation. The 3-time LIPUS exposure, however, did not statistically significantly increase cell proliferation compared with the 1-time LIPUS exposure.

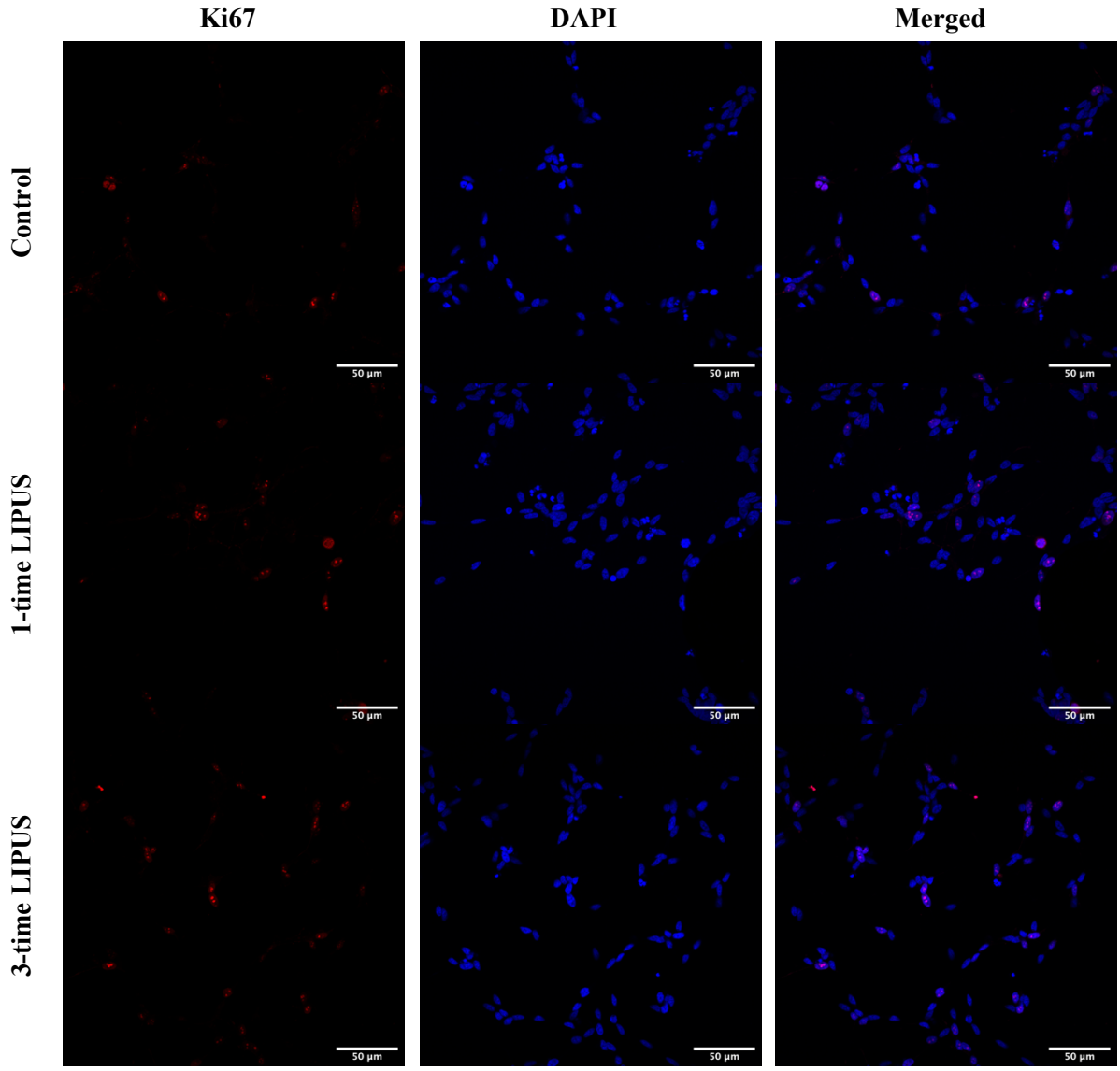

Figure 6.7 Immunocytochemical analysis of the proliferative nuclear protein marker (Ki67) in the d-SH-SY5Y neuroblastoma cells. The nuclei were stained with the Ki67 marker to determine the newly formed cells (red stain) and the DAPI to demonstrate the whole cell population (blue stain). Images were acquired using multi-track laser scanning under Zeiss LSM 700 confocal microscopy at a 40x magnification: n = 29. Scale bars are shown.

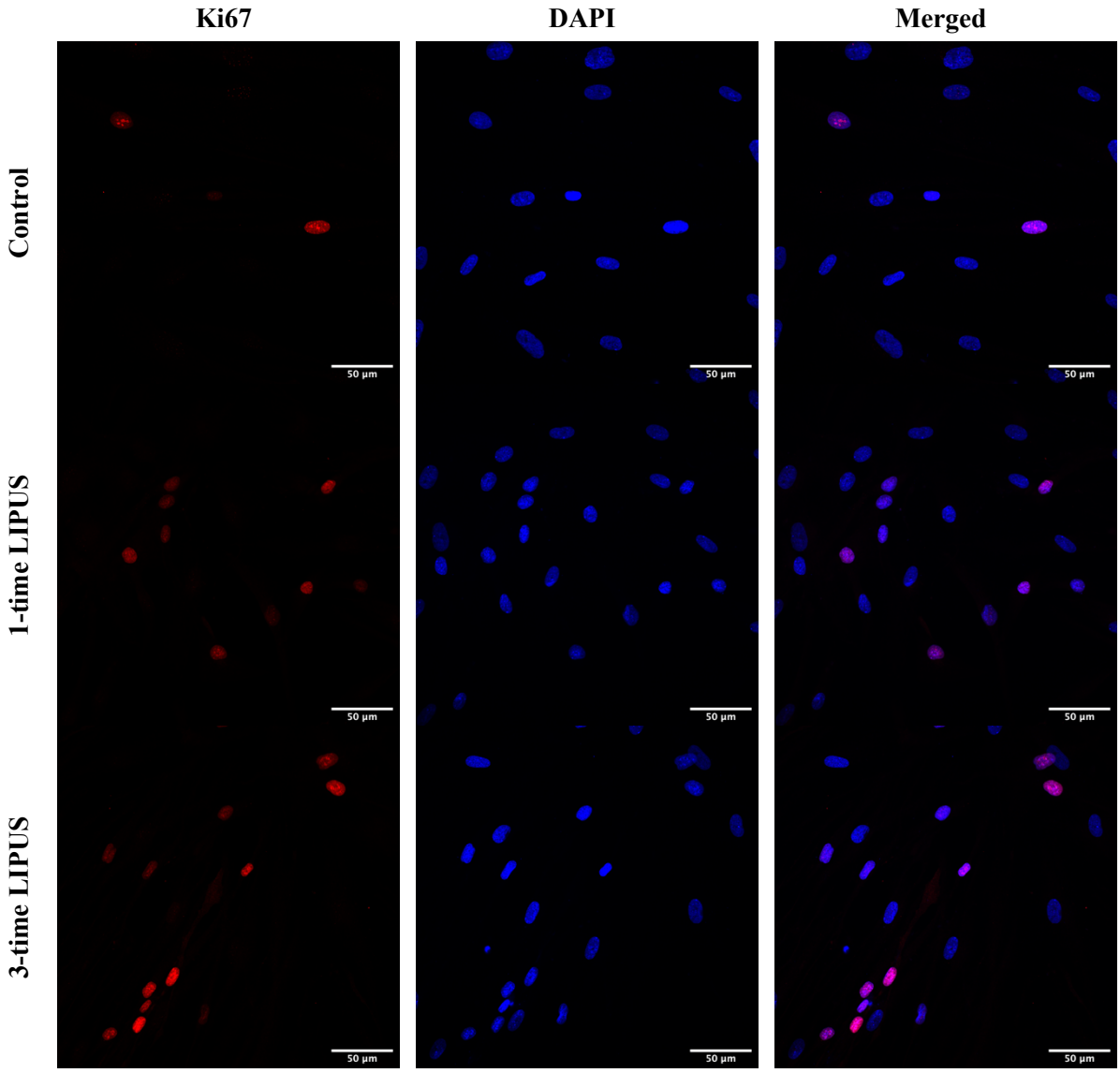

Figure 6.8 Immunocytochemical analysis of proliferative nuclear protein marker (Ki67) in the d-DPSCs. The nuclei were stained with the Ki67 marker to determine the newly formed cells (red stain) and the DAPI to demonstrate the whole cell population (blue stain). Images were acquired using multi-track laser scanning under Zeiss LSM 700 confocal microscopy at a 40x magnification: n = 33. Scale bars are shown.

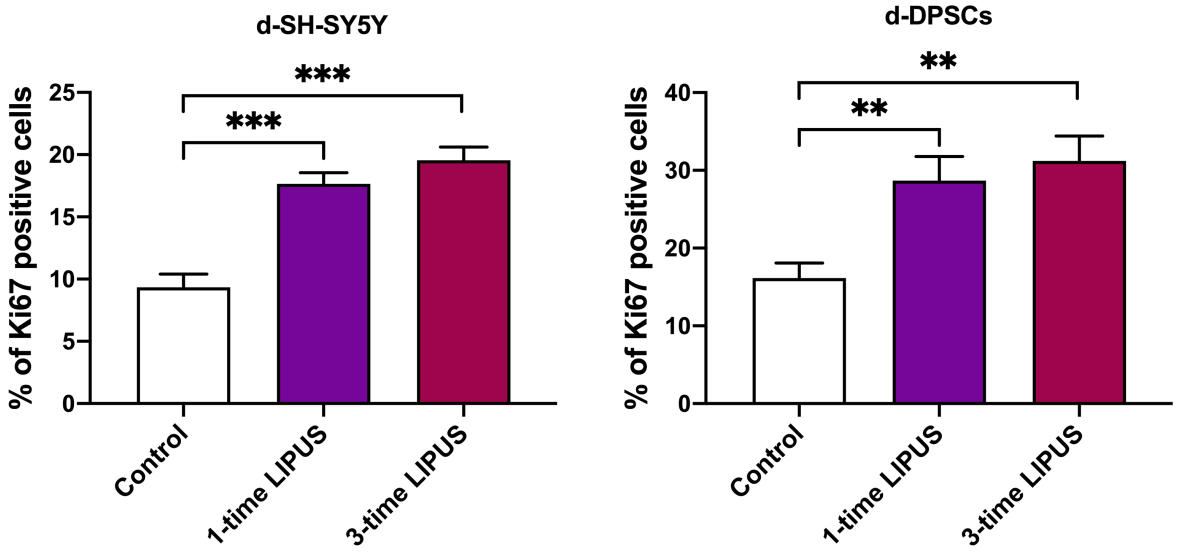

Figure 6.9 Quantified ratio of Ki67 positive cells. The Ki67 positively stained cells were counted and their percentage in the whole cell population (stained with DAPI) was determined. Data are plotted as mean ± SEM. The groups were statistically compared using One-way ANOVA and then Games-Howell post-hoc test for pairwise comparison between groups (d-SH-SY5Y: n = 29, d-DPSCs: n = 33; $^{**}p < 0.01$, and $^{***}p < 0.001$).

6.2.5. The involvement of the ERK/MAPK signalling pathway in the LIPUS-simulated cell proliferation

To determine whether the ERK signalling pathway is involved in the proliferative effect of LIPUS in d-SH-SY5Y and d-DPSCs, cultures were pretreated with and without the ERK1/2 inhibitor (MEK1/2 inhibitor: U0126) for 1h before a single 20-min LIPUS exposure. Subsequently, the cell cultures were either immediately lysed for ELISA to quantify the phosphorylated ERK1/2 (phsopho-p44/42 MAPK/p-ERK1/2) or 48h-incubated for Ki67 immunostaining to assess the proliferation levels in the presence or absence of the MEK1/2 inhibitor (U0126).

6.2.5.1. Proliferation ratio after LIPUS exposure in the presence or absence of the MEK1/2 inhibitor (U0126)

The proliferative Ki67 staining assay revealed that the LIPUS-treated group of both neuronal-like cell culture models exhibited the highest levels of Ki67-labelled immunopositive nuclei compared with other experimental groups (Figure 6.10 and Figure 6.11). This increase in the LIPUS-treated groups was markedly reduced in the presence of the MEK1/2 inhibitor (U0126) in the d-SH-SY5Y and the d-DPSCs.

Notably, the inhibition levels of Ki67-labelled immunopositive nuclei in LIPUS plus U0126 groups were different in the d-SH-SY5Y and d-DPSC cell cultures. The LIPUS plus U0126 group in the d-SH-SY5Y showed a noticeable reduction in levels of Ki67-labelled immunopositive nuclei compared with the LIPUS group, but still much higher levels compared with those of the control groups in the presence or absence of the U0126 inhibitor (Figure 6.10). In contrast, the levels of Ki67-labelled immunopositive nuclei in LIPUS plus U0126 group of the d-DPSC cell culture were comparable with those of the control with and without the U0126 inhibitor (Figure 6.11). Furthermore, there was a reduction in Ki67-labelled nuclei in control plus U0126 inhibitor compared with the control/sham group in both neuronal-like cell culture models.

Consequently, the proliferation ratio of the Ki67-labelled immunopositive nuclei to the whole cell population (DAPI stain) was calculated in all experimental groups of both neuronal-like cell cultures (Figure 6.12A). Statistical analysis revealed that there was a significant difference in the mean proliferation ratio of Ki67 positive cells between the experimental groups (Kruskal-Wallis test - Test statistics (df): the d-SH-SY5Y: H (3) = 43.835, p = 0.000 and d-DPSCs H (3) = 28.424, p = 0.000). The LIPUS-treated group demonstrated a statistically significantly higher percentage of Ki67 immunostaining cells compared with the control/sham

group in the presence or absence of U0126 inhibitor (LIPUS vs Control: d-SH-SY5Y: $p = 0.000$ and d-DPSCs: $p = 0.021$ and LIPUS vs Control+U0126: $p = 0.000$ in both cell types). The LIPUS-treated group also had a statistically significantly higher percentage of Ki67 labelled cells compared with LIPUS plus U0126 inhibitor group (d-SH-SY5Y: $p = 0.033$ and d-DPSCs: $p = 0.000$) which indicate the ability of MEK/ERK inhibitor to significantly reduce the cell proliferation induced by LIPUS. In contrast, the control/sham group did not show any statistically significant difference in the proliferation ratio of Ki67 positive cells compared with the control plus U0126 inhibitor group (d-SH-SY5Y: $p = 0.263$ and d-DPSCs: $p = 0.158$) nor the LIPUS plus U0126 inhibitor group (d-SH-SY5Y: $p = 0.823$ and d-DPSCs: $p = 0.266$). The LIPUS plus U0126 inhibitor group resulted in a statistically significant higher proliferation ratio of Ki67 positive cells compared with control plus U0126 inhibitor group in the d-SH-SY5Y ($p = 0.005$) but not in d-DPSC cell culture ($p = 0.210$).

The absolute number of Ki67 positively stained cell calculations supported the proliferation ratio results which showed similar trend results of the d-SH-SY5Y and d-DPSC cell cultures (Figure 6.12B: Kruskal-Wallis test - Test statistics (df): the d-SH-SY5Y: H (3) = 42.630, $p = 0.000$ and d-DPSCs H (3) = 41.169, $p = 0.000$). Notably, LIPUS plus U0126 inhibitor groups in both cell types demonstrated a significant higher number of Ki67 positively stained cells compared with the control plus U0126 inhibitor group (d-SH-SY5Y: $p = 0.001$ and d-DPSCs: $p = 0.004$: Figure 6.12B). This finding indicates that the MEK/ERK inhibitor partially inhibited the LIPUS-induced cell proliferation compared with control plus MEK/ERK inhibitor group. Thus, more than one pathway may be also involved in LIPUS-induced cell proliferation. Overall, the Ki67 results showed that LIPUS induced significant cell proliferation, and U0126 inhibitor pre-treatment significantly inhibited this cell proliferation.

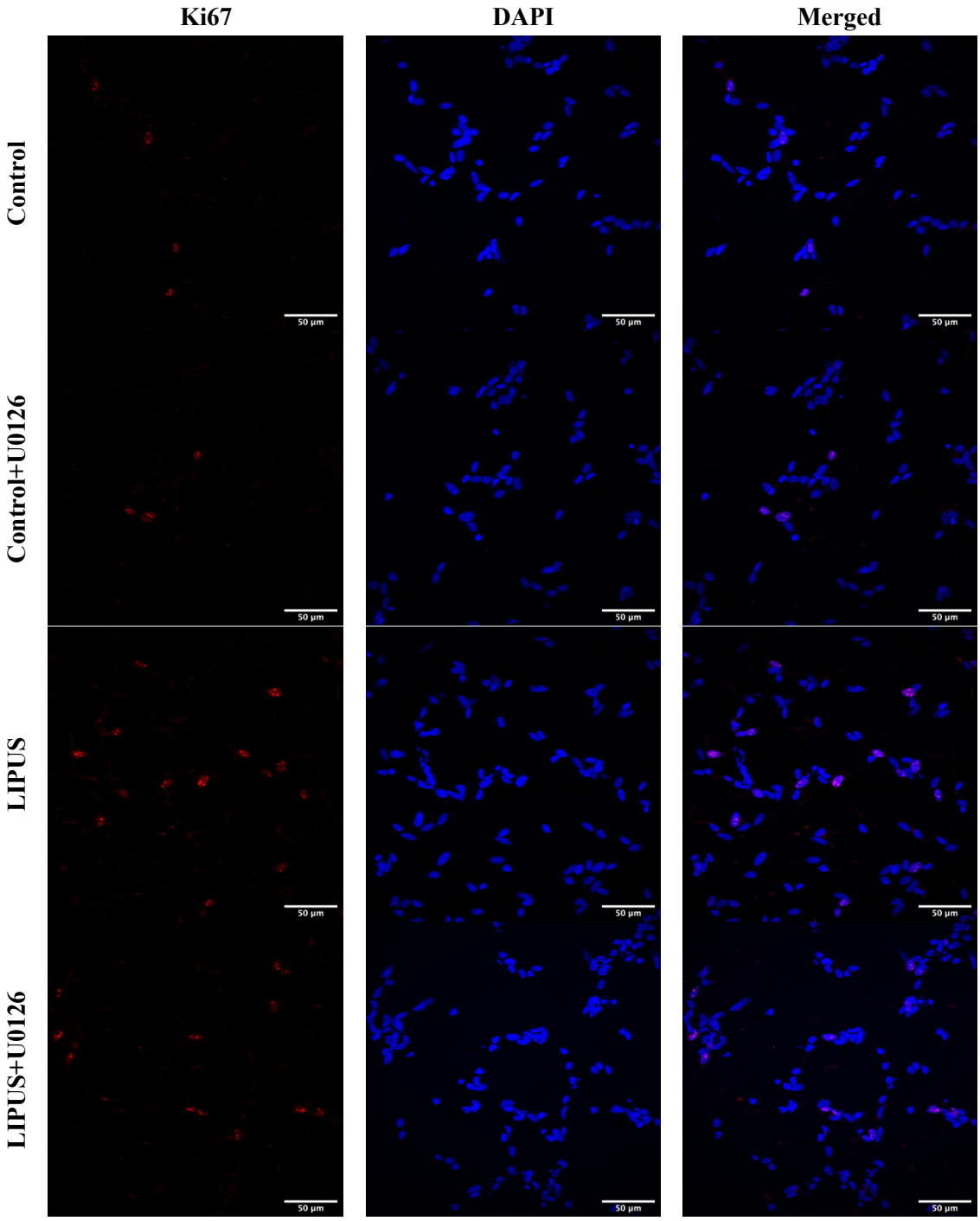

Figure 6.10 Immunocytochemical staining of the proliferation nuclear protein marker (Ki67) in the d-SH-SY5Y with and without the MEK inhibitor (U0126). The immunocytochemistry was performed after 48h incubation following LIPUS or sham exposure. The Ki67 marker was used to label newly formed cells (red stain) and the DAPI stain was used to demonstrate the whole cell population (blue stain). Images were acquired using multi-track laser scanning under Zeiss LSM 700 confocal microscopy with oil lens at a 40x magnification: control (n = 24). Scale bars are shown.

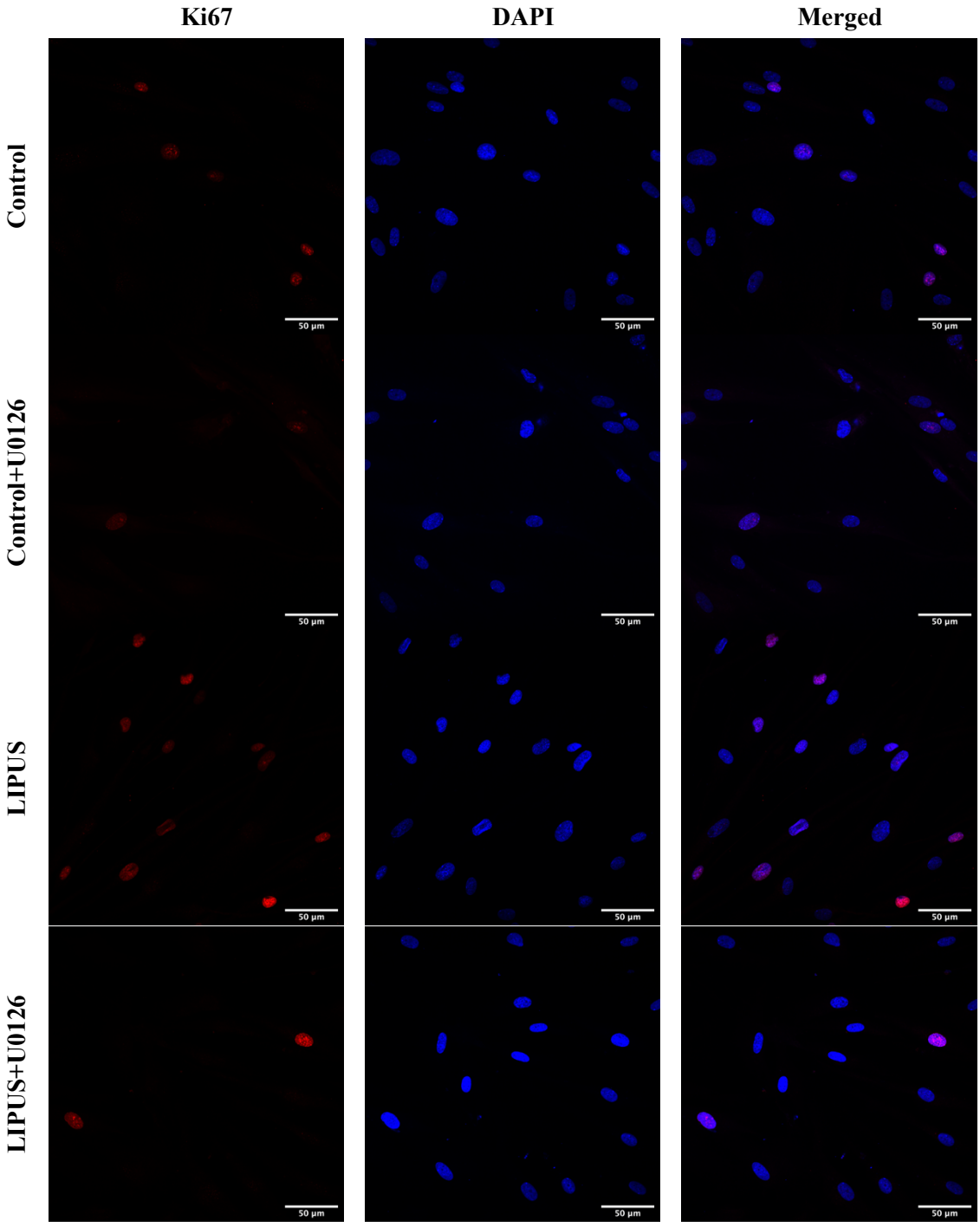

Figure 6.11 Immunocytochemical staining of the proliferation nuclear protein marker (Ki67) in the d-DPSCs with and without the MEK inhibitor (U0126). The immunocytochemistry was performed after 48h incubation following LIPUS or sham exposure. The Ki67 marker was used to label proliferating cells (red stain) and the DAPI stain was used to demonstrate the whole cell population (blue stain). Images were acquired using multi-track laser scanning under Zeiss LSM 700 confocal microscopy at a 40x magnification: n = 25. Scale bars are shown.

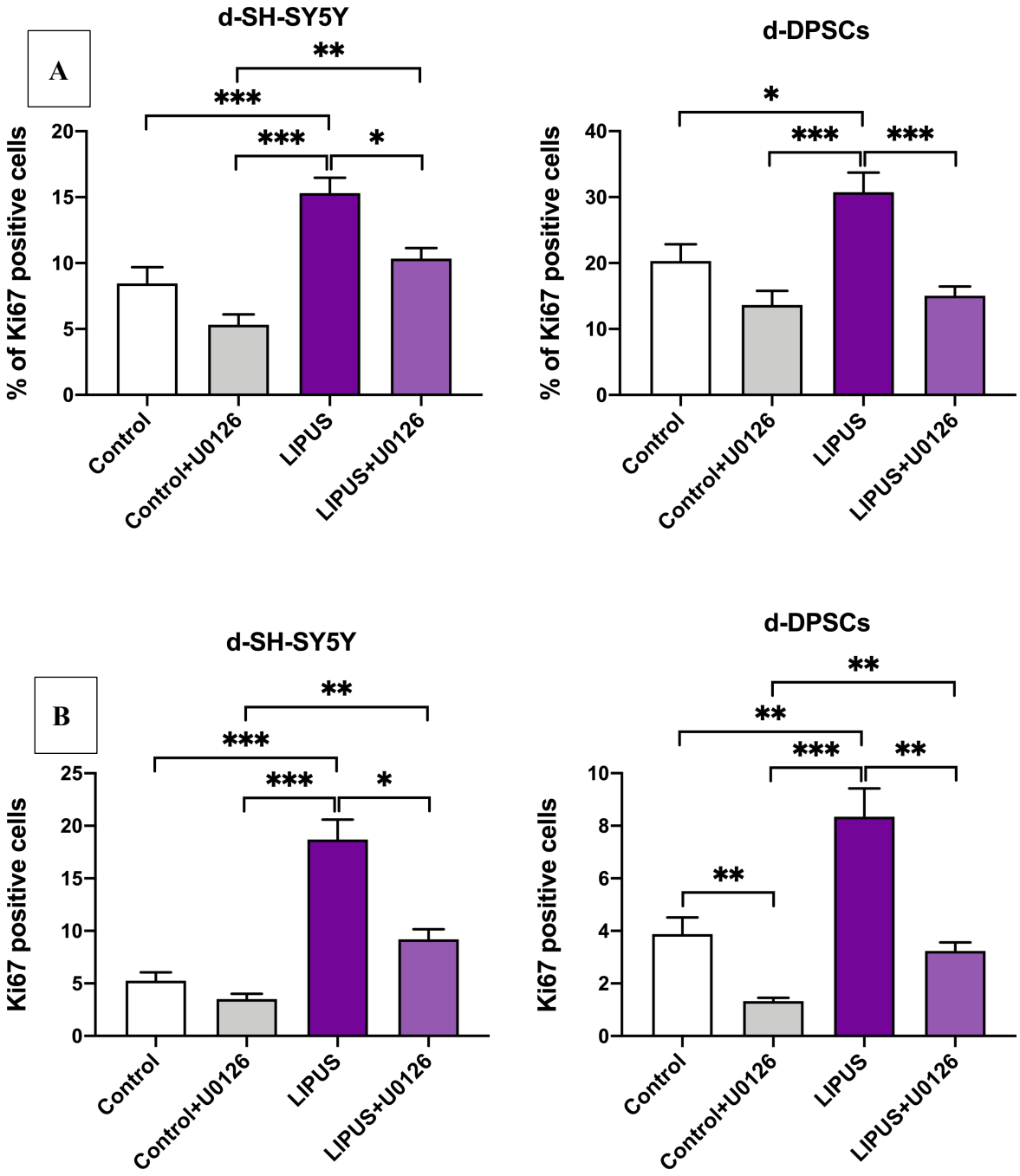

Figure 6.12 The quantified ratio and absolute number of Ki67 positive cells in the presence or absence of MEK inhibitor (U0126). A, The Ki67 ratio: the Ki67 positively stained cells (red-stained nuclei) were counted and the relative percentage of the Ki67 positively stained cells was determined to the whole cell population (DAPI stain: blue-stained nuclei) per captured image. B, Absolute number of the Ki67 positively stained cells (red-stained nuclei) per each group. Data are plotted as mean ± SEM. The groups were statistically compared using Kruskal-Wallis test with pairwise comparison; the significance values were adjusted by Bonferroni correction for multiple tests (d-SH-SY5Y: n = 24, d-DPSCs: n = 25; *$p < 0.05$, **$p < 0.01$, and ***$p < 0.001$).

6.2.5.2. Phospho-ERK1/2 (phospho-p44/42MAPK) levels in the presence or absence of the MEK1/2 inhibitor (U0126)

The results demonstrated that the LIPUS-treated groups in both differentiated cell models (d-SH-SY5Y and d-DPSCs) demonstrated the highest phospho-ERK1/2 (phospho-p44/42MAPK) levels compared with all the other experimental groups. Furthermore, the pre-treatment with the MEK/ERK inhibitor reduced the phospho-ERK1/2 protein levels in the control and LIPUS groups (Figure 6.13).

Statistical analysis confirmed that there was a significant difference in mean phospho-ERK1/2 levels between the experimental groups (Figure 6.13A: One-way ANOVA test - F statistics (df): the d-SH-SY5Y: F (3,48) = 41.822, p = 0.000 and d-DPSCs: F (3,48) = 20.995, p = 0.000). The LIPUS-treated group exhibited significantly increased levels of phospho-ERK1/2 protein compared with the LIPUS plus inhibitor group (p = 0.000) and control plus inhibitor group (p = 0.000). In comparison with the control group in absence of inhibitor, the statistically significant increase was only detected in the d-SH-SY5Y cell culture (d-SH-SY5Y: p = 0.040, and d-DPSC: p = 0.589). However, the relative percent increase of phospho-ERK1/2 levels in the LIPUS-treated group to the control group was roughly comparable in both cell types (d-SH-SY5Y: 17.3 ± 4.50% and d-DPSC: 19.5 ± 11.74% in Figure 6.13B). This increase in both cell types suggested that the LIPUS induced ERK1/2 phosphorylation, albeit the significant difference was only observed in the d-SH-SY5Y cell culture and the MEK/ERK inhibitor pre-treatment reduced this phosphorylation.

Similarly, the MEK/ERK-treated groups (control+U0126 and LIPUS+U0126) in both neuronal-like cell cultures showed a significantly lower phospho-ERK1/2 levels compared with the control (control+U0126 vs control: p = 0.000 and p = 0.001 in d-SH-SY5Y and d-DPSCs,

respectively whereas LIPUS+U0126 vs control: $p = 0.023$ and $p = 0.002$ in d-SH-SY5Y and d-DPSCs, respectively).

Notably, the phospho-ERK1/2 protein levels in the LIPUS plus U0126 group of the d-SH-SY5Y cell cultures were statistically significantly higher compared with the control plus U0126 group ($p = 0.003$). Whereas, in the d-DPSC cell culture, the levels of phospho-ERK1/2 protein of the LIPUS plus U0126 and control plus U0126 groups were comparable (d-DPSC: $p = 0.977$). This observation in the d-SH-SY5Y but not in d-DPSCs indicated that the upstream regulator (MEK1/2) might not be the sole activators of the ERK phosphorylation induced by LIPUS in the d-SH-SY5Y cell culture.

These phospho-ERK1/2 protein levels' results indicated the involvement of ERK1/2 signalling in the control and LIPUS-treated groups, but LIPUS-treated groups demonstrated higher activation levels of ERK1/2 signalling compared with controls.

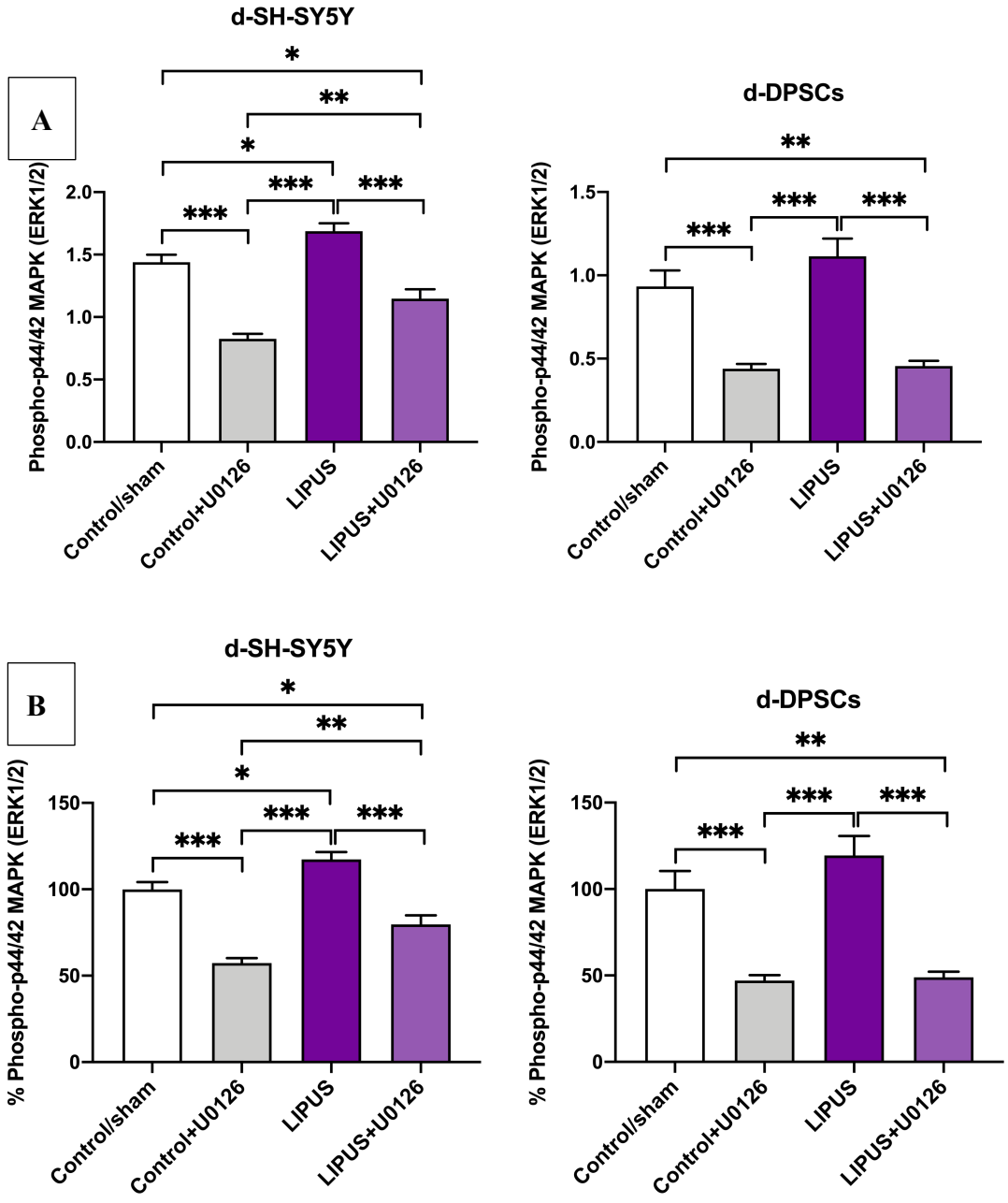

Figure 6.13 Phosphorylation of p44/42 MAPK (phosho-ERK1/2) in control/sham and LIPUS-treated groups in the presence or absence of MEK/ERK inhibitor (U0126). A, Phosho-ERK1/2 protein quantification levels. B, Relative percentage of phosho-ERK1/2 protein quantification levels in the experimental groups to those of the control group. These phosphorylation data were detected by quantitative sandwich ELISA, and absorbance readings were recorded at 450 nm. Data plotted are mean ± SEM analysed by One-way ANOVA and then Games-Howell post hoc for pairwise comparisons (d-DPSCs: n = 8, except for LIPUS, n=10; SH-SY5Y: n = 6, except for LIPUS, n = 8; *p < 0.05, **p < 0.01, and ***p < 0.001).

6.3. Discussion

Data shown in the present chapter demonstrates that LIPUS exposure promoted cell proliferation of neuronal-like cells derived from DPSCs and SH-SY5Y cells as determined by metabolic-based assays (AlamarBlue and CCK-8 assay) and also supported by Ki67 immunoreactive expression and quantification. In addition, the ERK/MAPK signalling is involved in the proliferative effect of LIPUS exposure on the established neuronal cell models. This was determined by phospho-ERK protein levels in association with Ki67 proliferation ratio in the presence and absence of the MEK/ERK inhibitor (U0126). To my knowledge, this study is the first to investigate the proliferative effect of LIPUS in *in vitro* differentiated neuronal-like cells.

LIPUS studies were conducted on neuronal-like cells differentiated from SH-SY5Y and DPSCs using the sequential supplementation: ATRA→BDNF protocol (as shown in chapter 3 and 4). Notably it has been reported that the cells exit from the proliferative phase once differentiated and remain in the stationary phase of the cell cycle (Li and Kirschner, 2014; Ruijtenberg and van den Heuvel, 2016). It also has been reported that the sequential supplementation method (ATRA→BDNF) arrests the SH-SY5Y derived neuronal-like cells in the stationary G1 phase of the cell cycle (Encinas *et al.*, 2000). Thus, both SH-SY5Y and DPSC-derived neuronal-like cells were kept cultured in the differentiated media (BDNF-supplemented serum-free media) to maintain the neuronal-like differentiated status to enable investigation of whether LIPUS exposure stimulated the cells to re-enter the active phase of the cell cycle and consequently proliferate.

Data demonstrated LIPUS at an intensity (I_{SATA}) of 60 mW/cm^2 significantly resulted in the highest percentage of viable cells compared with other groups, hence this was determined

to be the most optimal intensity for use in the subsequent experiments. The other LIPUS parameters applied were selected based on previous studies. For example, the 20-min LIPUS exposure time was commonly used as an effective stimulation for repair and regeneration in a variety of tissues such as nerve (Sato *et al.*, 2016), ligament injuries (Takakura *et al.*, 2002), periodontal wound healing (Ikai *et al.*, 2008), bone (Harrison *et al.*, 2016), and cartilage (Horne *et al.*, 2017). The selected pulse repetition frequency (100 Hz) was also reported in inducing neural stem cell proliferation, nerve repair and regeneration (Lv *et al.*, 2013; Xia *et al.*, 2019; Lv *et al.*, 2015). Thereby, the following LIPUS parameters were used: I_{SATA} of 60 mW/cm^2, 20-min exposure time, the pulse of 100 Hz (ratio of 1:5 - duty cycle 20%) with 1.5 MHz frequency transducer of the ultrasound device.

In both neuronal-like cell culture models, the AlamarBlue data revealed that the LIPUS exposure significantly increased the percentage of viable cell numbers compared with control. This increase was also in agreement with other LIPUS studies using different LIPUS parameters on undifferentiated cells as assessed by other cell viability assays in osteoblasts (Alvarenga *et al.*, 2010), neural stem cells (Lv *et al.*, 2013), and rat Schwann cells (Ren *et al.*, 2018). These studies observed a significant increase in cellular viability after LIPUS treatment. Similarly, the cell counting assay (CCK-8) revealed comparable results in both neuronal-like cell culture models in which the LIPUS exposure groups showed higher absorbance readings than those obtained in the control group, albeit no significant difference was detected between control and 1-time LIPUS group in the d-DPSC culture. These results are consistent with previous LIPUS studies which also evaluated by CCK-8 to assess the cell count numbers in keratinocytes (Leng *et al.*, 2018), and in stem cells (Ling *et al.*, 2017b). This consistency indicates that the LIPUS is able to promote metabolic activities and consequently result in increases in cell numbers.

The increase in proliferation was also supported by the Ki67 proliferation marker data (Miller *et al.*, 2018). The LIPUS exposure groups showed significantly higher number of immunopositive cells compared with the control. These findings were in agreement with other LIPUS studies which used Ki67 assay (Takeuchi *et al.*, 2008) as well as other proliferation indicators (Leng *et al.*, 2018; Ling *et al.*, 2017b; Lv *et al.*, 2013; Gao *et al.*, 2016b). These previous works reported that LIPUS promoted cell proliferation in chondrocytes, keratinocytes, and stem cells, respectively. He *et al.* (2015) also reported that LIPUS exposure promoted bone marrow stem cells to re-enter the proliferative phase from the stationary phase of the cell cycle, and consequently increased cell numbers. This is the most likely scenario reflecting the increase in numbers of the neuronal-like cells differentiated from DPSCs and SH-SY5Y cells of this study.

Data presented here demonstrates LIPUS induces cell proliferation in the neuronal-like cell culture models. Furthermore, this cell proliferation was increased proportionally with the number of LIPUS exposure times used; however, a statistically significant difference in both cell types was only noted in data obtained from the AlamarBlue assay. Thus, LIPUS exposure could be useful therapeutically to induce cell proliferation for neuronal repair and regeneration, including the differentiated neuronal cells, which are in the postmitotic/stationary phase. Notably, this concept of LIPUS exposure can induce neuronal proliferation/regeneration is consistent with several previous studies (Sato *et al.*, 2016; Jiang *et al.*, 2016; Yang *et al.*, 2017a; Ren *et al.*, 2018). However, there are other studies that have reported that LIPUS did not induce neuronal regeneration (Daeschler *et al.*, 2018), and suppressed cell proliferation and induced apoptosis in preadipocytes (Xu *et al.*, 2018). This disagreement in findings in the different LIPUS studies could be attributable to the different LIPUS parameters used, such as intensity, frequency, and exposure time (Tanaka *et al.*, 2015; Yang *et al.*, 2010). Also, different cell

responses to the stimulus were measured in different cell types (Janmey and McCulloch, 2007; Maul *et al.*, 2011). Therefore, further studies are required to set standard LIPUS parameters for each specific cell-type group.

Regardless of the differences in LIPUS parameters, this study results are consistent with previous LIPUS studies which reported ERK signalling underlying the proliferative effect of LIPUS in several cell types, such as mesenchymal stem cells (Ling *et al.*, 2017b; Gao *et al.*, 2016b; Xia *et al.*, 2019; Zhou *et al.*, 2004). The control group with MEK inhibitor also resulted in a reduction of basic ERK phosphorylation and proliferation in both neuronal-like cell cultures; however, the reduction in cell proliferation was not statistically significant. This reduction was expected as the ERK signalling pathway is mainly involved in cell proliferation and growth of mammalian cells (Meloche and Pouyssegur, 2007; Zhang and Liu, 2002). Thus, the ERK signalling pathway is involved in both control and LIPUS-treated groups, but the LIPUS exposure activated this pathway and subsequently resulted in higher significant cellular proliferation compared with control group.

Notably, the LIPUS plus U0126 inhibitor group of the d-SH-SY5Y cell cultures displayed significantly higher phospho-ERK1/2 levels and cell proliferation ratios compared with the control plus U0126 group. This finding indicating that the MEK inhibitor partially blocked the LIPUS-induced SH-SY5Y cell proliferation and ERK phosphorylation suggesting that other upstream signalling inducers are involved in this process. This interpretation is in agreement with findings studying LIPUS by Zhou *et al.* (2004) who reported that LIPUS also activated the Rho-associated coiled-coil-containing protein kinase (ROCK/Rho) upstream regulator, subsequently triggering ERK phosphorylation and cell proliferation. Consequently, Zhou *et al.* (2004) concluded the LIPUS induced cell proliferation of human skin fibroblasts via activation of ROCK/ERK and MEK/ERK signalling pathways. It has also been reported

that ERK/MAPK signalling could be activated by alternative components other than the MEK-ERK classical cascade (Yoon and Seger, 2006). In addition, Zuccarini *et al.* (2018) reported involvement of other upstream regulators (NO-cGMP-PKG) in directly activating ERK phosphorylation in the SH-SY5Y neuroblastoma cell line induced by another therapeutic modality. The findings of this study and that of Zhou *et al.* (2004) also support the concept of LIPUS stimulating more than one upstream regulator or even involvement of multiple cellular signalling pathways.

Indeed, there are many studies in the literature reporting involvement of other signalling pathways in the proliferative effect of LIPUS. For example, Ling *et al.* (2017b) also reported the involvement of PI3K-Akt signalling besides ERK/MAPK signalling pathway. A study by Gao *et al.* (2016b) demonstrated the involvement of the ERK signalling pathway in rat DPSCs whereas JNK or JNK and p38 signalling pathways were involved in rat bone marrow and periodontal ligament stem cells, respectively. Sato *et al.* (2014) reported the activation of all ERK, JNK and p38 MAPK pathways by LIPUS exposure in inducing proliferation of the rabbit synovial cells. Takeuchi *et al.* (2008) reported the involvement of PI3K-Akt signalling and not the ERK signalling pathway in the proliferation of porcine chondrocytes. In addition, other studies reported the involvement of notch, GSK-3β/β-catenin, and PI3K-Akt and JNK MAPK signalling pathways in the cell proliferation induced by LIPUS, respectively (Wu *et al.*, 2020b; Ren *et al.*, 2018; Leng *et al.*, 2018). These differences in the signalling pathways underlying LIPUS induced cell proliferation indicated that LIPUS might stimulate more than one signalling or even multiple signalling pathways simultaneously and be cell-type dependent. Hence, further investigation is required to reveal all involved signalling pathways induced by LIPUS and using genome sequencing approaches might be more specific and informative to reveal all activated key genes related to cellular signalling pathways (Ochsner *et al.*, 2019; Ramanan *et al.*, 2012).

6.4. Conclusion

The present study demonstrates that LIPUS exposure can promote cell proliferation in the neuronal-like cell culture models derived from SH-SY5Y cells and DPSCs. This study also shows that increasing the number of LIPUS exposures induces greater cell number increases. However, the one-time exposure is sufficient to stimulate significant cell number increases. In addition, the ERK/MAPK signalling pathway is involved in the proliferative effect of LIPUS exposure on the neuronal-like cell culture models derived from both cell types (SH-SY5Y cells and DPSCs). This study also highlights that LIPUS exposure may potentially trigger multiple cellular regulators and signalling pathways underlying the cell proliferation induced by LIPUS. In future, further studies are required to reinforce the clinical translation of the LIPUS effects on nerve regeneration using *in vivo* human models/settings. However, at this stage, this study can postulate that LIPUS could be useful therapeutic modality to induce neuronal/nerve regeneration. Also, the combination of LIPUS treatment and stem cell-derived neuronal cells would be beneficial therapeutic method to induced nerve regeneration for regenerative endodontics and nerve injuries.

CHAPTER 7: GENERAL DISCUSSION

7.1. Discussion of main findings

The nerve regeneration is required in the regenerative endodontic treatments to regain functional pulp which regulates all essential, defensive, and reparative processes of the healthy dentine-pulp complex (Diogenes, 2020; Byers, Suzuki and Maeda, 2003). In addition, it is required to treat the nerve injuries which negatively affect life quality, ranging from discomfort and numbness to severe pain and loss of function. Some of these nerve injuries are irreparable, and the symptoms are long-lasting or permanent (Snyder and Bartoshuk, 2016; Menorca, Fussell and Elfar, 2013). Consequently, there is a need to find a therapeutic approach to induce nerve regeneration for regenerative endodontics and nerve injuries. Although LIPUS has widely been recognised as an adjunct therapeutic approach for bone regeneration (Poolman *et al.*, 2017; Harrison *et al.*, 2016; Leighton *et al.*, 2017), it has not adequately been explored for nerve regeneration. Investigating such a therapeutic approach needs *in vitro* human neurons as a preclinical step, however, this is highly limited due to ethical issues. The other alternative source is using animal neurons. Although animal experimentation provides a basic advance in medicine, cellular and molecular differences exist between animal and human tissues. These differences lead to incomparable results to that of human neuronal cells, which can hinder the translation of therapies to human (Monteggia, Heimer and Nestler, 2018; Zhao and Bhattacharyya, 2018; Ransohoff, 2018). Therefore, developing *in vitro* human neuronal cell models derived from human stem cells (hDPSCs) and human neuroblastoma cell line (SH-SY5Y) were required to simulate nerves for LIPUS experimentation in the current research project. These human neuronal cell models might be useful for other nerve experimentations such as pharmacological purposes or testing other therapeutic approaches. In addition, the DPSC-derived neuronal cell model might be beneficial to be used in the stem cell

transplantation therapies for the regenerative endodontic procedures and nerve injuries to repair the neuronal loss.

Within the current project, the first hypothesis to optimise the neuronal differentiation was that the serum-reduced neurogenic differentiation medium condition would induce higher neuronal differentiation of the neuroblastoma cell line (SH-SY5Y). This hypothesis was not supported, and the alternative null hypothesis was accepted as the two groups studied (10% and 5% FBS) had nearly comparable neuronal differentiation results assessed by immunocytochemical and gene expression of neuronal markers. However, the 5% FBS neuronal cell models demonstrated a significantly lower cell viability percentage than the 10% FBS neuronal cell models (chapter 3). Hence, the serum reduction in the neurogenic media negatively affected the cell viability without any enhancing in the neuronal differentiation. This interpretation was supported by work done with bone marrow stem cells incubated in serum-free media (Croft and Przyborski, 2006). This study demonstrated that the serum deprivation does not induce actual neuronal differentiation and negatively affects the cell growth. Thereby, this study findings suggest that the neurogenic induction media should be supplemented with serum or alternative supplements such as growth factors to maintain the cellular viability and growth (Rodrigues, Griffith and Wells, 2010; Liu *et al.*, 2013). Consequently, the 10% FBS neuronal differentiation protocols (ATRA alone or ATRA→BDNF) were applied to the hDPSC cultures to examine the hypothesis that the hDPSCs would be comparably differentiated into functional neuronal cells to that of the SH-SY5Y cells. Subsequent hDPSC neuronal differentiation results supported the hypothesis in which the hDPSC-derived neuronal-like cells immunocytochemically, and transcriptionally expressed neuronal markers. Furthermore, these differentiated hDPSCs acquired electrophysiological voltage-dependent Na^+ and K^+ currents in ATRA→BDNF group compared with no currents in the control group (chapter 4). Comparison

between the two cell types (SH-SY5Y: chapter 3 and hDPSCs: chapter 4) revealed similar trends in expression of specific neuronal markers and functional electrophysiological profiles indicating the development of functional mature cholinergic sensory neuronal cell models in the sequential supplementation groups (ATRA→BDNF). However, the DPSC-derived neuronal cell model demonstrated lower neuronal marker expression and an electrophysiological recordings profile compared with SH-SY5Y-derived neuronal cell model. From a translational perspective, the neuronal lineage specifications of the developed neuronal cell models support their *in vitro* modelling for the sensory cholinergic neurons. In addition, their potential applications to replace the sensory cholinergic neuronal loss in the dental pulp regeneration and peripheral nerve injuries by the transplantation therapies are suggested.

It is known that cells exit the cell cycle and lose their proliferation capacity upon differentiation (Hardwick *et al.*, 2015; Buttitta and Edgar, 2007; Järvinen *et al.*, 2010). Hence, the established neuronal cell models were used to examine the hypothesis that LIPUS would induce cell proliferation of differentiated neuronal cells. In addition, to investigate whether increasing the number of LIPUS exposures would increase the cell proliferation. The results supported the hypotheses that 1-time LIPUS-treated groups demonstrated higher cellular proliferation than control groups and increasing LIPUS exposures (3-time LIPUS) resulted in more cellular proliferation, albeit insignificant increase compared with 1-time LIPUS was detected by some assay (chapter 6). Although the LIPUS-induced cell proliferation was shown in several cell types (Gao *et al.*, 2016b; Ling *et al.*, 2017b; Xie *et al.*, 2019; Lv *et al.*, 2013; Wu *et al.*, 2020b; Ren *et al.*, 2018; Nishikori *et al.*, 2002; Leng *et al.*, 2018), LIPUS-induced cell proliferation in *in vitro* differentiated neuronal cells, to the best of my knowledge, have not previously been reported. The observations that LIPUS-induced cellular proliferation of the neuronal cell models derived from two different cell types (DPSCs and SH-SY5Y) is

considered as additional evidence to the previous neuronal-related literature (Wu *et al.*, 2020b; Xia *et al.*, 2019; Ren *et al.*, 2018; Lv *et al.*, 2013) regarding the potentiality of LIPUS as an adjunct therapeutic approach to induce neuronal cell proliferation. The clinical relevance might be beneficial as an inducer for nerve regeneration or in combination with transplantation of differentiated neuronal cells derived from stem cells for regenerative endodontics and nerve injuries.

The positive neuronal differentiation and LIPUS-stimulated neuronal cell proliferation generated further questions concerning ERK/MAPK signalling, the reported activated signalling in the physiologically reparative nerve regeneration after peripheral nerve injury (Agthong *et al.*, 2006; Chierzi *et al.*, 2005; Tsuda, Kanje and Dahlin, 2011; Hausott and Klimaschewski, 2019), would be involved in these processes. The hypothesis was supported as the neuronal characteristics, and ERK1/2 phosphorylated protein levels (p-ERK1/2) induced by differentiation method were ablated in the presence of the ERK/MEK inhibitor (chapter 5). Similarly, LIPUS-stimulated cell proliferation and concomitant p-ERK1/2 levels were reduced in the presence of the ERK/MEK inhibitor, albeit p-ERK1/2 of the LIPUS-treated group in the DPSC-derived neuronal cell model showed an insignificant increase compared with the control group (chapter 6). The involved ERK/MAPK pathway in the neuronal differentiation and LIPUS-stimulated neuronal-like cell proliferation indicated that the ERK/MAPK signalling might therefore play an important and also a general role in nerve regeneration *in vivo* with and without LIPUS stimulation. Furthermore, direct stimulating/targeting of ERK signalling by specific inducers might be useful for peripheral nerve regeneration *in vivo* as suggested by Hausott and Klimaschewski (2019).

Regarding clinical translation aspects of this research project for oral and dental problems, LIPUS could be used as a step in regenerative endodontic treatment procedures to

restore the neuronal component of pulp regeneration. In a broader context, to induce regeneration of the whole dentin-pulp complex, as previously highlighted by some studies that ultrasound exposure induces cell proliferation of DPSCs (Gao *et al.*, 2016b), and odontoblast-like cells (Scheven *et al.*, 2009; Man *et al.*, 2012; Ghorayeb *et al.*, 2013). Hence, this approach could help in establishing holistic dentin-pulp complex regeneration for treatment of the irreversible pulpitis or pulp necrosis cases, instead of the traditional endodontic approaches. LIPUS waves could be delivered to the root canal system either via manufacturing intracanal transducer or modifying the endosonic file system with LIPUS settings, which is currently used in endodontics to activate the root canal irrigants. The LIPUS approach could be performed with traditional pulp revascularisation procedures or in combination with the cell transplantation approach to boost regeneration potential of the dentin-pulp complex. In this context, the established sensory cholinergic DPSC-derived neuronal model (chapter 4) would be a good option as neuronal transplants/component for nerve regeneration in dentin-pulp complex regeneration.

Another clinical translation, the LIPUS could be used as therapeutic modality for oral and dental related nerve injuries which may occur either due to traumatic accidents or oral and maxillofacial surgeries. As previously reported, 25 to ~37.5% of these nerve injuries are permanent and patients suffer from a range of symptoms such as pain, numbness, and disturbance or loss of taste sensation (Agbaje *et al.*, 2016; Renton *et al.*, 2013; Valmaseda-Castellón, Berini-Aytés and Gay-Escoda, 2001). LIPUS could be applied to the injured nerve area to induce nerve regeneration which may lead complete nerve recovery, including functional recovery. However, further research is required to reinforce the clinical translation of the present research and optimise settings for the treatment of oral and dental related nerve injuries. For example, the present project showed that a single LIPUS exposure can result in a

significant cell proliferation of the SH-SY5Y and DPSC-derived neuronal models (chapter 6) and this may not be the case in the clinical scenario. The combination of LIPUS and the established DPSC-derived neuronal model could also be another or better option for treating moderate or severe injuries which may need additional neuronal replacements.

7.2. Future work

The next logical extensions of this project are to:

I. Test the efficacy of the neuronal cell models to widely investigate other therapeutic approaches.

II. Study the potential effects of LIPUS on inducing other neurogenesis components: differentiation, migration, and integration within the surrounding tissue.

III. Investigate all activated signalling pathways in the LIPUS-treated cells/tissues using more specific and inclusive approaches such as genomic sequencing analyses to understand how the LIPUS stimulus works at the molecular levels.

IV. Test transplantation of DPSC-derived neuronal cells with and without LIPUS in transplantation therapies for regenerative endodontic procedures, and peripheral nerve injuries, including dental nerve injuries.

7.3. Conclusions

The results described in this project contribute to current knowledge on the development of neuronal cell models using hDPSCs, using a differentiation methodology that has not been adequately highlighted for differentiation of DPSCs. This approach enabled the study of the potential therapeutic role of LIPUS in comparison with neuronal cell line (SH-SY5Y). The characterisation findings indicated the established neuronal cell models are cholinergic sensory

neuronal lineage which would be beneficial as specialised neuronal cell models to simulate peripheral sensory nerves, including dental nerves in *in vitro* and *in vivo* settings. This study also demonstrated that LIPUS was able to induce cell proliferation of differentiated neuronal cell models. To the best of my knowledge, the proliferative effect of LIPUS is not previously reported in *in vitro* differentiated neuronal-like cells. These LIPUS findings might have clinical relevance as a potential therapeutic tool to induce nerve regeneration and also highlights an exciting opportunity for a combination of the DPSC-derived neuronal cells and LIPUS in the transplantation therapies for nerve regeneration. Finally, this project showed the involvement of ERK/MAPK signalling in the neuronal differentiation and LIPUS-induced neuronal cell proliferation, highlighting the critical role of ERK/MAPK signalling in nerve regeneration.

REFERENCES

Abe, N. and Cavalli, V. (2008) 'Nerve injury signaling', *Curr Opin Neurobiol,* 18(3), pp. 276-83.

Abeysinghe, H. C., Bokhari, L., Quigley, A., Choolani, M., Chan, J., Dusting, G. J., Crook, J. M., Kobayashi, N. R. and Roulston, C. L. (2015) 'Pre-differentiation of human neural stem cells into GABAergic neurons prior to transplant results in greater repopulation of the damaged brain and accelerates functional recovery after transient ischemic stroke', *Stem Cell Res Ther,* 6, pp. 186.

Abud, E. M., Ramirez, R. N., Martinez, E. S., Healy, L. M., Nguyen, C. H. H., Newman, S. A., Yeromin, A. V., Scarfone, V. M., Marsh, S. E., Fimbres, C., Caraway, C. A., Fote, G. M., Madany, A. M., Agrawal, A., Kayed, R., Gylys, K. H., Cahalan, M. D., Cummings, B. J., Antel, J. P., Mortazavi, A., Carson, M. J., Poon, W. W. and Blurton-Jones, M. (2017) 'iPSC-Derived Human Microglia-like Cells to Study Neurological Diseases', *Neuron,* 94(2), pp. 278-293.e9.

Acar, A. H., Yolcu, Ü., Altındiş, S., Gül, M., Alan, H. and Malkoç, S. (2016) 'Bone regeneration by low-level laser therapy and low-intensity pulsed ultrasound therapy in the rabbit calvarium', *Archives of oral biology,* 61, pp. 60-65.

Agbaje, J. O., Van de Casteele, E., Hiel, M., Verbaanderd, C., Lambrichts, I. and Politis, C. (2016) 'Neuropathy of Trigeminal Nerve Branches After Oral and Maxillofacial Treatment', *J Maxillofac Oral Surg,* 15(3), pp. 321-327.

Agholme, L., Lindström, T., Kågedal, K., Marcusson, J. and Hallbeck, M. (2010) 'An in vitro model for neuroscience: differentiation of SH-SY5Y cells into cells with morphological and biochemical characteristics of mature neurons', *Journal of Alzheimer's disease,* 20(4), pp. 1069-1082.

Agthong, S., Kaewsema, A., Tanomsridejchai, N. and Chentanez, V. (2006) 'Activation of MAPK ERK in peripheral nerve after injury', *BMC Neurosci,* 7, pp. 45.

Ahmadi, F., McLoughlin, I. V., Chauhan, S. and ter-Haar, G. (2012) 'Bio-effects and safety of low-intensity, low-frequency ultrasonic exposure', *Prog Biophys Mol Biol,* 108(3), pp. 119-38.

Akamatsu, W. (2017) '[Neural differentiation from induced pluripotent stem cells for disease modelling and drug discovery]', *Nihon Yakurigaku Zasshi,* 150(6), pp. 282-285.

Akin, E. J., Higerd, G. P., Mis, M. A., Tanaka, B. S., Adi, T., Liu, S., Dib-Hajj, F. B., Waxman, S. G. and Dib-Hajj, S. D. (2019) 'Building sensory axons: Delivery and distribution of Na', *Sci Adv,* 5(10), pp. eaax4755.

Al-Daghreer, S., Doschak, M., Sloan, A. J., Major, P. W., Heo, G., Scurtescu, C., Tsui, Y. Y. and El-Bialy, T. (2012) 'Long term effect of low intensity pulsed ultrasound on a human tooth slice organ culture', *Arch Oral Biol,* 57(6), pp. 760-8.

Al-Daghreer, S., Doschak, M., Sloan, A. J., Major, P. W., Heo, G., Scurtescu, C., Tsui, Y. Y. and El-Bialy, T. (2013) 'Short-term effect of low-intensity pulsed ultrasound on an ex-vivo 3-D tooth culture', *Ultrasound in medicine & biology,* 39(6), pp. 1066-1074.

Al-Sabbagh, M., Okeson, J. P., Bertoli, E., Medynski, D. C. and Khalaf, M. W. (2015) 'Persistent pain and neurosensory disturbance after dental implant surgery: prevention and treatment', *Dent Clin North Am,* 59(1), pp. 143-56.

Alberts, B., Johnson, A., Lewis, J., Raff, M., Roberts, K. and Walter, P. (2002) 'Neural Development', *Molecular Biology of the Cell.* 4th edition ed. New York: Garland Science.

Alessi, D. R., Cuenda, A., Cohen, P., Dudley, D. T. and Saltiel, A. R. (1995) 'PD 098059 is a specific inhibitor of the activation of mitogen-activated protein kinase kinase in vitro and in vivo', *J Biol Chem,* 270(46), pp. 27489-94.

Alvarenga, E. C., Rodrigues, R., Caricati-Neto, A., Silva-Filho, F. C., Paredes-Gamero, E. J. and Ferreira, A. T. (2010) 'Low-intensity pulsed ultrasound-dependent osteoblast proliferation occurs by via activation of the P2Y receptor: role of the P2Y1 receptor', *Bone,* 46(2), pp. 355-62.

Amano, T., Papanikolaou, T., Sung, L. Y., Lennington, J., Conover, J. and Yang, X. (2009) 'Nuclear transfer embryonic stem cells provide an in vitro culture model for Parkinson's disease', *Cloning Stem Cells,* 11(1), pp. 77-88.

Andersen, C. L., Jensen, J. L. and Orntoft, T. F. (2004) 'Normalization of real-time quantitative reverse transcription-PCR data: a model-based variance estimation approach to identify genes suited for normalization, applied to bladder and colon cancer data sets', *Cancer Res,* 64(15), pp. 5245-50.

Andrews, P. W. (1988) 'Human teratocarcinomas', *Biochim Biophys Acta,* 948(1), pp. 17-36.

Antonucci, F., Corradini, I., Fossati, G., Tomasoni, R., Menna, E. and Matteoli, M. (2016) 'SNAP-25, a Known Presynaptic Protein with Emerging Postsynaptic Functions', *Front Synaptic Neurosci,* 8, pp. 7.

Arber, S., Han, B., Mendelsohn, M., Smith, M., Jessell, T. M. and Sockanathan, S. (1999) 'Requirement for the homeobox gene Hb9 in the consolidation of motor neuron identity', *Neuron,* 23(4), pp. 659-74.

Arcangeli, A., Rosati, B., Crociani, O., Cherubini, A., Fontana, L., Passani, B., Wanke, E. and Olivotto, M. (1999) 'Modulation of HERG current and herg gene expression during retinoic acid treatment of human neuroblastoma cells: potentiating effects of BDNF', *J Neurobiol,* 40(2), pp. 214-25.

Arthur, A., Rychkov, G., Shi, S., Koblar, S. A. and Gronthos, S. (2008) 'Adult human dental pulp stem cells differentiate toward functionally active neurons under appropriate environmental cues', *Stem Cells,* 26(7), pp. 1787-95.

Arthur-Farraj, P., Wanek, K., Hantke, J., Davis, C. M., Jayakar, A., Parkinson, D. B., Mirsky, R. and Jessen, K. R. (2011) 'Mouse schwann cells need both NRG1 and cyclic AMP to myelinate', *Glia,* 59(5), pp. 720-33.

Austah, O., Joon, R., Fath, W. M., Chrepa, V., Diogenes, A., Ezeldeen, M., Couve, E. and Ruparel, N. B. (2018) 'Comprehensive Characterization of 2 Immature Teeth Treated with Regenerative Endodontic Procedures', *J Endod,* 44(12), pp. 1802-1811.

Austah, O., Widbiller, M., Tomson, P. L. and Diogenes, A. (2019) 'Expression of Neurotrophic Factors in Human Dentin and Their Regulation of Trigeminal Neurite Outgrowth', *J Endod,* 45(4), pp. 414-419.

Austah, O. N., Ruparel, N. B., Henry, M. A., Fajardo, R. J., Schmitz, J. E. and Diogenes, A. (2016) 'Capsaicin-sensitive Innervation Modulates the Development of Apical Periodontitis', *J Endod,* 42(10), pp. 1496-502.

Azari, H. and Reynolds, B. A. (2016) 'In Vitro Models for Neurogenesis', *Cold Spring Harb Perspect Biol,* 8(6).

Basi, G. S., Jacobson, R. D., Virág, I., Schilling, J. and Skene, J. H. (1987) 'Primary structure and transcriptional regulation of GAP-43, a protein associated with nerve growth', *Cell,* 49(6), pp. 785-91.

Becerra, P., Ricucci, D., Loghin, S., Gibbs, J. L. and Lin, L. M. (2014) 'Histologic study of a human immature permanent premolar with chronic apical abscess after revascularization/revitalization', *Journal of endodontics,* 40(1), pp. 133-139.

Bekelis, K., Missios, S. and Spinner, R. J. (2014) 'Restraints and peripheral nerve injuries in adult victims of motor vehicle crashes', *J Neurotrauma,* 31(12), pp. 1077-82.

Bekelis, K., Missios, S. and Spinner, R. J. (2015) 'Falls and peripheral nerve injuries: an age-dependent relationship', *J Neurosurg,* 123(5), pp. 1223-9.

Bell, N., Hann, V., Redfern, C. P. and Cheek, T. R. (2013) 'Store-operated Ca 2+ entry in proliferating and retinoic acid-differentiated N-and S-type neuroblastoma cells', *Biochimica et Biophysica Acta (BBA)-Molecular Cell Research,* 1833(3), pp. 643-651.

Belzberg, A. J. (2006) 'Peripheral Nerve Injury', in Johnson, R.T., Griffin, J.W. and McArthur, J.C. (eds.) *Current therapy in neurologic disease.* Seventh Edition ed: Mosby, pp. 244-253.

Biedler, J., Spengler, B. and Lyser, K. (1975) 'Morphological interconversion of human neuroblastoma cells', *Vitro,* 10, pp. 380.

Biedler, J. L., Helson, L. and Spengler, B. A. (1973) 'Morphology and growth, tumorigenicity, and cytogenetics of human neuroblastoma cells in continuous culture', *Cancer research,* 33(11), pp. 2643-2652.

Biedler, J. L., Roffler-Tarlov, S., Schachner, M. and Freedman, L. S. (1978) 'Multiple neurotransmitter synthesis by human neuroblastoma cell lines and clones', *Cancer Res,* 38(11 Pt 1), pp. 3751-7.

Bonaventura, G., La Cognata, V., Iemmolo, R., Zimbone, M., Contino, A., Maccarrone, G., Failla, B., Barcellona, M. L., Conforti, F. L., D'Agata, V. and Cavallaro, S. (2018) 'Ag-NPs induce apoptosis, mitochondrial damages and MT3/OSGIN2 expression changes in an in vitro model of human dental-pulp-stem-cells-derived neurons', *Neurotoxicology,* 67, pp. 84-93.

Bonnamain, V., Thinard, R., Sergent-Tanguy, S., Huet, P., Bienvenu, G., Naveilhan, P., Farges, J. C. and Alliot-Licht, B. (2013) 'Human dental pulp stem cells cultured in serum-free supplemented medium', *Front Physiol,* 4, pp. 357.

Bracken, M. B. (2009) 'Why animal studies are often poor predictors of human reactions to exposure', *J R Soc Med,* 102(3), pp. 120-2.

Braun, S. M. and Jessberger, S. (2014) 'Adult neurogenesis: mechanisms and functional significance', *Development,* 141(10), pp. 1983-6.

Brewer, G. J. (1995) 'Serum-free B27/neurobasal medium supports differentiated growth of neurons from the striatum, substantia nigra, septum, cerebral cortex, cerebellum, and dentate gyrus', *J Neurosci Res,* 42(5), pp. 674-83.

Brewer, G. J., Torricelli, J. R., Evege, E. K. and Price, P. J. (1993) 'Optimized survival of hippocampal neurons in B27-supplemented Neurobasal, a new serum-free medium combination', *J Neurosci Res,* 35(5), pp. 567-76.

Brown, A. M., Riddoch, F. C., Robson, A., Redfern, C. P. and Cheek, T. R. (2005) 'Mechanistic and functional changes in Ca2+ entry after retinoic acid-induced differentiation of neuroblastoma cells', *Biochemical Journal,* 388(3), pp. 941-948.

Bruyns, C. N., Jaquet, J.-B., Schreuders, T. A., Kalmijn, S., Kuypers, P. D. and Hovius, S. E. (2003) 'Predictors for return to work in patients with median and ulnar nerve injuries', *The Journal of hand surgery,* 28(1), pp. 28-34.

Budhiraja, G., Sahu, N. and Subramanian, A. (2018) 'Low-Intensity Ultrasound Upregulates the Expression of Cyclin-D1 and Promotes Cellular Proliferation in Human Mesenchymal Stem Cells', *Biotechnol J,* 13(4), pp. e1700382.

Busse, J. W., Bhandari, M., Kulkarni, A. V. and Tunks, E. (2002) 'The effect of low-intensity pulsed ultrasound therapy on time to fracture healing: a meta-analysis', *CMAJ,* 166(4), pp. 437-41.

Buttiglione, M., Vitiello, F., Sardella, E., Petrone, L., Nardulli, M., Favia, P., d'Agostino, R. and Gristina, R. (2007) 'Behaviour of SH-SY5Y neuroblastoma cell line grown in different media and on different chemically modified substrates', *Biomaterials,* 28(19), pp. 2932-45.

Buttitta, L. A. and Edgar, B. A. (2007) 'Mechanisms controlling cell cycle exit upon terminal differentiation', *Curr Opin Cell Biol,* 19(6), pp. 697-704.

Byers, M. and Taylor, P. (1993) 'Effect of sensory denervation on the response of rat molar pulp to exposure injury', *Journal of dental research,* 72(3), pp. 613-618.

Byers, M. R., Schatteman, G. C. and Bothwell, M. (1990) 'Multiple functions for NGF receptor in developing, aging and injured rat teeth are suggested by epithelial, mesenchymal and neural immunoreactivity', *Development,* 109(2), pp. 461-71.

Byers, M. R., Suzuki, H. and Maeda, T. (2003) 'Dental neuroplasticity, neuro-pulpal interactions, and nerve regeneration', *Microsc Res Tech,* 60(5), pp. 503-15.

Byers, M. R., Taylor, P. E., Khayat, B. G. and Kimberly, C. L. (1990) 'Effects of injury and inflammation on pulpal and periapical nerves', *J Endod,* 16(2), pp. 78-84.

Caceres, A., Banker, G., Steward, O., Binder, L. and Payne, M. (1984) 'MAP2 is localized to the dendrites of hippocampal neurons which develop in culture', *Brain Res,* 315(2), pp. 314-8.

Calland, J. W., Harris, S. E. and Carnes, D. L. (1997) 'Human pulp cells respond to calcitonin gene-related peptide in vitro', *J Endod,* 23(8), pp. 485-9.

Cambray-Deakin, M. (1991) 'Cytoskeleton of the growing axon', *The neuronal cytoskeleton*: Wiley-Liss New York, pp. 233-255.

Campbell, R. L., Shamaskin, R. G. and Harkins, S. W. (1987) 'Assessment of recovery from injury to inferior alveolar and mental nerves', *Oral Surgery, Oral Medicine, Oral Pathology,* 64(5), pp. 519-526.

Cao, J., Semenova, M. M., Solovyan, V. T., Han, J., Coffey, E. T. and Courtney, M. J. (2004) 'Distinct requirements for p38alpha and c-Jun N-terminal kinase stress-activated protein kinases in different forms of apoptotic neuronal death', *J Biol Chem,* 279(34), pp. 35903-13.

Casper, K. B. and McCarthy, K. D. (2006) 'GFAP-positive progenitor cells produce neurons and oligodendrocytes throughout the CNS', *Mol Cell Neurosci,* 31(4), pp. 676-84.

Cassidy, N., Fahey, M., Prime, S. S. and Smith, A. J. (1997) 'Comparative analysis of transforming growth factor-beta isoforms 1-3 in human and rabbit dentine matrices', *Arch Oral Biol,* 42(3), pp. 219-23.

Chailangkarn, T., Acab, A. and Muotri, A. R. (2012) 'Modeling neurodevelopmental disorders using human neurons', *Curr Opin Neurobiol,* 22(5), pp. 785-90.

Chambard, J. C., Lefloch, R., Pouysségur, J. and Lenormand, P. (2007) 'ERK implication in cell cycle regulation', *Biochim Biophys Acta,* 1773(8), pp. 1299-310.

Chan, W. S., Sideris, A., Sutachan, J. J., Montoya G, J. V., Blanck, T. J. and Recio-Pinto, E. (2013) 'Differential regulation of proliferation and neuronal differentiation in adult rat spinal cord neural stem/progenitors by ERK1/2, Akt, and PLCγ', *Front Mol Neurosci,* 6, pp. 23.

Chang, C. C., Chang, K. C., Tsai, S. J., Chang, H. H. and Lin, C. P. (2014) 'Neurogenic differentiation of dental pulp stem cells to neuron-like cells in dopaminergic and motor neuronal inductive media', *J Formos Med Assoc,* 113(12), pp. 956-65.

Chang, L. and Karin, M. (2001) 'Mammalian MAP kinase signalling cascades', *Nature,* 410(6824), pp. 37-40.

Chen, J., Chattopadhyay, B., Venkatakrishnan, G. and Ross, A. H. (1990) 'Nerve growth factor-induced differentiation of human neuroblastoma and neuroepithelioma cell lines', *Cell Growth Differ,* 1(2), pp. 79-85.

Chen, Y., Stevens, B., Chang, J., Milbrandt, J., Barres, B. A. and Hell, J. W. (2008) 'NS21: re-defined and modified supplement B27 for neuronal cultures', *J Neurosci Methods,* 171(2), pp. 239-47.

Cheng, Y., Ma, Z., Kim, B. H., Wu, W., Cayting, P., Boyle, A. P., Sundaram, V., Xing, X., Dogan, N., Li, J., Euskirchen, G., Lin, S., Lin, Y., Visel, A., Kawli, T., Yang, X., Patacsil, D., Keller, C. A., Giardine, B., Kundaje, A., Wang, T., Pennacchio, L. A., Weng, Z., Hardison, R. C., Snyder, M. P. and Consortium, m. E. (2014) 'Principles of regulatory information conservation between mouse and human', *Nature,* 515(7527), pp. 371-375.

Cheung, L. K., Leung, Y. Y., Chow, L. K., Wong, M. C., Chan, E. K. and Fok, Y. H. (2010) 'Incidence of neurosensory deficits and recovery after lower third molar surgery: a prospective clinical study of 4338 cases', *Int J Oral Maxillofac Surg,* 39(4), pp. 320-6.

Cheung, Y.-T., Lau, W. K.-W., Yu, M.-S., Lai, C. S.-W., Yeung, S.-C., So, K.-F. and Chang, R. C.-C. (2009a) 'Effects of all-trans-retinoic acid on human SH-SY5Y neuroblastoma as in vitro model in neurotoxicity research', *Neurotoxicology,* 30(1), pp. 127-135.

Cheung, Y. T., Lau, W. K., Yu, M. S., Lai, C. S., Yeung, S. C., So, K. F. and Chang, R. C. (2009b) 'Effects of all-trans-retinoic acid on human SH-SY5Y neuroblastoma as in vitro model in neurotoxicity research', *Neurotoxicology,* 30(1), pp. 127-35.

Chew, L. J., Coley, W., Cheng, Y. and Gallo, V. (2010) 'Mechanisms of regulation of oligodendrocyte development by p38 mitogen-activated protein kinase', *J Neurosci,* 30(33), pp. 11011-27.

Chiego, D. J., Klein, R. M., Avery, J. K. and Gruhl, I. M. (1986) 'Denervation-induced changes in cell proliferation in the rat molar after wounding', *Anat Rec,* 214(4), pp. 348-52.

Chierzi, S., Ratto, G. M., Verma, P. and Fawcett, J. W. (2005) 'The ability of axons to regenerate their growth cones depends on axonal type and age, and is regulated by calcium, cAMP and ERK', *Eur J Neurosci,* 21(8), pp. 2051-62.

Choi, S. H., Kim, Y. H., Hebisch, M., Sliwinski, C., Lee, S., D'Avanzo, C., Chen, H., Hooli, B., Asselin, C., Muffat, J., Klee, J. B., Zhang, C., Wainger, B. J., Peitz, M., Kovacs, D. M., Woolf, C. J., Wagner, S. L., Tanzi, R. E. and Kim, D. Y. (2014) 'A three-dimensional human neural cell culture model of Alzheimer's disease', *Nature,* 515(7526), pp. 274-8.

Chrepa, V., Henry, M. A., Daniel, B. J. and Diogenes, A. (2015) 'Delivery of Apical Mesenchymal Stem Cells into Root Canals of Mature Teeth', *J Dent Res,* 94(12), pp. 1653-9.

Christensen, J., Steain, M., Slobedman, B. and Abendroth, A. (2011) 'Differentiated neuroblastoma cells provide a highly efficient model for studies of productive varicella-zoster virus infection of neuronal cells', *J Virol,* 85(16), pp. 8436-42.

Chuang, J. H., Tung, L. C. and Lin, Y. (2015) 'Neural differentiation from embryonic stem cells in vitro: An overview of the signaling pathways', *World J Stem Cells,* 7(2), pp. 437-47.

Chun, S. Y., Soker, S., Jang, Y. J., Kwon, T. G. and Yoo, E. S. (2016) 'Differentiation of Human Dental Pulp Stem Cells into Dopaminergic Neuron-like Cells in Vitro', *J Korean Med Sci,* 31(2), pp. 171-7.

Ciccarone, V., Spengler, B. A., Meyers, M. B., Biedler, J. L. and Ross, R. A. (1989) 'Phenotypic diversification in human neuroblastoma cells: expression of distinct neural crest lineages', *Cancer Res,* 49(1), pp. 219-25.

Constantinescu, R., Constantinescu, A., Reichmann, H. and Janetzky, B. (2007) 'Neuronal differentiation and long-term culture of the human neuroblastoma line SH-SY5Y', *Neuropsychiatric disorders an integrative approach*, pp. 17-28.

Cooper, P. R., Holder, M. J. and Smith, A. J. (2014) 'Inflammation and regeneration in the dentin-pulp complex: a double-edged sword', *J Endod,* 40(4 Suppl), pp. S46-51.

Cordeiro, M. M., Dong, Z., Kaneko, T., Zhang, Z., Miyazawa, M., Shi, S., Smith, A. J. and Nör, J. E. (2008) 'Dental pulp tissue engineering with stem cells from exfoliated deciduous teeth', *J Endod,* 34(8), pp. 962-9.

Couve, E., Osorio, R. and Schmachtenberg, O. (2014) 'Reactionary Dentinogenesis and Neuroimmune Response in Dental Caries', *J Dent Res,* 93(8), pp. 788-93.

Crisci, A. R. and Ferreira, A. L. (2002) 'Low-intensity pulsed ultrasound accelerates the regeneration of the sciatic nerve after neurotomy in rats', *Ultrasound in medicine & biology,* 28(10), pp. 1335-1341.

Croft, A. P. and Przyborski, S. A. (2006) 'Formation of neurons by non-neural adult stem cells: potential mechanism implicates an artifact of growth in culture', *Stem Cells,* 24(8), pp. 1841-51.

Crum, L., Bailey, M., Hwang, J. H., Khokhlova, V. and Sapozhnikov, O. (2010) 'Therapeutic ultrasound: Recent trends and future perspectives', *Physics Procedia,* 3(1), pp. 25-34.

Cruz, C. D. and Cruz, F. (2007) 'The ERK 1 and 2 pathway in the nervous system: from basic aspects to possible clinical applications in pain and visceral dysfunction', *Curr Neuropharmacol,* 5(4), pp. 244-52.

Cui, J. H., Park, K., Park, S. R. and Min, B.-H. (2006) 'Effects of low-intensity ultrasound on chondrogenic differentiation of mesenchymal stem cells embedded in polyglycolic acid: an in vivo study', *Tissue engineering,* 12(1), pp. 75-82.

D'Aiuto, L., Naciri, J., Radio, N., Tekur, S., Clayton, D., Apodaca, G., Di Maio, R., Zhi, Y., Dimitrion, P., Piazza, P., Demers, M., Wood, J., Chu, C., Callio, J., McClain, L., Yolken, R., McNulty, J., Kinchington, P., Bloom, D. and Nimgaonkar, V. (2018) 'Generation of three-dimensional human neuronal cultures: application to modeling CNS viral infections', *Stem Cell Res Ther,* 9(1), pp. 134.

D'Angelo, E., Solinas, S., Garrido, J., Casellato, C., Pedrocchi, A., Mapelli, J., Gandolfi, D. and Prestori, F. (2013) 'Realistic modeling of neurons and networks: towards brain simulation', *Funct Neurol,* 28(3), pp. 153-66.

da Silva, L. A. B., Nelson-Filho, P., da Silva, R. A. B., Flores, D. S. H., Heilborn, C., Johnson, J. D. and Cohenca, N. (2010) 'Revascularization and periapical repair after endodontic treatment using apical negative pressure irrigation versus conventional irrigation plus triantibiotic intracanal dressing in dogs' teeth with apical periodontitis', *Oral Surgery, Oral Medicine, Oral Pathology, Oral Radiology, and Endodontology,* 109(5), pp. 779-787.

Dadon-Nachum, M., Sadan, O., Srugo, I., Melamed, E. and Offen, D. (2011) 'Differentiated mesenchymal stem cells for sciatic nerve injury', *Stem Cell Rev Rep,* 7(3), pp. 664-71.

Daeschler, S. C., Harhaus, L., Bergmeister, K. D., Boecker, A., Hoener, B., Kneser, U. and Schoenle, P. (2018) 'Clinically Available Low Intensity Ultrasound Devices do not Promote Axonal Regeneration After Peripheral Nerve Surgery-A Preclinical Investigation of an FDA-Approved Device', *Front Neurol,* 9, pp. 1057.

Darmon, M., Bottenstein, J. and Sato, G. (1981) 'Neural differentiation following culture of embryonal carcinoma cells in a serum-free defined medium', *Dev Biol,* 85(2), pp. 463-73.

Day, R. (1994) 'Diagnosis and treatment of trigeminal nerve injuries', *Journal of the California Dental Association,* 22(6), pp. 48.

de Albornoz, P. M., Delgado, P. J., Forriol, F. and Maffulli, N. (2011) 'Non-surgical therapies for peripheral nerve injury', *British medical bulletin*, pp. ldr005.

De Camilli, P., Cameron, R. and Greengard, P. (1983) 'Synapsin I (protein I), a nerve terminal-specific phosphoprotein. I. Its general distribution in synapses of the central and peripheral nervous system demonstrated by immunofluorescence in frozen and plastic sections', *J Cell Biol,* 96(5), pp. 1337-54.

de Lucas, B., Pérez, L. M., Bernal, A. and Gálvez, B. G. (2020) 'Ultrasound Therapy: Experiences and Perspectives for Regenerative Medicine', *Genes (Basel),* 11(9).

de Medeiros, L. M., De Bastiani, M. A., Rico, E. P., Schonhofen, P., Pfaffenseller, B., Wollenhaupt-Aguiar, B., Grun, L., Barbé-Tuana, F., Zimmer, E. R., Castro, M. A. A., Parsons, R. B. and Klamt, F. (2019) 'Cholinergic Differentiation of Human Neuroblastoma SH-SY5Y Cell Line and Its Potential Use as an In vitro Model for Alzheimer's Disease Studies', *Mol Neurobiol,* 56(11), pp. 7355-7367.

Deng, L. X., Hu, J., Liu, N., Wang, X., Smith, G. M., Wen, X. and Xu, X. M. (2011) 'GDNF modifies reactive astrogliosis allowing robust axonal regeneration through Schwann cell-seeded guidance channels after spinal cord injury', *Exp Neurol,* 229(2), pp. 238-50.

Deshmukh, R. S., Kovács, K. A. and Dinnyés, A. (2012) 'Drug discovery models and toxicity testing using embryonic and induced pluripotent stem-cell-derived cardiac and neuronal cells', *Stem Cells Int,* 2012, pp. 379569.

Deumens, R., Bozkurt, A., Meek, M. F., Marcus, M. A., Joosten, E. A., Weis, J. and Brook, G. A. (2010) 'Repairing injured peripheral nerves: Bridging the gap', *Prog Neurobiol,* 92(3), pp. 245-76.

Devey, G. B. and Wells, P. N. (1978) 'Ultrasound in medical diagnosis', *Scientific American,* 238(5), pp. 98-113.

Dezawa, M., Kanno, H., Hoshino, M., Cho, H., Matsumoto, N., Itokazu, Y., Tajima, N., Yamada, H., Sawada, H., Ishikawa, H., Mimura, T., Kitada, M., Suzuki, Y. and Ide, C. (2004) 'Specific induction of neuronal cells from bone marrow stromal cells and application for autologous transplantation', *J Clin Invest,* 113(12), pp. 1701-10.

Dib-Hajj, S. D., Yang, Y., Black, J. A. and Waxman, S. G. (2013) 'The Na(V)1.7 sodium channel: from molecule to man', *Nat Rev Neurosci,* 14(1), pp. 49-62.

Diogenes, A. (2020) 'Trigeminal Sensory Neurons and Pulp Regeneration', *J Endod,* 46(9S), pp. S71-S80.

Diogenes, A., Henry, M. A., Teixeira, F. B. and Hargreaves, K. M. (2013) 'An update on clinical regenerative endodontics', *Endodontic Topics,* 28(1), pp. 2-23.

Duan, H., Song, W., Zhao, W., Gao, Y., Yang, Z. and Li, X. (2016) 'Endogenous neurogenesis in adult mammals after spinal cord injury', *Sci China Life Sci,* 59(12), pp. 1313-1318.

Dubin, A. E. and Patapoutian, A. (2010) 'Nociceptors: the sensors of the pain pathway', *J Clin Invest,* 120(11), pp. 3760-72.

Duflocq, A., Le Bras, B., Bullier, E., Couraud, F. and Davenne, M. (2008) 'Nav1.1 is predominantly expressed in nodes of Ranvier and axon initial segments', *Mol Cell Neurosci,* 39(2), pp. 180-92.

Duncan, H. F., Smith, A. J., Fleming, G. J., Reid, C., Smith, G. and Cooper, P. R. (2017) 'Release of bio-active dentine extracellular matrix components by histone deacetylase inhibitors (HDACi)', *Int Endod J,* 50(1), pp. 24-38.

Dupin, E. and Le Douarin, N. M. (1995) 'Retinoic acid promotes the differentiation of adrenergic cells and melanocytes in quail neural crest cultures', *Dev Biol,* 168(2), pp. 529-48.

Ebisawa, K., Hata, K.-i., Okada, K., Kimata, K., Ueda, M., Torii, S. and Watanabe, H. (2004) 'Ultrasound enhances transforming growth factor β-mediated chondrocyte differentiation of human mesenchymal stem cells', *Tissue engineering,* 10(5-6), pp. 921-929.

Eckenstein, F. and Sofroniew, M. V. (1983) 'Identification of central cholinergic neurons containing both choline acetyltransferase and acetylcholinesterase and of central neurons containing only acetylcholinesterase', *J Neurosci,* 3(11), pp. 2286-91.

El-Bialy, T., Alhadlaq, A. and Lam, B. (2012) 'Effect of therapeutic ultrasound on human periodontal ligament cells for dental and periodontal tissue engineering', *Open Dent J,* 6, pp. 235-9.

Encinas, M., Iglesias, M., Liu, Y., Wang, H., Muhaisen, A., Ceña, V., Gallego, C. and Comella, J. X. (2000) 'Sequential treatment of SH-SY5Y cells with retinoic acid and brain-derived neurotrophic factor gives rise to fully differentiated, neurotrophic factor-dependent, human neuron-like cells', *J Neurochem,* 75(3), pp. 991-1003.

Encinas, M., Iglesias, M., Llecha, N. and Comella, J. X. (1999) 'Extracellular-regulated kinases and phosphatidylinositol 3-kinase are involved in brain-derived neurotrophic factor-mediated survival and neuritogenesis of the neuroblastoma cell line SH-SY5Y', *Journal of neurochemistry,* 73(4), pp. 1409-1421.

Eng, L. F., Ghirnikar, R. S. and Lee, Y. L. (2000) 'Glial fibrillary acidic protein: GFAP-thirty-one years (1969-2000)', *Neurochem Res,* 25(9-10), pp. 1439-51.

Eng, L. F., Vanderhaeghen, J. J., Bignami, A. and Gerstl, B. (1971) 'An acidic protein isolated from fibrous astrocytes', *Brain Res,* 28(2), pp. 351-4.

Ernsberger, U., Reissmann, E., Mason, I. and Rohrer, H. (2000) 'The expression of dopamine beta-hydroxylase, tyrosine hydroxylase, and Phox2 transcription factors in sympathetic neurons: evidence for common regulation during noradrenergic induction and diverging regulation later in development', *Mech Dev,* 92(2), pp. 169-77.

Esteves, A. R., Domingues, A. F., Ferreira, I. L., Januário, C., Swerdlow, R. H., Oliveira, C. R. and Cardoso, S. M. (2008) 'Mitochondrial function in Parkinson's disease cybrids containing an nt2 neuron-like nuclear background', *Mitochondrion,* 8(3), pp. 219-28.

Evans, G. R. (2001) 'Peripheral nerve injury: a review and approach to tissue engineered constructs', *The Anatomical Record,* 263(4), pp. 396-404.

Farkhondeh, A., Li, R., Gorshkov, K., Chen, K. G., Might, M., Rodems, S., Lo, D. C. and Zheng, W. (2019) 'Induced pluripotent stem cells for neural drug discovery', *Drug Discov Today,* 24(4), pp. 992-999.

Favata, M. F., Horiuchi, K. Y., Manos, E. J., Daulerio, A. J., Stradley, D. A., Feeser, W. S., Van Dyk, D. E., Pitts, W. J., Earl, R. A., Hobbs, F., Copeland, R. A., Magolda, R. L., Scherle, P. A. and Trzaskos, J. M. (1998) 'Identification of a novel inhibitor of mitogen-activated protein kinase kinase', *J Biol Chem,* 273(29), pp. 18623-32.

Festing, S. and Wilkinson, R. (2007) 'The ethics of animal research. Talking Point on the use of animals in scientific research', *EMBO Rep,* 8(6), pp. 526-30.

Fields, R. D. and Lancaster, M. V. (1993) 'Dual-attribute continuous monitoring of cell proliferation/cytotoxicity', *Am Biotechnol Lab,* 11(4), pp. 48-50.

Forster, J., Köglsberger, S., Trefois, C., Boyd, O., Baumuratov, A., Buck, L., Balling, R. and Antony, P. (2016) 'Characterization of differentiated SH-SY5Y as neuronal screening model reveals increased oxidative vulnerability', *Journal of biomolecular screening,* 21(5), pp. 496-509.

Foudah, D., Monfrini, M., Donzelli, E., Niada, S., Brini, A. T., Orciani, M., Tredici, G. and Miloso, M. (2014) 'Expression of neural markers by undifferentiated mesenchymal-like stem cells from different sources', *J Immunol Res,* 2014, pp. 987678.

Frebel, K. and Wiese, S. (2006) 'Signalling molecules essential for neuronal survival and differentiation', *Biochem Soc Trans,* 34(Pt 6), pp. 1287-90.
Fristad, I. (1997) 'Dental innervation: functions and plasticity after peripheral injury', *Acta Odontologica Scandinavica,* 55(4), pp. 236-254.
Gage, F. H. (2000) 'Mammalian neural stem cells', *Science,* 287(5457), pp. 1433-8.
Gakhar-Koppole, N., Hundeshagen, P., Mandl, C., Weyer, S. W., Allinquant, B., Müller, U. and Ciccolini, F. (2008) 'Activity requires soluble amyloid precursor protein alpha to promote neurite outgrowth in neural stem cell-derived neurons via activation of the MAPK pathway', *Eur J Neurosci,* 28(5), pp. 871-82.
Gao, F., Chiu, S. M., Motan, D. A., Zhang, Z., Chen, L., Ji, H. L., Tse, H. F., Fu, Q. L. and Lian, Q. (2016a) 'Mesenchymal stem cells and immunomodulation: current status and future prospects', *Cell Death Dis,* 7, pp. e2062.
Gao, Q., Cooper, P. R., Walmsley, A. D. and Scheven, B. A. (2017) 'Role of Piezo Channels in Ultrasound-stimulated Dental Stem Cells', *Journal of Endodontics*.
Gao, Q., Walmsley, A. D., Cooper, P. R. and Scheven, B. A. (2016b) 'Ultrasound Stimulation of Different Dental Stem Cell Populations: Role of Mitogen-activated Protein Kinase Signaling', *Journal of endodontics,* 42(3), pp. 425-431.
Gatta, V., Drago, D., Fincati, K., Valenti, M. T., Dalle Carbonare, L., Sensi, S. L. and Zatta, P. (2011) 'Microarray analysis on human neuroblastoma cells exposed to aluminum, β(1-42)-amyloid or the β(1-42)-amyloid aluminum complex', *PLoS One,* 6(1), pp. e15965.
Geisler, T. M. (2012) 'Clinical considerations for regenerative endodontic procedures', *Dental Clinics of North America,* 56(3), pp. 603-626.
Geng, Y. W., Zhang, Z., Liu, M. Y. and Hu, W. P. (2017) 'Differentiation of human dental pulp stem cells into neuronal by resveratrol', *Cell Biol Int,* 41(12), pp. 1391-1398.
Gervois, P., Struys, T., Hilkens, P., Bronckaers, A., Ratajczak, J., Politis, C., Brône, B., Lambrichts, I. and Martens, W. (2015) 'Neurogenic maturation of human dental pulp stem cells following neurosphere generation induces morphological and electrophysiological characteristics of functional neurons', *Stem Cells Dev,* 24(3), pp. 296-311.
Gervois, P., Wolfs, E., Dillen, Y., Hilkens, P., Ratajczak, J., Driesen, R. B., Vangansewinkel, T., Bronckaers, A., Brone, B., Struys, T. and Lambrichts, I. (2017) 'Paracrine Maturation and Migration of SH-SY5Y Cells by Dental Pulp Stem Cells', *Journal of Dental Research,* 96(6), pp. 654-662.
Ghorayeb, S. R., Patel, U. S., Walmsley, A. D. and Scheven, B. A. (2013) 'Biophysical characterization of low-frequency ultrasound interaction with dental pulp stem cells', *Journal of therapeutic ultrasound,* 1(1), pp. 12.
Gimenez-Cassina, A., Lim, F. and Diaz-Nido, J. (2006) 'Differentiation of a human neuroblastoma into neuron-like cells increases their susceptibility to transduction by herpesviral vectors', *J Neurosci Res,* 84(4), pp. 755-67.
Gnanasegaran, N., Govindasamy, V. and Abu Kasim, N. H. (2016) 'Differentiation of stem cells derived from carious teeth into dopaminergic-like cells', *Int Endod J,* 49(10), pp. 937-49.
Goldie, B. J., Barnett, M. M. and Cairns, M. J. (2014) 'BDNF and the maturation of posttranscriptional regulatory networks in human SH-SY5Y neuroblast differentiation', *Front Cell Neurosci,* 8, pp. 325.
Gonmanee, T., Sritanaudomchai, H., Vongsavan, K., Faisaikarm, T., Songsaad, A., White, K. L. and Thonabulsombat, C. (2020) 'Neuronal differentiation of dental pulp stem cells from human permanent and deciduous teeth following coculture with rat auditory brainstem slices', *Anat Rec (Hoboken),* 303(11), pp. 2931-2946.

Gonmanee, T., Thonabulsombat, C., Vongsavan, K. and Sritanaudomchai, H. (2018) 'Differentiation of stem cells from human deciduous and permanent teeth into spiral ganglion neuron-like cells', *Arch Oral Biol,* 88, pp. 34-41.
Gonzalez-Perez, F., Udina, E. and Navarro, X. (2013) 'Extracellular matrix components in peripheral nerve regeneration', *Int Rev Neurobiol,* 108, pp. 257-75.
Goorha, S. and Reiter, L. T. (2017) 'Culturing and Neuronal Differentiation of Human Dental Pulp Stem Cells', *Curr Protoc Hum Genet,* 92, pp. 21.6.1-21.6.10.
Gordon, J., Amini, S. and White, M. K. (2013) 'General overview of neuronal cell culture', *Methods Mol Biol,* 1078, pp. 1-8.
Gordon, T., Chan, K. M., Sulaiman, O. A., Udina, E., Amirjani, N. and Brushart, T. M. (2009) 'Accelerating axon growth to overcome limitations in functional recovery after peripheral nerve injury', *Neurosurgery,* 65(4), pp. A132-A144.
Gordon, T., Sulaiman, O. and Boyd, J. G. (2003) 'Experimental strategies to promote functional recovery after peripheral nerve injuries', *J Peripher Nerv Syst,* 8(4), pp. 236-50.
Goshi, N., Morgan, R. K., Lein, P. J. and Seker, E. (2020) 'A primary neural cell culture model to study neuron, astrocyte, and microglia interactions in neuroinflammation', *J Neuroinflammation,* 17(1), pp. 155.
Goudarzi, G., Hamidabadi, H. G., Bojnordi, M. N., Hedayatpour, A., Niapour, A., Zahiri, M., Absalan, F. and Darabi, S. (2020) 'Role of cerebrospinal fluid in differentiation of human dental pulp stem cells into neuron-like cells', *Anat Cell Biol,* 53(3), pp. 292-300.
Grade, S. and Götz, M. (2017) 'Neuronal replacement therapy: previous achievements and challenges ahead', *NPJ Regen Med,* 2, pp. 29.
Greene, L. A. and Tischler, A. S. (1976) 'Establishment of a noradrenergic clonal line of rat adrenal pheochromocytoma cells which respond to nerve growth factor', *Proc Natl Acad Sci U S A,* 73(7), pp. 2424-8.
Griffin, M. F., Malahias, M., Hindocha, S. and Khan, W. S. (2014) 'Peripheral nerve injury: principles for repair and regeneration', *Open Orthop J,* 8, pp. 199-203.
Grinsell, D. and Keating, C. P. (2014) 'Peripheral nerve reconstruction after injury: a review of clinical and experimental therapies', *Biomed Res Int,* 2014, pp. 698256.
Haas, D. A. and Lennon, D. (1995) 'A 21 year retrospective study of reports of paresthesia following local anesthetic administration', *Journal (Canadian Dental Association),* 61(4), pp. 319-20, 323-6, 329-30.
Haines, J. D., Fulton, D. L., Richard, S. and Almazan, G. (2015) 'p38 Mitogen-Activated Protein Kinase Pathway Regulates Genes during Proliferation and Differentiation in Oligodendrocytes', *PLoS One,* 10(12), pp. e0145843.
Han, S. B., Shin, Y. J., Hyon, J. Y. and Wee, W. R. (2011) 'Cytotoxicity of voriconazole on cultured human corneal endothelial cells', *Antimicrob Agents Chemother,* 55(10), pp. 4519-23.
Hancock, M. K., Kopp, L., Kaur, N. and Hanson, B. J. (2015) 'A facile method for simultaneously measuring neuronal cell viability and neurite outgrowth', *Curr Chem Genom Transl Med,* 9, pp. 6-16.
Harada, A., Teng, J., Takei, Y., Oguchi, K. and Hirokawa, N. (2002) 'MAP2 is required for dendrite elongation, PKA anchoring in dendrites, and proper PKA signal transduction', *J Cell Biol,* 158(3), pp. 541-9.
Haratizadeh, S., Nazm Bojnordi, M., Darabi, S., Karimi, N., Naghikhani, M., Ghasemi Hamidabadi, H. and Seifi, M. (2017) 'Condition medium of cerebrospinal fluid and retinoic acid induces the transdifferentiation of human dental pulp stem cells into neuroglia and neural like cells', *Anat Cell Biol,* 50(2), pp. 107-114.

Hardwick, L. J., Ali, F. R., Azzarelli, R. and Philpott, A. (2015) 'Cell cycle regulation of proliferation versus differentiation in the central nervous system', *Cell Tissue Res,* 359(1), pp. 187-200.
Hardwick, L. J. and Philpott, A. (2014) 'Nervous decision-making: to divide or differentiate', *Trends Genet,* 30(6), pp. 254-61.
Hargreaves, K. M., Diogenes, A. and Teixeira, F. B. (2013) 'Treatment options: biological basis of regenerative endodontic procedures', *Journal of endodontics,* 39(3), pp. S30-S43.
Harrington, J., Sloan, A. J. and Waddington, R. J. (2014) 'Quantification of clonal heterogeneity of mesenchymal progenitor cells in dental pulp and bone marrow', *Connect Tissue Res,* 55 Suppl 1, pp. 62-7.
Harrison, A., Lin, S., Pounder, N. and Mikuni-Takagaki, Y. (2016) 'Mode & mechanism of low intensity pulsed ultrasound (LIPUS) in fracture repair', *Ultrasonics,* 70, pp. 45-52.
Hartman, B. K., Zide, D. and Udenfriend, S. (1972) 'The use of dopamine -hydroxylase as a marker for the central noradrenergic nervous system in rat brain', *Proc Natl Acad Sci U S A,* 69(9), pp. 2722-6.
Hartmann, A., Seeberger, R., Bittner, M., Rolke, R., Welte-Jzyk, C. and Daubländer, M. (2017) 'Profiling intraoral neuropathic disturbances following lingual nerve injury and in burning mouth syndrome', *BMC Oral Health,* 17(1), pp. 68.
Hausott, B. and Klimaschewski, L. (2019) 'Promotion of Peripheral Nerve Regeneration by Stimulation of the Extracellular Signal-Regulated Kinase (ERK) Pathway', *Anat Rec (Hoboken),* 302(8), pp. 1261-1267.
He, R., Zhou, W., Zhang, Y., Hu, S., Yu, H., Luo, Y., Liu, B., Ran, J., Wu, J., Wang, Y. and Chen, W. (2015) 'Combination of low-intensity pulsed ultrasound and C3H10T1/2 cells promotes bone-defect healing', *Int Orthop,* 39(11), pp. 2181-9.
Heller, B. A., Ghidinelli, M., Voelkl, J., Einheber, S., Smith, R., Grund, E., Morahan, G., Chandler, D., Kalaydjieva, L., Giancotti, F., King, R. H., Fejes-Toth, A. N., Fejes-Toth, G., Feltri, M. L., Lang, F. and Salzer, J. L. (2014) 'Functionally distinct PI 3-kinase pathways regulate myelination in the peripheral nervous system', *J Cell Biol,* 204(7), pp. 1219-36.
Heng, B. C., Lim, L. W., Wu, W. and Zhang, C. (2016) 'An Overview of Protocols for the Neural Induction of Dental and Oral Stem Cells In Vitro', *Tissue Eng Part B Rev,* 22(3), pp. 220-50.
Henry, M. A. and Hargreaves, K. M. (2007) 'Peripheral mechanisms of odontogenic pain', *Dent Clin North Am,* 51(1), pp. 19-44, v.
Hentz, V. R., Rosen, J. M., Xiao, S.-J., McGill, K. C. and Abraham, G. (1991) 'A comparison of suture and tubulization nerve repair techniques in a primate', *The Journal of hand surgery,* 16(2), pp. 251-261.
Hill, E. J., Jiménez-González, C., Tarczyluk, M., Nagel, D. A., Coleman, M. D. and Parri, H. R. (2012) 'NT2 derived neuronal and astrocytic network signalling', *PLoS One,* 7(5), pp. e36098.
Hillerup, S. (2007) 'Iatrogenic injury to oral branches of the trigeminal nerve: records of 449 cases', *Clin Oral Investig,* 11(2), pp. 133-42.
Hillion, J. A., Takahashi, K., Maric, D., Ruetzler, C., Barker, J. L. and Hallenbeck, J. M. (2005) 'Development of an ischemic tolerance model in a PC12 cell line', *J Cereb Blood Flow Metab,* 25(2), pp. 154-162.
Hodge, R. D., Bakken, T. E., Miller, J. A., Smith, K. A., Barkan, E. R., Graybuck, L. T., Close, J. L., Long, B., Johansen, N., Penn, O., Yao, Z., Eggermont, J., Höllt, T., Levi, B. P., Shehata, S. I., Aevermann, B., Beller, A., Bertagnolli, D., Brouner, K., Casper, T., Cobbs,

C., Dalley, R., Dee, N., Ding, S. L., Ellenbogen, R. G., Fong, O., Garren, E., Goldy, J., Gwinn, R. P., Hirschstein, D., Keene, C. D., Keshk, M., Ko, A. L., Lathia, K., Mahfouz, A., Maltzer, Z., McGraw, M., Nguyen, T. N., Nyhus, J., Ojemann, J. G., Oldre, A., Parry, S., Reynolds, S., Rimorin, C., Shapovalova, N. V., Somasundaram, S., Szafer, A., Thomsen, E. R., Tieu, M., Quon, G., Scheuermann, R. H., Yuste, R., Sunkin, S. M., Lelieveldt, B., Feng, D., Ng, L., Bernard, A., Hawrylycz, M., Phillips, J. W., Tasic, B., Zeng, H., Jones, A. R., Koch, C. and Lein, E. S. (2019) 'Conserved cell types with divergent features in human versus mouse cortex', *Nature,* 573(7772), pp. 61-68.

Horne, D., Jones, P., Salgaonkar, V., Adams, M., Ozilgen, B. A., Zahos, P., Tang, X., Liebenburg, E., Coughlin, D., Lotz, J. and Diederich, C. (2017) 'Low intensity pulsed ultrasound (LIPUS) for the treatment of intervertebral disc degeneration', *Proc SPIE Int Soc Opt Eng,* 10066.

Hossini, A. M., Megges, M., Prigione, A., Lichtner, B., Toliat, M. R., Wruck, W., Schröter, F., Nuernberg, P., Kroll, H., Makrantonaki, E., Zouboulis, C. C., Zouboulis, C. C. and Adjaye, J. (2015) 'Induced pluripotent stem cell-derived neuronal cells from a sporadic Alzheimer's disease donor as a model for investigating AD-associated gene regulatory networks', *BMC Genomics,* 16, pp. 84.

Hu, F., Zhang, X., Liu, H., Xu, P., Doulathunnisa, Teng, G. and Xiao, Z. (2017) 'Neuronally differentiated adipose-derived stem cells and aligned PHBV nanofiber nerve scaffolds promote sciatic nerve regeneration', *Biochem Biophys Res Commun,* 489(2), pp. 171-178.

Huang, D., Gao, Y., Wang, S., Zhang, W., Cao, H., Zheng, L., Chen, Y., Zhang, S. and Chen, J. (2020) 'Impact of low-intensity pulsed ultrasound on transcription and metabolite compositions in proliferation and functionalization of human adipose-derived mesenchymal stromal cells', *Sci Rep,* 10(1), pp. 13690.

Huang, G. T., Yamaza, T., Shea, L. D., Djouad, F., Kuhn, N. Z., Tuan, R. S. and Shi, S. (2010) 'Stem/progenitor cell-mediated de novo regeneration of dental pulp with newly deposited continuous layer of dentin in an in vivo model', *Tissue Eng Part A,* 16(2), pp. 605-15.

Huckhagel, T., Nuchtern, J., Regelsberger, J. and Lefering, R. (2018) 'Nerve injury in severe trauma with upper extremity involvement: evaluation of 49,382 patients from the TraumaRegister DGU(R) between 2002 and 2015', *Scand J Trauma Resusc Emerg Med,* 26(1), pp. 76.

Ibarretxe, G., Crende, O., Aurrekoetxea, M., García-Murga, V., Etxaniz, J. and Unda, F. (2012) 'Neural crest stem cells from dental tissues: a new hope for dental and neural regeneration', *Stem Cells Int,* 2012, pp. 103503.

Ichihara, S., Inada, Y. and Nakamura, T. (2008) 'Artificial nerve tubes and their application for repair of peripheral nerve injury: an update of current concepts', *Injury,* 39 Suppl 4, pp. 29-39.

Ikai, H., Tamura, T., Watanabe, T., Itou, M., Sugaya, A., Iwabuchi, S., Mikuni-Takagaki, Y. and Deguchi, S. (2008) 'Low-intensity pulsed ultrasound accelerates periodontal wound healing after flap surgery', *J Periodontal Res,* 43(2), pp. 212-6.

Iohara, K., Imabayashi, K., Ishizaka, R., Watanabe, A., Nabekura, J., Ito, M., Matsushita, K., Nakamura, H. and Nakashima, M. (2011) 'Complete pulp regeneration after pulpectomy by transplantation of CD105+ stem cells with stromal cell-derived factor-1', *Tissue Eng Part A,* 17(15-16), pp. 1911-20.

Iohara, K., Murakami, M., Takeuchi, N., Osako, Y., Ito, M., Ishizaka, R., Utunomiya, S., Nakamura, H., Matsushita, K. and Nakashima, M. (2013) 'A novel combinatorial therapy with pulp stem cells and granulocyte colony-stimulating factor for total pulp regeneration', *Stem Cells Transl Med,* 2(7), pp. 521-33.

Iohara, K., Nakashima, M., Ito, M., Ishikawa, M., Nakasima, A. and Akamine, A. (2004) 'Dentin regeneration by dental pulp stem cell therapy with recombinant human bone morphogenetic protein 2', *J Dent Res,* 83(8), pp. 590-5.

Iohara, K., Utsunomiya, S., Kohara, S. and Nakashima, M. (2018) 'Allogeneic transplantation of mobilized dental pulp stem cells with the mismatched dog leukocyte antigen type is safe and efficacious for total pulp regeneration', *Stem Cell Res Ther,* 9(1), pp. 116.

Iohara, K., Zheng, L., Ito, M., Ishizaka, R., Nakamura, H., Into, T., Matsushita, K. and Nakashima, M. (2009) 'Regeneration of dental pulp after pulpotomy by transplantation of CD31(-)/CD146(-) side population cells from a canine tooth', *Regen Med,* 4(3), pp. 377-85.

Irion, S., Zabierowski, S. E. and Tomishima, M. J. (2017) 'Bringing Neural Cell Therapies to the Clinic: Past and Future Strategies', *Mol Ther Methods Clin Dev,* 4, pp. 72-82.

Ishikawa, N., Suzuki, Y., Dezawa, M., Kataoka, K., Ohta, M., Cho, H. and Ide, C. (2009) 'Peripheral nerve regeneration by transplantation of BMSC-derived Schwann cells as chitosan gel sponge scaffolds', *J Biomed Mater Res A,* 89(4), pp. 1118-24.

Isobe, Y., Koyama, N., Nakao, K., Osawa, K., Ikeno, M., Yamanaka, S., Okubo, Y., Fujimura, K. and Bessho, K. (2016) 'Comparison of human mesenchymal stem cells derived from bone marrow, synovial fluid, adult dental pulp, and exfoliated deciduous tooth pulp', *Int J Oral Maxillofac Surg,* 45(1), pp. 124-31.

Israel, M. A., Yuan, S. H., Bardy, C., Reyna, S. M., Mu, Y., Herrera, C., Hefferan, M. P., Van Gorp, S., Nazor, K. L., Boscolo, F. S., Carson, C. T., Laurent, L. C., Marsala, M., Gage, F. H., Remes, A. M., Koo, E. H. and Goldstein, L. S. (2012) 'Probing sporadic and familial Alzheimer's disease using induced pluripotent stem cells', *Nature,* 482(7384), pp. 216-20.

Jaiswal, R. K., Jaiswal, N., Bruder, S. P., Mbalaviele, G., Marshak, D. R. and Pittenger, M. F. (2000) 'Adult human mesenchymal stem cell differentiation to the osteogenic or adipogenic lineage is regulated by mitogen-activated protein kinase', *J Biol Chem,* 275(13), pp. 9645-52.

Jang, S., Kang, Y. H., Ullah, I., Shivakumar, S. B., Rho, G. J., Cho, Y. C., Sung, I. Y. and Park, B. W. (2018) 'Cholinergic Nerve Differentiation of Mesenchymal Stem Cells Derived from Long-Term Cryopreserved Human Dental Pulp In Vitro and Analysis of Their Motor Nerve Regeneration Potential In Vivo', *Int J Mol Sci,* 19(8).

Janmey, P. A. and McCulloch, C. A. (2007) 'Cell mechanics: integrating cell responses to mechanical stimuli', *Annu Rev Biomed Eng,* 9, pp. 1-34.

Jansen, K., Pou Casellas, C., Groenink, L., Wever, K. E. and Masereeuw, R. (2020) 'Humans are animals, but are animals human enough? A systematic review and meta-analysis on interspecies differences in renal drug clearance', *Drug Discov Today,* 25(4), pp. 706-717.

Jerjes, W., Upile, T., Shah, P., Nhembe, F., Gudka, D., Kafas, P., McCarthy, E., Abbas, S., Patel, S., Hamdoon, Z., Abiola, J., Vourvachis, M., Kalkani, M., Al-Khawalde, M., Leeson, R., Banu, B., Rob, J., El-Maaytah, M. and Hopper, C. (2010) 'Risk factors associated with injury to the inferior alveolar and lingual nerves following third molar surgery-revisited', *Oral Surg Oral Med Oral Pathol Oral Radiol Endod,* 109(3), pp. 335-45.

Jessen, K. R. and Mirsky, R. (2016) 'The repair Schwann cell and its function in regenerating nerves', *J Physiol,* 594(13), pp. 3521-31.

Jiang, W., Wang, Y., Tang, J., Peng, J., Guo, Q., Guo, Z., Li, P., Xiao, B. and Zhang, J. (2016) 'Low-intensity pulsed ultrasound treatment improved the rate of autograft peripheral nerve regeneration in rat', *Sci Rep,* 6, pp. 22773.

Jones, I., Yelhekar, T. D., Wiberg, R., Kingham, P. J., Johansson, S., Wiberg, M. and Carlsson, L. (2018) 'Development and validation of an in vitro model system to study peripheral sensory neuron development and injury', *Sci Rep,* 8(1), pp. 15961.

Jones, R. E., Foster, D. S., Hu, M. S. and Longaker, M. T. (2019) 'Wound healing and fibrosis: current stem cell therapies', *Transfusion,* 59(S1), pp. 884-892.

Jung, J., Kim, J. W., Moon, H. J., Hong, J. Y. and Hyun, J. K. (2016) 'Characterization of Neurogenic Potential of Dental Pulp Stem Cells Cultured in Xeno/Serum-Free Condition: In Vitro and In Vivo Assessment', *Stem Cells Int,* 2016, pp. 6921097.

Jämsä, A., Hasslund, K., Cowburn, R. F., Bäckström, A. and Vasänge, M. (2004) 'The retinoic acid and brain-derived neurotrophic factor differentiated SH-SY5Y cell line as a model for Alzheimer's disease-like tau phosphorylation', *Biochem Biophys Res Commun,* 319(3), pp. 993-1000.

Järvinen, E., Angers-Loustau, A., Osiceanu, A. M. and Wartiovaara, K. (2010) 'Timing of the cell cycle exit of differentiating hippocampal neural stem cells', *Int J Stem Cells,* 3(1), pp. 46-53.

Kabir, R., Gupta, M., Aggarwal, A., Sharma, D., Sarin, A. and Kola, M. Z. (2014) 'Imperative role of dental pulp stem cells in regenerative therapies: a systematic review', *Niger J Surg,* 20(1), pp. 1-8.

Kahler, B., Mistry, S., Moule, A., Ringsmuth, A. K., Case, P., Thomson, A. and Holcombe, T. (2014) 'Revascularization outcomes: a prospective analysis of 16 consecutive cases', *J Endod,* 40(3), pp. 333-8.

Kalinina, N. I., Sysoeva, V. Y., Rubina, K. A., Parfenova, Y. V. and Tkachuk, V. A. (2011) 'Mesenchymal stem cells in tissue growth and repair', *Acta Naturae,* 3(4), pp. 30-7.

Kanafi, M., Majumdar, D., Bhonde, R., Gupta, P. and Datta, I. (2014) 'Midbrain cues dictate differentiation of human dental pulp stem cells towards functional dopaminergic neurons', *J Cell Physiol,* 229(10), pp. 1369-77.

Kandemir Demirci, G., Güneri, P. and Çalışkan, M. K. (2020) 'Regenerative Endodontic Therapy with Platelet Rich Fibrin: Case Series', *J Clin Pediatr Dent,* 44(1), pp. 15-19.

Kaplan, D. R., Matsumoto, K., Lucarelli, E. and Thiele, C. J. (1993) 'Induction of TrkB by retinoic acid mediates biologic responsiveness to BDNF and differentiation of human neuroblastoma cells. Eukaryotic Signal Transduction Group', *Neuron,* 11(2), pp. 321-31.

Kaplan, D. R. and Miller, F. D. (2000) 'Neurotrophin signal transduction in the nervous system', *Curr Opin Neurobiol,* 10(3), pp. 381-91.

Karnieli, O., Friedner, O. M., Allickson, J. G., Zhang, N., Jung, S., Fiorentini, D., Abraham, E., Eaker, S. S., Yong, T. K., Chan, A., Griffiths, S., Wehn, A. K. and Oh, S. (2017) 'A consensus introduction to serum replacements and serum-free media for cellular therapies', *Cytotherapy,* 19(2), pp. 155-169.

Karumuri, S. K., Rastogi, T., Beeraka, K., Penumatcha, M. R. and Olepu, S. R. (2016) 'Ultrasound: A Revenant Therapeutic Modality in Dentistry', *J Clin Diagn Res,* 10(7), pp. ZE08-12.

Katsetos, C. D., Legido, A., Perentes, E. and Mörk, S. J. (2003) 'Class III beta-tubulin isotype: a key cytoskeletal protein at the crossroads of developmental neurobiology and tumor neuropathology', *J Child Neurol,* 18(12), pp. 851-66; discussion 867.

Kempermann, G., Gage, F. H., Aigner, L., Song, H., Curtis, M. A., Thuret, S., Kuhn, H. G., Jessberger, S., Frankland, P. W., Cameron, H. A., Gould, E., Hen, R., Abrous, D. N., Toni, N., Schinder, A. F., Zhao, X., Lucassen, P. J. and Frisén, J. (2018) 'Human Adult Neurogenesis: Evidence and Remaining Questions', *Cell Stem Cell,* 23(1), pp. 25-30.

Kerezoudis, N., Olgart, L. and Edwall, L. (1994) 'Involvement of substance P but not nitric oxide or calcitonin gene-related peptide in neurogenic plasma extravasation in rat incisor pulp and lip', *Archives of oral biology,* 39(9), pp. 769-774.

Khanna, A., Nelmes, R. T., Gougoulias, N., Maffulli, N. and Gray, J. (2009) 'The effects of LIPUS on soft-tissue healing: a review of literature', *Br Med Bull,* 89, pp. 169-82.

Kikuchi, M., Tenneti, L. and Lipton, S. A. (2000) 'Role of p38 mitogen-activated protein kinase in axotomy-induced apoptosis of rat retinal ganglion cells', *J Neurosci,* 20(13), pp. 5037-44.

Kim, C., Hwang, K. G. and Park, C. J. (2018) 'Local anesthesia for mandibular third molar extraction', *J Dent Anesth Pain Med,* 18(5), pp. 287-294.

Kim, J. R., Oh, S. H., Kwon, G. B., Namgung, U., Song, K. S., Jeon, B. H. and Lee, J. H. (2013) 'Acceleration of peripheral nerve regeneration through asymmetrically porous nerve guide conduit applied with biological/physical stimulation', *Tissue Eng Part A,* 19(23-24), pp. 2674-85.

Kim, J. Y., Xin, X., Moioli, E. K., Chung, J., Lee, C. H., Chen, M., Fu, S. Y., Koch, P. D. and Mao, J. J. (2010) 'Regeneration of dental-pulp-like tissue by chemotaxis-induced cell homing', *Tissue Eng Part A,* 16(10), pp. 3023-31.

Kim, S. G., Malek, M., Sigurdsson, A., Lin, L. M. and Kahler, B. (2018) 'Regenerative endodontics: a comprehensive review', *Int Endod J,* 51(12), pp. 1367-1388.

Kim, S. S., Choi, J. M., Kim, J. W., Ham, D. S., Ghil, S. H., Kim, M. K., Kim-Kwon, Y., Hong, S. Y., Ahn, S. C., Kim, S. U., Lee, Y. D. and Suh-Kim, H. (2005) 'cAMP induces neuronal differentiation of mesenchymal stem cells via activation of extracellular signal-regulated kinase/MAPK', *Neuroreport,* 16(12), pp. 1357-61.

Kim, S. S., Yoo, S. W., Park, T. S., Ahn, S. C., Jeong, H. S., Kim, J. W., Chang, D. Y., Cho, K. G., Kim, S. U., Huh, Y., Lee, J. E., Lee, S. Y., Lee, Y. D. and Suh-Kim, H. (2008) 'Neural induction with neurogenin1 increases the therapeutic effects of mesenchymal stem cells in the ischemic brain', *Stem Cells,* 26(9), pp. 2217-28.

Kimberly, C. L. and Byers, M. R. (1988) 'Inflammation of rat molar pulp and periodontium causes increased calcitonin gene-related peptide and axonal sprouting', *Anat Rec,* 222(3), pp. 289-300.

Király, M., Kádár, K., Horváthy, D. B., Nardai, P., Rácz, G. Z., Lacza, Z., Varga, G. and Gerber, G. (2011) 'Integration of neuronally predifferentiated human dental pulp stem cells into rat brain in vivo', *Neurochem Int,* 59(3), pp. 371-81.

Király, M., Porcsalmy, B., Pataki, A., Kádár, K., Jelitai, M., Molnár, B., Hermann, P., Gera, I., Grimm, W.-D. and Ganss, B. (2009) 'Simultaneous PKC and cAMP activation induces differentiation of human dental pulp stem cells into functionally active neurons', *Neurochemistry international,* 55(5), pp. 323-332.

Klazen, Y., Van der Cruyssen, F., Vranckx, M., Van Vlierberghe, M., Politis, C., Renton, T. and Jacobs, R. (2018) 'Iatrogenic trigeminal post-traumatic neuropathy: a retrospective two-year cohort study', *Int J Oral Maxillofac Surg,* 47(6), pp. 789-793.

Koch, P., Opitz, T., Steinbeck, J. A., Ladewig, J. and Brüstle, O. (2009) 'A rosette-type, self-renewing human ES cell-derived neural stem cell with potential for in vitro instruction and synaptic integration', *Proc Natl Acad Sci U S A,* 106(9), pp. 3225-30.

Kochlamazashvili, G. and Haucke, V. (2013) 'A dual role of SNAP-25 as carrier and guardian of synaptic transmission', *EMBO Rep,* 14(7), pp. 579-80.

Kogo, Y., Seto, C., Totani, Y., Mochizuki, M., Nakahara, T., Oka, K., Yoshioka, T. and Ito, E. (2020) 'Rapid differentiation of human dental pulp stem cells to neuron-like cells by high K', *Biophys Physicobiol,* 17, pp. 132-139.

Kouyoumdjian, J. A. (2006) 'Peripheral nerve injuries: a retrospective survey of 456 cases', *Muscle Nerve,* 34(6), pp. 785-8.
Kovalevich, J. and Langford, D. (2013) 'Considerations for the use of SH-SY5Y neuroblastoma cells in neurobiology', *Neuronal Cell Culture: Methods and Protocols*, pp. 9-21.
Krivickas, L. S. and Wilbourn, A. J. (2000) 'Peripheral nerve injuries in athletes: a case series of over 200 injuries', *Semin Neurol,* 20(2), pp. 225-32.
Kumar, M. and Katyal, A. (2018) 'Data on retinoic acid and reduced serum concentration induced differentiation of Neuro-2a neuroblastoma cells', *Data Brief,* 21, pp. 2435-2440.
Kume, T., Kawato, Y., Osakada, F., Izumi, Y., Katsuki, H., Nakagawa, T., Kaneko, S., Niidome, T., Takada-Takatori, Y. and Akaike, A. (2008) 'Dibutyryl cyclic AMP induces differentiation of human neuroblastoma SH-SY5Y cells into a noradrenergic phenotype', *Neurosci Lett,* 443(3), pp. 199-203.
Ladak, A., Olson, J., Tredget, E. E. and Gordon, T. (2011) 'Differentiation of mesenchymal stem cells to support peripheral nerve regeneration in a rat model', *Exp Neurol,* 228(2), pp. 242-52.
Lambrichts, I., Driesen, R. B., Dillen, Y., Gervois, P., Ratajczak, J., Vangansewinkel, T., Wolfs, E., Bronckaers, A. and Hilkens, P. (2017) 'Dental Pulp Stem Cells: Their Potential in Reinnervation and Angiogenesis by Using Scaffolds', *J Endod,* 43(9S), pp. S12-S16.
Lang, C., Shu, X., Peng, L. and Yu, X. (2019) 'The ERK signaling pathway is involved in cardiotrophin-1-induced neural differentiation of human umbilical cord blood mesenchymal stem cells in vitro', *Cytotechnology,* 71(5), pp. 977-988.
Lanier, J., Quina, L. A., Eng, S. R., Cox, E. and Turner, E. E. (2007) 'Brn3a target gene recognition in embryonic sensory neurons', *Dev Biol,* 302(2), pp. 703-16.
Laudani, S., La Cognata, V., Iemmolo, R., Bonaventura, G., Villaggio, G., Saccone, S., Barcellona, M. L., Cavallaro, S. and Sinatra, F. (2020) 'Effect of a Bone Marrow-Derived Extracellular Matrix on Cell Adhesion and Neural Induction of Dental Pulp Stem Cells', *Front Cell Dev Biol,* 8, pp. 100.
Law, A. S. (2013) 'Considerations for regeneration procedures', *J Endod,* 39(3 Suppl), pp. S44-56.
Lee, H., Shamy, G. A., Elkabetz, Y., Schofield, C. M., Harrsion, N. L., Panagiotakos, G., Socci, N. D., Tabar, V. and Studer, L. (2007) 'Directed differentiation and transplantation of human embryonic stem cell-derived motoneurons', *Stem Cells,* 25(8), pp. 1931-9.
Lee, H. J., Choi, B. H., Min, B. H., Son, Y. S. and Park, S. R. (2006) 'Low-intensity Ultrasound Stimulation Enhances Chondrogenic Differentiation in Alginate Culture of Mesenchymal Stem Cells', *Artificial organs,* 30(9), pp. 707-715.
Lee, J. E., Lim, M. S., Park, J. H., Park, C. H. and Koh, H. C. (2016) 'PTEN Promotes Dopaminergic Neuronal Differentiation Through Regulation of ERK-Dependent Inhibition of S6K Signaling in Human Neural Stem Cells', *Stem Cells Transl Med,* 5(10), pp. 1319-1329.
Lee, S. K. and Wolfe, S. W. (2000) 'Peripheral nerve injury and repair', *J Am Acad Orthop Surg,* 8(4), pp. 243-52.
Lei, L., Chen, Y., Zhou, R., Huang, X. and Cai, Z. (2015) 'Histologic and immunohistochemical findings of a human immature permanent tooth with apical periodontitis after regenerative endodontic treatment', *Journal of endodontics,* 41(7), pp. 1172-1179.
Leighton, R., Watson, J. T., Giannoudis, P., Papakostidis, C., Harrison, A. and Steen, R. G. (2017) 'Healing of fracture nonunions treated with low-intensity pulsed ultrasound (LIPUS): A systematic review and meta-analysis', *Injury,* 48(7), pp. 1339-1347.

Lendahl, U., Zimmerman, L. B. and McKay, R. D. (1990) 'CNS stem cells express a new class of intermediate filament protein', *Cell,* 60(4), pp. 585-95.
Leng, X., Shang, J., Gao, D. and Wu, J. (2018) 'Low-intensity pulsed ultrasound promotes proliferation and migration of HaCaT keratinocytes through the PI3K/AKT and JNK pathways', *Braz J Med Biol Res,* 51(12), pp. e7862.
Leventhal, P. S., Randolph, A. E., Vesbit, T. E., Schenone, A., Windebank, A. and Feldman, E. L. (1995) 'Insulin-like growth factor-II as a paracrine growth factor in human neuroblastoma cells', *Exp Cell Res,* 221(1), pp. 179-86.
Li, D., Zou, X. Y., El-Ayachi, I., Romero, L. O., Yu, Z., Iglesias-Linares, A., Cordero-Morales, J. F. and Huang, G. T. (2019) 'Human Dental Pulp Stem Cells and Gingival Mesenchymal Stem Cells Display Action Potential Capacity In Vitro after Neuronogenic Differentiation', *Stem Cell Rev Rep,* 15(1), pp. 67-81.
Li, J., Han, J., Hu, Y. and Yang, J. (2016) 'Selection of Reference Genes for Quantitative Real-Time PCR during Flower Development in Tree Peony (Paeonia suffruticosa Andr.)', *Front Plant Sci,* 7, pp. 516.
Li, J., Zhang, H. and Ren, C. (2012) 'Effect of Low-Intensity Pulsed Ultrasound on Nerve Repair', *Tissue Regeneration-From Basic Biology to Clinical Application*: InTech.
Li, V. C. and Kirschner, M. W. (2014) 'Molecular ties between the cell cycle and differentiation in embryonic stem cells', *Proc Natl Acad Sci U S A,* 111(26), pp. 9503-8.
Li, X. J., Du, Z. W., Zarnowska, E. D., Pankratz, M., Hansen, L. O., Pearce, R. A. and Zhang, S. C. (2005) 'Specification of motoneurons from human embryonic stem cells', *Nat Biotechnol,* 23(2), pp. 215-21.
Li, X. J., Hu, B. Y., Jones, S. A., Zhang, Y. S., Lavaute, T., Du, Z. W. and Zhang, S. C. (2008) 'Directed differentiation of ventral spinal progenitors and motor neurons from human embryonic stem cells by small molecules', *Stem Cells,* 26(4), pp. 886-93.
Lim, D. A. and Alvarez-Buylla, A. (2016) 'The Adult Ventricular-Subventricular Zone (V-SVZ) and Olfactory Bulb (OB) Neurogenesis', *Cold Spring Harb Perspect Biol,* 8(5).
Lim, J. Y., Park, S. I., Kim, S. M., Jun, J. A., Oh, J. H., Ryu, C. H., Jeong, C. H., Park, S. H., Park, S. A., Oh, W., Chang, J. W. and Jeun, S. S. (2011) 'Neural differentiation of brain-derived neurotrophic factor-expressing human umbilical cord blood-derived mesenchymal stem cells in culture via TrkB-mediated ERK and β-catenin phosphorylation and following transplantation into the developing brain', *Cell Transplant,* 20(11-12), pp. 1855-66.
Lim, J. Y., Park, S. I., Oh, J. H., Kim, S. M., Jeong, C. H., Jun, J. A., Lee, K. S., Oh, W., Lee, J. K. and Jeun, S. S. (2008) 'Brain-derived neurotrophic factor stimulates the neural differentiation of human umbilical cord blood-derived mesenchymal stem cells and survival of differentiated cells through MAPK/ERK and PI3K/Akt-dependent signaling pathways', *J Neurosci Res,* 86(10), pp. 2168-78.
Lin, S., Lin, Y., Nery, J. R., Urich, M. A., Breschi, A., Davis, C. A., Dobin, A., Zaleski, C., Beer, M. A., Chapman, W. C., Gingeras, T. R., Ecker, J. R. and Snyder, M. P. (2014) 'Comparison of the transcriptional landscapes between human and mouse tissues', *Proc Natl Acad Sci U S A,* 111(48), pp. 17224-9.
Lin, S. L., Duan, H., Wang, S. and Li, J. J. (2020) 'Overexpression of Lin28B Promoted the Proliferation of Adenomyotic Smooth Muscle Cells of the Junctional Zone via Regulating Let-7a', *Reprod Sci*.
Lindwall, C. and Kanje, M. (2005) 'The role of p-c-Jun in survival and outgrowth of developing sensory neurons', *Neuroreport,* 16(15), pp. 1655-9.

Ling, L., Feng, X., Wei, T., Wang, Y., Zhang, W., He, L., Wang, Z., Zeng, Q. and Xiong, Z. (2017a) 'Effects of low-intensity pulsed ultrasound (LIPUS)-pretreated human amnion-derived mesenchymal stem cell (hAD-MSC) transplantation on primary ovarian insufficiency in rats', *Stem Cell Res Ther,* 8(1), pp. 283.

Ling, L., Wei, T., He, L., Wang, Y., Wang, Y., Feng, X., Zhang, W. and Xiong, Z. (2017b) 'Low-intensity pulsed ultrasound activates ERK1/2 and PI3K-Akt signalling pathways and promotes the proliferation of human amnion-derived mesenchymal stem cells', *Cell proliferation,* 50(6), pp. 10.1111/cpr.12383.

Liu, D. D., Ullah, M., Concepcion, W., Dahl, J. J. and Thakor, A. S. (2020) 'The role of ultrasound in enhancing mesenchymal stromal cell-based therapies', *Stem Cells Transl Med,* 9(8), pp. 850-866.

Liu, S., Kam, W. R., Ding, J., Hatton, M. P. and Sullivan, D. A. (2013) 'Effect of growth factors on the proliferation and gene expression of human meibomian gland epithelial cells', *Invest Ophthalmol Vis Sci,* 54(4), pp. 2541-50.

Liu, Y., Namba, T., Liu, J., Suzuki, R., Shioda, S. and Seki, T. (2010) 'Glial fibrillary acidic protein-expressing neural progenitors give rise to immature neurons via early intermediate progenitors expressing both glial fibrillary acidic protein and neuronal markers in the adult hippocampus', *Neuroscience,* 166(1), pp. 241-51.

Lopes, F. M., Schröder, R., da Frota Júnior, M. L. C., Zanotto-Filho, A., Müller, C. B., Pires, A. S., Meurer, R. T., Colpo, G. D., Gelain, D. P. and Kapczinski, F. (2010) 'Comparison between proliferative and neuron-like SH-SY5Y cells as an in vitro model for Parkinson disease studies', *Brain research,* 1337, pp. 85-94.

Lovelace, T. W., Henry, M. A., Hargreaves, K. M. and Diogenes, A. (2011) 'Evaluation of the delivery of mesenchymal stem cells into the root canal space of necrotic immature teeth after clinical regenerative endodontic procedure', *J Endod,* 37(2), pp. 133-8.

Lovicu, F. J. and McAvoy, J. W. (2001) 'FGF-induced lens cell proliferation and differentiation is dependent on MAPK (ERK1/2) signalling', *Development,* 128(24), pp. 5075-84.

Lu, J., Moochhala, S., Moore, X. L., Ng, K. C., Tan, M. H., Lee, L. K., He, B., Wong, M. C. and Ling, E. A. (2006) 'Adult bone marrow cells differentiate into neural phenotypes and improve functional recovery in rats following traumatic brain injury', *Neurosci Lett,* 398(1-2), pp. 12-7.

Lu, P., Blesch, A. and Tuszynski, M. H. (2004) 'Induction of bone marrow stromal cells to neurons: differentiation, transdifferentiation, or artifact?', *J Neurosci Res,* 77(2), pp. 174-91.

Luke, A. M., Patnaik, R., Kuriadom, S., Abu-Fanas, S., Mathew, S. and Shetty, K. P. (2020) 'Human dental pulp stem cells differentiation to neural cells, osteocytes and adipocytes-An', *Heliyon,* 6(1), pp. e03054.

Lundy, F. T., El karim, I. and Scheven, B. A. (2019) 'Current and Future Views on Pulpal Pain and Neurogenesis', in Duncan, H. and Cooper, P. (eds.) *Clinical Approaches in Endodontic Regeneration*: Springer, Cham.

Luo, L., Albashari, A. A., Wang, X., Jin, L., Zhang, Y., Zheng, L., Xia, J., Xu, H., Zhao, Y., Xiao, J., He, Y. and Ye, Q. (2018) 'Effects of Transplanted Heparin-Poloxamer Hydrogel Combining Dental Pulp Stem Cells and bFGF on Spinal Cord Injury Repair', *Stem Cells Int,* 2018, pp. 2398521.

Luo, L., He, Y., Jin, L., Zhang, Y., Guastaldi, F. P., Albashari, A. A., Hu, F., Wang, X., Wang, L., Xiao, J., Li, L., Wang, J., Higuchi, A. and Ye, Q. (2021) 'Application of bioactive hydrogels combined with dental pulp stem cells for the repair of large gap peripheral nerve injuries', *Bioact Mater,* 6(3), pp. 638-654.

Luo, W., Wickramasinghe, S. R., Savitt, J. M., Griffin, J. W., Dawson, T. M. and Ginty, D. D. (2007) 'A hierarchical NGF signaling cascade controls Ret-dependent and Ret-independent events during development of nonpeptidergic DRG neurons', *Neuron,* 54(5), pp. 739-54.

Luzuriaga, J., Pineda, J. R., Irastorza, I., Uribe-Etxebarria, V., García-Gallastegui, P., Encinas, J. M., Chamero, P., Unda, F. and Ibarretxe, G. (2019) 'BDNF and NT3 Reprogram Human Ectomesenchymal Dental Pulp Stem Cells to Neurogenic and Gliogenic Neural Crest Progenitors Cultured in Serum-Free Medium', *Cell Physiol Biochem,* 52(6), pp. 1361-1380.

Lv, Y., Nan, P., Chen, G., Sha, Y., Xia, B. and Yang, L. (2015) 'In vivo repair of rat transected sciatic nerve by low-intensity pulsed ultrasound and induced pluripotent stem cells-derived neural crest stem cells', *Biotechnol Lett,* 37(12), pp. 2497-506.

Lv, Y., Zhao, P., Chen, G., Sha, Y. and Yang, L. (2013) 'Effects of low-intensity pulsed ultrasound on cell viability, proliferation and neural differentiation of induced pluripotent stem cells-derived neural crest stem cells', *Biotechnol Lett,* 35(12), pp. 2201-12.

Madanagopal, T. T., Franco-Obregón, A. and Rosa, V. (2020) 'Comparative study of xeno-free induction protocols for neural differentiation of human dental pulp stem cells in vitro', *Arch Oral Biol,* 109, pp. 104572.

Man, J., Shelton, R. M., Cooper, P. R. and Scheven, B. A. (2012) 'Low-intensity low-frequency ultrasound promotes proliferation and differentiation of odontoblast-like cells', *Journal of endodontics,* 38(5), pp. 608-613.

Marangos, P. J., Schmechel, D. E., Parma, A. M. and Goodwin, F. K. (1980) 'Developmental profile of neuron-specific (NSE) and non-neuronal (NNE) enolase', *Brain Res,* 190(1), pp. 185-93.

Marangos, P. J., Zomzely-Neurath, C. and York, C. (1976) 'Determination and characterization of neuron specific protein (NSP) associated enolase activity', *Biochem Biophys Res Commun,* 68(4), pp. 1309-16.

Martens, W., Sanen, K., Georgiou, M., Struys, T., Bronckaers, A., Ameloot, M., Phillips, J. and Lambrichts, I. (2014) 'Human dental pulp stem cells can differentiate into Schwann cells and promote and guide neurite outgrowth in an aligned tissue-engineered collagen construct in vitro', *Faseb j,* 28(4), pp. 1634-43.

Martens, W., Wolfs, E., Struys, T., Politis, C., Bronckaers, A. and Lambrichts, I. (2012) 'Expression pattern of basal markers in human dental pulp stem cells and tissue', *Cells Tissues Organs,* 196(6), pp. 490-500.

Martin, G., Ricucci, D., Gibbs, J. L. and Lin, L. M. (2013) 'Histological findings of revascularized/revitalized immature permanent molar with apical periodontitis using platelet-rich plasma', *Journal of endodontics,* 39(1), pp. 138-144.

Maul, T. M., Chew, D. W., Nieponice, A. and Vorp, D. A. (2011) 'Mechanical stimuli differentially control stem cell behavior: morphology, proliferation, and differentiation', *Biomech Model Mechanobiol,* 10(6), pp. 939-53.

McDermott, L. A., Weir, G. A., Themistocleous, A. C., Segerdahl, A. R., Blesneac, I., Baskozos, G., Clark, A. J., Millar, V., Peck, L. J., Ebner, D., Tracey, I., Serra, J. and Bennett, D. L. (2019) 'Defining the Functional Role of Na', *Neuron,* 101(5), pp. 905-919.e8.

McGillicuddy, N., Floris, P., Albrecht, S. and Bones, J. (2018) 'Examining the sources of variability in cell culture media used for biopharmaceutical production', *Biotechnol Lett,* 40(1), pp. 5-21.

Meijering, E. (2010) 'Neuron tracing in perspective', *Cytometry A,* 77(7), pp. 693-704.

Meijering, E., Jacob, M., Sarria, J. C., Steiner, P., Hirling, H. and Unser, M. (2004) 'Design and validation of a tool for neurite tracing and analysis in fluorescence microscopy images', *Cytometry A,* 58(2), pp. 167-76.

Meloche, S. and Pouyssegur, J. (2007) 'The ERK1/2 mitogen-activated protein kinase pathway as a master regulator of the G1- to S-phase transition', *Oncogene,* 26(22), pp. 3227-39.

Menorca, R. M., Fussell, T. S. and Elfar, J. C. (2013) 'Nerve physiology: mechanisms of injury and recovery', *Hand Clin,* 29(3), pp. 317-30.

Meschi, N., Hilkens, P., Lambrichts, I., Van den Eynde, K., Mavridou, A., Strijbos, O., De Ketelaere, M., Van Gorp, G. and Lambrechts, P. (2016) 'Regenerative endodontic procedure of an infected immature permanent human tooth: an immunohistological study', *Clinical oral investigations,* 20(4), pp. 807-814.

Milhas, D., Andrieu-Abadie, N., Levade, T., Benoist, H. and Segui, B. (2012) 'The tricyclodecan-9-yl-xanthogenate D609 triggers ceramide increase and enhances FasL-induced caspase-dependent and -independent cell death in T lymphocytes', *Int J Mol Sci,* 13(7), pp. 8834-52.

Miller, I., Min, M., Yang, C., Tian, C., Gookin, S., Carter, D. and Spencer, S. L. (2018) 'Ki67 is a Graded Rather than a Binary Marker of Proliferation versus Quiescence', *Cell Rep,* 24(5), pp. 1105-1112.e5.

Mimura, T., Dezawa, M., Kanno, H., Sawada, H. and Yamamoto, I. (2004) 'Peripheral nerve regeneration by transplantation of bone marrow stromal cell-derived Schwann cells in adult rats', *J Neurosurg,* 101(5), pp. 806-12.

Missios, S., Bekelis, K. and Spinner, R. J. (2014) 'Traumatic peripheral nerve injuries in children: epidemiology and socioeconomics', *J Neurosurg Pediatr,* 14(6), pp. 688-94.

Miyasaka, M., Nakata, H., Hao, J., Kim, Y.-K., Kasugai, S. and Kuroda, S. (2015) 'Low-Intensity Pulsed Ultrasound Stimulation Enhances Heat-Shock Protein 90 and Mineralized Nodule Formation in Mouse Calvaria-Derived Osteoblasts', *Tissue Engineering Part A,* 21(23-24), pp. 2829-2839.

Moayeri, A., Nazm Bojnordi, M., Haratizadeh, S., Esmaeilnejad-Moghadam, A., Alizadeh, R. and Ghasemi Hamidabadi, H. (2017) 'Transdifferentiation of Human Dental Pulp Stem Cells Into Oligoprogenitor Cells', *Basic Clin Neurosci,* 8(5), pp. 387-394.

Monk, K. R., Naylor, S. G., Glenn, T. D., Mercurio, S., Perlin, J. R., Dominguez, C., Moens, C. B. and Talbot, W. S. (2009) 'A G protein-coupled receptor is essential for Schwann cells to initiate myelination', *Science,* 325(5946), pp. 1402-5.

Monteggia, L. M., Heimer, H. and Nestler, E. J. (2018) 'Meeting Report: Can We Make Animal Models of Human Mental Illness?', *Biol Psychiatry,* 84(7), pp. 542-545.

Monteiro, M. C., de la Cruz, M., Cantizani, J., Moreno, C., Tormo, J. R., Mellado, E., De Lucas, J. R., Asensio, F., Valiante, V., Brakhage, A. A., Latge, J. P., Genilloud, O. and Vicente, F. (2012) 'A new approach to drug discovery: high-throughput screening of microbial natural extracts against Aspergillus fumigatus using resazurin', *J Biomol Screen,* 17(4), pp. 542-9.

Moore, A. M., MacEwan, M., Santosa, K. B., Chenard, K. E., Ray, W. Z., Hunter, D. A., Mackinnon, S. E. and Johnson, P. J. (2011) 'Acellular nerve allografts in peripheral nerve regeneration: a comparative study', *Muscle Nerve,* 44(2), pp. 221-34.

Moreno-Jiménez, E. P., Flor-García, M., Terreros-Roncal, J., Rábano, A., Cafini, F., Pallas-Bazarra, N., Ávila, J. and Llorens-Martín, M. (2019) 'Adult hippocampal neurogenesis is abundant in neurologically healthy subjects and drops sharply in patients with Alzheimer's disease', *Nat Med,* 25(4), pp. 554-560.

Mukai, S., Ito, H., Nakagawa, Y., Akiyama, H., Miyamoto, M. and Nakamura, T. (2005) 'Transforming growth factor-β 1 mediates the effects of low-intensity pulsed ultrasound in chondrocytes', *Ultrasound in medicine & biology,* 31(12), pp. 1713-1721.

Murphy, L. O. and Blenis, J. (2006) 'MAPK signal specificity: the right place at the right time', *Trends Biochem Sci,* 31(5), pp. 268-75.

Murray, P. E., Garcia-Godoy, F. and Hargreaves, K. M. (2007) 'Regenerative endodontics: a review of current status and a call for action', *Journal of endodontics,* 33(4), pp. 377-390.

Mårtensson, L., Gustavsson, P., Dahlin, L. B. and Kanje, M. (2007) 'Activation of extracellular-signal-regulated kinase-1/2 precedes and is required for injury-induced Schwann cell proliferation', *Neuroreport,* 18(10), pp. 957-61.

Nageh, M., Ahmed, G. M. and El-Baz, A. A. (2018) 'Assessment of Regaining Pulp Sensibility in Mature Necrotic Teeth Using a Modified Revascularization Technique with Platelet-rich Fibrin: A Clinical Study', *J Endod,* 44(10), pp. 1526-1533.

Nakajima, M. and Schmitt, L. I. (2020) 'Understanding the circuit basis of cognitive functions using mouse models', *Neurosci Res,* 152, pp. 44-58.

Nakanishi, M., Niidome, T., Matsuda, S., Akaike, A., Kihara, T. and Sugimoto, H. (2007) 'Microglia-derived interleukin-6 and leukaemia inhibitory factor promote astrocytic differentiation of neural stem/progenitor cells', *Eur J Neurosci,* 25(3), pp. 649-58.

Nakashima, M. and Akamine, A. (2005) 'The application of tissue engineering to regeneration of pulp and dentin in endodontics', *Journal of endodontics,* 31(10), pp. 711-718.

Nakashima, M. and Iohara, K. (2011) 'Regeneration of dental pulp by stem cells', *Adv Dent Res,* 23(3), pp. 313-9.

Nakashima, M., Iohara, K., Murakami, M., Nakamura, H., Sato, Y., Ariji, Y. and Matsushita, K. (2017) 'Pulp regeneration by transplantation of dental pulp stem cells in pulpitis: a pilot clinical study', *Stem Cell Res Ther,* 8(1), pp. 61.

Namour, M. and Theys, S. (2014) 'Pulp revascularization of immature permanent teeth: a review of the literature and a proposal of a new clinical protocol', *The Scientific World Journal,* 2014.

Navarro Quiroz, E., Navarro Quiroz, R., Ahmad, M., Gomez Escorcia, L., Villarreal, J. L., Fernandez Ponce, C. and Aroca Martinez, G. (2018) 'Cell Signaling in Neuronal Stem Cells', *Cells,* 7(7).

Neelamurthy, P. S., Kumar, R. A., Balakrishnan, V., Venkatesan, S. M., Narayan, G. S. and I, K. (2018) 'Revascularization in Immature and Mature Teeth with Necrotic Pulp: A Clinical Study', *J Contemp Dent Pract,* 19(11), pp. 1393-1399.

Ng, Y. W. and Say, Y. H. (2018) 'Palmitic acid induces neurotoxicity and gliatoxicity in SH-SY5Y human neuroblastoma and T98G human glioblastoma cells', *PeerJ,* 6, pp. e4696.

Nguyen, E., Grubor, D. and Chandu, A. (2014) 'Risk factors for permanent injury of inferior alveolar and lingual nerves during third molar surgery', *J Oral Maxillofac Surg,* 72(12), pp. 2394-401.

Nicolini, G., Miloso, M., Zoia, C., Di Silvestro, A., Cavaletti, G. and Tredici, G. (1998) 'Retinoic acid differentiated SH-SY5Y human neuroblastoma cells: an in vitro model to assess drug neurotoxicity', *Anticancer research,* 18(4A), pp. 2477-2481.

Ning, G. Z., Song, W. Y., Xu, H., Zhu, R. S., Wu, Q. L., Wu, Y., Zhu, S. B., Li, J. Q., Wang, M., Qu, Z. G. and Feng, S. Q. (2019) 'Bone marrow mesenchymal stem cells stimulated with low-intensity pulsed ultrasound: Better choice of transplantation treatment for spinal cord injury: Treatment for SCI by LIPUS-BMSCs transplantation', *CNS Neurosci Ther,* 25(4), pp. 496-508.

Nirenberg, M. J., Chan, J., Vaughan, R. A., Uhl, G. R., Kuhar, M. J. and Pickel, V. M. (1997) 'Immunogold localization of the dopamine transporter: an ultrastructural study of the rat ventral tegmental area', *J Neurosci,* 17(11), pp. 4037-44.

Nishikori, T., Ochi, M., Uchio, Y., Maniwa, S., Kataoka, H., Kawasaki, K., Katsube, K. and Kuriwaka, M. (2002) 'Effects of low-intensity pulsed ultrasound on proliferation and chondroitin sulfate synthesis of cultured chondrocytes embedded in Atelocollagen gel', *J Biomed Mater Res,* 59(2), pp. 201-6.

O'Brien, D. E., Alter, B. J., Satomoto, M., Morgan, C. D., Davidson, S., Vogt, S. K., Norman, M. E., Gereau, G. B., Demaro, J. A., Landreth, G. E., Golden, J. P. and Gereau, R. W. (2015) 'ERK2 Alone Drives Inflammatory Pain But Cooperates with ERK1 in Sensory Neuron Survival', *J Neurosci,* 35(25), pp. 9491-507.

O'Brien, J., Wilson, I., Orton, T. and Pognan, F. (2000) 'Investigation of the Alamar Blue (resazurin) fluorescent dye for the assessment of mammalian cell cytotoxicity', *Eur J Biochem,* 267(17), pp. 5421-6.

Ochsner, S. A., Abraham, D., Martin, K., Ding, W., McOwiti, A., Kankanamge, W., Wang, Z., Andreano, K., Hamilton, R. A., Chen, Y., Hamilton, A., Gantner, M. L., Dehart, M., Qu, S., Hilsenbeck, S. G., Becnel, L. B., Bridges, D., Ma'ayan, A., Huss, J. M., Stossi, F., Foulds, C. E., Kralli, A., McDonnell, D. P. and McKenna, N. J. (2019) 'The Signaling Pathways Project, an integrated 'omics knowledgebase for mammalian cellular signaling pathways', *Sci Data,* 6(1), pp. 252.

Olgart, L. (1985) 'The role of local factors in dentin and pulp in intradental pain mechanisms', *Journal of dental research,* 64(4), pp. 572-578.

Olgart, L. (1996) 'Neural control of pulpal blood flow', *Critical Reviews in Oral Biology & Medicine,* 7(2), pp. 159-171.

Osathanon, T., Sawangmake, C., Nowwarote, N. and Pavasant, P. (2014) 'Neurogenic differentiation of human dental pulp stem cells using different induction protocols', *Oral Dis,* 20(4), pp. 352-8.

Osteen, J. D., Herzig, V., Gilchrist, J., Emrick, J. J., Zhang, C., Wang, X., Castro, J., Garcia-Caraballo, S., Grundy, L., Rychkov, G. Y., Weyer, A. D., Dekan, Z., Undheim, E. A., Alewood, P., Stucky, C. L., Brierley, S. M., Basbaum, A. I., Bosmans, F., King, G. F. and Julius, D. (2016) 'Selective spider toxins reveal a role for the Nav1.1 channel in mechanical pain', *Nature,* 534(7608), pp. 494-9.

Pagella, P., Miran, S., Neto, E., Martin, I., Lamghari, M. and Mitsiadis, T. A. (2020) 'Human dental pulp stem cells exhibit enhanced properties in comparison to human bone marrow stem cells on neurites outgrowth', *FASEB J,* 34(4), pp. 5499-5511.

Pan, S., Dangaria, S., Gopinathan, G., Yan, X., Lu, X., Kolokythas, A., Niu, Y. and Luan, X. (2013) 'SCF promotes dental pulp progenitor migration, neovascularization, and collagen remodeling - potential applications as a homing factor in dental pulp regeneration', *Stem Cell Rev Rep,* 9(5), pp. 655-67.

Patodia, S. and Raivich, G. (2012) 'Role of transcription factors in peripheral nerve regeneration', *Front Mol Neurosci,* 5, pp. 8.

Pavlova, G., Lopatina, T., Kalinina, N., Rybalkina, E., Parfyonova, Y., Tkachuk, V. and Revishchin, A. (2012) 'In vitro neuronal induction of adipose-derived stem cells and their fate after transplantation into injured mouse brain', *Curr Med Chem,* 19(30), pp. 5170-7.

Pfaffl, M. W. (2001) 'A new mathematical model for relative quantification in real-time RT-PCR', *Nucleic Acids Res,* 29(9), pp. e45.

Pfaffl, M. W., Tichopad, A., Prgomet, C. and Neuvians, T. P. (2004) 'Determination of stable housekeeping genes, differentially regulated target genes and sample integrity:

BestKeeper--Excel-based tool using pair-wise correlations', *Biotechnol Lett,* 26(6), pp. 509-15.
Phonchai, R., Phermthai, T., Kitiyanant, N., Suwanjang, W., Kotchabhakdi, N. and Chetsawang, B. (2019) 'Potential effects and molecular mechanisms of melatonin on the dopaminergic neuronal differentiation of human amniotic fluid mesenchymal stem cells', *Neurochem Int,* 124, pp. 82-93.
Piehler, A. P., Grimholt, R. M., Ovstebo, R. and Berg, J. P. (2010) 'Gene expression results in lipopolysaccharide-stimulated monocytes depend significantly on the choice of reference genes', *BMC Immunol,* 11, pp. 21.
Pierdomenico, L., Bonsi, L., Calvitti, M., Rondelli, D., Arpinati, M., Chirumbolo, G., Becchetti, E., Marchionni, C., Alviano, F., Fossati, V., Staffolani, N., Franchina, M., Grossi, A. and Bagnara, G. P. (2005) 'Multipotent mesenchymal stem cells with immunosuppressive activity can be easily isolated from dental pulp', *Transplantation,* 80(6), pp. 836-42.
Pires, A. O., Neves-Carvalho, A., Sousa, N. and Salgado, A. J. (2014) 'The Secretome of Bone Marrow and Wharton Jelly Derived Mesenchymal Stem Cells Induces Differentiation and Neurite Outgrowth in SH-SY5Y Cells', *Stem Cells Int,* 2014, pp. 438352.
Podrygajlo, G., Tegenge, M. A., Gierse, A., Paquet-Durand, F., Tan, S., Bicker, G. and Stern, M. (2009) 'Cellular phenotypes of human model neurons (NT2) after differentiation in aggregate culture', *Cell Tissue Res,* 336(3), pp. 439-52.
Pogrel, M. A. (2017) 'Nerve damage in dentistry', *Gen Dent,* 65(2), pp. 34-41.
Pogrel, M. A., Jergensen, R., Burgon, E. and Hulme, D. (2011) 'Long-term outcome of trigeminal nerve injuries related to dental treatment', *J Oral Maxillofac Surg,* 69(9), pp. 2284-8.
Pogrel, M. A. and Thamby, S. (2000) 'Permanent nerve involvement resulting: from inferior alveolar nerve blocks', *The Journal of the American Dental Association,* 131(7), pp. 901-907.
Polleux, F. and Snider, W. (2010) 'Initiating and growing an axon', *Cold Spring Harb Perspect Biol,* 2(4), pp. a001925.
Pomini, K. T., Andreo, J. C., de C Rodrigues, A., de O, G., Jéssica, B., Daré, L. R., German, I. J., Rosa, G. M. and Buchaim, R. L. (2014) 'Effect of Low-Intensity Pulsed Ultrasound on Bone Regeneration', *Journal of Ultrasound in Medicine,* 33(4), pp. 713-717.
Poolman, R. W., Agoritsas, T., Siemieniuk, R. A., Harris, I. A., Schipper, I. B., Mollon, B., Smith, M., Albin, A., Nador, S., Sasges, W., Schandelmaier, S., Lytvyn, L., Kuijpers, T., van Beers, L. W., Verhofstad, M. H. and Vandvik, P. O. (2017) 'Low intensity pulsed ultrasound (LIPUS) for bone healing: a clinical practice guideline', *BMJ,* 356, pp. j576.
Portier, M. M., de Néchaud, B. and Gros, F. (1983) 'Peripherin, a new member of the intermediate filament protein family', *Dev Neurosci,* 6(6), pp. 335-44.
Prescott, R. S., Alsanea, R., Fayad, M. I., Johnson, B. R., Wenckus, C. S., Hao, J., John, A. S. and George, A. (2008) 'In vivo generation of dental pulp-like tissue by using dental pulp stem cells, a collagen scaffold, and dentin matrix protein 1 after subcutaneous transplantation in mice', *J Endod,* 34(4), pp. 421-6.
Presgraves, S. P., Ahmed, T., Borwege, S. and Joyce, J. N. (2004) 'Terminally differentiated SH-SY5Y cells provide a model system for studying neuroprotective effects of dopamine agonists', *Neurotox Res,* 5(8), pp. 579-98.
Påhlman, S., Hoehner, J. C., Nånberg, E., Hedborg, F., Fagerström, S., Gestblom, C., Johansson, I., Larsson, U., Lavenius, E. and Ortoft, E. (1995) 'Differentiation and survival influences of growth factors in human neuroblastoma', *Eur J Cancer,* 31A(4), pp. 453-8.

Påhlman, S., Odelstad, L., Larsson, E., Grotte, G. and Nilsson, K. (1981) 'Phenotypic changes of human neuroblastoma cells in culture induced by 12-O-tetradecanoyl-phorbol-13-acetate', *International journal of cancer,* 28(5), pp. 583-589.

Påhlman, S., Ruusala, A.-I., Abrahamsson, L., Mattsson, M. E. and Esscher, T. (1984) 'Retinoic acid-induced differentiation of cultured human neuroblastoma cells: a comparison with phorbolester-induced differentiation', *Cell differentiation,* 14(2), pp. 135-144.

Raab, W. (1992) 'Temperature related changes in pulpal microcirculation', *Proc Finn Dent Soc,* 88(Suppl 1), pp. 469-479.

Rafiee, F., Pourteymourfard-Tabrizi, Z., Mahmoudian-Sani, M. R., Mehri-Ghahfarrokhi, A., Soltani, A., Hashemzadeh-Chaleshtori, M. and Jami, M. S. (2020) 'Differentiation of dental pulp stem cells into neuron-like cells', *Int J Neurosci,* 130(2), pp. 107-116.

Raivich, G., Bohatschek, M., Da Costa, C., Iwata, O., Galiano, M., Hristova, M., Nateri, A. S., Makwana, M., Riera-Sans, L., Wolfer, D. P., Lipp, H. P., Aguzzi, A., Wagner, E. F. and Behrens, A. (2004) 'The AP-1 transcription factor c-Jun is required for efficient axonal regeneration', *Neuron,* 43(1), pp. 57-67.

Raivich, G. and Makwana, M. (2007) 'The making of successful axonal regeneration: genes, molecules and signal transduction pathways', *Brain Res Rev,* 53(2), pp. 287-311.

Ramanan, V. K., Shen, L., Moore, J. H. and Saykin, A. J. (2012) 'Pathway analysis of genomic data: concepts, methods, and prospects for future development', *Trends Genet,* 28(7), pp. 323-32.

Rampersad, S. N. (2012) 'Multiple applications of Alamar Blue as an indicator of metabolic function and cellular health in cell viability bioassays', *Sensors (Basel),* 12(9), pp. 12347-60.

Randall, A. D. (2016) 'Are stem cell-derived neural cells physiologically credible?', *J Physiol,* 594(22), pp. 6569-6572.

Ransohoff, R. M. (2018) 'All (animal) models (of neurodegeneration) are wrong. Are they also useful?', *J Exp Med,* 215(12), pp. 2955-2958.

Raso, V. V. M., Barbieri, C. H., Mazzer, N. and Fasan, V. S. (2005) 'Can therapeutic ultrasound influence the regeneration of peripheral nerves?', *Journal of neuroscience methods,* 142(2), pp. 185-192.

Ray, B., Simon, J. R. and Lahiri, D. K. (2009) 'Determination of high-affinity choline uptake (HACU) and choline acetyltransferase (ChAT) activity in the same population of cultured cells', *Brain Res,* 1297, pp. 160-8.

Rayner, M. L. D., Laranjeira, S., Evans, R. E., Shipley, R. J., Healy, J. and Phillips, J. B. (2018) 'Developing an In Vitro Model to Screen Drugs for Nerve Regeneration', *Anat Rec (Hoboken),* 301(10), pp. 1628-1637.

Reese, D. and Drapeau, P. (1998) 'Neurite growth patterns leading to functional synapses in an identified embryonic neuron', *J Neurosci,* 18(15), pp. 5652-62.

Reher, P., Elbeshir el-NI, Harvey, W., Meghji, S. and Harris, M. (1997) 'The stimulation of bone formation in vitro by therapeutic ultrasound', *Ultrasound Med Biol,* 23(8), pp. 1251-8.

Reid, A. J., Sun, M., Wiberg, M., Downes, S., Terenghi, G. and Kingham, P. J. (2011) 'Nerve repair with adipose-derived stem cells protects dorsal root ganglia neurons from apoptosis', *Neuroscience,* 199, pp. 515-22.

Ren, C., Chen, X., Du, N., Geng, S., Hu, Y., Liu, X., Wu, X., Lin, Y., Bai, X., Yin, W., Cheng, S., Yang, L. and Zhang, Y. (2018) 'Low-intensity pulsed ultrasound promotes Schwann cell viability and proliferation via the GSK-3β/β-catenin signaling pathway', *Int J Biol Sci,* 14(5), pp. 497-507.

Ren, L., Yang, Z., Song, J., Wang, Z., Deng, F. and Li, W. (2013) 'Involvement of p38 MAPK pathway in low intensity pulsed ultrasound induced osteogenic differentiation of human periodontal ligament cells', *Ultrasonics,* 53(3), pp. 686-690.

Renton, T. (2011) 'Persistent Pain after Dental Surgery', *Rev Pain,* 5(1), pp. 8-17.

Renton, T., Adey-Viscuso, D., Meechan, J. G. and Yilmaz, Z. (2010) 'Trigeminal nerve injuries in relation to the local anaesthesia in mandibular injections', *Br Dent J,* 209(9), pp. E15.

Renton, T., Janjua, H., Gallagher, J. E., Dalgleish, M. and Yilmaz, Z. (2013) 'UK dentists' experience of iatrogenic trigeminal nerve injuries in relation to routine dental procedures: why, when and how often?', *Br Dent J,* 214(12), pp. 633-42.

Revay, R., Vaughan, R., Grant, S. and Kuhar, M. J. (1996) 'Dopamine transporter immunohistochemistry in median eminence, amygdala, and other areas of the rat brain', *Synapse,* 22(2), pp. 93-9.

Riccio, M., Marchesini, A., Pugliese, P. and De Francesco, F. (2019) 'Nerve repair and regeneration: Biological tubulization limits and future perspectives', *J Cell Physiol,* 234(4), pp. 3362-3375.

Rodrigues, M., Griffith, L. G. and Wells, A. (2010) 'Growth factor regulation of proliferation and survival of multipotential stromal cells', *Stem Cell Res Ther,* 1(4), pp. 32.

Rosberg, H., Carlsson, K., Höjgård, S., Lindgren, B., Lundborg, G. and Dahlin, L. (2005) 'Injury to the human median and ulnar nerves in the forearm–analysis of costs for treatment and rehabilitation of 69 patients in southern Sweden', *Journal of Hand Surgery,* 30(1), pp. 35-39.

Ross, R. A., Spengler, B. A. and Biedler, J. L. (1983) 'Coordinate morphological and biochemical interconversion of human neuroblastoma cells', *J Natl Cancer Inst,* 71(4), pp. 741-7.

Rostamian Delavar, M., Baghi, M., Safaeinejad, Z., Kiani-Esfahani, A., Ghaedi, K. and Nasr-Esfahani, M. H. (2018) 'Differential expression of miR-34a, miR-141, and miR-9 in MPP+-treated differentiated PC12 cells as a model of Parkinson's disease', *Gene,* 662, pp. 54-65.

Rosén, A., Tardast, A. and Shi, T. J. (2016) 'How Far Have We Come in the Field of Nerve Regeneration After Trigeminal Nerve Injury?', *Curr Oral Health Rep,* 3(4), pp. 309-313.

Rosén, B., Chemnitz, A., Weibull, A., Andersson, G., Dahlin, L. B. and Björkman, A. (2012) 'Cerebral changes after injury to the median nerve: a long-term follow up', *Journal of plastic surgery and hand surgery,* 46(2), pp. 106-112.

Rotshenker, S. (2011) 'Wallerian degeneration: the innate-immune response to traumatic nerve injury', *J Neuroinflammation,* 8, pp. 109.

Ruangsawasdi, N., Zehnder, M., Patcas, R., Ghayor, C., Siegenthaler, B., Gjoksi, B. and Weber, F. E. (2017) 'Effects of Stem Cell Factor on Cell Homing During Functional Pulp Regeneration in Human Immature Teeth', *Tissue Eng Part A,* 23(3-4), pp. 115-123.

Rubin, C., Bolander, M., Ryaby, J. P. and Hadjiargyrou, M. (2001) 'The use of low-intensity ultrasound to accelerate the healing of fractures', *J Bone Joint Surg Am,* 83(2), pp. 259-70.

Rubinfeld, H. and Seger, R. (2005) 'The ERK cascade: a prototype of MAPK signaling', *Mol Biotechnol,* 31(2), pp. 151-74.

Ruijtenberg, S. and van den Heuvel, S. (2016) 'Coordinating cell proliferation and differentiation: Antagonism between cell cycle regulators and cell type-specific gene expression', *Cell Cycle,* 15(2), pp. 196-212.

Rutten, S., van den Bekerom, M. P., Sierevelt, I. N. and Nolte, P. A. (2016) 'Enhancement of Bone-Healing by Low-Intensity Pulsed Ultrasound: A Systematic Review', *JBJS Rev,* 4(3).

Sadée, W., Yu, V. C., Richards, M. L., Preis, P. N., Schwab, M. R., Brodsky, F. M. and Biedler, J. L. (1987) 'Expression of neurotransmitter receptors and myc protooncogenes in subclones of a human neuroblastoma cell line', *Cancer Res,* 47(19), pp. 5207-12.

Sakai, K., Yamamoto, A., Matsubara, K., Nakamura, S., Naruse, M., Yamagata, M., Sakamoto, K., Tauchi, R., Wakao, N., Imagama, S., Hibi, H., Kadomatsu, K., Ishiguro, N. and Ueda, M. (2012) 'Human dental pulp-derived stem cells promote locomotor recovery after complete transection of the rat spinal cord by multiple neuro-regenerative mechanisms', *J Clin Invest,* 122(1), pp. 80-90.

Sandstedt, P. and Sörensen, S. (1995) 'Neurosensory disturbances of the trigeminal nerve: a long-term follow-up of traumatic injuries', *Journal of oral and maxillofacial surgery,* 53(5), pp. 498-505.

Sanen, K., Martens, W., Georgiou, M., Ameloot, M., Lambrichts, I. and Phillips, J. (2017) 'Engineered neural tissue with Schwann cell differentiated human dental pulp stem cells: potential for peripheral nerve repair?', *J Tissue Eng Regen Med,* 11(12), pp. 3362-3372.

Saoud, T. M. A., Ricucci, D., Lin, L. M. and Gaengler, P. (2016) 'Regeneration and Repair in Endodontics—A Special Issue of the Regenerative Endodontics—A New Era in Clinical Endodontics', *Dentistry Journal,* 4(1), pp. 3.

Sarikov, R. and Juodzbalys, G. (2014) 'Inferior alveolar nerve injury after mandibular third molar extraction: a literature review', *J Oral Maxillofac Res,* 5(4), pp. e1.

Sato, M., Motoyoshi, M., Shinoda, M., Iwata, K. and Shimizu, N. (2016) 'Low-intensity pulsed ultrasound accelerates nerve regeneration following inferior alveolar nerve transection in rats', *Eur J Oral Sci,* 124(3), pp. 246-50.

Sato, M., Nagata, K., Kuroda, S., Horiuchi, S., Nakamura, T., Karima, M., Inubushi, T. and Tanaka, E. (2014) 'Low-intensity pulsed ultrasound activates integrin-mediated mechanotransduction pathway in synovial cells', *Ann Biomed Eng,* 42(10), pp. 2156-63.

Sawai, Y., Murata, H., Koto, K., Matsui, T., Horie, N., Ashihara, E., Maekawa, T., Fushiki, S. and Kubo, T. (2012) 'Effects of low-intensity pulsed ultrasound on osteosarcoma and cancer cells', *Oncol Rep,* 28(2), pp. 481-6.

Scarnati, M. S., Halikere, A. and Pang, Z. P. (2019) 'Using human stem cells as a model system to understand the neural mechanisms of alcohol use disorders: Current status and outlook', *Alcohol,* 74, pp. 83-93.

Scheven, B., Man, J., Millard, J., Cooper, P., Lea, S., Walmsley, A. and Smith, A. (2009) 'VEGF and odontoblast-like cells: stimulation by low frequency ultrasound', *Archives of oral biology,* 54(2), pp. 185-191.

Schindelin, J., Arganda-Carreras, I., Frise, E., Kaynig, V., Longair, M., Pietzsch, T., Preibisch, S., Rueden, C., Saalfeld, S., Schmid, B., Tinevez, J. Y., White, D. J., Hartenstein, V., Eliceiri, K., Tomancak, P. and Cardona, A. (2012) 'Fiji: an open-source platform for biological-image analysis', *Nat Methods,* 9(7), pp. 676-82.

Schrope, B. A. and Goel, N. (2014) 'Physical Principles of Ultrasound', in E., H. and J., M. (eds.) *Abdominal Ultrasound for Surgeons*. New York, NY.: Springer, pp. 7-15.

Seddon, H. (1942) 'A classification of nerve injuries', *British medical journal,* 2(4260), pp. 237.

Seddon, H. (1943) 'Three types of nerve injury', *Brain,* 66(4), pp. 237-288.

Seeds, N. W., Gilman, A. G., Amano, T. and Nirenberg, M. W. (1970) 'Regulation of axon formation by clonal lines of a neural tumor', *Proc Natl Acad Sci U S A,* 66(1), pp. 160-7.

Shafer, T. J. and Atchison, W. D. (1991) 'Transmitter, ion channel and receptor properties of pheochromocytoma (PC12) cells: a model for neurotoxicological studies', *Neurotoxicology,* 12(3), pp. 473-92.
Shamir, C., Venugopal, C. and Dhanushkodi, A. (2015) 'Dental pulp stem cells for treating neurodegenerative diseases', *Neural Regen Res,* 10(12), pp. 1910-1.
Shanks, N., Greek, R. and Greek, J. (2009) 'Are animal models predictive for humans?', *Philos Ethics Humanit Med,* 4, pp. 2.
Sharow, K. A., Temkin, B. and Asson-Batres, M. A. (2012) 'Retinoic acid stability in stem cell cultures', *Int J Dev Biol,* 56(4), pp. 273-8.
Shi, X., Mao, J. and Liu, Y. (2020) 'Pulp stem cells derived from human permanent and deciduous teeth: Biological characteristics and therapeutic applications', *Stem Cells Transl Med,* 9(4), pp. 445-464.
Shimizu, E., Ricucci, D., Albert, J., Alobaid, A. S., Gibbs, J. L., Huang, G. T.-J. and Lin, L. M. (2013) 'Clinical, radiographic, and histological observation of a human immature permanent tooth with chronic apical abscess after revitalization treatment', *Journal of endodontics,* 39(8), pp. 1078-1083.
Shinoda, Y., Ahmed, S., Ramachandran, B., Bharat, V., Brockelt, D., Altas, B. and Dean, C. (2014) 'BDNF enhances spontaneous and activity-dependent neurotransmitter release at excitatory terminals but not at inhibitory terminals in hippocampal neurons', *Front Synaptic Neurosci,* 6, pp. 27.
Shipley, M. M., Mangold, C. A. and Szpara, M. L. (2016) 'Differentiation of the SH-SY5Y human neuroblastoma cell line', *Journal of visualized experiments: JoVE,* (108), pp. 53193.
Skene, J. H. and Willard, M. (1981) 'Axonally transported proteins associated with axon growth in rabbit central and peripheral nervous systems', *J Cell Biol,* 89(1), pp. 96-103.
Slack, R., Lach, B., Gregor, A., al-Mazidi, H. and Proulx, P. (1992) 'Retinoic acid- and staurosporine-induced bidirectional differentiation of human neuroblastoma cell lines', *Exp Cell Res,* 202(1), pp. 17-27.
Smith, A., Scheven, B., Takahashi, Y., Ferracane, J., Shelton, R. and Cooper, P. (2012) 'Dentine as a bioactive extracellular matrix', *Archives of oral biology,* 57(2), pp. 109-121.
Smith, A. J., Duncan, H. F., Diogenes, A., Simon, S. and Cooper, P. R. (2016) 'Exploiting the Bioactive Properties of the Dentin-Pulp Complex in Regenerative Endodontics', *J Endod,* 42(1), pp. 47-56.
Smith, J. G., Elias, L. A., Yilmaz, Z., Barker, S., Shah, K., Shah, S. and Renton, T. (2013) 'The psychosocial and affective burden of posttraumatic neuropathy following injuries to the trigeminal nerve', *J Orofac Pain,* 27(4), pp. 293-303.
Smith, M. H. and Lung, K. E. (2006) 'Nerve injuries after dental injection: a review of the literature', *Journal-Canadian Dental Association,* 72(6), pp. 559.
Snyder, D. J. and Bartoshuk, L. M. (2016) 'Oral sensory nerve damage: Causes and consequences', *Rev Endocr Metab Disord,* 17(2), pp. 149-58.
Soler López, F. (2013) 'Ultrasound applications to medicine', *Tecciencia,* 7(14), pp. 77-89.
Solis-Castro, O. O., Boissonade, F. M. and Rivolta, M. N. (2020) 'Establishment and neural differentiation of neural crest-derived stem cells from human dental pulp in serum-free conditions', *Stem Cells Transl Med,* 9(11), pp. 1462-1476.
Sorrells, S. F., Paredes, M. F., Cebrian-Silla, A., Sandoval, K., Qi, D., Kelley, K. W., James, D., Mayer, S., Chang, J., Auguste, K. I., Chang, E. F., Gutierrez, A. J., Kriegstein, A. R., Mathern, G. W., Oldham, M. C., Huang, E. J., Garcia-Verdugo, J. M., Yang, Z. and

Alvarez-Buylla, A. (2018) 'Human hippocampal neurogenesis drops sharply in children to undetectable levels in adults', *Nature,* 555(7696), pp. 377-381.
Spencer, C. I., Yuill, K. H., Borg, J. J., Hancox, J. C. and Kozlowski, R. Z. (2001) 'Actions of pyrethroid insecticides on sodium currents, action potentials, and contractile rhythm in isolated mammalian ventricular myocytes and perfused hearts', *J Pharmacol Exp Ther,* 298(3), pp. 1067-82.
Srikanth, P. and Young-Pearse, T. L. (2014) 'Stem cells on the brain: modeling neurodevelopmental and neurodegenerative diseases using human induced pluripotent stem cells', *J Neurogenet,* 28(1-2), pp. 5-29.
Stern, M., Gierse, A., Tan, S. and Bicker, G. (2014) 'Human Ntera2 cells as a predictive in vitro test system for developmental neurotoxicity', *Arch Toxicol,* 88(1), pp. 127-36.
Sterneckert, J. L., Reinhardt, P. and Schöler, H. R. (2014) 'Investigating human disease using stem cell models', *Nat Rev Genet,* 15(9), pp. 625-39.
Stifani, N. (2014) 'Motor neurons and the generation of spinal motor neuron diversity', *Front Cell Neurosci,* 8, pp. 293.
Stoll, G. and Müller, H. W. (1999) 'Nerve injury, axonal degeneration and neural regeneration: basic insights', *Brain Pathol,* 9(2), pp. 313-25.
Suga, M., Kondo, T. and Inoue, H. (2019) 'Modeling Neurological Disorders with Human Pluripotent Stem Cell-Derived Astrocytes', *Int J Mol Sci,* 20(16).
Sun, H. H., Jin, T., Yu, Q. and Chen, F. M. (2011) 'Biological approaches toward dental pulp regeneration by tissue engineering', *Journal of tissue engineering and regenerative medicine,* 5(4), pp. e1-e16.
Sun, Z., Yang, H., Shi, Y., Wei, M., Xian, J. and Hu, W. (2010) '[Establishment of a cell model system of herpes simplex virus type II latent infection and reactivation in SH-SY5Y cells]', *Wei Sheng Wu Xue Bao,* 50(1), pp. 98-106.
Sunderland, S. and Williams, H. B. 1992. Nerve injuries and their repair: a critical appraisal. LWW.
Suzuki, A., Takayama, T., Suzuki, N., Sato, M., Fukuda, T. and Ito, K. (2009) 'Daily low-intensity pulsed ultrasound-mediated osteogenic differentiation in rat osteoblasts', *Acta Biochim Biophys Sin (Shanghai),* 41(2), pp. 108-15.
Suzuki, T., Lee, C. H., Chen, M., Zhao, W., Fu, S. Y., Qi, J. J., Chotkowski, G., Eisig, S. B., Wong, A. and Mao, J. J. (2011) 'Induced migration of dental pulp stem cells for in vivo pulp regeneration', *J Dent Res,* 90(8), pp. 1013-8.
Takahashi, K. and Yamanaka, S. (2006) 'Induction of pluripotent stem cells from mouse embryonic and adult fibroblast cultures by defined factors', *Cell,* 126(4), pp. 663-76.
Takakura, Y., Matsui, N., Yoshiya, S., Fujioka, H., Muratsu, H., Tsunoda, M. and Kurosaka, M. (2002) 'Low-intensity pulsed ultrasound enhances early healing of medial collateral ligament injuries in rats', *J Ultrasound Med,* 21(3), pp. 283-8.
Takeuchi, N., Hayashi, Y., Murakami, M., Alvarez, F. J., Horibe, H., Iohara, K., Nakata, K., Nakamura, H. and Nakashima, M. (2015) 'Similar in vitro effects and pulp regeneration in ectopic tooth transplantation by basic fibroblast growth factor and granulocyte-colony stimulating factor', *Oral Dis,* 21(1), pp. 113-22.
Takeuchi, R., Ryo, A., Komitsu, N., Mikuni-Takagaki, Y., Fukui, A., Takagi, Y., Shiraishi, T., Morishita, S., Yamazaki, Y., Kumagai, K., Aoki, I. and Saito, T. (2008) 'Low-intensity pulsed ultrasound activates the phosphatidylinositol 3 kinase/Akt pathway and stimulates the growth of chondrocytes in three-dimensional cultures: a basic science study', *Arthritis Res Ther,* 10(4), pp. R77.

Tamaki, Y., Nakahara, T., Ishikawa, H. and Sato, S. (2013) 'In vitro analysis of mesenchymal stem cells derived from human teeth and bone marrow', *Odontology,* 101(2), pp. 121-32.
Tamburini, C. and Li, M. (2017) 'Understanding neurodevelopmental disorders using human pluripotent stem cell-derived neurons', *Brain Pathol,* 27(4), pp. 508-517.
Tanaka, E., Kuroda, S., Horiuchi, S., Tabata, A. and El-Bialy, T. (2015) 'Low-intensity pulsed ultrasound in dentofacial tissue engineering', *Annals of biomedical engineering,* 43(4), pp. 871-886.
Taylor, M. A., Kan, H. L., Gollapudi, B. B. and Marty, M. S. (2019) 'An in vitro developmental neurotoxicity screening assay for retinoic acid-induced neuronal differentiation using the human NT2/D1 cell line', *Neurotoxicology,* 73, pp. 258-264.
ter Haar, G. (1999) 'Therapeutic ultrasound', *Eur J Ultrasound,* 9(1), pp. 3-9.
ter Haar, G. (2007) 'Therapeutic applications of ultrasound', *Prog Biophys Mol Biol,* 93(1-3), pp. 111-29.
Thaler, J., Harrison, K., Sharma, K., Lettieri, K., Kehrl, J. and Pfaff, S. L. (1999) 'Active suppression of interneuron programs within developing motor neurons revealed by analysis of homeodomain factor HB9', *Neuron,* 23(4), pp. 675-87.
Theyel, B. (2018) 'Animal Models in Psychiatric Disease: A Circuit-Search Approach', *Harv Rev Psychiatry,* 26(5), pp. 298-303.
Thiel, G. (1993) 'Synapsin I, synapsin II, and synaptophysin: marker proteins of synaptic vesicles', *Brain Pathol,* 3(1), pp. 87-95.
Tınastepe, N. and Oral, K. (2013) 'Neuropathic pain after dental treatment', *Agri,* 25(1), pp. 1-6.
Tohyama, T., Lee, V. M., Rorke, L. B., Marvin, M., McKay, R. D. and Trojanowski, J. Q. (1992) 'Nestin expression in embryonic human neuroepithelium and in human neuroepithelial tumor cells', *Lab Invest,* 66(3), pp. 303-13.
Tojyo, I., Nakanishi, T., Shintani, Y., Okamoto, K., Hiraishi, Y. and Fujita, S. (2019) 'Risk of lingual nerve injuries in removal of mandibular third molars: a retrospective case-control study', *Maxillofac Plast Reconstr Surg,* 41(1), pp. 40.
Tomson, P. L., Grover, L. M., Lumley, P. J., Sloan, A. J., Smith, A. J. and Cooper, P. R. (2007) 'Dissolution of bio-active dentine matrix components by mineral trioxide aggregate', *J Dent,* 35(8), pp. 636-42.
Torabinejad, M., Alexander, A., Vahdati, S. A., Grandhi, A., Baylink, D. and Shabahang, S. (2018) 'Effect of Residual Dental Pulp Tissue on Regeneration of Dentin-pulp Complex: An In Vivo Investigation', *J Endod,* 44(12), pp. 1796-1801.
Trantor, I. R., Messer, H. H. and Birner, R. (1995) 'The effects of neuropeptides (calcitonin gene-related peptide and substance P) on cultured human pulp cells', *J Dent Res,* 74(4), pp. 1066-71.
Traverse, S., Gomez, N., Paterson, H., Marshall, C. and Cohen, P. (1992) 'Sustained activation of the mitogen-activated protein (MAP) kinase cascade may be required for differentiation of PC12 cells. Comparison of the effects of nerve growth factor and epidermal growth factor', *Biochem J,* 288 (Pt 2), pp. 351-5.
Trojanowski, J. Q., Walkenstein, N. and Lee, V. M. (1986) 'Expression of neurofilament subunits in neurons of the central and peripheral nervous system: an immunohistochemical study with monoclonal antibodies', *J Neurosci,* 6(3), pp. 650-60.
Tsai, C. L., Chang, W. H. and Liu, T. K. (1992) 'Preliminary studies of duration and intensity of ultrasonic treatments on fracture repair', *Chin J Physiol,* 35(1), pp. 21-6.
Tsokos, M., Scarpa, S., Ross, R. A. and Triche, T. J. (1987) 'Differentiation of human neuroblastoma recapitulates neural crest development. Study of morphology,

neurotransmitter enzymes, and extracellular matrix proteins', *Am J Pathol,* 128(3), pp. 484-96.
Tsuda, Y., Kanje, M. and Dahlin, L. B. (2011) 'Axonal outgrowth is associated with increased ERK 1/2 activation but decreased caspase 3 linked cell death in Schwann cells after immediate nerve repair in rats', *BMC Neurosci,* 12, pp. 12.
Tyler, W. J. and Pozzo-Miller, L. D. (2001) 'BDNF enhances quantal neurotransmitter release and increases the number of docked vesicles at the active zones of hippocampal excitatory synapses', *J Neurosci,* 21(12), pp. 4249-58.
Tzeng, H. H., Hsu, C. H., Chung, T. H., Lee, W. C., Lin, C. H., Wang, W. C., Hsiao, C. Y., Leu, Y. W. and Wang, T. H. (2015) 'Cell Signaling and Differential Protein Expression in Neuronal Differentiation of Bone Marrow Mesenchymal Stem Cells with Hypermethylated Salvador/Warts/Hippo (SWH) Pathway Genes', *PLoS One,* 10(12), pp. e0145542.
Ullah, I., Subbarao, R. B., Kim, E. J., Bharti, D., Jang, S. J., Park, J. S., Shivakumar, S. B., Lee, S. L., Kang, D., Byun, J. H., Park, B. W. and Rho, G. J. (2016) 'In vitro comparative analysis of human dental stem cells from a single donor and its neuronal differentiation potential evaluated by electrophysiology', *Life Sci,* 154, pp. 39-51.
Ulusoy, A. T., Turedi, I., Cimen, M. and Cehreli, Z. C. (2019) 'Evaluation of Blood Clot, Platelet-rich Plasma, Platelet-rich Fibrin, and Platelet Pellet as Scaffolds in Regenerative Endodontic Treatment: A Prospective Randomized Trial', *J Endod,* 45(5), pp. 560-566.
Vagaska, B., Gillham, O. and Ferretti, P. (2020) 'Modelling human CNS injury with human neural stem cells in 2- and 3-Dimensional cultures', *Sci Rep,* 10(1), pp. 6785.
Valmaseda-Castellón, E., Berini-Aytés, L. and Gay-Escoda, C. (2001) 'Inferior alveolar nerve damage after lower third molar surgical extraction: a prospective study of 1117 surgical extractions', *Oral Surg Oral Med Oral Pathol Oral Radiol Endod,* 92(4), pp. 377-83.
Vaudry, D., Chen, Y., Hsu, C. M. and Eiden, L. E. (2002) 'PC12 cells as a model to study the neurotrophic activities of PACAP', *Ann N Y Acad Sci,* 971, pp. 491-6.
Veitz-Keenan, A. and Keenan, J. R. (2015) 'Trials needed to identify best management of iatrogenic inferior alveolar and lingual nerve injuries', *Evid Based Dent,* 16(1), pp. 29.
Ventre, D. M. and Koppes, A. N. (2016) 'The Body Acoustic: Ultrasonic Neuromodulation for Translational Medicine', *Cells Tissues Organs,* 202(1-2), pp. 23-41.
Verma, P., Nosrat, A., Kim, J. R., Price, J. B., Wang, P., Bair, E., Xu, H. H. and Fouad, A. F. (2017) 'Effect of Residual Bacteria on the Outcome of Pulp Regeneration In Vivo', *J Dent Res,* 96(1), pp. 100-106.
Vetter, I., Mozar, C. A., Durek, T., Wingerd, J. S., Alewood, P. F., Christie, M. J. and Lewis, R. J. (2012) 'Characterisation of Na(v) types endogenously expressed in human SH-SY5Y neuroblastoma cells', *Biochem Pharmacol,* 83(11), pp. 1562-71.
Wada, T. and Penninger, J. M. (2004) 'Mitogen-activated protein kinases in apoptosis regulation', *Oncogene,* 23(16), pp. 2838-49.
Walker, M. J. and Xu, X. M. (2018) 'History of Glial Cell Line-Derived Neurotrophic Factor (GDNF) and Its Use for Spinal Cord Injury Repair', *Brain Sci,* 8(6).
Walmsley, A., Laird, W. and Lumley, P. (1992) 'Ultrasound in dentistry. Part 2—periodontology and endodontics', *Journal of dentistry,* 20(1), pp. 11-17.
Wan, W., Cao, L., Kalionis, B., Xia, S. and Tai, X. (2015) 'Applications of Induced Pluripotent Stem Cells in Studying the Neurodegenerative Diseases', *Stem Cells Int,* 2015, pp. 382530.

Wang, F., Li, Y., Yang, Z., Lu, K., Zuo, J. and Zhou, Z. (2017a) 'Effect of Low-Intensity Pulsed Ultrasound on a Rat Model of Dentin–Dental Pulp Injury and Repair', *Ultrasound in Medicine & Biology,* 43(1), pp. 163-175.

Wang, F., Zuo, J., Li, Y., Yang, Z. and Luo, J. (2017b) '[Effect of low intensity pulsed ultrasound on expression of TGF-β1 and Smads during dentin injury and repair]', *Zhong Nan Da Xue Xue Bao Yi Xue Ban,* 42(9), pp. 1030-1036.

Wang, S., Xia, B., Qiao, Z., Duan, L., Wang, G., Meng, W., Liu, Z., Wang, Y. and Zhang, M. (2019) 'Tetramethylpyrazine attenuated bupivacaine-induced neurotoxicity in SH-SY5Y cells through regulating apoptosis, autophagy and oxidative damage', *Drug Des Devel Ther,* 13, pp. 1187-1196.

Wang, T., Choi, E., Monaco, M. C., Campanac, E., Medynets, M., Do, T., Rao, P., Johnson, K. R., Elkahloun, A. G., Von Geldern, G., Johnson, T., Subramaniam, S., Hoffman, D. A., Hoffman, D., Major, E. and Nath, A. (2013) 'Derivation of neural stem cells from human adult peripheral CD34+ cells for an autologous model of neuroinflammation', *PLoS One,* 8(11), pp. e81720.

Wang, X., Thibodeau, B., Trope, M., Lin, L. M. and Huang, G. T.-J. (2010) 'Histologic characterization of regenerated tissues in canal space after the revitalization/revascularization procedure of immature dog teeth with apical periodontitis', *Journal of endodontics,* 36(1), pp. 56-63.

Warden, S. J. (2003) 'A new direction for ultrasound therapy in sports medicine', *Sports Med,* 33(2), pp. 95-107.

Watanabe, Y., Harada, T., Ito, T., Ishiguro, Y., Ando, H., Seo, T., Kobayashi, S., Takahashi, M. and Nimura, Y. (1997) 'ret Proto-oncogene product is a useful marker of lineage determination in the development of the enteric nervous system in rats', *J Pediatr Surg,* 32(1), pp. 28-33.

Wichterle, H., Lieberam, I., Porter, J. A. and Jessell, T. M. (2002) 'Directed differentiation of embryonic stem cells into motor neurons', *Cell,* 110(3), pp. 385-97.

Wichterle, H. and Peljto, M. (2008) 'Differentiation of mouse embryonic stem cells to spinal motor neurons', *Curr Protoc Stem Cell Biol,* Chapter 1, pp. Unit 1H.1.1-1H.1.9.

Wilson, E. S. and Newell-Litwa, K. (2018) 'Stem cell models of human synapse development and degeneration', *Mol Biol Cell,* 29(24), pp. 2913-2921.

Wojtkiewicz, D. M., Saunders, J., Domeshek, L., Novak, C. B., Kaskutas, V. and Mackinnon, S. E. (2015) 'Social impact of peripheral nerve injuries', *Hand (N Y),* 10(2), pp. 161-7.

Wu, P. K. and Park, J. I. (2015) 'MEK1/2 Inhibitors: Molecular Activity and Resistance Mechanisms', *Semin Oncol,* 42(6), pp. 849-62.

Wu, T., Xu, W., Chen, H., Li, S., Dou, R., Shen, H., Liu, X., Hong, Y. and He, J. (2020a) 'Comparison of the differentiation of dental pulp stem cells and periodontal ligament stem cells into neuron-like cells and their effects on focal cerebral ischemia', *Acta Biochim Biophys Sin (Shanghai),* 52(9), pp. 1016-1029.

Wu, Y., Gao, Q., Zhu, S., Wu, Q., Zhu, R., Zhong, H., Xing, C., Qu, H., Wang, D., Li, B., Ning, G. and Feng, S. (2020b) 'Low-intensity pulsed ultrasound regulates proliferation and differentiation of neural stem cells through notch signaling pathway', *Biochem Biophys Res Commun,* 526(3), pp. 793-798.

Xia, B., Chen, G., Zou, Y., Yang, L., Pan, J. and Lv, Y. (2019) 'Low-intensity pulsed ultrasound combination with induced pluripotent stem cells-derived neural crest stem cells and growth differentiation factor 5 promotes sciatic nerve regeneration and functional recovery', *J Tissue Eng Regen Med,* 13(4), pp. 625-636.

Xicoy, H., Wieringa, B. and Martens, G. J. (2017) 'The SH-SY5Y cell line in Parkinson's disease research: a systematic review', *Mol Neurodegener,* 12(1), pp. 10.
Xie, S., Jiang, X., Wang, R., Hua, Y., Zhou, S., Yang, Y. and Zhang, J. (2019) 'Low-intensity pulsed ultrasound promotes the proliferation of human bone mesenchymal stem cells by activating PI3K/AKt signaling pathways', *J Cell Biochem,* 120(9), pp. 15823-15833.
Xin, Z., Lin, G., Lei, H., Lue, T. F. and Guo, Y. (2016) 'Clinical applications of low-intensity pulsed ultrasound and its potential role in urology', *Transl Androl Urol,* 5(2), pp. 255-66.
Xu, T., Gu, J., Li, C., Guo, X., Tu, J., Zhang, D., Sun, W. and Kong, X. (2018) 'Low-intensity pulsed ultrasound suppresses proliferation and promotes apoptosis via p38 MAPK signaling in rat visceral preadipocytes', *Am J Transl Res,* 10(3), pp. 948-956.
Xuan, K., Li, B., Guo, H., Sun, W., Kou, X., He, X., Zhang, Y., Sun, J., Liu, A., Liao, L., Liu, S., Liu, W., Hu, C., Shi, S. and Jin, Y. (2018) 'Deciduous autologous tooth stem cells regenerate dental pulp after implantation into injured teeth', *Sci Transl Med,* 10(455).
Yadav, S., Verma, A. and Sachdeva, A. (2014) 'Assessment of lingual nerve injury using different surgical variables for mandibular third molar surgery: a clinical study', *Int J Oral Maxillofac Surg,* 43(7), pp. 889-93.
Yamamoto, D., Tada, K., Suganuma, S., Hayashi, K., Nakajima, T., Nakada, M., Matsuta, M. and Tsuchiya, H. (2020) 'Differentiated adipose-derived stem cells promote peripheral nerve regeneration', *Muscle Nerve,* 62(1), pp. 119-127.
Yamauchi, N., Yamauchi, S., Nagaoka, H., Duggan, D., Zhong, S., Lee, S. M., Teixeira, F. B. and Yamauchi, M. (2011) 'Tissue engineering strategies for immature teeth with apical periodontitis', *J Endod,* 37(3), pp. 390-7.
Yang, B., Wu, Q., Zhang, L., Guo, Y. and Gong, P. (2017a) 'Effect of Low-intensity Pulsed Ultrasound on the Mandibular Remodeling Following Inferior Alveolar Nerve Transection', *Zhongguo Yi Xue Ke Xue Yuan Xue Bao,* 39(2), pp. 215-224.
Yang, C., Li, X., Sun, L., Guo, W. and Tian, W. (2017b) 'Potential of human dental stem cells in repairing the complete transection of rat spinal cord', *J Neural Eng,* 14(2), pp. 026005.
Yang, H., Xie, Z., Wei, L., Yang, S., Zhu, Z., Wang, P., Zhao, C. and Bi, J. (2013) 'Human umbilical cord mesenchymal stem cell-derived neuron-like cells rescue memory deficits and reduce amyloid-beta deposition in an AβPP/PS1 transgenic mouse model', *Stem Cell Res Ther,* 4(4), pp. 76.
Yang, J., Yuan, G. and Chen, Z. (2016) 'Pulp Regeneration: Current Approaches and Future Challenges', *Front Physiol,* 7, pp. 58.
Yang, J. W., Zhang, Y. F., Wan, C. Y., Sun, Z. Y., Nie, S., Jian, S. J., Zhang, L., Song, G. T. and Chen, Z. (2015) 'Autophagy in SDF-1α-mediated DPSC migration and pulp regeneration', *Biomaterials,* 44, pp. 11-23.
Yang, M. H., Lim, K. T., Choung, P. H., Cho, C. S. and Chung, J. H. (2010) 'Application of ultrasound stimulation in bone tissue engineering', *Int J Stem Cells,* 3(2), pp. 74-9.
Yang, S. W., Kuo, C. L., Chang, S. J., Chen, P. C., Lin, Y. T., Manousakas, I. and Kuo, S. M. (2014) 'Does low-intensity pulsed ultrasound treatment repair articular cartilage injury? A rabbit model study', *BMC Musculoskelet Disord,* 15, pp. 36.
Yap, M. S., Nathan, K. R., Yeo, Y., Lim, L. W., Poh, C. L., Richards, M., Lim, W. L., Othman, I. and Heng, B. C. (2015) 'Neural Differentiation of Human Pluripotent Stem Cells for Nontherapeutic Applications: Toxicology, Pharmacology, and In Vitro Disease Modeling', *Stem Cells Int,* 2015, pp. 105172.
Yin, K., Baillie, G. J. and Vetter, I. (2016) 'Neuronal cell lines as model dorsal root ganglion neurons: A transcriptomic comparison', *Mol Pain,* 12.

Yin, Y., Huang, P., Han, Z., Wei, G., Zhou, C., Wen, J., Su, B., Wang, X. and Wang, Y. (2014) 'Collagen nanofibers facilitated presynaptic maturation in differentiated neurons from spinal-cord-derived neural stem cells through MAPK/ERK1/2-Synapsin I signaling pathway', *Biomacromolecules,* 15(7), pp. 2449-60.

Yoon, J. H., Roh, E. Y., Shin, S., Jung, N. H., Song, E. Y., Lee, D. S., Han, K. S., Kim, J. S., Kim, B. J., Jeon, H. W. and Yoon, K. S. (2009) 'Introducing pulsed low-intensity ultrasound to culturing human umbilical cord-derived mesenchymal stem cells', *Biotechnol Lett,* 31(3), pp. 329-35.

Yoon, S. and Seger, R. (2006) 'The extracellular signal-regulated kinase: multiple substrates regulate diverse cellular functions', *Growth Factors,* 24(1), pp. 21-44.

Yoshimura, K., Tanimoto, A., Abe, T., Ogawa, M., Yutsudo, T., Kashimura, M. and Yoshida, S. (2002) 'Shiga toxin 1 and 2 induce apoptosis in the amniotic cell line WISH', *J Soc Gynecol Investig,* 9(1), pp. 22-6.

Young, F. I., Telezhkin, V., Youde, S. J., Langley, M. S., Stack, M., Kemp, P. J., Waddington, R. J., Sloan, A. J. and Song, B. (2016) 'Clonal Heterogeneity in the Neuronal and Glial Differentiation of Dental Pulp Stem/Progenitor Cells', *Stem Cells Int,* 2016, pp. 1290561.

Yousefi, F., Lavi Arab, F., Nikkhah, K., Amiri, H. and Mahmoudi, M. (2019) 'Novel approaches using mesenchymal stem cells for curing peripheral nerve injuries', *Life Sci,* 221, pp. 99-108.

Yuan, A., Sasaki, T., Kumar, A., Peterhoff, C. M., Rao, M. V., Liem, R. K., Julien, J. P. and Nixon, R. A. (2012) 'Peripherin is a subunit of peripheral nerve neurofilaments: implications for differential vulnerability of CNS and peripheral nervous system axons', *J Neurosci,* 32(25), pp. 8501-8.

Yuan, A., Sershen, H., Veeranna, Basavarajappa, B. S., Kumar, A., Hashim, A., Berg, M., Lee, J. H., Sato, Y., Rao, M. V., Mohan, P. S., Dyakin, V., Julien, J. P., Lee, V. M. and Nixon, R. A. (2015) 'Neurofilament subunits are integral components of synapses and modulate neurotransmission and behavior in vivo', *Mol Psychiatry,* 20(8), pp. 986-94.

Yue, Y., Yang, X., Zhang, L., Xiao, X., Nabar, N. R., Lin, Y., Hao, L., Zhang, D., Huo, J. and Li, J. (2016) 'Low-intensity pulsed ultrasound upregulates pro-myelination indicators of Schwann cells enhanced by co-culture with adipose-derived stem cells', *Cell Proliferation,* 49(6), pp. 720-728.

Zeng, Q., Nguyen, S., Zhang, H., Chebrolu, H. P., Alzebdeh, D., Badi, M. A., Kim, J. R., Ling, J. and Yang, M. (2016) 'Release of Growth Factors into Root Canal by Irrigations in Regenerative Endodontics', *J Endod,* 42(12), pp. 1760-1766.

Zhang, H., Lin, X., Wan, H., Li, J. H. and Li, J. M. (2009) 'Effect of low-intensity pulsed ultrasound on the expression of neurotrophin-3 and brain-derived neurotrophic factor in cultured Schwann cells', *Microsurgery,* 29(6), pp. 479-485.

Zhang, J. and Jiao, J. (2015) 'Molecular Biomarkers for Embryonic and Adult Neural Stem Cell and Neurogenesis', *Biomed Res Int,* 2015, pp. 727542.

Zhang, J., Lian, M., Cao, P., Bao, G., Xu, G., Sun, Y., Wang, L., Chen, J., Wang, Y., Feng, G. and Cui, Z. (2017) 'Effects of Nerve Growth Factor and Basic Fibroblast Growth Factor Promote Human Dental Pulp Stem Cells to Neural Differentiation', *Neurochem Res,* 42(4), pp. 1015-1025.

Zhang, J., Lu, X., Feng, G., Gu, Z., Sun, Y., Bao, G., Xu, G., Lu, Y., Chen, J., Xu, L., Feng, X. and Cui, Z. (2016a) 'Chitosan scaffolds induce human dental pulp stem cells to neural differentiation: potential roles for spinal cord injury therapy', *Cell Tissue Res,* 366(1), pp. 129-42.

Zhang, L. X., Shen, L. L., Ge, S. H., Wang, L. M., Yu, X. J., Xu, Q. C., Yang, P. S. and Yang, C. Z. (2015) 'Systemic BMSC homing in the regeneration of pulp-like tissue and the enhancing effect of stromal cell-derived factor-1 on BMSC homing', *Int J Clin Exp Pathol,* 8(9), pp. 10261-71.

Zhang, W. and Liu, H. T. (2002) 'MAPK signal pathways in the regulation of cell proliferation in mammalian cells', *Cell Res,* 12(1), pp. 9-18.

Zhang, X., Zhou, Y., Li, H., Wang, R., Yang, D., Li, B. and Fu, J. (2018) 'Intravenous administration of DPSCs and BDNF improves neurological performance in rats with focal cerebral ischemia', *Int J Mol Med,* 41(6), pp. 3185-3194.

Zhang, Z., Hou, L., Li, X., Ju, C., Zhang, J., Wang, X., Liu, C., Lv, Y. and Wang, Y. (2016b) 'Neuroprotection of inositol hexaphosphate and changes of mitochondrion mediated apoptotic pathway and α-synuclein aggregation in 6-OHDA induced parkinson's disease cell model', *Brain Res,* 1633, pp. 87-95.

Zhao, L., Feng, Y., Hu, H., Shi, A., Zhang, L. and Wan, M. (2016) 'Low-Intensity Pulsed Ultrasound Enhances Nerve Growth Factor-Induced Neurite Outgrowth through Mechanotransduction-Mediated ERK1/2-CREB-Trx-1 Signaling', *Ultrasound Med Biol,* 42(12), pp. 2914-2925.

Zhao, X. and Bhattacharyya, A. (2018) 'Human Models Are Needed for Studying Human Neurodevelopmental Disorders', *Am J Hum Genet,* 103(6), pp. 829-857.

Zheng, K., Feng, G., Zhang, J., Xing, J., Huang, D., Lian, M., Zhang, W., Wu, W., Hu, Y., Lu, X. and Feng, X. (2020) 'Basic fibroblast growth factor promotes human dental pulp stem cells cultured in 3D porous chitosan scaffolds to neural differentiation', *Int J Neurosci*, pp. 1-9.

Zhou, S., Schmelz, A., Seufferlein, T., Li, Y., Zhao, J. and Bachem, M. G. (2004) 'Molecular mechanisms of low intensity pulsed ultrasound in human skin fibroblasts', *J Biol Chem,* 279(52), pp. 54463-9.

Zoli, M. (2000) 'Distribution of Cholinergic Neurons in the Mammalian Brain with Special Reference to their Relationship with Neuronal Nicotinic Acetylcholine Receptors.', in Clementi, F., Fornasari, D. and Gotti, C. (eds.) *Handbook of Experimental Pharmacology*. Berlin, Heidelberg: Springer, pp. 13-30.

Zou, M., Li, S., Klein, W. H. and Xiang, M. (2012) 'Brn3a/Pou4f1 regulates dorsal root ganglion sensory neuron specification and axonal projection into the spinal cord', *Dev Biol,* 364(2), pp. 114-27.

Zuccarini, M., Giuliani, P., Frinchi, M., Mudò, G., Serio, R. M., Belluardo, N., Buccella, S., Carluccio, M., Condorelli, D. F., Caciagli, F., Ciccarelli, R. and Di Iorio, P. (2018) 'Uncovering the Signaling Pathway behind Extracellular Guanine-Induced Activation of NO System: New Perspectives in Memory-Related Disorders', *Front Pharmacol,* 9, pp. 110.

Zuniga, J. R. and LaBanc, J. P. (1993) 'Advances in microsurgical nerve repair', *Journal of oral and maxillofacial surgery,* 51(1), pp. 62-68.

Zuo, J., Zhen, J., Wang, F., Li, Y. and Zhou, Z. (2018) 'Effect of Low-Intensity Pulsed Ultrasound on the Expression of Calcium Ion Transport-Related Proteins during Tertiary Dentin Formation', *Ultrasound Med Biol,* 44(1), pp. 223-233.

APPENDICES

Appendix I: Stability value ‘SD value’ of the qPCR reference genes

Housekeeping genes	SH-SY5Y	DPSCs
HPRT1	0.213	0.264
RPLA13	0.259	0.677
GAPDH	0.284	0.691
B2M	0.307	0.283

.

Appendix II: The specificity of the neuronal markers

Marker name	Specificity	References
NES	Neuroepithelial neuron marker	Lendahl, Zimmerman, and McKay (1990) and Tohyama *et al.* (1992)
TUBB3	Neuronal cytoskeleton marker	Cambray-Deakin (1991) and Katsetos *et al.* (2003)
RET	Neuronal development marker	Watanabe *et al.* (1997) and Luo *et al.* (2007)
GAP43	Neuronal growth marker	Basi *et al.* (1987) and Skene and Willard (1981)
NF-M/NEFM	Mature and specific neuron marker	Trojanowski, Walkenstein and Lee (1986) and Yuan *et al.* (2015)
ENO2/NSE		Marangos *et al.* (1980) and Marangos, Zomzely-Neurath and York (1976)
MAP2	Dendritic marker	Harada *et al.* (2002) and Caceres *et al.* (1984)
GFAP	Astrocyte glial cell marker	Eng *et al.* (1971) and Eng, Ghirnikar and Lee (2000)
ACHE and CHAT	Cholinergic neuron markers	Eckenstein and Sofroniew (1983), Zoli (2000), and Ray, Simon, and Lahiri (2009)
DBH	Noradrenergic neuron marker	Hartman, Zide, and Udenfriend (1972) and Ernsberger *et al.* (2000)
DAT	Dopaminergic neuron marker	Nirenberg *et al.* (1997) and Revay *et al.* (1996)
SYN1	Synaptic marker	Thiel (1993) and De Camilli, Cameron and Greengard (1983)
SNAP25		Kochlamazashvili and Haucke (2013) and Antonucci *et al.* (2016)
SCN1A/$Na_v1.1$	General voltage-gated sodium channel in motor and sensory neurons	Duflocq *et al.* (2008) and Osteen *et al.* (2016)
SCN9A/$Na_v1.7$	Specific sensory and nociceptive voltage-gated sodium channel	Dib-Hajj *et al.* (2013), Akin *et al.* (2019), and McDermott *et al.* (2019)
PRPH/Peripherin	Peripheral nervous system marker	Portier, de Néchaud, and Gros (1983) and Yuan *et al.* (2012)
POU4F1/BRN3A	Sensory neuron marker	Zou et al. (2012) and Lanier *et al.* (2007)
MNX1/HLXB9/HB9	Motor neuron marker	Arber *et al.* (1999), Thaler *et al.* (1999), and Stifani (2014)

Appendix III: Conference and scientific meeting presentations

Al-Maswary A., Walmsley D., Cooper P., Scheven B. Low Intensity Pulsed Ultrasound (LIPUS) Effects on Proliferation and Differentiation of Neural cells. Ultrasurge IAB Meeting, University of Birmingham, UK, January 23-24th, 2020 (oral presentation- invited speaker).

Al-Maswary A., Walmsley D., Cooper P., Scheven B. Neurogenic Differentiation of Dental Pulp Stem Cells. British Society for Oral and Dental Research (BSODR), Leeds, UK, September 3-5th, 2019 (oral presentation).

Al-Maswary A., Walmsley D., Cooper P., Scheven B. A Low Intensity Pulsed Ultrasound (LIPUS) Promotes Proliferation and Differentiation of Neuronal Cells. IADR/AADR/CADR General Session and Exhibition, Vancouver, Canada, June 19-22nd, 2019 (oral presentation).

Al-Maswary A., Walmsley D., Cooper P., Scheven B. Establishing Neuronal Cell Differentiation Models Using Dental Pulp Cells. IADR/PER General Session and Exhibition, London, UK, July 25-28th, 2018 (Poster presentation- Won a prize, 2018 Travel Award for post-graduate category for excellence in pulp biology regeneration research, pulp biology and regeneration group (PBRG)).

Al-Maswary A., Walmsley D., Cooper P., Scheven B. Neuronal Wiring. Competition of doctoral early research image presentation. College of Medical and Dental Sciences, Festival of Graduate Research, University of Birmingham, UK, April 11th, 2019 (poster presentation- Joint Winner).

UNIVERSITY OF BIRMINGHAM | COLLEGE OF MEDICAL AND DENTAL SCIENCES | SCHOOL OF DENTISTRY

INSTITUTE OF CLINICAL SCIENCES

Neuronal wiring

Arwa A Al-Maswary, A. Damien Walmsley, Paul R Cooper, Ben A Scheven

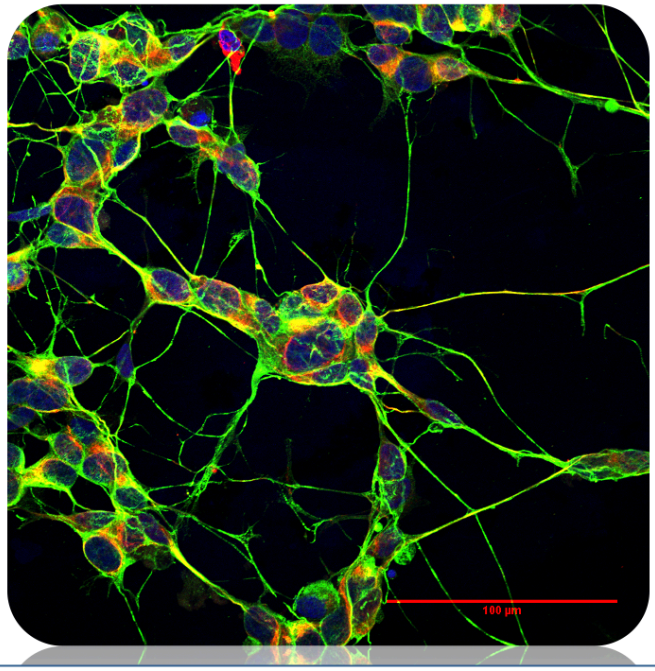

"Miscommunication is the number one cause of all problems" Earl Sweatshirt

Neuronal wiring is the key to neuronal cell to cell communication to convey messages and perform sensory or motor function. Our neuronal-like wiring model was established from human neuroblastoma SH-SY5Y cell line. The cells were differentiated into neuronal-like cells incorporating 10µM all trans retinoic acid (ATRA) with 10% FBS DMEM/F12 medium for 5 days, followed by 7-days'culture in serum-free media supplemented with 50ng/ml brain-derived neurotrophic factor (BDNF). Double immunofluorescence (neurofilament-medium (NF-M), and beta III tubulin) with nuclear stain (DAPI) showed the cytoskeleton and neurite-like extensions. The image was captured by confocal microscopy.